University of Bradford eThesis

STRUCTURAL INTEGRITY OF EYES DIAGNOSED WITH AMBLYOPIA

The measurement of retinal structure in amblyopia using Optical Coherence Tomography

Alison BRUCE MA DBO (D)

Submitted for the degree of Doctor of Philosophy

School of Optometry and Vision Science
University of Bradford

2010

Abstract

Alison Bruce

Structural Integrity of Eyes Diagnosed with Amblyopia

Amblyopia is the leading cause of monocular visual impairment in children. Therapy for amblyopia is extremely beneficial in some children but ineffective in others. It is critical that the reasons for this discrepancy are understood. Emerging evidence indicates that current clinical protocols for the diagnosis of amblyopia may not be sufficiently sensitive in identifying individuals who, on more detailed examination, exhibit subtle structural defects of the eye. Presently, the magnitude of this problem is unknown.

The aim of this study was to establish the prevalence of subtle retinal/optic nerve head defects in eyes diagnosed with amblyopia, to distinguish between possible explanations for the origin of such defects and to investigate the relationship between quantitative measures of retinal structure, retinal nerve fibre layer thickness and optic nerve head dimensions. Using the imaging technique of Optical Coherence Tomography (OCT) retinal structure has been investigated in detail, following the visual pathway across the retina from the fovea, via the paramacular

bundle to the optic disc, where peripapillary retinal nerve fibre thickness has been imaged and subjected to detailed measures along with optic disc size and shape. The study formed two phases, the first imaging the eyes of visually normal adults and children, comparing them to amblyopes, both adults and children who had completed their treatment. The second phase, a longitudinal study, investigated retinal structure of amblyopic children undertaking occlusion therapy for the first time. By relating pre-therapy quantitative measures to the visual outcome the second phase of the study aimed to examine whether OCT imaging could identify children achieving a poor final outcome.

The results show a clear picture of inter-ocular symmetry structure in all individuals, visually normal and amblyopic. Optic disc characteristics revealed no structural abnormalities in amblyopes, in any of the measured parameters, nor was there any association between the level of visual acuity and the measured structure.

At the fovea differences were shown to occur in the presence of amblyopia, with thickening of the fovea and reduction of the foveal pit depth. The structural changes were found to be both bilateral and symmetrical with the fellow eye also affected. In the longitudinal phase of the study these changes were demonstrated to a greater extent in children who "failed" to respond to treatment. This bilateral, symmetrical structural change found at the fovea, which has not been previously reported, cannot therefore be the primary cause of the visual loss which has been diagnosed as amblyopia.

Acknowledgements

For Andrew, Ewan and James

I would like to thank both Dr Brendan Barrett and Dr Ian Pacey for their guidance, encouragement, and patience.

"Take a chance! All life is a chance. The man who goes the furthest is generally the one who is willing to do and dare. The "sure thing" boat never gets you far from shore."

Dale Carnegie

Contents

9

Chapter 1. The Human Visual Pathway

1.1 Introduction

The primary aim of this study is to investigate the retinal structure of amblyopes. In order to explore retinal structure in the presence of amblyopia, it is necessary to consider both the structure and development of the normal adult human visual pathway and the detail of the retinal structure. This chapter will firstly present information relating to structure in the normal human adult, which will provide a background against which any structural differences found during the study can be compared. Secondly this chapter will provide information on the development of the visual pathway and retinal structure. This study investigates the structure of the retina, in the adult amblyope and in amblyopic children during treatment. It is essential to this study that the development of both the visual pathway and the retina be considered in detail. Given the exceedingly complex, multi-layered structure of the adult human visual pathway from the retina to the primary visual cortex, it is of interest to particularly consider if the retinal structure and visual pathway, in its adult form is present at birth, and to what extent it develops postnatally.

The scientific investigation into the structure and development of the visual pathway has mainly been based on results of experiments in animals, both primates and non-primates. Many of the retinal investigations have been carried

15

out on chickens(Frohns et al., 2009; Liang et al., 1995; Troilo et al., 1996) and most of the retinogeniculate and cortical investigations have used kittens and monkeys of varying species(Briggs and Usrey, 2007; Levitt et al., 2001; Symonds and Rosenquist, 1984; Wiesel and Hubel, 1963). Research on humans has been limited with a few notable studies having examined the anatomical structure of the retina at post-mortem and post-termination (Curcio and Allen, 1990; Provis and Hendrickson, 2008). Post-mortem studies produce particular difficulties in ensuring that tissue samples do not shrink and are not distorted by the laboratory processing (Curcio and Allen, 1990). It is only recently that neuroimaging techniques have been developed to the degree where they are suitable for in vivo human investigations. The consequence of this diversity in investigation, over a variety of species, is that in areas where there is variation in anatomical structure controversy arises as to the interpretation of the results (Livingstone and Hubel, 1984) and their subsequent analysis and understanding when related to the human visual system (Horton and Hoyt, 1991b; Huberman, 2007; Landisman and Ts'o, 2002). Recently new techniques are being developed (Duong et al., 2008; Van Velthoven et al., 2007; Zhang et al., 2008) which will allow researchers to perform detailed non-invasive examinations of the structure and function of the human visual pathway.

1.2 Structure of the Adult Human Visual Pathway

1.2.1 Retinal Structure

The human retina consists of an intricate architectural structure of over 110 million neurones, forming a layered organisation, except in the area of the fovea; here the inner nuclear layer and the ganglion cell layers are laterally displaced allowing light to fall directly onto the cones. This structural formation of the fovea facilitates a high level of spatial resolution. The retinal layers contain a number of differing types of neurones; photoreceptors (rods and cones), horizontal cells, bipolar cells, amacrine cells and ganglion cells, as well as glial cells such as astrocytes and Muller cells (Miller, 2005) (Figure 1.1). There are approximately 92 million rods and 4.6 million cones in the human eye; 50% of the cones are located in the macular area (Curcio and Allen, 1990). This number has been revised down from the much quoted study by Osterberg (1935) due to the improvement in histological techniques (Curcio and Allen, 1990; Osterberg, 1935). Structurally the photoreceptors link to the ganglion cells via the bipolar and amacrine cells, synapsing with the bipolar cells in the outer plexiform layer, and the bipolar cells linking with both amacrine and ganglion cells in the inner plexiform layer (Bruce V et al., 2004).
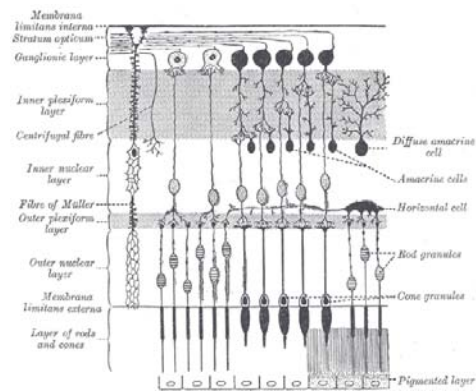
Figure 1.1: Retinal Structure depicting the retinal cell layers.
From http://upload.wikimedia.org July 2009.

Photoreceptors, both rods and cones respond to wavelengths of light (400-700nm) and are responsible for converting light into an electrochemical signal that is transmitted along the visual pathway to the visual cortex, where it is encoded in terms of its position, time and wavelength. The rods and cones are packed into the retina in a mosaic like fashion with their long axes parallel to the direction of the incident light and their outer segment pointing away from the incoming beam; consequently light must pass through the layers of the retina to stimulate the photoreceptors (Bruce V et al., 2004).

1.2.2 Macula

The terms macula, fovea and foveola are used interchangeably within the field of ophthalmic literature; this may lead to confusion or misinterpretation of research findings. It is of particular importance in this research study, investigating retinal structure related to amblyopia and visual development, to define the position and extent of the macular region and in particular to define the region of the fovea.

The term macula (Figure 1.2) refers to the region in the retina bound by the perifoveal area, where the retinal ganglion cells are reduced to a single layer, this may be seen on ophthalmic examination as an annular reflex. The human macula is located approximately 13.5º (4 mm) on the temporal side of the optic nerve; it has a total diameter of 5.5 mm. The fovea (meaning pit in Latin) is the specialised central area, where there is displacement of the ganglion cell and the inner nuclear layers, it is approximately 1.5 mm in diameter. In the centre of the pit is located the foveola (diameter 0.35 mm) a smaller central area where only cones and glial cells are situated (Provis and Hendrickson, 2008). The majority of scientific papers investigating foveal structure use the term fovea to encompass both the fovea and foveola, therefore for the remainder of this document the term fovea will be used to define both the fovea and the foveola, unless otherwise stated.

19

.
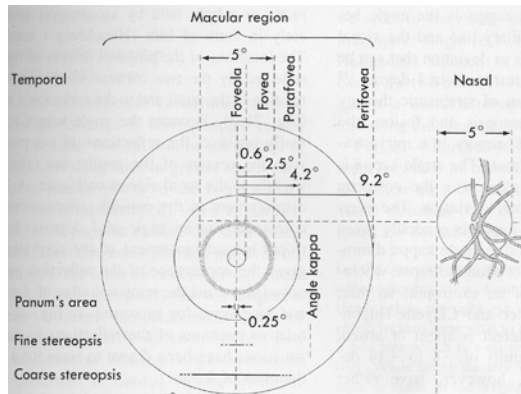
Figure 1.2: Diagram of the macular and foveal regions. Adapted from Adler's Physiology of the Eye (Moses, 1981)

1.2.2.1 Macular Pigment

The characteristic yellow appearance of the macula is produced by macular pigment; this is comprised of two carotenoid pigments, lutein and zeaxanthin. Lutein and zeaxanthin are found in the photoreceptor axon and inner plexiform layers and it is likely that they protect the macula by acting as a short wavelength filter of blue light (Neuringer et al., 2004; Snodderly et al., 1984). Their ability to filter blue light can be measured as macular pigment optical density (MPOD), this measure can be directly related to the lutein and zeaxanthin levels in the macula (Richer et al., 2004). The optical density and spatial distribution of macular pigment varies significantly between individuals (Bone and Landrum, 1992; Hammond and

20

Fuld, 1992) and it has been suggested that this is related to the spatial distribution of the cones, which decrease rapidly away from the centre of the fovea (Elsner et al., 1998). A study investigating the spatial profile of macular pigment has demonstrated a positive association between foveal macular pigment and the width of the fovea (Nolan et al., 2008) and the authors of the latter study suggest that the association may be determined by the length of the Henlé fibres, with increased length of the fibres being found in wider foveas.

1.2.3 Fovea

The fovea is characterised by being an avascular, rod-free zone. In this area, exclusive to cone photoreceptors, the highest density of cones are found. The cones connect individually with either one or two bipolar cells; this low connection ratio allows the high spatial resolution of visual stimuli. A peak density of 100,000 – 324,000 cones per mm^2 is found in the human fovea; the foveal cones are elongated with the diameter of each cone inner segment measuring 2-3 μm and individual outer segments measuring 1-2 μm (Curcio and Allen, 1990). The distinctive characteristic of the fovea is the displacement of the connecting cells onto the rim (Figure 1.3) this configuration is believed to prevent light scatter, enabling a high spatial resolution (Rowe and Dreher, 1982). In order to connect with the bipolar cells found on the rim of the fovea the cone axons are lengthened; these specialist axonal structures are known as the Fibres of Henlé, reaching radially up to 0.4mm to connect with their bipolar cells. Information regarding the topography of the human foveal pit is limited and is variable due to the small

21

number of studies and differing investigative techniques. (Williams, 1980) attempted to mathematically model the slope of the foveal pit and estimated it to be 43⁰, (Polyak, 1941) measured the slope of an excised human retina to be 20⁰ and most recently utilising OCT technology, (Dubis et al., 2009) measured the foveal slope to be 12⁰ but found significant variation in pit structure between individuals although not between right and left eyes.
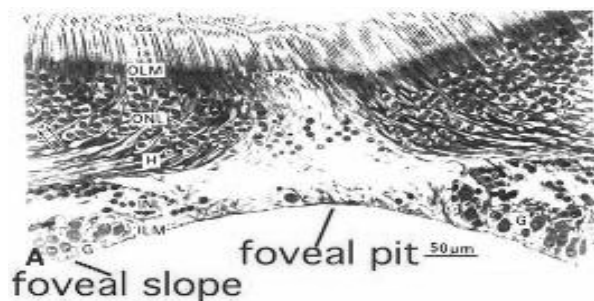
Figure 1.3: Histological section of the human fovea. os, outer segments; is, inner segments; OLM, outer limiting membrane; ONL, outer nuclear layer; H, fibres of Henlé; INL, inner nuclear layer; ILM, inner limiting membrane; G, ganglion cells. From (Yamada, 1969).
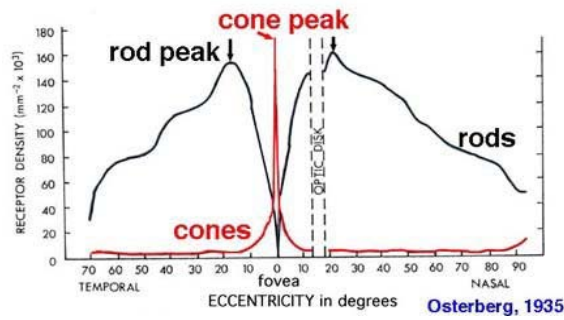
Figure 1.4: Graph of the cone:rod density across the retina From (Osterberg, 1935).

The concentration of cones reduces exponentially away from the fovea, outside of the macular region there are few cones and the retina is dominated by rods (Miller, 2005) (Figure 1.4).

1.2.4 Retinal Ganglion Cells

In the human adult there are approximately 1 million retinal ganglion cells (Miller, 2005; Nassi and Callaway, 2009). The highest density of ganglion cells is found in central retina with a peak density of 5,000 cells/mm^2 1mm from the foveal centre. The nasal retina has been shown to have more than 3 times as many ganglion cells as corresponding sites in temporal retina (Curcio and Allen, 1990). Early studies suggested a 1:1 ratio of cone photoreceptors to ganglion cells in the foveal area (Polyak, 1941) however more recent studies have demonstrated that the ratio is closer to 1:2 or 1:3 (Curcio and Allen, 1990; Missotten, 1974). Curcio (1990)

hypothesises that this configuration of cones to ganglion cells is consistent with a magnified representation in the primary visual cortex; the cortical magnification factor being proportional to the retinal ganglion cell density (For further explanation see Figure 1.9) (Curcio and Allen, 1990).

In the primate eye, research has shown at least 17 different ganglion cell types distributed throughout the retina. Each type of retinal ganglion cell has a specific anatomy (Rockhill et al., 2002) and a small number have been identified as having a specific physiology (Dacey et al., 2003). Three types of retinal ganglion cell have been shown to fall into distinct categories due to their characteristic responses (Nassi and Callaway, 2009). Midget ganglion cells provide the origin of the parvocellular (P) pathway to the lateral geniculate nucleus. These cells convey a red-green colour–opponent signal. They typically have small receptive fields, low contrast sensitivity, slow axonal velocities and are sensitive to high spatial and low temporal frequencies (Callaway, 2005). Parasol ganglion cells provide the origin of the magnocellular (M) pathway to the lateral geniculate nucleus. These cells lack colour opponency and transmit a broadband achromatic signal, they have large receptive fields high contrast sensitivity, fast axonal conduction velocity and are sensitive to high temporal and low spatial frequencies (Yücel et al., 2003). The third type of ganglion cells are made up of bistratified cells and form the koniocellular (K) pathway. These cells convey a blue-on, yellow-off colour-opponent signal to the lateral geniculate nucleus (Bruce V et al., 2004; Chatterjee and Callaway, 2003; Nassi and Callaway, 2009). Chromatic information is consequently conveyed from the retina to the lateral geniculate nucleus by

anatomically segregated colour-opponent systems and on to the primary visual cortex, to be combined (Chatterjee and Callaway, 2003).

1.2.4.1 Melanopsin Containing Ganglion Cells

The rod and cone photoreceptors detect and relay light through the retinal ganglion cells to the visual cortex via a multisynaptic pathway. Not only is pattern vision relayed to the brain using this pathway, but also non-image forming functions such as the papillary light reflex and circadian photoentrainment. These non-image forming functions are maintained by the rods, cones and the melanopsin-containing intrinsically photosensitive retinal ganglion cells (ipRGCs) (Berson et al., 2002; Hattar et al., 2002). In animal studies it has been shown that loss of ipRGCs does not influence image formation, suggesting that the role of ipRGCs in vision is modulatory (Barnard et al., 2006) whereas non-image forming functions are significantly reduced (Guler et al., 2008; Markwell et al., 2010).

1.2.5 The Optic Nerve, Chiasm and Tract

The retinal ganglion cell axons traverse the visual pathway, exiting via the intraocular segment of the optic nerve known as the optic nerve head and navigate the path to the lateral geniculate nucleus via the optic chiasm and optic tract. The distribution of the retinal ganglion cell axons generally corresponds to the retinotopic map. The axons travelling from the papillomacular bundle are located temporally within the anterior portion of the optic nerve and traverse to a more central position in the posterior portion of the optic nerve (Miller, 2005). The optic

nerve head varies in its appearance and dimensions, the size of the optic cup generally being associated with the size of the sclera canal. The size of the optic nerve head has been shown to have a positive correlation with the retinal surface area, the number of retinal ganglion cell axons and the number of photoreceptors (Jonas et al., 1999; Jonas et al., 1992). It has also been shown to be correlated with refractive error, with an increase in size being associated with increasing myopia (Wang et al., 2006). The orbital section of the human adult optic nerve is approximately 25 mm in length and lacks tension, allowing for ease of movement (Miller, 2005). As the optic nerve exits the orbit via the optic foramen it becomes tightly held within the bony optic canal and as a consequence has greater rigidity. At the optic chiasm the optic nerves from the right and left eyes merge together, in a highly specific pattern. Generally, the axons from nasal retina cross, while those from temporal retina remain uncrossed. The retinal ganglion cell axons from the fovea/papillomacular bundle project both in the crossed and the uncrossed fibres in the optic chiasm; mainly concentrated dorsally and centrally. This configuration of fibres allows the retention of visual acuity in the presence of chiasmal disorders, such as pituitary adenoma or lateral chiasmal disorders (Frisen, 1980; Polyak, 1941).

The emerging crossed and uncrossed axons form the optic tract rearrange themselves to some extent; the larger axons of the magnocellular (M) pathway becoming more superficial than those of the parvocellular (P) axons prior to reaching their destination in the lateral geniculate nucleus.

1.2.6 Lateral Geniculate Nucleus

The lateral geniculate nucleus is the principal thalamic visual relay centre linking the retina and the visual cortex (Miller, 2005). Having passed through the optic nerve and chiasm, retinal ganglion cells synapse in a corresponding number of neurones in the lateral geniculate nucleus (Callaway, 2005) and finally connect to the neurones in the primary visual cortex (Figure 1.5). The lateral geniculate nucleus demonstrates a laminar segregation which is related to the distinct retinal ganglion cells pathways, parvocellular (P) magnocellular (M) and koniocellular (K), emerging from the retina (Parker, 2007). The lateral geniculate nucleus is divided into 6 clear layers, the two inner layers (1 & 2) receiving input from the magnocellular neurones, and the dorsal layers (3, 4, 5 & 6) of the lateral geniculate nucleus generally receiving input from midget ganglion cells of the parvocellular pathway. The koniocellular pathway consists of K neurones, the smallest type of neurone, located within and between the M and P layers (Hendry and Reid, 2000). In the human visual system, retinal ganglion cell axons are organised in an eye specific way, forming set layers. Lateral geniculate nucleus layers 1, 4 and 6 receive input from the contralateral eye (crossed axons) and layers 2, 3 and 5 receive input from the ipsilateral eye (uncrossed axons) (Yücel et al., 2003). The lateral geniculate nucleus segregation has been shown in ferrets to be disrupted by inhibiting retinal activity (Stellwagen and Shatz, 2002).

27

.
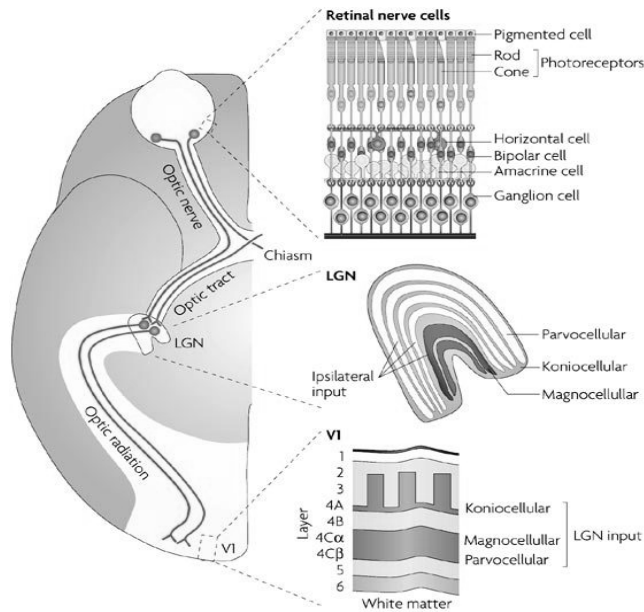
Figure 1.5: Illustration of the pathway from the retina to the primary visual cortex (V1) via the lateral geniculate nucleus. From (Solomon and Lennie, 2007)

Retinal images are mapped topographically and transmitted as a neural code allowing the interpretation of sensory information. Cartesian coordinates of the eye are mapped precisely; axons arising from nasal retina projecting to the posterior end of the tectum and axons from temporal retina projecting to the anterior area. Dorsal-ventral axis information is mapped to the dorsal-ventral axis of the tectum (Erskine and Herrera, 2007). Studies in mammals (mice and ferrets) investigating retinotopic mapping indicate involvement of a group of cell receptor proteins, the Eph receptors and ephrin molecules. The studies have shown that loss of EphrinA

or overexpression of EphAs induces eye specific targeting errors in the LGN, indicating their key role in this process of retinotopic mapping along the length of the visual pathway (Huberman et al., 2005; Pfeiffenberger et al., 2005). There are no binocularly driven neurones in the visual pathway at the level of the lateral geniculate nucleus in the human adult (Haynes et al., 2005).

1.2.7 Optic Radiations

The optic radiations fan out from the lateral geniculate nucleus extending into the primary visual cortex (V1) (Figure 1.6). The radiations are separated into three bundles, classified by the direction of the fibres as they leave the lateral geniculate nucleus; direct, central and Meyer's loop. Meyer's loop is the lowest bundle and initially projects into the anterior temporal lobe before looping back to the posterior cortex (Sherbondy et al., 2008). The central bundle is the largest projection and contains the macular fibres. Within the radiations there are also a significant number of fibres projecting back from the visual cortex, to the lateral geniculate nucleus, ensuring feedback between the visual cortex and the lateral geniculate nucleus.
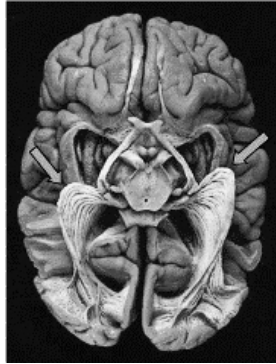
Figure 1.6: Anatomy of the optic tracts and optic radiations feeding into the visual cortices. The anterior extension of the optic radiations, Meyer's loop is indicated by the arrows. From Sherbondy et al (2008).

1.2.8 Primary Visual Cortex (V1)

The primary visual cortex is also referred to as the striate cortex and/or V1, the extrastriate cortex being V2, V3, V4 and V5 (Miller, 2005) (Figure 1.7). In humans V1 is situated in the posterior pole of the occipital cortex extending along the superior and inferior margins of the calcarine fissure. It receives its main afferent input from the optic radiations emanating from the lateral geniculate nucleus. Histological examination of this highly folded sheet of nerve cells shows that V1 is divided into 6 functionally distinct layers with layer 4 receiving the majority of its input from the lateral geniculate nucleus (Callaway, 1998). Layer 4 provides a multitude of intra-cortical connections to other layers; its structure has recently been revised and further subdivided into sublayers: 4α, 4ctr and 4β. The layers identified previously as 4A and 4B have now been revised to layer 3Bβ and layer

3C (Boyd et al., 2000). The newly defined layer 4α receives input from the

magnocellular (M) pathway, and 4β receives its main input from the parvocellular

(P) pathway. Input into 4ctr is currently believed to be from a combination of both

the M and P pathways. The sublayers; 4α, 4ctr and 4β input directly into the layer 3

sublayers; 3A, 3B (α and β) and 3C. The koniocellular (K) pathway projects to layer

3Bα leading to an increasing mix of the M, P and K pathways in V1 (Boyd et al.,

2000; Yoshioka and Hendry, 1995).
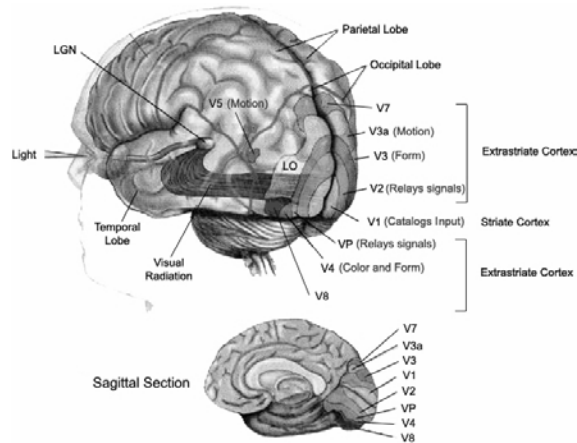
Figure 1.7: Illustration of the represented areas within the Primary Visual
Cortex and the Extrastriate Cortex. From www.colarado.edu July 2009.

Three types of neurones have been identified within the primary visual cortex, simple cells, complex cells and end-stopped cells. Simple cells display a linear receptive field and are highly sensitive to long, narrow slits of light; they demonstrate either an ON or an OFF response, and are orientation selective, responding maximally to a stimulus inclined at a particular angle (Hubel, 1963). They are also particularly selective about the position of the stimulus within their receptive field. Simple cells are mainly located in layer 4 of V1.

Complex cells are also orientation selective but in addition are motion sensitive, being sensitive to both direction and speed. They respond inconsistently to stationary stimulus but respond vigorously to a moving stimulus orientated at their preferred angle and speed (Hubel and Wiesel, 1968). Unlike simple cells they will respond to a stimulus regardless of its position within the receptive field as long as it is of the appropriate orientation and speed. Complex cells are mainly located above and below layer 4 and are found in greater numbers than simple cells (Miller, 2005). Hubel and Weisel (1998) first proposed that complex cells are constructed from the convergence of inputs from a number of simple cells, this appears to have been confirmed by a more recent study investigating the receptive fields of the cat primary visual cortex (V1) (Martinez and Alonso, 2001).

End-stopped cells have an inhibitory area surround, beyond which their response decreases. Therefore they respond to short line segments contained within their activating surround. End-stopped cells are also located above and below layer 4 (Miller, 2005).

The primary visual cortex (V1) combines the visual information from the right and the left eyes. The complex and end-stopped cells receive only binocular input, while the simple cells receive both binocular and uniocular input. This means that layer 4 receives predominantly monocular input and the remaining layers receive predominantly binocular input.

Cells that respond to horizontal and vertical disparity are located within the foveal representation of V1 and the parafoveal areas of V1 and V2. These cells detect both horizontal and vertical disparity between corresponding features from both retinas. This disparity provides the information that determines stereoscopic depth perception (Durand et al., 2002; Trotter et al., 2004).

The organisation within the primary visual cortex (V1) is not exclusively the 6 parallel layers; there is further organisation into columns running at right angles to the surface (Figure 1.8). The columns, formed from neurones are known as ocular dominance columns, these receive eye specific input. This pattern of alternating eye specific input spans the thickness of the cortex (Hubel et al., 1977; Levay et al., 1980). The ocular dominance columns are not solely eye specific but also encompass groups of neurones that are orientation specific, the orientation changing systematically in small steps covering a 180° rotation (Figure 1.8) (Hubel et al., 1978). This highly specific arrangement of cortical neurones results in precise cellular activity responses, reacting to the defined orientation of a line stimulus. Staining with the enzyme cytochrome oxidase (CO) which is a marker for

33

areas of high metabolic activity exposes patches aligned within the ocular

dominance columns these are referred to as "blobs". Cells within the blobs do not

demonstrate orientation selectivity and are believed to process colour information

within the striate cortex, running parallel to but separate from the orientation

specific system (Livingstone and Hubel, 1984).
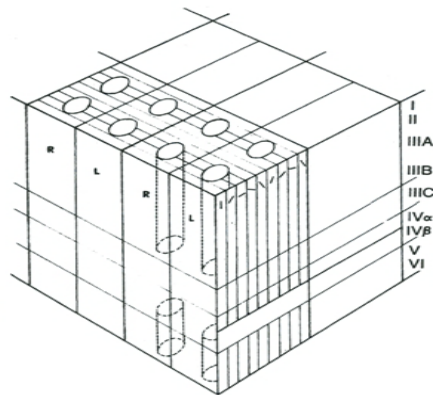
Figure 1.8: Illustration of the striate cortex depicting the eye specific ocular dominance columns, orientation columns and blobs. The subdivision of layer 4 (4ctr) is not shown. From Miller, 2005 July 2009.

The retinotopic mapping found in the lateral geniculate nucleus continues into the

primary visual cortex (V1) (Figure 1.9).The retinotopic organisation in humans can

be demonstrated in the representation of visual field testing (Mc Fadzean et al.,

1994). A number of studies have documented and revised the human retinotopic

map (Fox et al., 1987; Holmes, 1945; Horton and Hoyt, 1991b) by correlating visual

field defects with cortical lesions. The representation of the fovea on the posterior

pole of V1 is disproportionately large, the macular (central 10°) region of retina occupying approximately 50% of V1 surface area and the foveal (central 1°) region occupying 5% (Figure 1.9). This magnified representation of the macular area in V1 results in nearly double the amount of cortex being dedicated to processing macular information than might have been expected from the numbers of retinal ganglion cells (Curcio and Allen, 1990).
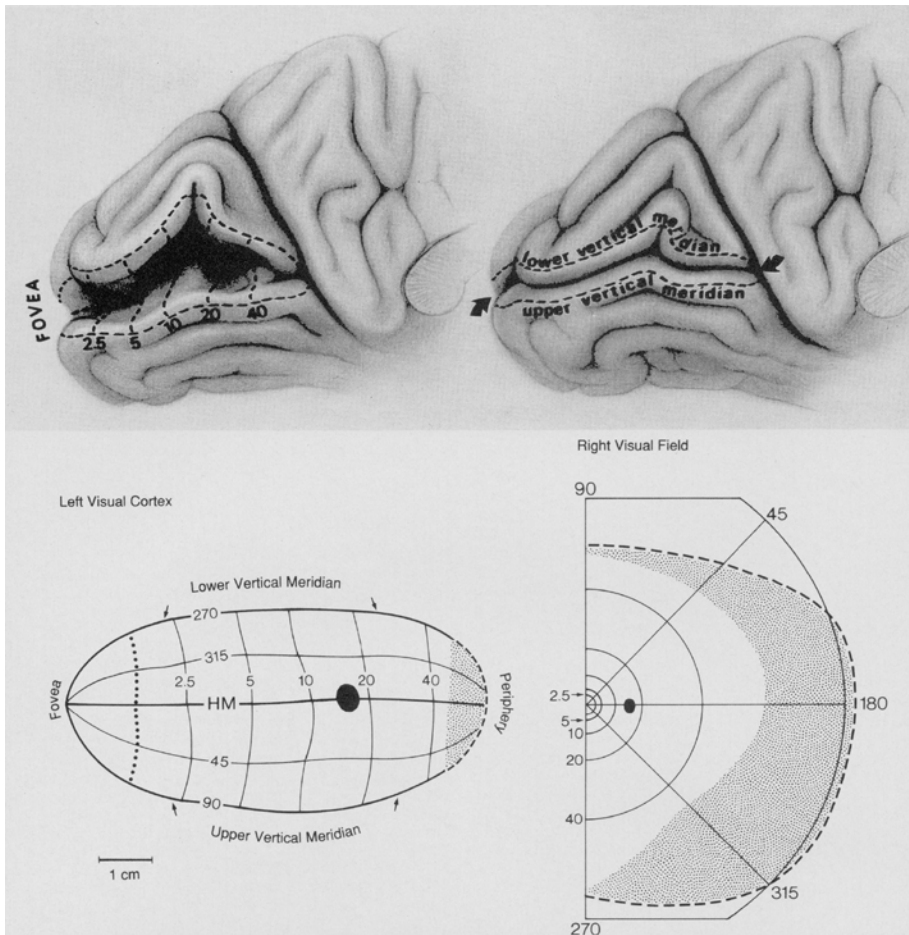
Figure 1.9: Retinotopic map of the human primary visual cortex (V1) with representation of the visual field. Numbers denote the distance from the fovea(°) or the meridional angle. The central 1° of field is represented from the fovea to the dotted line. HM=horizontal meridian and the black oval =blind spot. From Horton and Hoyt (1991).

1.2.9 V2

The majority of input to V1 passes from V1 to area V2. V2 lies within the occipital lobe bordering V1 and anatomically is divided into quadrants, representing the dorsal, ventral and left and right hemispheres. The connections between V1 and V2 are between neurones located at the same depth and are retinotopically organised (Horton and Hoyt, 1991a).

V2 connects contralaterally via the corpus callosum to the fellow area V2 thus representing opposite halves of the visual field (Miller, 2005).

V2 receives its input from two pathways, either from the blob or inter-blob areas of V1 (Sincich and Horton, 2002). The majority of the neurones in V2 are colour-selective and orientation-selective and the neurones located within the thick striped areas process information from both eyes, responding to retinal spatial disparity (Thomas et al., 2002). Many of the V2 cells have been shown to have multifaceted responses, responding to both colour and retinal disparity and demonstrating larger receptive fields (Ts'o et al., 2001).

1.2.10 V3

Area V2 lies proximal to area V3 and projects ipsilaterally to V4 and V5. Area V3 also exhibits a retinotopic organisation, with the border of V2 and V3 representing the horizontal meridian of the visual field (Horton and Hoyt, 1991a) and foveal representation lying in the area where V2 and V3 lie side by side (Zeki, 1969). The

37

anatomical arrangement of V3 is controversial with some researchers who have carried out studies in monkeys proposing that V3 is subdivided into a dorsal and a ventral area (Lyon and Kaas, 2002; Lyon et al., 2002) and others suggesting that there is in fact no area V3 but a separate and different area labelled V6 (Rosa et al., 2005).

1.2.11 V4

Area V4 lies in proximity to V2 from which it receives its greatest input. Its neurones respond to a number of stimulus attributes, including shape, colour, and texture. A recent study in humans using fMRI suggests that V4 contains neurones that are important for encoding properties of visible surfaces (Bouvier et al., 2008).

1.2.12 V5 (MT)

Area V5 also referred to as MT due to its location in the middle temporal gyrus (Miller, 2005) has been shown to be predominantly involved in the processing of motion information. The input to V5 from V1 is directionally selective and has been shown to be also involved in the processing of second-order movement where movement is defined by changing contrast or texture, rather than a change in luminance which is found in first order movement (Smith et al., 1998).

The outputs from the striate to the extrastriate cortex represent the segregation of signals into two main information pathways, the dorsal and the ventral streams (Nassi and Callaway, 2009). The dorsal pathway processes the direction of

movement of the eyes, head and body, in effect providing information on the positioning of objects i.e. *where* objects are in space. The ventral pathway, in contrast, interacts visual processing with memory processing allowing the ability to produce complex actions i.e. *what* objects are (Bruce V et al., 2004; Goodale et al., 1994). The two pathways therefore provide a pathway for perception and a pathway for action. Consequently, one interpretation is that the dorsal and ventral pathways process the same information but for different aims, carrying out parallel processing of visual information to enable the interpretation of our surroundings.

There is an extensive organization of interconnections throughout the visual pathway. These connections appear to provide both a free flow of visual information and a reciprocal feedback mechanism. The commonality of these visual areas is that they are all linked retinotopically optimising the neural transmission of visual information (Briggs and Usrey, 2008; Erskine and Herrera, 2007; Symonds and Rosenquist, 1984).

1.3 Development of the Human Visual Pathway

1.3.1 Embryogenesis of the Eye

The development of the eye is a continuous process both during embryogenesis and in the post-natal period. The ocular tissues mature at differing rates and co-ordination of this growth is essential so that all the elements of the visual system develop correctly, producing a complete, mature visual system extending from the eye to the brain in the adult. The human eyes develop early in the process of embryogenesis and consists of neuroectoderm, surface ectoderm, mesoderm and migrated neural crest cells (Barishak, 1992). The optic sulcus develops from neuroectoderm around the third week of gestation with the optic pits appearing at week 5, extending to form the optic vesicles. The lens and cornea form from surface ectoderm, the lens first appearing at 4 weeks of gestation. The retina, pigment epithelium and optic nerve form from neural ectoderm, the retinal disc first appearing at 4 weeks (Figure 1.10). The extraocular muscles, vasculature and sclera are formed from mesoderm also around week 4. By 12 weeks of gestation the main anatomical structures are in place (Moller, 2005).

The neonate eye appears to be a similar size to the fully formed adult eye, with the corneal diameter only 1.7mm smaller (Adams, 2005) The newborn's axial length is approximately 17 mm and the eye continues to grow in a non-uniform fashion mainly from posterior elongation. The axial length of the matured eye (23mm) is not finally achieved until approximately 13 years of age (Adams, 2005).

40

Figure 1.10: (**a**) Embryology of the eye begins with the outpocketing of the optic vesicle (OV). The optic vesicle is in contact with the overlying ectoderm (Ect), which thickens to form the lens placode (LP). As the optic cup (OC) develops, the placode forms a vesicle that pinches off from the ectoderm to form the lens. Adapted from (Weaver and Hogan, 2001)

1.3.2 Retinal Development

In any investigation of retinal structure consideration of retinal development and the process of retinal cell arrangement requires deliberation. The process of maturation of central retina and particularly foveal development is important as it is the fovea that is the area responsible for the highest level of visual acuity, although the fovea starts to develop before peripheral retina it is still immature at birth (Adams, 2005) accounting for the relatively poor level of visual acuity found in human infants (Moller, 2005).Understanding the maturation process of the retina and in particularly the fovea is relevant to the understanding amblyopia and its visual consequences.

Cell generation occurs by mitotic division, it occurs in a centro-peripheral sequence of retinal maturation. Mitosis occurs across the entire surface of the retina between

10 -12 weeks of human gestation. The rate is not uniform and the mitosis is greatest in the nasal area. At this time the ganglion cell layer becomes evident, but only in central retina, it is clearly defined against the inner plexiform layer (Provis et al., 1985). At around 14 weeks of gestation a "cold spot" (Rapaport and Stone, 1982) emerges in central retina where mitosis ceases. Within this cold spot a rod free zone is established, with cones developing exclusively in the photoreceptor layer of the developing macula (Provis et al., 1985). The cold spot increases along the horizontal axis reaching the optic disc and quickly extending beyond by approximately 20 weeks of gestation. The ganglion cell layer initially identified centrally by mid-gestation is defined throughout the retina. At 20 weeks of gestation, 77.5% of the retinal surface contains mitotic cells; this has declined by 24 weeks when mitosis is only found in the periphery. Mitosis ceases around 30 weeks of gestation and the retinal laminae can be identified across the whole retinal area.

1.3.3 Apoptosis

Cell death (apoptosis) is common in embryogenesis, allowing a natural process for eliminating excess neurons produced in the development of the central nervous system. All neurones contain the mechanism for apoptosis, in that the cell itself produces the proteins that destroy it. Although it is not yet known what triggers the cell to self destruct, it is known that it is the presence of neurotrophins, activating a reaction with the receptors in the cell membrane that prevents the apoptosis from occurring (Levi-Montalcini, 1975). (Provis, 1987) demonstrated that the process of

cell death in the ganglion cell layer develops in a centro-peripheral fashion.
Pyknotic figures have been identified in the area of the developing macula around
18 weeks of gestation, the period of cell death spanning from 18- 30 weeks of
gestation. This time scale coinciding with the period of loss of axons from the optic
nerve, initially gave rise to the theory that the pyknotic figures were derived from
the retinal ganglion cells (Provis, 1987). However, further research(Georges et al.,
1999) suggests that it is in fact bipolar cells that are affected, with a wave of bipolar
cell death emminating from the developing fovea from around 15 weeks gestation
and extending in a centroperipheral fashion across the retina. Apoptosis in the
ganglion cell layer has not, therefore, been found to be a significant factor in the
morphogenesis of the foveal depression.

The process of bipolar cell apoptosis closely follows the pattern of synapse
formation in both the inner and outer plexiform layers (Vandriel et al., 1990).
Bipolar cells transfer the impulses from photoreceptors to ganglion cells, matching
specific photoreceptor cells: rods; long wavelength sensitive cones; medium
wavelength sensitive cones; and short wavelength sensitive cones, with specific
types of ganglion cells. The implication from Georges' (1999) research is that the
elimination of bipolar cells during retinal synaptogenesis could be a mechanism for
obtaining appropriate connections between specific photoreceptors and ganglion
cells; a synaptic mismatch between photoreceptor type and ganglion cell type may
result in the death of the intervening bipolar cell. The timing of the bipolar cell loss
in the foveal area at 15-20 weeks post-gestation coincides with the period of onset

of the expression of L- and M-opsin from the cones (Cornish et al., 2004; Georges et al., 1999) .

In animal studies apoptosis has also been shown to occur in response to disease processes such as glaucoma and altered visual experiences such as monocular deprivation(Nucci et al., 2000; Quigley et al., 2000). In particular studies in rats where a sustained elevation in intraocular pressure was induced the retrograde transport of neurotrophic factor was obstructed, resulting in the deprivation of the neurotrophins required for retinal ganglion cell support, triggering apoptosis (Johnson et al., 2009; Quigley et al., 2000) .

Apoptosis has also been suggested to have a role in the occurrence of amblyopia in the developing human visual system. Yen's study of the optic nerve head using optical coherence tomography (OCT) speculates that the retinal nerve fibre layer thickness in anisometropic amblyopes is thicker due to a lack of apoptosis (Yen et al., 2004). Studies by Nucci of induced monocular visual deprivation in rats demonstrated a molecular chain reaction triggering apoptosis in the lateral geniculate nucleus (Nucci et al., 2003; Nucci et al., 2000{Nucci, 2003 #543).It is therefore clear from these studies that apoptosis and in particular the complex molecular interactions contributing to apoptosis play a crucial role in the normal development along the entire visual pathway.

1.3.4 Foveal Development

Development of the foveal pit occurs with the centripetal migration of photoreceptors and the centrifugal displacement of the inner nuclear and ganglion cell layer. The process of foveal pit formation is believed to result from the presence of an avascular zone encompassing the fovea {Provis, 1998 #105; Springer, 2004 #167; Provis, 2008 #314}. Provis et al (1998) propose a three stage model of foveal development in humans. Initially, in the early stages of gestation around 12 weeks, all retinal layers are to be found in the central area. Cones begin to accumulate in the central area at around 17 weeks of gestation with the surrounding area becoming thicker and of a domed appearance on the retinal surface, due to the migration of the ganglion cells and bipolar cells, along with the migrating cones they are connected to. At around 24 weeks of gestation Provis (2008) suggests that the presence of the avascular zone leads to starvation of the inner retina, triggering the centrifugal displacement of the inner retinal cells towards the capillary network located in the surrounding parafoveal area (Figure 1.11).

In a further study Provis (Provis and Hendrickson, 2008) suggests the hypothesis that, not only is the foveal region avascular during its development, but that any instance of vascularisation in this area would lead to malformation of the foveal pit and subsequent visual loss (Mc Guire et al., 2003; Meyer et al., 2002).Springer and Hendrickson, (2004) hypothesise that this avascular area of retina produces retinal tissue that is extremely malleable, this in turn allows a combination of mechanical force from the intra-ocular pressure (IOP) and growth induced retinal stretch

producing an elasticity gradient from which the foveal pit is formed. The pit formation is characterised by rapid increase in depth prenatally followed by a widening of the pit postnatally (Springer and Hendrickson, 2005).

A. 12 WG - Differentiation of the Central Area

GCL

VL

Ch
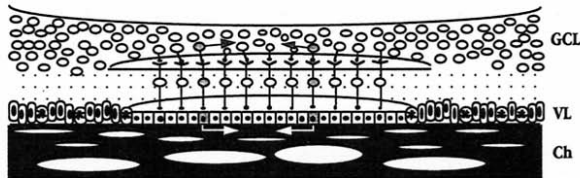
B. 17 WG - Doming of the Retinal Surface

GCL

INL

ONL

Ch
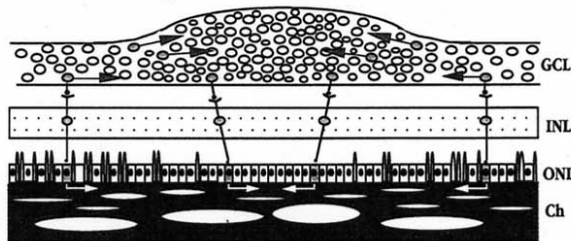
C. 24 WG - Foveal Depression Evident

GCL

INL

ONL

Ch
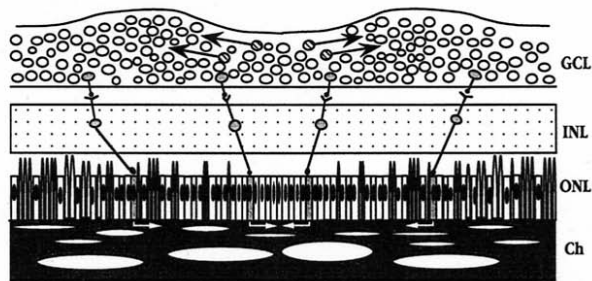
KEY:

centripetal displacement of photoreceptors

centripetal displacement of inner neurons

centrifugal migration of inner neurons

centripetal cone displacements

dendrite - cell body - axon (bipolar cell)

ONL   Outer nuclear layer

dividing cells

rod photoreceptors

cone photoreceptors

choroidal vessels

GCL   Ganglion cell layer

INL   Inner nuclear layer

Figure 1.11: Three stage model of human foveal development. (A) 12 weeks of gestation: All retinal layers are evident in the central area of retina. (B) 17 weeks of gestation: Cones accumulate in the central area with their accompanying bipolar and ganglion cells, giving the retinal surface a domed appearance. (C) 24 weeks of gestation: The foveal depression is evident, formed by the centrifugal migration of GCL (black arrows) and INL from the central area. Cone photoreceptors continue to migrate centripetally (white arrows). From Provis et al (1998).

As the foveal pit forms, the cones change in orientation and length, the inner and outer segments forming elongated appendages. The cone axons elongate forming the fibres of Henle´. The development of the fibres of Henle´ coincides with pit formation in late gestation, with the ganglion cell layer, inner plexiform layer and inner nuclear layer displacement from the foveal area. At this time there is an increase in cone density, changing the single cell layer to a multi-cell layer in the fovea. In the development of the human eye, cone density has been shown to achieve adult proportions around the age of 4-7 years (Provis et al., 1998; Yuodelis and Hendrickson, 1986). This protracted anatomical development of the fovea is reflected in the achievement of visual acuity levels in the developing infant; with a newborn infants visual acuity being estimated at a measurement of 6/60 equivalent and adult levels of 6/6 or better only being achieved around the age of 5 years (Adams, 2005). The timing of any disruptive element is likely to halt or interfere with this developmental sequence and crucially impact on the ultimate visual acuity.

1.3.5 Optic nerve and chiasm

Ganglion cells are the only retinal cell to produce axons that navigate out of the retina, and over a million retinal ganglion cell axons find their way out of the optic disc, to form the optic nerve. The formation of the optic nerve, chiasm and tract is mainly based on information from animal studies(Mann et al., 2004; Oster et al., 2004; Oster and Sretavan, 2003). Newly formed axons amass with the previously generated axons and form small tight bundles travelling together. This is known as fasciculation (Oster et al., 2004).

Axon navigation starts immediately on differentiation of the retinal ganglion cells. Guided by specialised structures on the axon tips known as growth cones, the axons respond to various cues in their micro-environment (Taylor, 2005). The growth cone moves forward from a combination of being both pushed and pulled. As the axon navigates through its environment it adds new material to the cell membrane, extending its length and pushing it forward. The pulling emanates from the thin membrane protrusions of the growth cones, composed of actin filaments and known as filopodia. The actin filaments in the filopodia are able to contract pulling the growth cone along. The growth cone is continuously pulled by the filopodia, the amount of force being dependant on the size and also its ability to adhere to its surroundings (Oster and Sretavan, 2003). Adhesive ability is important to the growth cone as it allows it to progress along a pathway. The receptor molecules on the filopodia interact either by attraction or repulsion to molecules on the surfaces of surrounding cells, this is known as chemotactic guidance. The filopodia also respond to more distant cues in the extra cellular environment, these are known as chemotropic factors, and consist of molecules that diffuse through the environment, either attracting or repelling the growth cone from its appropriate target. On arrival at the target growth stops and the growth cone converts into a synapse. In this way the axons find their route towards the optic nerve head to enter the optic nerve (Mann et al., 2004; Oster et al., 2004; Oster and Sretavan, 2003; Van Horck et al., 2004).

Axon fasciculation is believed to play a key role in axon route finding; however it is dependant on the first axons pioneering the correct pathway. Animal studies have

49

shown that proteins from the immunoglobulin (Ig) family are critical to the process
of fasciculation (Oster et al., 2004). These growth promoting proteins e.g. L1, found
on the retinal ganglion cell axons, function by binding the axons together. In
conjunction with guidance molecules such as L1, attractant molecules exist guiding
the axons towards areas such as the optic nerve head (Oster and Sretavan, 2003)
(Figure 1.12).
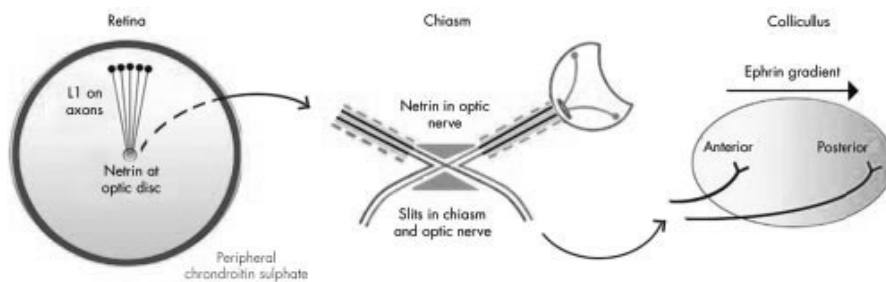
Figure 1.12: Mechanisms of axon guidance in the vertebrate visual system.
From Oster and Sretavan 2003.

Netrin-1, is expressed by neuroepithelial cells at the optic nerve head and appears
to act at short range to attract the retinal ganglion cell growth cones. Genetic
deletion of netrin-1 in mice has resulted in the failure of retinal ganglion cell axons
to accurately exit the eye reducing the size of the optic nerve and producing optic
nerve hypoplasia (Deiner et al., 1997). Having exited the optic nerve head retinal

ganglion cell axons become insensitive to netrin-1 and further along the visual pathway at the optic tract are subsequently strongly repelled by it (Mann et al., 2004).

The cell receptor proteins, Eph receptors and ephrin molecules have been shown to enhance the accuracy of retinal ganglion cell axon targeting in the embryonic mouse retina (Oster et al., 2004). Eph receptors and ephrins have the ability to initiate bi-directional signalling. Dorsal- ventral gradient of Eph/ephrin expression allows axons located in dorsal retina to find their route to the optic nerve. EphB receptor proteins generally have a high ventral to low dorsal gradient while ephrin-B proteins demonstrate the opposite, a high dorsal to low ventral pattern.

EphA and ephrin-A molecules demonstrate similar gradients but along the nasal-temporal axis. Ephrins demonstrate an inhibitory action. This is illustrated where the axons from temporal retina transporting a significant number of Eph receptors avoid the posterior colliculus, an area where ephrins are produced in significant quantities. Conversely axons travelling from nasal retina transport lesser numbers of Eph receptors and show the ability to map to more posterior sites. This complex system of gradients and inhibitory guidance acting on the RGC axons allows the generation of retinotopic mapping of the visual pathway in the lateral geniculate nucleus and superior colliculus (Feldheim et al., 1998; Oster and Sretavan, 2003).

During embryological development the main pathway from the eye to the brain, the optic nerve (ON) is a micro-environment of axonal growth promotion, but within this

environment it has also been shown that inhibitory guidance forces are also present in order to guide the retinal ganglion cell axons. Semaphorins are the largest family of inhibitory guidance molecules consisting of 7 different classes. Sema3A has been reported to cause L1 to switch from inhibition to attraction (Oster et al., 2003). In studies of the optic nerve in rats Sema5A has been shown to induce the collapse of retinal ganglion cell growth cones inhibiting axon re-growth (Goldberg et al., 2004). The presence of Sema5A in the optic nerve is thought to form an inhibitory sheath around the developing structure, maintaining the tight fasciculation of the axon bundles (Oster et al., 2004). Sema5A, however, is not the sole guidance molecule present in the optic nerve; L1 and netrin-1 continue to be expressed in the optic nerve and it is likely that their combined presence ensures the retinal ganglion cell axons assume the correct position and travel the required route to their final destination.

In humans the optic chiasm appears around 4 weeks of gestation (Taylor, 2005).The highly specific pattern of the chiasmal axons namely that nasal fibres cross and temporal fibres remain uncrossed, is essential for the development of the human visual system. The precise mapping of the retinal ganglion cells from each eye to the contra-lateral adjacent layers of the lateral geniculate nucleus is dependant upon the retinal ganglion cell axons continuing on the correct pathway, undertaking decussation or remaining ipsi-lateral in order to arrive at their precise position in the lateral geniculate nucleus. Protein receptor molecules known as Slit molecules, have been shown to be instrumental in the formation of the optic

chiasm in studies of the drosophila and the mouse (Brose et al., 1999; Kidd et al., 1999; Plump et al., 2002). Initially Slit proteins were described as inhibitory molecules inhibiting retinal growth cones. However, further research has shown a synergistic role of these proteins in the chiasm regulating the axonal pathway by promoting fasciculation and establishing a repellent tract to ensure the exact position at which the chiasm forms (Kidd et al., 1999; Plump et al., 2002) (Figure 1.12).

The mechanism by which the retinal ganglion cell axons traverse the pathway between eye and brain is a highly complex and sophisticated process involving a multiplicity of synergistic interactions between the retinal ganglion cell axons and the protein molecules along the entire length of the visual pathway between eye and brain. It is therefore remarkable that errors in axonal pathfinding appear to be rare (Sretavan, 1990).

1.3.6 Development of the Lateral Geniculate Nucleus

The development of the lateral geniculate nucleus in humans appears to be substantially completed during the pre-natal period and by birth the structure is comparable to that of adults (Morita et al., 2000). However, in a similar process to the axonal development in the retina the number of axons terminating in the lateral geniculate nucleus is refined in a process of eye specific segregation. Accelerated development has been shown to occur around week 16 -17 of gestation in humans with the number of retinal axons achieving synaptic connection in the lateral

geniculate nucleus peaking at this time (Khan et al., 1994; Provis et al., 1985). The number of axons then diminishes significantly (Provis et al., 1985). The completion of histological development of the lateral geniculate nucleus appears to be reflected in physiological development which has also been shown to be largely complete by birth (Blakemore and Vitaldurand, 1986).

Recent animal studies have identified a cortico-thalamic feedback system processing information and shaping the receptive fields of thalamic neurones (Bal et al., 2000; Briggs and Usrey, 2005, 2007, 2008). It is thought that this feedback system fine tunes and enhances the transmission of sensory information to and from the visual cortex. Thus the lateral geniculate nucleus is a fundamental component of an important multi-channel circuit, processing and communicating sensory information between the retina and the visual cortex (Briggs and Usrey, 2008).

1.3.7 Primary Visual Cortex (V1)

The ocular dominance columns within layer 4 of V1 have been shown in the rhesus monkey to be formed prior to visual experience (Horton and Hocking, 1996a). In humans the timing of the ocular dominance column development is controversial (Adams and Horton, 2009; Huberman, 2007) with debate arising around whether spontaneous retinal activity which influences the synaptic refinement process of the retinal axons synapsing in the lateral geniculate nucleus also drives the early ocular dominance column formation prior to visual experience (Del Rio and Feller, 2006; Huberman et al., 2006). The development of ocular dominance columns was

thought to be linked to the critical period of post-natal visual development, during which the columnar arrangement is vulnerable to alterations in visual stimuli such as monocular deprivation(Del Rio and Feller, 2006). However, recent findings in cats, monkeys and ferrets show that the ocular dominance columns develop earlier than was previously assumed indicating that the initial formation of cortical architecture and its subsequent plasticity during the critical period are distinct developmental phases that might reflect differing mechanisms (Crowley and Katz, 2002; Katz and Crowley, 2002). Significant variability in both the size and numbers of ocular dominance columns have been found in studies of the Macaque monkey (Horton and Hocking, 1996b). This variability must be considered when interpreting the results of studies where monocular visual abnormalities such as enucleation, strabismus and anisometropia have been experimentally induced. A post-mortem study of monkeys and humans demonstrated shrinkage of the ocular dominance columns resulting from monocular enucleation. (Horton and Hocking, 1998). The degree of shrinkage appears to be related to the timing of the assault during the critical period, the earlier the enucleation, the greater the shrinkage. In a separate post-mortem study (Horton and Hocking, 1996c) of an adult human with a history of accommodative esotropia and amblyopia (childhood onset) no shrinkage of the ocular dominance columns was found suggesting that the ocular dominance columns are not susceptible to shrinkage after a currently undefined short sensitive period of plasticity. The Horton and Hocking (1996c) study does not however concur with the findings of a study of monkeys raised with strabismus and anisometropia (Crawford and Harwerth, 2004). Crawford and Harwerth (2004)

55

found a reduction in width of the ocular dominance columns in monkeys raised with either strabismus or anisometropia. They further linked the amount of shrinkage to the age of onset and the duration of the visual abnormality.

The development of the ocular dominance columns is important in humans when considering the impact of amblyogenic factors such as strabismus and anisometropia on the development of the primary visual cortex. The timing of the structural formation is important in understanding the impact that amblyopia may have on the developing human visual system.

Chapter 2. Laboratory Investigation of Amblyopia

2.1 Defining Amblyopia

Amblyopia can be defined as a form of reversible cerebral visual impairment (typically visual acuity) despite optimal optical correction. It is caused by a disturbance in visual development during the sensitive period of development and is never found in isolation, generally being associated with strabismus and or anisometropia (Holmes and Clarke, 2006). Although amblyopia has long been recognised (De Buffon, 1743; Worth, 1901), it has remained elusive, with little known about the natural history of amblyopic development in humans. It is therefore defined more by what it is not, than what it is. It has been the subject of numerous publications, with 6573 publications listed on PubMed as of 28/10/2010, yet there is still a lack of understanding regarding its aetiology, with continuing debate regarding the best form of treatment (Pediatric Eye Disease Investigator, 2008), or indeed whether mild forms of amblyopia should even be treated (Clarke et al., 2003; Rahi et al., 2006; Stewart-Brown and Snowdon, 1998). Despite the pioneering neuro-anatomical and physiological studies of Hubel and Wiesel (Hubel, 1963; Hubel and Wiesel, 1965, 1968, 1998), nearly half a century later, clinical consensus regarding treatment methodology, treatment success and even the definition of amblyopia itself is still under debate (Barrett et al., 2004; Campos, 1995; Clarke, 2010; Cleary, 2007). This may be due to the fact that the vast majority of our knowledge of amblyopia comes from animal studies where

amblyopia is experimentally generated. The use of animal models limits the

comparison to humans; however, experimental data derived from humans is also

limited, anatomically mainly to post-mortem studies, and developmentally to

retrospective studies, producing perpetual difficulties in accumulating information.

This chapter will define amblyopia, in terms of its neural basis from research

studies carried out on the visual pathway of animals and humans. In Chapter three,

amblyopia will be considered in terms of the clinical definition, detailing the factors

affecting visual outcome following treatment.

2.2 The Site of Neural Deficit in Amblyopia

2.2.1 The Visual Cortex

The experimental research of Hubel and Weisel has been central in defining our

current thinking on amblyopia (Hubel, 1963; Hubel and Wiesel, 1965, 1968; Hubel

et al., 1977; Hubel et al., 1978). Their research, firstly investigating the visual

cortex of kittens and subsequently macaque monkeys, has contributed

substantially to our knowledge on visual development and, in particular, introduced

the concept that in amblyopia the principal abnormality lies at the level of the visual

cortex. Their questioning of what the brain does with the visual information it

receives from the retina led to a number of significant discoveries. Using the

technique of single-cell recording in the visual cortex they were able to differentiate

between the functions of the cortical cells (Hubel, 1963; Hubel et al., 1978). They

established the presence of simple cells. These cells are cells which demonstrate a linear response to light falling in their receptive field and are highly sensitive to long, narrow slits of light. They demonstrate either an ON or an OFF response, responding maximally to a stimulus inclined at a particular angle (Hubel, 1963). They also established the presence of complex cells. Complex cells are both orientation selective and motion sensitive, responding to both direction and speed (Hubel and Wiesel, 1968) (see Chapter 1).These animal studies utilising techniques of monocular deprivation and artificially induced strabismus, provided evidence for the formation of two independent systems of columns, one system for orientation (Hubel et al., 1978) and one for ocular dominance (see Chapter 1, Figure 1.8) in the visual cortex (Hubel and Wiesel, 1965). On the basis of their studies, Hubel and Wiesel were the first to propose the concept of ocular "competition"; ocular dominance plasticity being a reflection of competitive interaction between the two eyes for synaptic space (Figure 2.1). These changes to cortical structure were observed to occur within the early period of visual development and the concept of the "critical period" was formed. The structure of the ocular dominance columns has been shown to "adult-like" at birth in fetal monkeys (Horton and Hocking, 1996) suggesting that visual experience is not a requirement for their development. Monocular deprivation studies have demonstrated shrinkage of the ocular dominance columns both in monkeys and in humans (Hubel et al., 1977; Horton and Hocking, 1998; Adams et al 2007). It has been suggested that this shrinkage is associated with the timing of the visual assault with the monocular deprivation (usually taking the form of unilateral eyelid

suturing in monkeys) occurring shortly after birth. In studies of anisometropia both in humans (Adams et al., 2007, Horton and Stryker., 1993) and in monkeys (Horton., et al 1997), shrinkage of the ocular dominance columns has not been revealed. This may be due to the natural development of the anisometropia, development occurring after the critical period of cortical development. It could also be due to the presence of binocular function which tends to be maintained to a limited extent in anisometropes despite the presence of amblyopia.
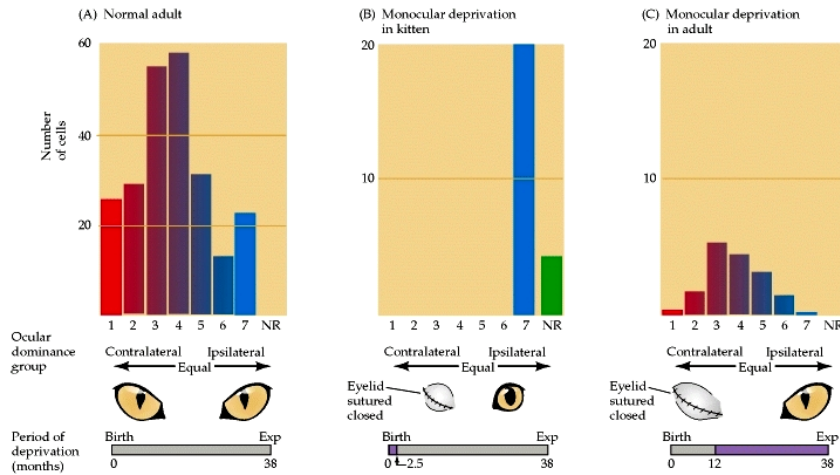
Figure 2.1: Effect of early closure of one eye on the distribution of cortical neurons driven by stimulation of both eyes. (A) Ocular dominance distribution of single unit recordings from a large number of neurons in the primary visual cortex of normal adult cats. Cells in group 1 were activated exclusively by the contralateral eye, cells in group 7 by the ipsilateral eye. Diagrams below these graphs indicate procedure, and bars indicate duration of deprivation (purple). "Exp"= time when experimental observations were made. (B) Following closure of one eye from 1 week after birth until 2.5 months of age (indicated by the bar underneath the graph), no cells could be activated by the deprived (contralateral) eye. Some cells could not be activated by either eye (NR). Note that the closed eye is opened at the time of the experimental observations, and that the recordings are not restricted to any particular cortical layer. (C) A much longer period of monocular deprivation in an adult cat has little effect on ocular dominance (although overall cortical activity is diminished). In this case, the contralateral eye was closed from 12 to 38 months of age. (A after Hubel and Weisel, 1962; B after Wiesel and Hubel, 1963; C after Hubel and Wiesel, 1970.From Neuroscience 2nd edition Chapter 24, Effects of Visual Deprivation on Ocular Dominance.(Purves et al., 2001).

61

The theory of ocular competition has been further developed and refined with the publication of more recent evidence suggesting that neurotrophins play a role in the process of attracting synaptic connections, synaptic stabilisation and rearrangement of the ocular dominance columns in the visual cortex (Bienenstock et al., 1982; Bonhoeffer, 1996; Mc Allister et al., 1999). The model of synaptic modification presented by Bienenstock, Cooper and Munro (BCM) (Bienenstock et al., 1982) provides a mathematical framework from which synaptic change can be modelled for various simulated visual experiences (Clothiaux et al., 1991). The model predicts the results from monocular deprivation experiments where recovery occurs sooner if binocular stimulation is resumed, as opposed to deprivation of the original non-deprived eye (Kind et al., 2002; Mitchell et al., 2003). This finding may have implications when considering the treatment of amblyopia in humans with occlusion therapy, and may account for the reason that amblyopia responds as well to partial occlusion from atropine, as it does to total deprivation from traditional occlusion (Pediatric Eye Disease Investigator, 2008) and also with part-time occlusion as opposed to full-time occlusion (Wallace et al., 2006).It could also explain or partly explain why refractive correction alone is so useful in the treatment of amblyopia.

Studies in human amblyopes using visual evoked potentials (VEP) have confirmed abnormalities at a cortical level (Lawwill, 1978; Levi and Manny, 1982). Amblyopes have been shown to have longer reaction times, demonstrating an increased latency of response in both the treated amblyopic eye and the fellow eye (Watts et

al., 2002). The signal from the cortex in the electrophysiological technique, however, is not refined enough to identify the exact location of the abnormality. More recent research into cortical structure and function has been strengthened with the technological development of imaging techniques allowing greater exploration of human visual cortex and brain function in particular. The technique of fMRI investigates activity within the brain, it does not directly record neural activity, but detects the changes in the blood oxygen level (BOLD) associated with neural activity in the cortex (Barnes et al., 2001) (Figure 2.2).
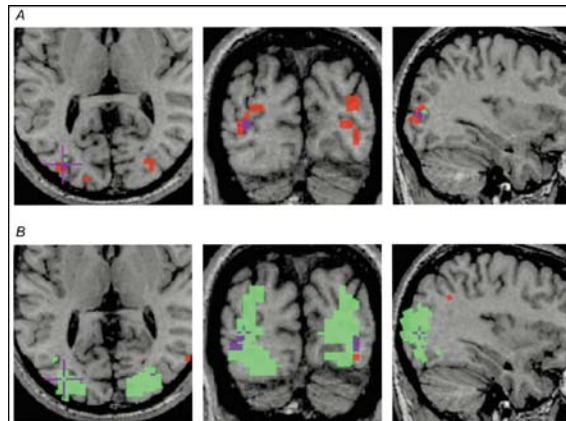
Figure 2.2: fMRI results detailing axial (left), coronal (middle) and sagittal (right) images of an amblyopic adult **A.** The response to a 11 c.p.d grating, and **B.** The response to a 4 c.p.d. grating, showing a large area of cortex driven by the fixing eye (green) but little detectable activation when the amblyopic eye (red) is stimulated. Purple indicates area of overlap. Adapted from Barnes et al (2001).

In a number of studies investigating amblyopia, Magnetic Resonance Imaging (MRI), producing detailed anatomic images of the brain, has been combined with voxel-based morphometry (VBM) (Chan et al., 2004; Mendola et al., 2005; Xiao et al., 2007). Voxel-based morphometry (VBM) is an automated statistical technique that compares multiple images of the cortical gray matter as imaged by MRI, producing a quantitative measurement of the difference in the amount of gray matter within the cortex (Ashburner and Friston, 2000). Both functional magnetic resonance imaging (fMRI) and voxel-based morphometry (VBM) in conjunction with magnetic resonance images have been used to investigate amblyopia (Anderson and Swettenham, 2006; Barnes et al., 2001; Chan et al., 2004; Mendola et al., 2005), functionally demonstrating the effect of reduced activity in the visual cortex (Anderson and Swettenham, 2006; Barnes et al., 2001) and structurally demonstrating a redistribution of the volume of gray matter from the visual cortex to the cortical oculomotor processing areas in amblyopes (Chan et al., 2004; Mendola et al., 2005; Xiao et al., 2007). It has been suggested that this redistribution is compatible with a hypothesis of plasticity in the oculomotor regions to compensate for the visual deficit of the amblyopia in the visual processing areas (Chan et al., 2004). This assertion has however, recently come into question by Barnes et al (2010), investigating both structure and function of the lateral geniculate nucleus (LGN) and visual cortex. This latter study did not find any reduction in gray matter within the visual cortex of amblyopes and further found no relationship between functional deficit and the level of gray matter in the visual cortex (V1). The study

did, however, find that functional deficit at the level of the cortex was predicted by the anatomical structure of the lateral geniculate nucleus (LGN).

2.2.2 The Lateral Geniculate Nucleus (LGN)

The effect of amblyopia on the structure of the lateral geniculate nucleus (LGN) is clear with a number of studies reporting structural abnormalities in the presence of amblyopia. The majority of studies have been animal studies investigating the effect of both monocular deprivation and strabismus in kittens and monkeys. These animal studies have demonstrated shrinkage of lateral geniculate nucleus cells in induced amblyopia of differing types (Headon et al., 1985; Levitt et al., 2001; Maguire et al., 1982) (Figure 2.3). This shrinkage has been attributed to secondary changes from the visual cortex (V1).
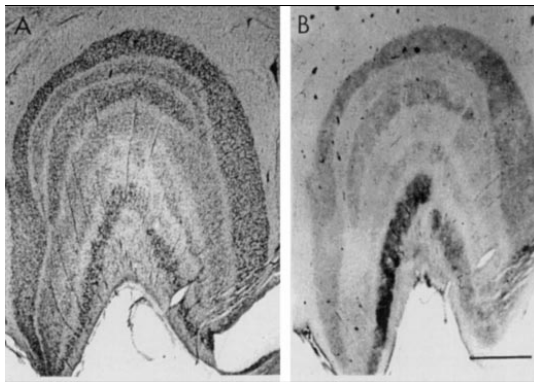
Figure 2.3: Photomicrographs of Nissl (*A*)- and nearby Cat-301 (*B*)-stained sections from the right hemisphere of a monocularly deprived animal's LGN. In both panels, the *top* of the figure is dorsal, and the *right* side is medial. Adapted from Levitt et al, 2001.

Studies of the anatomical structure of the lateral geniculate nucleus in humans are extremely rare, but there is one histological study of the lateral geniculate nucleus in a human diagnosed with anisometropic amblyopia. This showed a decrease in cell size located in the parvocellular layers of the lateral geniculate nucleus connected to the amblyopic eye (Von Noorden et al., 1983). Most recently VBM in conjunction with fMRI has been used to investigate both structure and function of the lateral geniculate nucleus (LGN) and visual cortex, identifying structural abnormalities in the LGN of amblyopes (Barnes et al., 2010), with the LGN of amblyopes demonstrating less gray matter than the LGN of the control group (p<0.04). However, although the presence of structural abnormalities may have been demonstrated, the involvement of the lateral geniculate nucleus (LGN) in amblyopia is contentious. Neurophysiology studies have provided mixed results. Investigation of the lateral geniculate nucleus cells in monkeys have demonstrated normal function with little or no deficit (Blakemore and Vitaldurand, 1986; Sasaki et al., 1998), yet other studies have found subtle effects on the response properties of the lateral geniculate nucleus (Levitt et al., 2001). Until recently the technique of fMRI had not been sensitive enough to provide accurate responses from the lateral geniculate nucleus in humans (Fujita et al., 2001). However, with the further development of this technique the functional integrity of the lateral geniculate nucleus has been recently assessed in amblyopia (Hess et al., 2009). This study found that the response from the lateral geniculate nucleus was significantly reduced when driven by the amblyopic eye (Figure 2.4).
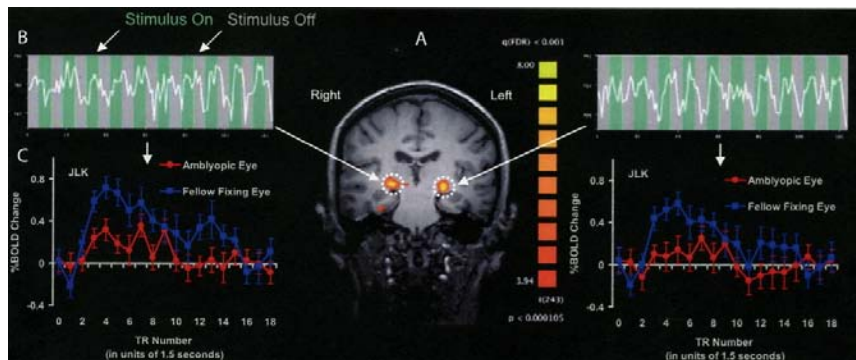
Figure 2.4: Reproduction fo fMRI result, demonstrating a significantly reduced response from the LGN when driven by the amblyopic eye (red line) in comparison to the fellow fixing eye (blue line). From Hess et al.,2009.

Although its structure had been shown to be affected (Cleary, 2000), lateral geniculate nucleus function had generally been viewed as normal in amblyopia (Blakemore and Vitaldurand, 1986) until the recent publication by Hess presenting evidence of deficient responses in amblyopes (Hess et al., 2009). This paper is significant as it provides evidence using the most up-to-date technology that the amblyopic deficit is not confined to the cortex. The question still remains, however, whether the deficit demonstrated in the lateral geniculate nucleus (LGN) is a primary defect, or is secondary to a deficit of the visual cortex. The most recent evidence (Barnes et al., 2010) suggests that the reduced responses found at the LGN of amblyopes may be linked to the reduction in the volume of gray matter affecting both LGN and cortical function in amblyopes.

67

2.2.3 The Retina

As with LGN involvement, retinal involvement in amblyopia is controversial (Hess, 2001). There have been many previous investigations into the retinal contribution in amblyopia, in particular the research of Ikeda and her team who used the neurophysiological technique of single-cell recording from retinal cells in kittens (Ikeda and Tremain, 1979; Ikeda and Wright, 1974). Their research differentiated two distinct types of retinal ganglion cells, sustained (X) cells which were found in the area centralis of the cat responding to fine contrast and spatial discrimination, allowing high levels of visual acuity, and transient (Y) cells which are located in more peripheral retina and detect movement, and which initiate the fixation reflex (Ikeda and Wright, 1972b). The sustained cells were shown to require specific stimulation in the form of a clearly focused image in order to develop (Ikeda and Wright, 1972a). If the appropriate stimulation was not provided, then an arrest of visual development occurred. Ikeda and colleagues, hypothesised that amblyopia was a result of a habitual blur arresting visual development, arising from either the presence of a strabismus or refractive error during the critical period of development (Ikeda, 1980). The findings from Ikeda's work have, however, been heavily criticised, particularly as other studies have been unable to replicate the effects they described and indeed found no evidence of loss of spatial resolution at retinal level (Cleland et al., 1982); (Blakemore and Vital-Durand, 1979). These deprivation studies carried out in both kittens and monkeys found no neurophysiological reduction in spatial resolution, other than in the visual cortex. It has been suggested that the methodology used by Ikeda, (specifically in relation to

68

the method used to artificially induce the convergent strabismus, produced by avulsion of the lateral rectus muscle, leading to a fixed strabismus with the animal unable to move the eye to take up fixation) may have led to the resultant responses from the retinal ganglion cells (Hess, 2001). Unlike Ikeda's research, Cleland investigated retinal responses in kittens with different types of induced strabismus, esotropia, exotropia and cyclotropia (Cleland et al., 1982). These differing types of strabismus would lead to stimulation of different retinal locations (nasal retina in esotropia, temporal retina in exotropia) and may not have produced similar amblyopic deficits to the esotropic kittens investigated by Ikeda (Donnelly et al., 2005; Ikeda, 1980; Williams et al., 2008) and indeed the study produced different findings. The procedure used to artificially induce strabismus and consequently amblyopia has thus been deemed a major factor in determining the outcome of animal studies of retinal physiology. It is therefore important that testing with naturally occurring strabismus and amblyopia in humans is used to substantiate the findings of the animal studies. In human electro-physiological studies using pattern-evoked electroretinograms (ERG's), results have also been variable. In human amblyopes, Hess was unable to substantiate the findings of Ikeda's animal studies (Hess et al., 1985) or replicate results from other human electrophysiological studies (Arden et al., 1980; Arden and Wooding, 1985; Persson and Wanger, 1982), and suggested that the findings from these latter studies, a reduction in pattern-evoked ERG's in the amblyopic eye, was produced by lack of fixation stability, fixation alignment and optical defocus. In particular Hess et al (1985) found amblyopic eyes with unsteady fixation produced reduced

69

amplitude in the pattern ERG. In order to compensate for poor fixation in the amblyopic eye, fixation by the fellow eye was allowed with centration of the corneal reflection in the amblyopic eye to obtain the correct presentation of the stimulus. It is important during the pattern ERG to ensure central fixation as the response from the fovea is greater and unsteady eye movements will result in poor responses, a significant problem in amblyopic eyes (Hess et al., 1985). However, the technique of centration, used by Hess is unlikely to provide accurate foveal stimulation in cases of dense amblyopia where there is likely to be the presence of eccentric fixation (Brock and Givner, 1952; Burian and Cortimiglia, 1962) which cannot be adequately adapted for by centring corneal reflections (Choi and Kushner, 1998). Unusually Hess recruited amblyopic subjects all with the presence of exotropia, this type of strabismus is atypical of what would be found in the general population (Williams et al., 2008) and may have contributed to the lack of ERG anomalies detected in the amblyopes. Contrary to Hess' findings, pattern-ERG's in children attending an ophthalmic clinic for treatment of their amblyopia by occlusion therapy and adults previously treated for amblyopia have been shown to be reduced in response in the amblyopic eye, even when fixation and refractive error were accounted for (Arden et al., 1980; Arden and Wooding, 1985; Persson and Wanger, 1982). Electrophysiology therefore provides contradictory evidence concerning possible retinal involvement in amblyopia.

Recent research using digital photography to image retinal structure in amblyopia has suggested that a subtle organic cause exists in amblyopes, particularly those that have failed to respond to occlusion therapy (Lempert, 2000; Lempert, 2003, 2004, 2008). Lempert's series of studies found a significant reduction in disc size in hypermetropic and strabismic eyes in comparison to eyes without amblyopia or strabismus. The findings have led him to suggest that the smaller optic disc size found in amblyopes indicates a reduction in retinal nerve fibres, and that this is in turn responsible for the reduction in the level of visual acuity in amblyopic eyes (Lempert, 2003). With the development of imaging techniques, the last decade has seen an increasing number of research studies using the developing technologies to measure retinal structure in amblyopia (Huynh et al., 2009; Repka et al., 2009b; Yen et al., 2004). However, these studies have produced interesting but ambiguous results (see Chapter 4 for discussion). With ever improving retinal imaging techniques the opportunity to further explore retinal structure using the most advanced imaging technology, establishing once and for all the possible contribution of the retina in the presence of amblyopia is provided. This is the subject area for the research presented in this thesis.

Based on the published literature, currently the consensus on the aetiology of amblyopia is that it is cortical in nature (Barrett et al., 2004), founded on the initial research evidence from Hubel and Wiesel that cortical structure and function is abnormal (Hubel and Wiesel, 1998) and confirmed by the most recent cortical fMRI research (Barnes et al., 2001; Chan et al., 2004). However, with the continuing development of techniques enabling detailed anatomical investigations such as

71

those producing images of the lateral geniculate nucleus we are beginning to both add to and refine our knowledge and understanding of the functioning of the entire visual pathway and how it may be affected in amblyopia.

2.3 Amblyopia, Anisometropia and Strabismus

The animal data has significantly expanded our knowledge with regards to the mechanisms involved in amblyopia. The animal experiments allowed precise interventions such as monocular deprivation and artificially induced strabismus to be applied at particular periods during development and monitored over exact periods of time. In contrast to this, in human amblyopia there is the presence of a combination of many differing factors coexisting and interacting, which develop longitudinally in a pattern and about which we are still uncertain.

Amblyopia rarely presents as an isolated condition in humans, with very few reported cases of amblyopia occurring with no associated anomaly such as strabismus or anisometropia (Von Noorden, 1985). In a small proportion of cases, the visual deficit results from form deprivation early in life (e.g. congenital cataract). However, in the vast majority of cases, amblyopia co-exists with strabismus and/or anisometropia. The terms "strabismic amblyopia" and "anisometropic amblyopia" are in common use and current belief asserts that the presence of strabismus or anisometropia causes anomalous brain development via either chronic unilateral suppression or chronic unilateral blurring, respectively (Sireteanu and Fronius, 1981; Smith et al., 1985). Amblyopia can therefore be seen as a disorder of visual

development as amblyopia and its associated conditions of anisometropia and strabismus result in visual deficit in the developing infant, but do not result in permanent visual deficit when they occur in adults. The exact timing of this sensitive period of visual development is not known and, crucially, differing visual functions appear to be sensitive to differing conditions at varying periods of time (Harwerth et al., 1986), although the time span in humans is thought to be within the first 7- 8 years of life (Daw, 1998).

2.3.1 Anisometropic Amblyopia

Anisometropia, a difference of the refractive state between the two eyes, is generally believed to produce a difference in image quality between the two eyes when the refractive difference is greater than 1 dioptre (DS) (Attebo et al., 1998; Ciuffreda et al., 1991; Stewart et al., 2005). Anisometropia is thought to cause amblyopia due to the difference in the refractive state between the two eyes, the eye with the lower degree of ametropia dictating the degree of accommodative focus, leaving the fellow eye with an out of focus image. The severity of amblyopia is less in myopic as opposed to hypermetropic anisometropia, as the more myopic eye may be used for near fixation (Hilz et al., 1977). The optical difference between the eyes in anisometropia can also produce aniseikonia with significant disparity in size contributing towards the differentiation between images (Bradley et al., 1983). Despite evidence from animal models attributing anisometropia as a cause of amblyopia (Blakemore and Eggers, 1978) there is support from the limited number of longitudinal studies in humans that anisometropia may not be a primary cause

but rather may be secondary to the amblyopia (Almeder et al., 1990). The longitudinal study by Almeder (1990) investigated the relationship of infant anisometropia to amblyopia over a 10 year period. From a population of 686 children 293 were reviewed and of those only 24 children were identified as having anisometropia; the anisometropia was persistent in only 2 subjects, both of whom had strabismus. A similar longitudinal study documenting astigmatism in children found that high degrees of increasing astigmatism between the ages of 1 to 4 years was associated with the development of amblyopia (Abrahamsson et al., 1990).

2.3.2 Strabismic Amblyopia

Anisometropia is not only correlated to amblyopia, it is also closely linked to strabismus, with both factors being proposed as causal agents for amblyopia (Campos, 1989). Indeed studies in humans have shown that the development of anisometropia may be secondary to the presence of strabismus perhaps reflecting a failure of the emmetropisation process in infants (Ingram et al., 2003; Lepard, 1975) and in animal studies anisometropia has been shown to follow the presence of amblyopia caused by strabismus (Kiorpes and Wallman, 1995). The presence of strabismus producing a misalignment of the visual axis results in the fixation target being projected onto peripheral retina in the deviated eye (nasal retina in convergent strabismus) causing diplopia and a differing target being projected onto the fovea of the deviating eye causing "confusion" (Von Noorden, 1985) (Figure 2.5). In infantile strabismus, with onset during the critical period of visual

development the confused and diplopic images are suppressed. Traditionally the suppression of images has been thought to cause amblyopia, with the degree of the amblyopia being related to the position of the eye, nasal retina having a deeper degree of amblyopia than temporal retina and a well correlated depth of suppression (Sireteanu and Fronius, 1981). This evidence supports a causal role for strabismus in the development of amblyopia.

secondary or false object   visual axes   object of regard

left eye   right eye

fovea   fovea
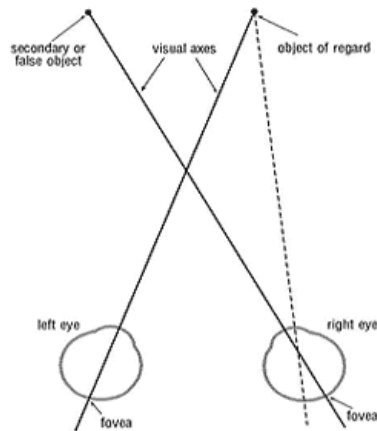
Figure 2.5: Schematic diagram of a RE Esotropia demonstrating stimulation of the right fovea by a secondary object leading to confusion and stimulation of a nasal retinal point by the object of regard (diplopia).Adapted from Von Noorden (1985).

The presence of strabismus, however, is not always indicative of the development of amblyopia, with amblyopia less likely to develop in alternating or intermittent deviations. In animal studies where a unilateral and constant strabismus has been

artificially produced, the development of amblyopia has been demonstrated (Blakemore and Eggers, 1978; Hubel and Wiesel, 1965). However, it has been shown that early form deprivation in humans, such as that experienced from unilateral cataract, causing amblyopia will lead to the development of strabismus (Brown et al., 1999; Helveston et al., 1980; Weisberg et al., 2005). Strabismus has also been shown to arise secondary to anisometropia (Helveston and Von Noorden, 1967), with the occurrence of microstrabismus being invariably linked to anisometropia, and the suggestion of its development being caused by the anisometropia. Therefore, despite the experimental animal literature supporting the hypothesis that amblyopia is the result of strabismus and anisometropia, in humans the cause and effect relationship of anisometropia and strabismus in the development of amblyopia is far from clear. A longitudinal study investigating monocular visual acuity using preferential-looking (PL) techniques in infantile esotropia, between 3 to 14 months of age, demonstrated a reduction of the level of visual acuity and stereopsis following the onset of esotropia (Birch and Stager, 1985).

2.3.3 Psychophysical Investigation

The measurement of visual acuity in amblyopia represents only one method of recording visual deficit. It provides information on the minimum resolution of the eye tested at maximum contrast. In natural viewing situations the visual system is however, subjected to both low and high spatial frequency images at varying levels of contrast. The amblyopic eye has been shown to respond in an atypical fashion

to certain stimuli; responding better to acuity measurement using single letters rather than to linear testing (crowding phenomenon) (Levi et al., 2008) and although contrast sensitivity has been shown to be reduced in amblyopes, this does not appear to be related to the level of acuity loss (Birch and Swanson, 2000). Contrast sensitivity function provides information about visual sensitivity at all spatial frequencies, from coarse to fine, whereas acuity provides a measure only of fine resolution. The defining visual characteristics of both anisometropic and strabismic amblyopes is that they typically demonstrate reduced contrast sensitivity at higher spatial frequencies (Bradley and Freeman, 1981; Katz et al., 1984) as would be expected given the acuity deficit. The binocular enhancement shown to be present in normal observers is found to be absent in amblyopes (Harwerth and Levi, 1983). In a study of visual development in monkeys the contrast sensitivity has been shown to gradually shift to higher levels of contrast along with the increase of sensitivity to higher spatial scales and indeed in a comparison of normal infant function to amblyopic adult function in the monkeys, the results were similar (Kiorpes and Kiper, 1996) suggesting that amblyopia can be characterised as an underdeveloped visual system. A number of studies have considered this deficit of contrast sensitivity as a function of retinal location, examining the degree of loss across the field of vision (Bradley et al., 1985; Hess and Pointer, 1985; Katz et al., 1984). The deficit has been shown to differ between the two 'types' of amblyopia with anisometropic amblyopes demonstrating a uniform deficit across the field of vision and strabismic amblyopes showing an asymmetrical loss (Hess and Pointer, 1985). It has been suggested that this difference is a reflection of the

blur produced in anisometropia where the defocus will have an effect across all eccentricities (Ciuffreda et al., 1991). It is also possible that the difference occurs due to the loss of binocularity. This latter theory of binocular competition is supported by research that demonstrated a deficit in contrast sensitivity in anisometropic amblyopes extending over the binocular field of vision, which disappeared when the monocular field was tested (Hess and Pointer, 1985). The amblyopic eye has been shown to be less affected by reduced luminance levels than the fellow eye (Burian, 1967) and the influence of luminance levels has been examined as to its effect on contrast sensitivity in both strabismic and anisometropic amblyopia (Hess et al., 1980); in strabismic amblyopes the loss of contrast sensitivity reduced with decreasing luminance. Differing hypotheses have been suggested for this finding, firstly that it is due to the fact that the amblyopic deficit is confined to the photopic pathway, predominately affecting the cone photoreceptors (Burian, 1967). Alternatively strabismic amblyopia may be confined to the central visual field as is suggested from the research reporting asymmetrical contrast sensitivity loss, with the strabismic amblyope using the abnormal central field under photopic conditions and the normal peripheral retina under scotopic conditions (Hess et al., 1980).

Strabismic amblyopes have reported perceptual distortions such as ghosting of letters on the acuity chart (Selenow and Ciuffreda, 1986). These perceptual distortions are difficult to assess in terms of their impact on visual performance (Bradley and Freeman, 1985). Judgements of horizontal and vertical alignment in

78

strabismic amblyopes have also been shown to produce consistent systematic errors. This has been attributed to abnormal binocular interactions (Bedell and Flom, 1981). A similar explanation could be that the misjudgement is due to eccentric fixation which is present in a significant proportion of strabismic amblyopes (Cleary, 2000; Stewart et al., 2005). A further study comparing the precision and accuracy of spatial localisation judgements compared with visual acuity levels found that the errors were not accounted for by the presence of eccentric fixation but were linked to the severity of the amblyopia (Bedell et al., 1985). It has been suggested that the presence of the spatial distortion found in strabismic amblyopia could be the result of disorder of the normally well-organized retinotopic map of visual space (Hess, 1982). This would effectively "scramble" the image producing loss of visual acuity but is less likely to reduce contrast sensitivity. A second hypothesis suggests that the distortions arise from retinotopic undersampling at fine spatial scales (Levi et al., 1987; Williams, 1985). However, these results may be a reflection of the methodology of the task, with amblyopes relying upon lower than normal spatial frequencies (Barrett et al., 2003). Where traditional grating stimuli have been used the investigators have failed to find evidence of retinotopic undersampling (Coletta and Williams, 1987). A third hypothesis is that the spatial distortions could be accounted for by a neural misrepresentation of stimulus orientation in the visual cortex, with the amblyope perceiving a single orientation as a pair of orientations (Barrett et al., 2003).

Experimentally, any differences between strabismic and anisometropic amblyopia responses have yet to be clarified. Clinically the two conditions, although both similarly presenting some behavioural overlap, with a reduced spatial acuity measure and reduced contrast sensitivity at high spatial frequencies, differ in the presence or absence of binocular vision. It is this binocular status that appears to influence the differing results from the research studies documenting the psychophysical investigations (Bedell et al., 1990; Hess and Pointer, 1985; Kee et al., 2003). There is a great deal of evidence that amblyopia produces a broad range of neural, perceptual and clinical abnormalities (Barrett et al., 2004; Kiorpes, 2006; Levi, 2006) however, precisely how these factors interact is still unknown. The purpose of the research presented here is to examine retinal and optic disc structure in detail in amblyopia using the latest available imaging technology.

Chapter 3. Amblyopia in Clinical Practice

3.1 Introduction

In this chapter amblyopia will be defined in clinical terms. As will become apparent, amblyopia is defined as a deficit of visual acuity but sometimes there is an additional element in the definition which refers to some minimum difference between the visual acuities of the amblyopic eye its fellow. The treatments for amblyopia will be briefly described and the issues surrounding the definition of a successful treatment outcome will also be discussed.

Depending upon precisely how it is defined, amblyopia is thought to have a prevalence of between 1- 4% (Attebo et al., 1998; Clarke et al., 2003; Williams et al., 2008) and is the most frequently encountered disorder by paediatric ophthalmologists (Rahi et al., 2006). Generally speaking, the period when treatment is believed to be most effective is up to 7 or 8 years of age (Jakobsson et al., 2002; Moseley and Fielder, 2001) as this coincides with the sensitive period of visual development. Traditionally treatment consists of occlusion therapy combined with the prescription of the full refractive correction when required (Clarke, 2010).

3.2 Visual Acuity in Amblyopia: Criterion for Diagnosis

Amblyopia is defined clinically by a measured visual acuity. Given that amblyopia is usually a monocular condition, some definitions also state some minimum difference that should exist between the acuities in the amblyopic and fellow eye (Ciuffreda et al., 1991). Until fairly recently, visual acuity was been measured using Snellen-based testing; however, this does not produce a standardised score and is difficult to determine reliably when testing young children (Mc Graw et al., 1995). There has therefore been a gradual change in clinical practice to the use of logMAR acuity tests (where each individual letter is scored) particularly with the development of validated paediatric versions (Mc Graw et al., 1995; Mc Graw et al., 2000; Stewart, 2000).

Repeatability and reproducibility of the visual acuity test are essential to continuous treatment and monitoring; any improvement in log score between treatment consultations must be deemed to arise from the treatment of the condition and not from any variability in the test result. The test-retest reliability of visual acuity testing has been shown to be within 0.1 log unit using a logMAR crowded test (Holmes et al., 2001; Mc Graw et al., 2000) consequently only differences of >0.1 log unit can be reliably considered as a genuine response to the treatment.

Visual acuity improves with age in the paediatric population. This is believed to be related to neural maturation (Adams, 2005; Moller, 2005). Using age-appropriate logMAR tests in a normative group of 4-5 year old children, mean visual acuity has been shown to be approximately 0·1logMAR (Stewart, 2000). The definition of amblyopia determined for this research study, based on these research findings is

a visual acuity in the amblyopic eye of 0.2 log units or more and a greater than 0.1logMAR (one line) difference between the eyes in best-corrected visual acuity. Since, test-retest variability is around one line, the inter-ocular acuity difference that features in any definition for amblyopia needs to exceed this amount. (Holmes et al., 2001; Kheterpal et al., 1996; Mc Graw et al., 2000). Other studies investigating amblyopia have also used this visual acuity standard (Attebo et al., 1998; Holmes and Clarke, 2006; Lempert, 2000; Williams et al., 2003b)

The prevalence of amblyopia has been reported to vary between 1– 4% (Attebo et al., 1998; Clarke et al., 2003; Williams et al., 2008). Prevalence, however, depends critically on the criterion used to diagnose amblyopia. Reduced visual acuity is the most notable feature of amblyopia and is generally the main criteria used to classify amblyopic eyes. However, to use the level of visual acuity of the amblyopic eye using an acuity criterion of 0.00 logMAR (6/6 Snellens equivalent) would include a proportion of normal eyes (Bedell and Flom, 1985; Flom and Bedell, 1985). Generally therefore the use of a visual acuity level for the amblyopic eye combined with a defined acuity difference between the amblyopic eye and the fellow eye is used to define amblyopia (Attebo et al., 1998; Holmes and Clarke, 2006). Setting the definition as visual acuity of worse than 0.2 logMAR (6/9 Snellen), studies have reported estimates of between 0.63% and 1.81% children in screened populations as presenting with amblyopia (Jensen and Goldschmidt, 1986; Ohlsson et al., 2002; Williams et al., 2003b; Williams et al., 2002).

3.3 Defining Treatment Success

There is considerable variability in terms of what constitutes success in the clinical treatment of amblyopia. This has resulted in a large disparity in reported results with 'definitions of success' varying widely. Some of the criteria for "success" include: (i) any improvement in visual acuity (Bowman et al., 1998; Olson and Scott, 1997), (ii) a defined level of visual acuity achieved, such as 6/9 (Woodruff et al., 1994) or a defined level of difference between the two eyes e.g. <0.1log unit difference (Cleary, 2000) (Figure 3.1).
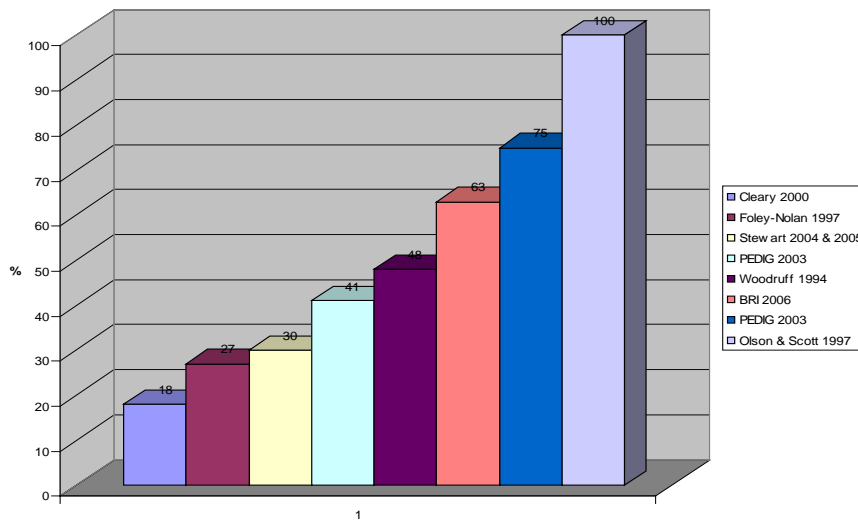
Figure 3.1: Amblyopia treatment success rates (%) from a range of published studies. Adapted from (Cleary, 2007).

The Monitored Occlusion Treatment in Amblyopia Study (MOTAS) determined a "success" rate by also incorporating the level of visual acuity of the fellow eye(Stewart et al., 2003) (Equation 3.1). This gives a comparison of any bilateral changes that may occur. The advantage of this proportional improvement measure is that it provides both an indication of the proportion of the amblyopia treated and a measure of any residual amblyopia. The disadvantage of this success measure is that the visual acuity of the fellow eye may change for various reasons, such as, improving with a training effect, visual maturation, or indeed reducing due to the development of occlusion amblyopia. Any small reduction in the visual acuity of the fellow eye due to variation in testing will also have the effect of disproportionately affecting the improvement score (Holmes et al., 2001).

$$\text{Proportion of visual deficit corrected (\%)} = \frac{\text{Amblyopic VA (start)} - \text{Amblyopic VA (end)}}{\text{Amblyopic VA (start)} - \text{Fellow eye VA (end)}}$$

Equation 3.1: The success rate as determined by the Monitored Occlusion Treatment in Amblyopia Study (MOTAS). Adapted from Stewart (2003).

The lack of a universally-accepted definition of amblyopia inevitably makes data on treatment success from published studies difficult to compare with little agreement on a definition for the treatment success of amblyopia (Clarke et al., 2003; Foley-Nolan et al., 1997; Stewart et al., 2005; Stewart et al., 2004b; Woodruff et al., 1994).

The final visual outcome in the longitudinal phase of this study (Chapter 11) will be reported in separate 3 ways

- Final level of the logMAR score visual acuity in the amblyopic eye.
- Difference in the logMAR score visual acuity after refractive adaptation,and between starting occlusion treatment and final recorded visual acuity when occlusion ceased.
- Proportional improvement criteria as designed by the Monitored Occlusion Treatment Amblyopia Study (MOTAS) group(Stewart et al., 2003).

The reason for using different methods of success evaluation is to ensure that the pattern of results is not unduly influenced by over-reliance on one success index.

3.4 Treatment of Amblyopia

The long-established treatment for amblyopia consists of full correction of any existing refractive error accompanied by occlusion therapy i.e. depriving the better eye of visual input by using a patch (De Buffon, 1743; Worth, 1901) or, less commonly, by optical or pharmaceutical penalisation. This traditional treatment has been supported by the neurophysiologic evidence that in amblyopia, the fellow eye is believed to have established a competitive advantage over the amblyopic eye; thus, in order to overcome this inequity the input to the fellow eye needs to be restricted (Wiesel and Hubel, 1963, 1965).

Prior to commencing occlusion the presence of refractive error should be corrected and in deprivation amblyopia, the cause of the visual deprivation (e.g. ptosis or cataract) needs to be addressed. With the optimum refractive correction in place and the absence of pathology any residual visual deficit is, by definition due to amblyopia. Occlusion of the fellow eye can be carried out by a number of methods:

- Total occlusion: Excluding both form and light, this traditionally takes the form of an occlusive patch. Total occlusion can be prescribed for either full-time or part-time wear, this is generally 6 to 8 hours a day.
- Partial occlusion: Reduces form vision but allows the eye to be stimulated by light. Frosting of the lens by adhesive tape or the use of optical penalisation is used to blur the image in the fellow eye, stimulating the amblyopic eye.
- Pharmacological: Cycloplegic drugs, generally atropine sulphate, are used to blur the vision of the non-amblyopic eye. Since accommodation is temporarily disabled the degree of blurring will restrict the level of acuity. This ensures that the amblyopic eye is likely to be the eye with the clearer vision for near fixation.

A combination of the above options can be used to treat amblyopia but generally total occlusion is the favoured treatment by clinicians (Loudon et al., 2004; Tan et al., 2003) in cases where glasses alone have not treated the amblyopia.

3.4.1 Refractive Correction

Clinically, the conventional treatment of amblyopia combines the correction of refractive error with occlusion therapy, with the occlusion commencing around 6 weeks after the prescription of the optical correction (Awan et al., 2005; Clarke et al., 2003; The Pediatric Eye Disease Investigator, 2003). The full optical correction, generally hypermetropia, is prescribed in order to firstly ensure a clearly focused retinal image and secondly to ensure the correct balance between accommodative effort and convergence (Burian and Von Noorden, 1980). Recent studies however, have provided evidence that correction of the refractive error alone can produce substantial improvement in the level of visual acuity reducing or even negating the requirement for occlusion (Chen et al., 2007; Clarke, 2010; Moseley et al., 1997; Moseley et al., 2002). This improvement in visual acuity from correction of the refractive error alone has been termed 'refractive adaptation' (Moseley et al., 2002). The studies investigating refractive adaptation (Chen et al., 2007; Cotter et al., 2006; Stewart et al., 2004a) demonstrated similar rates of improvement from the wearing of refractive correction alone, with a peak visual acuity recorded at 12 weeks but with some children demonstrating continued improvement up to 18-20 weeks. It has been suggested that the gain in visual acuity could be due to a practice effect, particularly where the testing was carried out on a weekly basis; however, in a similar group of amblyopes tested less frequently the same improvement effect was found (Moseley et al., 2002). Research studies have demonstrated an improvement in visual acuity solely from refractive correction, not only in anisometropic amblyopes but also in strabismic amblyopes, with no

significant difference between the these two types of amblyopia (Clarke et al., 2003; Moseley et al., 2002; Stewart et al., 2004a).

Anisometropic amblyopia is characterised by a substantial difference in refractive error (e.g. 1D or more difference) between the two eyes. Since the accommodation in the two eyes is yoked, the effect of uncorrected anisometropia and the refractive correction is that the two eyes never simultaneously receive a clear image. If the same eye is chronically defocused, there is a belief that this can lead to amblyopia. The exact degree of difference between the two eyes that produces this amblyogenic blur, leading to unilateral amblyopia has however not been identified, although the majority of research studies define anisometropia as a difference of greater than 1 dioptre (DS) between the two eyes. In anisometropic amblyopia the correction of the refractive error will eliminate the retinal blur. In strabismic amblyopia combined with anisometropia or significant ametropia the improvement has been attributed to the correction of the optical component of the amblyopia, suggesting a combined effect from the strabismus and the refractive error, possibly with the anisometropia being the cause of the initial deficit (Moseley et al., 2002). However, it could also be explained by the absence of binocularity in strabismic amblyopes, which would reduce the overall level of visually evoked activity as presented by the BCM model (see Chapter 2) (Bienenstock et al., 1982; Kind et al., 2002; Mitchell et al., 2003).

The theory of competitive interaction introduced by (Hubel, 1963) (discussed in Chapter 2) between the two eyes in amblyopia, is the basis for occlusion therapy. The dominance of this theory has recently come into question with experimental

animal studies demonstrating greater improvement in amblyopic eyes when binocular stimulation is initiated after experimentally- induced amblyopia in comparison to monocular stimulation of the amblyopic eye (Kind et al., 2002; Mitchell et al., 2003). If, as is suggested by these findings, visual recovery is dependent on the absolute level of visual input to an eye rather than the competitive interaction between the eyes, then this could have an impact on future strategies for treating amblyopia in humans. (Kind et al., 2002; Mitchell et al., 2003).

3.4.2 Occlusion Therapy

Evidence for the effectiveness of treatment for amblyopia has increased substantially in the last decade. Following a major review criticising the efficacy, and challenging the effectiveness, of the treatment of amblyopia (Stewart-Brown and Snowdon, 1998) (Powell et al., 2005a; Powell et al., 2005b) a number of research studies designed to evaluate the effectiveness of amblyopia treatment were initiated (Beck and Grp, 2003; Clarke et al., 2003; Pediatric Eye Disease Investigator, 2008; The Pediatric Eye Disease Investigator, 2003). These studies have investigated differing aspects of the treatment of amblyopia, including treatment by refractive correction alone (Moseley et al., 2002), occlusion therapy and the combined effect of both (Williams et al., 2003a). Studies monitoring the dose response of occlusion have demonstrated that there is an optimum amount of occlusion time within which maximum improvement can be achieved (Cleary, 2000; Stewart et al., 2004b; Stewart et al., 2007).The respective roles of treatment by refractive correction and treatment by occlusion therapy have therefore become

more clearly defined over the last few years (Shotton et al., 2008). Prior to this the optical prescription and occlusion therapy were generally instigated together and it was difficult, or impossible, to establish the relative contribution of each.

3.4.3 Occlusion Hours – The dose-response effect

The impact of occlusion on the treatment and outcome of amblyopia has been difficult to assess, particularly with the prescribed dose of occlusion differing significantly between clinical practitioners (Loudon et al., 2004);(Tan et al., 2003) and because of discrepancies between the amount prescribed and the amount actually completed (i.e. problems with compliance). The lack of standardisation in the amount of occlusion prescribed has resulted in occlusion therapy ranging from one hour daily to constant all day occlusion, with the treatment continuing in some cases over a period of years. A study investigating the optimal amount of occlusion required in the treatment of amblyopia monitored both strabismic and mixed amblyopes and reported a dose-response relationship, with the most significant improvement occurring within the first 400 hours of prescribed occlusion and within the first six months of treatment (Cleary, 2000). The study used parental diaries to monitor compliance with the treatment. Research investigating the dose-response effect has been enhanced by the development of a device which provides accurate monitoring of the actual dosage of occlusion. The 'occlusion dose monitor' has been developed over the last 10 years (Fielder et al., 1995; Moseley et al., 1997; Stewart et al., 2002) and used in a number of studies examining the dose-response effect in amblyopia treatment. The Monitored Occlusion Treatment in

Amblyopia Study (MOTAS) group carried out prospective monitoring of occlusion therapy and confirmed a dose-response effect (Stewart et al., 2004b) demonstrating that 82% of the improvement occurred within the first six weeks, with some continuing improvement up to 12 weeks. The study also found that dose rates of 2 hours and 6 hours daily produced the same final outcome, although amblyopes being treated with the higher dose of occlusion achieved this more rapidly. The initial improvement in visual acuity, followed by a plateau is similar to the findings of Hug's retrospective study examining the effect of full-time versus part-time occlusion (Hug, 2004). The "success" criterion of Hug's study (6/9 or better) was achieved within 6 weeks for the group receiving full-time total occlusion, compared to those receiving part-time total occlusion, where success occurred after on average 26 weeks. In a further study by the MOTAS group comparing part-time (6 hours) versus full-time (12 hours) occlusion (Stewart et al., 2007) similar outcomes were found for both groups. The total amount of occlusion hours was, however, very similar in both groups (4.2 hours (part-time) v 6.2 hours (full-time)) and this may account for the final result.

The Paediatric Eye Disease Investigator Group (PEDIG) have carried out a number of large scale multi-centre randomised trials investigating the dose-response of occlusion (Holmes et al., 2003; Pediatric Eye Disease Investigator, 2008; Wallace et al., 2006). In two studies comparing the effect of two hours, six hours and twelve hours occlusion in "moderate" and "severe" amblyopia no difference was found between either of the part-time regimes (2 hours or 6 hours) (Beck and Grp, 2003). This study did not include a period of refractive adaptation

which may have influenced the final outcome, although both groups would have been affected by this. The PEDIG suggest that the actual amount of occlusion prescribed may not have been the amount actually undertaken. This may have affected the groups differently and there is some evidence from the MOTAS study that prescribing greater amounts of occlusion results in a reduction of compliance (Stewart et al., 2007). It may also be possible that there is a limit to the achievable improvement gain, with the initial gain influenced by the amount of occlusion and providing the maximum improvement. Stewart et al (2007) found a plateau of improvement outcome with around 4 hours of daily occlusion over 9 weeks (range 2-26 weeks).

In all the studies investigating the treatment of amblyopia there is however a small proportion of amblyopes who fail to achieve any improvement and it is not known why there is lack of response to treatment (Shotton et al., 2008). In the large-scale investigation of occlusion therapy (The Pediatric Eye Disease Investigator, 2002a), around 15% of children showed no improvement at all after 6 months of therapy and a further 20% of children showed an extremely modest improvement following therapy. In the prospective randomised controlled study by Clarke et al. (2003), over half of those with unilateral acuity impairment at screening received little benefit from treatment. One proposed explanation is that the treatment response is limited by an underlying and undetected abnormality of the visual system, preventing treatment success (Lempert, 2000; Lempert, 2003, 2004, 2008). The research described in this thesis aims to investigate the anatomical integrity of the retinal and disc structure in amblyopia in order to establish if some of those

diagnosed with amblyopia have an underlying, subtle ocular defect. The aim is to either confirm or reject the hypothesis that visual loss in some patients presumed to be amblyopic is due in part to a co-existing structural abnormality.

3.4.4 Compliance

Compliance is crucial to the outcome of amblyopia treatment and has been shown to be one of the most critical factors in predicting visual outcome (Lithander and Sjostrand, 1991). The series of studies monitoring occlusion therapy in amblyopia by both the PEDIG and the MOTAS groups have included measures for monitoring compliance. The PEDIG studies monitored concordance with calendars and the MOTAS studies have utilised the occlusion dose monitors (Stewart et al., 2007; The Pediatric Eye Disease Investigator, 2003). These studies have reported a variation in compliance, comparing the prescribed dose to the received dose, with reduced compliance found in the groups prescribed the greatest amount of occlusion. A study investigating the factors associated with good compliance reported parental fluency in the national language and level of education were the main contributory factors in compliance (Loudon et al., 2006). These factors, however, may be linked to the socio-economic profile of the children presenting with amblyopia who have been shown to have a decreased socio-economic status (Williams et al., 2008). Loudon et al (2006) also noted that the starting level of visual acuity was a predictor of compliance, with poor initial visual acuity resulting in reduced levels of compliance. This is perhaps not surprising since visual acuity is poorer when the fellow eye is covered. The starting level of visual acuity was

also noted to be a significant factor affecting compliance in the MOTAS study, along with age of presentation (Stewart et al., 2004b). Self-reported compliance with occlusion therapy has shown an adherence to prescribed occlusion of 54% (Searle et al., 2002); perhaps surprisingly, levels of compliance were not found to increase significantly using occlusion dose monitors (Stewart et al., 2007) with compliance in the part-time (six hour) group being 66% and that of the full-time (12 hour) group being 50%. Occlusion diaries operate in a similar way to the calendar system used by the PEDIG studies, with the amount of occlusion being documented by the parent/guardian on a daily basis. A diary system has been compared to occlusion dose monitoring and been found to compare well with a good correlation between the two systems, despite some issues over legibility of handwriting (Fielder et al., 1995).

3.4.5 Pharmacologic Penalisation

Pharmacological penalisation of the fellow eye in the treatment of amblyopia has provided an alternative to occlusion therapy over the last century. Atropine sulphate is a long acting topical drug that both induces cycloplegia and prevents accommodation by temporarily paralysing the ciliary muscle, stopping the lens from changing shape in response to a near accommodative stimuli (Elkington et al., 1999). The overall effect is to blur the vision of the fellow eye, therefore biasing the image quality at near in favour of the amblyopic eye. Atropine penalisation can be used in isolation or used in combination with optical penalisation, when the strength of the hypermetropic correction required by the fellow eye is altered

effectively blurring the vision for both near and distance fixation (Foley-Nolan et al., 1997).(Repka et al., 2005) Clinical practitioners have tended to use atropine as a second line of treatment when conventional occlusion therapy has failed, mainly due to the risks presented by the use of atropine sulphate; it's potential toxicity and the risk of reverse amblyopia occurring in the fellow eye (Hainline et al., 2009). Reverse amblyopia is most likely to occur when the atropine is continued over a protracted period of time without the visual acuity being measured accurately. This has been shown to arise mainly when patients fail to attend their follow-up appointments and in children of a young age (Hainline et al., 2009; Simons et al., 1997).

The concentration of atropine sulphate is generally 1% for children over 1 year (0.5% for children younger than 1 year). The regime for the prescription does, however, vary. In two studies atropine sulphate 1% was prescribed once daily (Foley-Nolan 1997 and PEDIG 2002) and in another study it was prescribed twice weekly during active treatment and once weekly for maintenance therapy. A further study by the PEDIG (Repka et al., 2009a) investigating the prescription regime of atropine demonstrated that atropine used on two consecutive days (weekend) produced a similar result to the improvement of atropine used on a daily basis in a group of moderate amblyopes (0.3 to 0.6 logMAR) aged between 3 and 7 years. This is not surprising as the cycoplegic effect from the atropine sulphate continues for approximately 7 days; therefore a daily prescription should not be necessary. A comparison of the visual outcome of amblyopes treated by traditional occlusion therapy versus a group of amblyopes treated by atropine penalisation reported that

after periods of six months and twenty-four months of treatment, both groups had improved and there was no significant difference between the groups (The Pediatric Eye Disease Investigator, 2002b). This parity of improvement was found to be maintained over long term follow-up (Pediatric Eye Disease Investigator, 2008).

Similar findings were reported by Foley-Nolan (1997) who found no significant difference between two groups of amblyopes one of which was treated with conventional occlusion and the other with atropine penalisation. This study did not, however, use a standardised protocol with differing regimes of occlusion being prescribed, differing methods of measuring final visual acuity and the final visual acuity being recorded at differing time points. This makes it difficult to directly compare the results with the PEDIG studies (Pediatric Eye Disease Investigator, 2008; The Pediatric Eye Disease Investigator, 2002b, 2005).

Reported compliance with the use of atropine penalisation has been consistently good, with 49% of cases recorded as having good compliance in the occlusion arm of the PEDIG (2002) study and 78% of compliance in the atropine penalisation group. Foley-Nolan reported 55% compliance in their occlusion group in comparison to their atropine penalisation group who were reported to have 94% compliance. As discussed previously, compliance with the treatment for amblyopia is a significant factor in its treatment efficacy (Lithander and Sjostrand, 1991).

One of the factors for atropine penalisation not being the primary treatment of choice is the side effects and in particular the impact of reverse amblyopia that may occur. In the PEDIG (2002) study of the 204 participants receiving atropine

penalisation 47 were found to have a reduction of visual acuity in the penalised eye, with one child requiring active treatment to improve the vision in this eye. This compares with the 215 receiving traditional occlusion, of whom 17 children had a reduced vision in the fellow eye, although none required further treatment with visual acuity subsequently improving. Tejedor, 2008 reported one case of reverse amblyopia in their atropine penalisation group (1/35) (Tejedor and Ogallar, 2008). In a comparative study of atropine penalisation with optical penalisation (Tejedor and Ogallar, 2008) both groups demonstrated an improvement in comparison to their base line measured visual acuity, however, the authors do not report the difference between the two groups. In a Cochrane review the findings of this and other studies were reviewed and the group treated with atropine penalisation were found to have a greater improvement (Li and Shotton, 2009).

Thus atropine penalisation appears to be as effective as conventional occlusion therapy, has been shown to produce few side effects and provides improved compliance with the treatment regime. There is, therefore, no reason why atropine could not be used as the primary treatment of choice when managing amblyopia.

There has been a considerable body of evidence provided by studies taking up the challenge of the clinical reviews of amblyopia (Powell et al., 2005a; Powell et al., 2005b; Stewart-Brown and Snowdon, 1998) and it would seem that there is now strong evidence available demonstrating that amblyopia can be treated successfully. The current literature provides practitioners with guidance on the time span for refractive adaptation (Awan et al., 2005; Moseley et al., 2002; Steele et al., 2006), dose of occlusion (Cleary, 2000; Stewart et al., 2005; Stewart et al., 2007),

and guidance on the level of acuity at which to commence treatment (Clarke et al., 2003; Group, 2003). The criteria for the longitudinal phase of this research study investigating the structural integrity of the retina on amblyopia have been based upon this body of recently published literature.

Chapter 4. Retinal Imaging

4.1 Introduction

The ocular imaging technique to be used in this study, investigating the retinal structure in amblyopes, is Optical Coherence Tomography (OCT). This advanced technology will be used to determine retinal nerve fibre layer thickness and evaluate macular, retinal and optic nerve head structure. It is therefore fundamental to the study that there is understanding of the instrumentation, the basic principles of image acquisition and data processing as well as recognition of the techniques limitations. The aim of this chapter is to out-line the process of OCT and provide information on its basic principles and limitations.

4.2 Optical Coherence Tomography (OCT)

Optical Coherence Tomography (OCT) allows the visualisation of structures that have limited light absorption and that reflect light with minimal scatter. It is an examination technique that is non-contact and non-invasive making it an attractive method of assessment. OCT has been used in a diverse number of medical and surgical specialties; cardiology where it has been used to provide detailed images of vessel walls, in particular it has proved useful in the investigation of small vessels previously problematic to image with computed tomography (CT) (Coxson et al., 2008; Gerckens et al., 2003; Gonzalo et al., 2009) ; oncology where it is

difficult to observe the growth and development of micron size tumours (Evans et al., 2009) and gastroenterology where using a catheter probe epithelial structure of the gastrointestinal tract can be imaged aiding diagnostic accuracy (Testoni, 2007). The greatest development of OCT however has been in the field of ophthalmology. The reason for the technological advance in the ophthalmic arena is that the eye and its media are fundamentally transparent, with the retinal layers being ordered in a stratified fashion (see Chapter 1.1). This ocular arrangement produces minimal scattering of light, allowing good axial image resolution from OCT techniques (Drexler, 2007) and produces an in vivo image of the retina closely resembling histological sections (Blumenthal et al., 2009; Drexler and Fujimoto, 2008).

The development of OCT which utilises the properties of light, and the differing characteristics of retinal tissue to produce high resolution, tomographic cross sections, has allowed detailed investigation into retinal structure (Huang et al., 1991). OCT therefore provides a non-invasive method of ocular imaging and its routine use in clinical practice has developed exponentially over the past few years. It is utilised clinically, to detect and measure changes in macular thickness and evaluate both qualitatively and quantitatively the thickness of the nerve fibre layer around the optic disc in glaucoma (Chen and Lee, 2007; Sakata et al., 2009) providing detailed information about retinal architecture and associated disease processes.

OCT was first introduced into ophthalmic practice in the form of Time Domain OCT (Huang et al., 1991). Time Domain OCT has been and continues to be, the main

type of OCT utilised in clinical practice. The technique has been gradually developed and updated, with three generations of OCT's having been introduced into practice. The main 3rd generation Time Domain OCT in current use is the Stratus OCT (Carl Zeiss Meditec). OCT technology has developed rapidly and most recently the Fourier Domain/ Spectral Domain OCT is being introduced into ophthalmic practice. The initial pioneering studies using OCT to establish retinal morphology have been with Time Domain OCT and research using Fourier Domain OCT is only beginning to appear in the literature. It is therefore important to this research to describe and discuss both techniques. The principles of both Time Domain and Fourier Domain OCT will therefore be covered in this chapter.

4.2.1 Time Domain OCT

Standard OCT, also described as Time Domain OCT e.g. Stratus OCT (Carl Zeiss Meditec), operates by measuring the time delay of light reflected back from the retinal layers (Figure 4.1). The measurement of the echo reflectivity versus depth is known as an axial scan (A-scan) and consecutive A-scans set side by side together produce a two-dimensional B-scan (Costa et al., 2006) (Figure 4.2). Acquiring approximately 400 axial scans per second, a standard 512 A-scan OCT image is obtained in around 1.3 seconds (Wojtkowski et al., 2005).
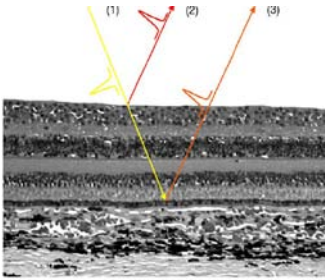
Figure 4.1: OCT beam (1) scanning across the retina. The delay of a superficial reflection (2) is shorter than that of a deeper reflection (3).From (Huang, 2006).
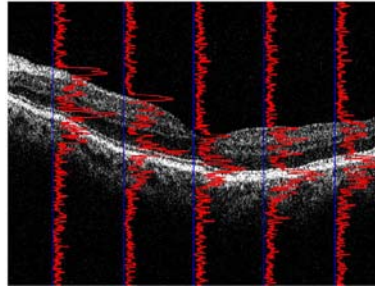
Figure 4.2: OCT B-scan (gray-scale image) produced from multiple A-scans (red lines) set side by side. From (Huang, 2006).

Time Domain OCT employs the optical principles of interferometry and coherence in order to produce tomographic images on a micron scale. The light source utilised in OCT imaging is generally a near infra-red light source, this low coherent light source encompasses a wide range of wavelengths (800nm - 1400 nm), producing the optimum balance between light scatter and light absorption created by the ocular media (Van Velthoven et al., 2007). In order to obtain micron scale imaging the wavelength of the light source must produce minimal scatter and have minimal absorption. In most morphological tissues scatter increases with decreasing wavelength and absorption occurs between 200-600 nm by haemoglobin and above 1000 nm by water (Van Velthoven et al., 2007). Therefore, in general the majority of OCT technology uses a super luminescent diode (SLD) source of emitting light, bandwidth 20 – 30nm centred around a wavelength of

830nm (Figure 4.3) this produces an axial image resolution of approximately 10 µm (Drexler and Fujimoto, 2008).
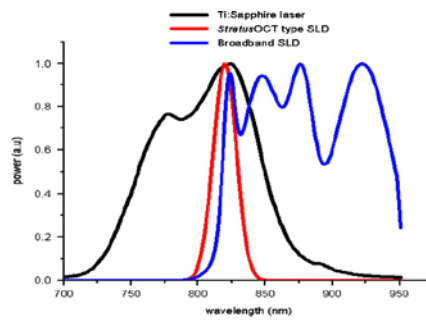
Figure 4.3 Spectral bandwidth profiles of the light sources currently used in Optical Coherence Tomography imaging. From (Van Velthoven et al., 2007)

4.2.2 Interferometry

In contrast to sound waves the rapid speed of light (3×10^8 m/s) prevents the direct measurement of reflected light in the same way as ultrasound is captured, therefore in the standard OCT system a Michelson interferometer is employed (Costa et al., 2006; Huang, 2006; Van Velthoven et al., 2007). Interferometry measures the effect of combining two light waves; this is achieved in OCT by

comparing the delays of sample reflections with reference reflections of known delay.

Characteristically in Time Domain OCT a Michelson interferometer is employed to measure the light reflected from the retinal surfaces. Within the interferometer the originating super luminescent diode (SLD) light source is split into a reference and a measurement beam, the measurement beam having traversed the eye and the reference beam having travelled a known path length are recombined in the interferometer producing an interference signal attributable to the summation of the two wave patterns (Figure 4.4).

The differential between the echo time delay of the reflected light from the reference beam and the measurement beam allows the distance (thickness) and reflectivity of the intraocular microstructures to be measured in detail to approximately 10 μm (Medeiros et al., 2004).The distance travelled by each of the multiple echoes is calculated by continually varying the position of the reference mirror.
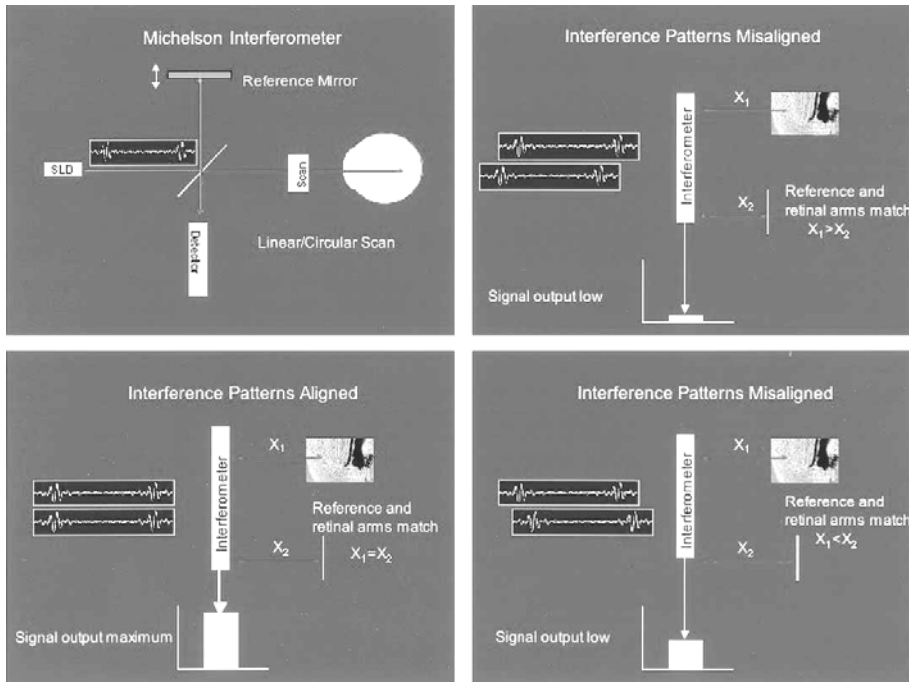
Figure 4.4: Configuration of the Michelson interferometer.
(Top left) The reference mirror is moved in and out to match the signal returning from the imaged area of the retina.
(Top right) When the reference and retinal measurement arms (X1 > X2) are not matched, the interference patterns are not aligned, and the returned signal is low.
(Bottom left) When the distance between the reference and retinal measurement arms (X1 = X2) are matched, the interference patterns are aligned, and the return signal is at a maximum, this represents the measurement detected by the instrument.
(Bottom right) When the reference mirror is moved further, the retinal arm is longer than the reference length X1 < X2, the interference patterns are not aligned, and the return signal is again low. Reproduced from (Jaffe and Caprioli, 2004).

4.2.3 Coherence

The combination of the interference signals, across a range of wavelengths, combines to produce a wave pulse (Figure 4.5). At the point where the wave forms match the interference signals are lined up peak to peak and trough to trough in a coherent fashion, producing large peaks and troughs (interferometric modulation). When the wave forms are mismatched and the peaks and troughs are not lined up, the interference pattern adds up to a flat line. This summed interference pattern is known as a wave pulse. The width of this pulse is the coherence length and it is the coherence length that determines the axial resolution of the OCT system (Costa et al., 2006; Huang, 2006). A monochromatic light source (single wavelength) has a broad coherence length producing interference fringes over a large range of path length differences. A low coherent light source such as that used in OCT, with a wide range of wavelengths will produce interference fringes over a small range of path length differences leading to a small coherence length and subsequently a micron scale axial resolution (Huang et al., 1991; Van Velthoven et al., 2007). With a broad spectral bandwidth the coherence length/ axial resolution is typically between 20 μm and 1μm. The axial resolution, determined by the coherence length (l_c) is inversely proportional to the wavelength range (spectral bandwidth- Δλ) (Van Velthoven et al., 2007).

Transverse resolution is determined by the focused spot size of the light source, with OCT the light beam is generally 1-2 mm, producing a transverse resolution of ~ 20μm (Drexler and Fujimoto, 2008).
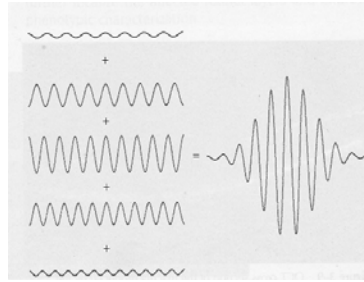
Figure 4.5: Combined interference signals from a range of wavelengths (left) produces a wave pulse (right). The width of the pulse determines the axial resolution of the OCT. From (Huang, 2006).

4.2.4 Performance

There are several factors that can affect the sensitivity of OCT imaging, light absorption, light scatter, speckle and motion artefacts can all affect the image quality. The performance of an OCT system is defined by the signal to noise ratio (SNR). This is influenced by the signal amplitude and the noise produced by the system, it is measured in decibels (dB) and can be calculated by the formula

$$\text{SNR [dB]} = 20 \,.^{10}\log \frac{\text{Signal}}{\text{noise}_{sd}}$$

The lower the noise level the higher the level of performance. Noise is produced from the internal processing of the OCT system and should be kept to a minimum in order to ensure optimal performance (Hee et al., 1995; Van Velthoven et al., 2007).

4.2.5 Speckle

Speckle noise reduces OCT image quality creating a grainy appearance and reduces the accuracy of the segmentation algorithms (Adler et al., 2004). Speckle is a fundamental characteristic of a light source with low coherence (Schmitt et al., 1999). It is by created by the presence of tiny particles in the imaged tissue which lead to interference when the reflected light from the retinal layers meet the light from the reference beam. The spot size of the light source and the axial resolution of the system determine the scale of the speckle, therefore ultra high resolution (UHR) OCT systems produce less speckle than time domain OCT systems due to their reduced axial resolution (Drexler and Fujimoto, 2008; Van Velthoven et al., 2007).

4.2.6 Scatter

Ocular tissue, although virtually transparent, still causes a diffuse light distribution. The OCT image quality can be significantly reduced by this light scatter within the intraocular media. Clinically the presence of lens opacities is common and leads to a diminished OCT beam, reducing the signal and degrading the images (Drexler and Fujimoto, 2008). The scatter caused by lens opacities is determined by the wavelength of the light source; scatter decreasing with increase in wavelength. Scatter is also affected by the density of the opacity, increasing with the increasing density of the opacity. The use of a light source of a longer wavelength (1050 nm) has been shown to improve the image quality but requires adaptation of the OCT

technology to allow capture of the image; this is currently at the research stage (Povazay et al., 2007).

4.2.7 Motion Artefacts

OCT imaging is always subject to involuntary eye movement during the scanning process. Although cross section B-scans can now be imaged in milliseconds, the construction of a full 3D retinal scan taking several seconds can be affected by motion artefacts. In observers with normal levels of visual acuity and good fixation involuntary microsaccades with amplitudes of several hundred microns occur; this is larger than the transverse image resolution of the first, second and third generation OCT systems and affects image quality (Hammer et al., 2005b). In order to address this concern retinal tracking devices have been devised and are now being integrated into OCT technology (Hammer et al., 2005a). Retinal tracking devises have a secondary sensing beam that locks on to common fundus features, detecting transverse eye movement and repositions the OCT beam to fixed retinal coordinates leading to improvement in image quality (Ferguson et al., 2004; Hammer et al., 2005a).

4.2.8 Imaging Protocols

With time domain OCT systems, such as the Stratus OCT, specific imaging protocols are used for the thickness measurements of the macula, retinal nerve fibre layer (RNFL) and optic disc parameters (Hee et al., 2004). The image

acquired of the macula is obtained by 6 radial scans spaced at 30⁰ apart. Standard

OCT utilises a system that interpolates the measurements between the scan lines,

however this may lead to crucial information being missed (Wojtkowski et al., 2005)

(Figure 4.6). The optic disc parameters are measured in the same way with 6 radial

scans centred over the optic disc; the retinal nerve fibre layer (RNFL) thickness

around the optic nerve head is measured by three repeated circumpapillary scans

around the optic disc.
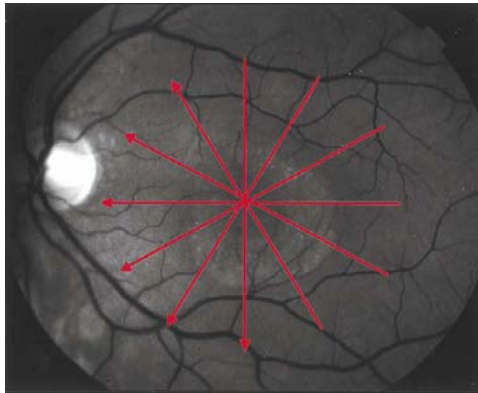
Figure 4.6: Orientation, location of six radial scans obtained with retinal thickness and fast macular thickness mapping program used for Time Domain OCT. Reproduced from (Jaffe and Caprioli, 2004).

Studies have demonstrated the reproducibility of the first (Blumenthal et al., 2000), second and third generation OCT (Stratus OCT, Carl Zeiss Meditec, Dublin, CA) instruments (Budenz et al., 2005; Paunescu et al., 2004; Polito et al., 2005). These time domain OCT studies have found good repeatability and reproducibility of measurements for both imaging of the macula and the retinal nerve fibre layer (RNFL) around the optic nerve head(Paunescu et al., 2004; Polito et al., 2005) Paunescu et al. (2004) reported an interclass correlation coefficient (ICC) of 94% for high-density (512 A-scans per image) macular scans, with no significant difference after dilation using the Stratus OCT-3.

The Stratus OCT has been shown to produce repeatable measurements (Paunescu et al., 2004) but it has also been criticised for the inconsistencies that its automatic detection software can produce (Costa et al., 2004; Sadda et al., 2006). The OCT detects the inner and outer layers of the retina and the retinal nerve fibre layer and bases the retinal thickness measurements upon these structures (Fernandez et al., 2005). The retinal thickness is determined by the OCT identifying both the internal limiting membrane and the retinal pigment epithelium (RPE). The distance between these two layers is used to calculate the retinal thickness. Studies using the Stratus OCT have shown that imaging of the retina detects two highly reflective layers in the outer retina, these are believed to correspond to the inner and outer segment junction of the photoreceptors (inner reflective layer) and the thicker retinal pigment epithelium (outer reflective layer) (Costa et al., 2004; Pons and Garcia-Valenzuela, 2005). Pons and Garcia-

Valenzuela (2005) are critical of the Stratus OCT software analysis due to its use of the inner reflective layer (photoreceptor junction) in retinal thickness measurement and analysis, leading to an underestimation of total retinal thickness. This requires consideration particularly as the use of differing borders for measurement will lead to differences in the retinal thickness measurements between studies. Depending on which layers have been used for measurement, this may lead to differing studies producing contradictory normative data regarding retinal thickness. In the presence of macular disease where the inner layer becomes indiscernible and the OCT reverts to utilising the outer reflective layer in the calculation of its measurements, this will also lead to inconsistencies. Some authors suggest that as the inner layer is constantly used as the retinal boundary across the entire scan it cannot be seen as an error (Sadda et al., 2006). This may be acceptable in clinical practice where patients are being monitored regularly with the same technology and only changes in the retinal structure are being considered. However, it is not acceptable in research studies where measurements in retinal structure are being used to define a normative range with which to compare to. The retinal boundary used for measurement in this case must therefore be taken into account when comparing the measurement results of differing modalities of OCT. The 3D OCT-1000 (Topcon, Tokyo, Japan) used in the present research defines the outer retinal border as that above the retinal pigment epithelium. This will result in an increase in the total retinal thickness measurement in comparison with the Stratus OCT, which defines the border as the junction

113

between the outer and inner segments of the photoreceptors (Menke et al., 2008)

(Figure 4.7).
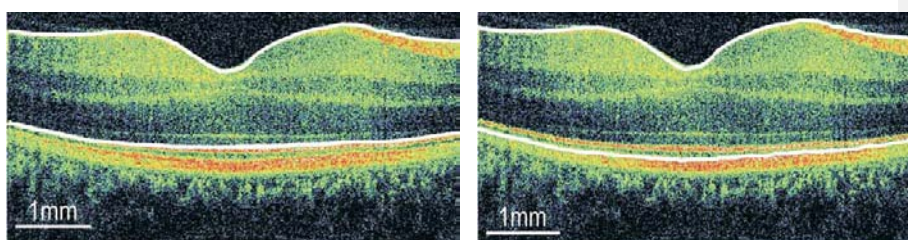
Figure 4.7: Colour B-scan of normal retina **A**. Showing 2 white algorithmic lines placed automatically by the Stratus OCT thickness analyser program. The outer white line is placed above the inner segment /outer segment of the photoreceptor layer. **B**. Fourier Domain OCT scan showing the outer white line placed above the retinal pigment epithelium (RPE) layer resulting in an increase of total retinal thickness. Reproduced from (Wojtkowski et al., 2005).

OCT technology is rapidly developing with the introduction of ultrahigh-resolution OCT improving the digital image axial resolution from 10-15 µm to 3µm (Drexler and Fujimoto, 2008). Ultrahigh-resolution OCT allows an exceptionally detailed image of the intra-retinal structures to be captured, providing visualisation of the ganglion cell layer (GCL), photoreceptors detailing both the inner and outer segments and retinal pigment epithelium (RPE) (Ko et al., 2004).This enhancement in the detail of the image is produced by a modification in the band-width of the light source, the axial resolution in OCT images being determined by the band-width of the coherent light source. Ultrahigh-resolution OCT utilises laser

light with up to 165nm band-width producing axial images of 3μm axial resolution. The limiting factor in achieving maximal sensitivity retinal imaging is the degree of retinal exposure to the broadband laser illumination. Ultrahigh-resolution OCT utilises the maximum recommended broadband width (Drexler et al., 2003). A number of studies have demonstrated the improved visualisation of intra-retinal morphology using ultra-high resolution OCT highlighting the potential for this technique in contributing to improved clinical diagnosis and management of retinal disease (Drexler et al., 2003; Ergun et al., 2005; Ko et al., 2004). However, the use of ultra-high resolution OCT combined with the standard echo time delay capturing system is slow since only around 150 to 250 axial scans per second can be acquired (Ko et al., 2004) this can lead to motion artefacts in the retinal images (Wojtkowski et al., 2005). To counteract this specialised protocols have been developed to improve the image quality obtained from standard OCT (Fernandez et al., 2005). Recent development of ultrahigh-resolution OCT combined with Fourier domain/ spectral detection techniques has lead to dramatic improvements in both image quality and speed of acquisition (Wojtkowski et al., 2004).

4.3 Fourier Domain OCT / Spectral Domain OCT (3D OCT)

Fourier Domain OCT, also known as Spectral Domain OCT was first developed by Wojtkowski in 2002 (Wojtkowski et al., 2002). In Fourier domain OCT the interferometer is replaced by a spectrometer, the reference mirror is static and the OCT echoes reflected from differing axial positions are obtained simultaneously rather than sequentially and interpreted by comparing the complete spectrum of

the reflected interference pattern returned from the retina in the measurement arm to the light from the stationary reference arm (Figure 4.8). The echo time delay of the reflected light from the retina back to the spectrometer is mathematically extracted using Fourier transform calculations that utilize the frequency spectrum of the OCT signal to transform the signal to a numerical measurement thus calculating the quantitative retinal depth information (Chen and Lee, 2007; Nassif et al., 2004).

The information obtained by a single detector element in a spectrometer is equivalent to an A-scan but provides a significant advantage in speed due to the simultaneous detection of reflected light over a range of depths and a significant improvement in image quality due to the reduction in motion artefacts (Huang, 2006).
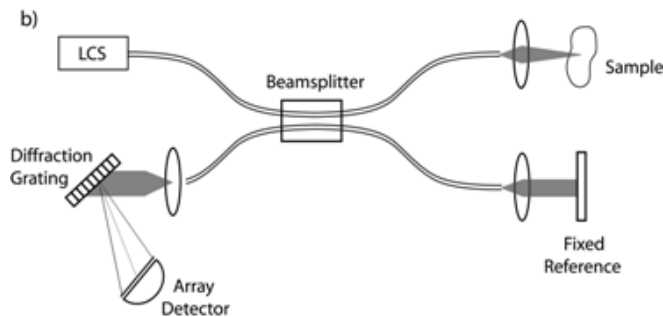
Figure 4.8: Schematic diagram of Fourier Domain OCT. A diffraction grating and array detector act as a spectrometer measuring spectral modulations produced by interference between the measurement sample and the reference beam.

116

In combination with the introduction of the spectrometer and Fourier transform the introduction of a raster scan technique provides Fourier Domain OCT with an improved scan coverage and resolution. The raster scan pattern allows the acquisition of highly detailed scans, acquiring consecutive A-scans at equally spaced lateral intervals imaged sequentially over a rectangular grid (Figure 4.9). This system has the advantage over the standard OCT system of radial scans (Figure 3.6) as it measures an increased number of transverse points and negates the requirement for the interpolation of data between measurements, reducing the odds of focal pathology being missed (Wojtkowski et al., 2005).

A.

B.

D.

C.
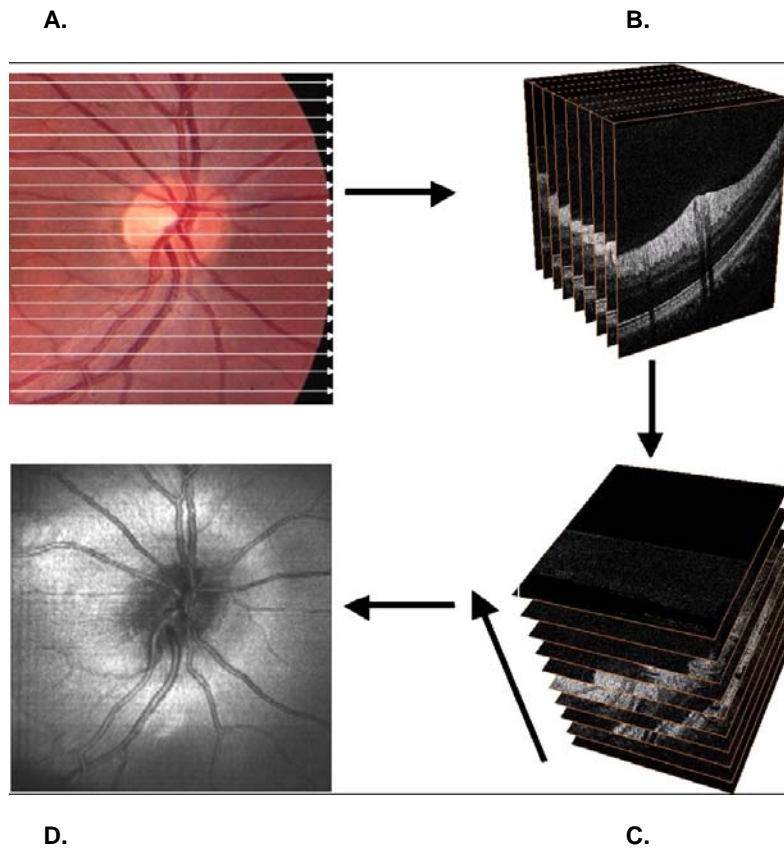
Figure 4.9: Raster scanning and post-processing protocols of 3D OCT.Several planes (B-scans) of a whole retinal volume can be scanned (**A**), resulting in a stack of adjacent B-scans (**B**). The acquired data can be summed along the axial direction (**C**) to generate an OCT fundus image (**D**) similar to the one obtained by standard fundus photography. This OCT fundus image is generated by summing the A-scan signal along the axial direction, thereby resulting in a brightness pixel value for each axial scan. Adapted from (Wojtkowski et al., 2005).

118

Fourier domain OCT provides an OCT image of considerably increased resolution, combined with a significantly reduced retinal image acquisition time. Fourier domain OCT allows the collection of high density volumetric data of the retina, producing 3-dimensional (3D) OCT data and providing comprehensive intra-retinal structure images and measurements (Figure 4.10).

With the continuing development of OCT in areas such as adaptive optics, polarisation, Doppler OCT and optophysiology (OCT combined with electrodiagnostic testing) the implication for the development of OCT techniques on clinical detection and management of ophthalmic disease is considerable (Drexler and Fujimoto, 2008; Van Velthoven et al., 2007).
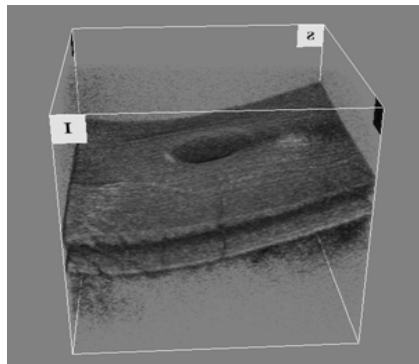
Figure 4.10: Example of a 3D OCT Macula Scan imaged by the Topcon 3D OCT-1000. 6x6 mm (256 x 256 A-scans).

4.4 Retinal Imaging and Amblyopia

Amblyopia, a condition of defective visual function, despite optimal optical correction and the absence of any overt pathology has remained an elusive condition (Chapter 2). The current consensus of opinion regarding the aetiology of amblyopia is that the primary sites of anatomical change and area of reduced function are in the visual cortex and lateral geniculate nucleus (Blakemore and Vitaldurand, 1986; Hess, 2001; Hess et al., 2009; Hubel and Wiesel, 1998; Mendola et al., 2005).Retinal involvement in amblyopia has long been controversial (Cleland et al., 1982; Hess, 2001; Ikeda and Tremain, 1979) (Chapter 2). Recent studies (Lempert, 2000; Lempert, 2003, 2008) have presented data suggesting that a difference exists in the retinal structure of amblyopic eyes. Lempert (2003) found a significant reduction in disc size in hypermetropic and strabismic eyes in comparison to eyes without amblyopia or strabismus, signifying retinal involvement as a factor in amblyopia. These findings have an implication for the aetiology of amblyopia, and in particular the hypothesis generated i.e. that amblyopia may have an underlying but undetected structural defect. Indeed, if amblyopia is caused by the presence of a subtle structural abnormality its very existence, as it is currently defined, is in question. The coincidence of the development of imaging technology and the continued questioning of the aetiology and development of amblyopia has been the catalyst for a small number of studies to reconsider the hypothesis of retinal involvement in amblyopia. Investigators have begun to examine retinal topography; measuring the optic disc dimensions, the thickness of the retinal nerve

120

fibre layer and macular thickness in amblyopic eyes (Baddini-Caramelli et al., 2001; Rabbione et al., 2004; Repka et al., 2006; Yen et al., 2004). These studies have used a variety of methodologies, Optical Coherence Topography (OCT), Scanning Laser Ophthalmoscopy (SLO), Scanning Laser Polarimetry (SLP) and retinal imaging using digital photography. The studies not only utilise a variety of techniques, they sample different retinal sites, include different types of amblyopia, and also measure different levels of amblyopia. It is therefore perhaps not surprising that the findings from the research studies are variable.

The development of the different imaging techniques, to obtain *in vivo* retinal measurements, has allowed further detailed investigation into the retinal status of amblyopic eyes. Since Lemperts' initial study (Lempert, 2000) using digital imaging photography two main techniques have been utilised to image the retinal nerve fibre layer of amblyopes, Optical Coherence Tomography (OCT) and Scanning Laser Polarimetry (SLP) using the GDx.

4.5 Imaging Retinal Structure - Scanning Laser Polarimetry

Scanning Laser Polarimetry (SLP) has not been employed as an imaging technique in this research. However, in order to understand and interpret the findings of the studies that used this technique investigating retinal structure, it is appropriate to briefly review the technology used. The majority of studies using the technique of Scanning Laser Polarimetry (SLP) utilise the GDx nerve fibre analyser with variable corneal compensator (VCC) system (Carl Zeiss Meditec). Polarised light is transmitted into the eye by scanning the beam of an infrared laser in a

raster pattern. The polariser separates the light beam into horizontal and vertical

wave components. This system exploits the birefringence properties of the retinal

nerve fibre layer which cause a change in the polarisation of the light beam

(retardation). The light waves travelling parallel to the retinal nerve fibre layer pass

through relatively undisturbed, whereas the waves travelling perpendicular to the

retinal nerve fibre layer are impeded; this impedance between the wave

components is known as retardation. The GDx measures the retardation of the

light reflected back from the parallel retinal nerve fibre layer fibres and provides an

estimate of retinal nerve fibre layer thickness in the peripapillary area (Huang, 2006)

(Figure 4.11).
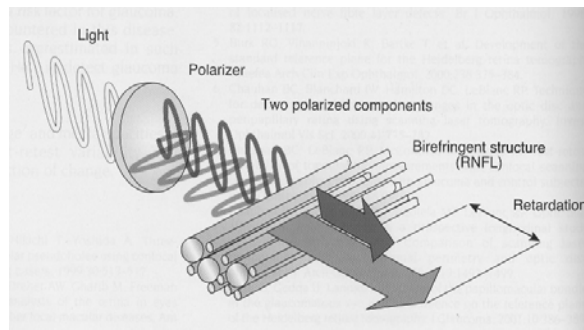
Figure 4.11: Retardation of polarised light passing through a
birefringent structure (RNFL). From Huang (2006).

The GDx was primarily designed for investigating glaucoma; the systems

parameters having been designed to detect retinal nerve fibre loss and monitor

change around the optic disc (Weinreb et al., 1998). A print out is produced

depicting the area of the retinal nerve fibre layer scanned around the optic disc

along with a fundus image (Figure 4.12). The images are colour coded to indicate

the degree of thickness, based on a comparison of the subjects results evaluated

against a normative database (approx 500 eyes) (Medeiros et al., 2004). The

printed output compares the right and left eyes. Subsequent images can be

compared and progression monitored.
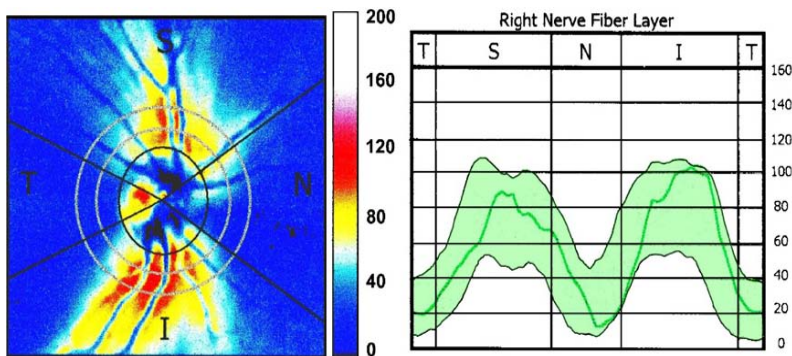
Figure 4.12: Example of a scan imaged by polarization-sensitive technology; performed by GDX VCC. RNFL thickness map (left) and circumpapillary RNFL thickness measurements (right). Adapted from Wojtkowski et al. (2005).

Within the human optical system not only does the retinal nerve fibre layer have

birefringence properties, but the cornea also has birefringence properties. The

original version of the GDx employed a fixed corneal compensation system

(Weinreb et al., 1998) which lead to the reporting of a wide variation in the retinal nerve fibre layer (RNFL) thickness among healthy individuals and an overlap between healthy and glaucomatous groups.

A wide variation in corneal birefringence has since been demonstrated (Greenfield et al., 2002; Weinreb et al., 2002) and in order to minimise the confounding effects from the cornea the GDx has been developed from a fixed corneal compensation system to a variable corneal compensation system. This development has resulted in an improvement in the diagnostic accuracy of the GDx measurements when used to identify the presence of glaucoma (Weinreb et al., 2003).

With the variable corneal compensation system a polarised image of the macula is initially measured. The macula is imaged as it contains no retinal ganglion cell axons and is not affected by polarisation; this image represents the combined polarising effect from the cornea, lens and the fibres of Henlé. An image is then taken of the circumpapillary retinal nerve fibre layer, the final measurement value is produced having subtracted out the initial macula data (Katsanos et al., 2004). In all the imaging studies of amblyopic eyes where Scanning Laser Polarimetry (SLP) has been utilised the GDx VCC was the instrument of choice (Baddini-Caramelli et al., 2001; Bozkurt et al., 2003; Colen et al., 2000).The GDx VCC system is designed only to image the optic disc area and does not provide the facility to image and measure the macular area of the retina, therefore all studies investigating amblyopia using the GDx VCC measure the retinal nerve fibre layer (RNFL) around the optic disc.

4.6 Imaging Retinal Structure - Optical Coherence Tomography (OCT)

The main imaging system to date used in studies of retinal structure in amblyopia is time domain OCT. Two measurement strategies are typically used, the circular scan and the radial scan. The circular scan measures a 360° papillary area around the optic disc evaluating the nerve fibres from the retina entering the optic nerve and providing topographic measurements of retinal nerve fibre layer (RNFL) thickness. The thickness of the retinal nerve fibre layer (RNFL) is compared to the OCT's normative database (328 eyes) (Medeiros et al., 2004) and a graph is presented of the thickness measurement in comparison to the normative data. The circular scan of the optic nerve head utilises a fixed diameter scan of 3.4 mm. Retinal nerve fibre layer thickness decreases away from the optic nerve head (Conradi and Sjostrand, 1993) therefore the utilisation of a fixed diameter scan may lead to an overestimation of the retinal nerve fibre layer thickness in the presence of a large optic disc, as the retina will be measured closer to the disc edge (Savini et al., 2005).

The radial scan strategy of the OCT can be used to measure the thickness area and volume of the macula (Figure 4.7) or the area and volume of the optic disc, producing a topographical thickness map and a comparison between both eyes. A small number of studies have chosen to image the macular area due to the lower individual variability in comparison to the increased variability of the optic disc (Altintas et al., 2005; Jonas et al., 1999).

4.7 The Published Research of Philip Lempert

Lempert (Lempert, 2000) was one of the first investigators to image the retinal structure of amblyopes, using digital photography. In particular he studied the size of the optic disc demonstrating a degree of optic disc hypoplasia. His studies suggest that a subtle organic cause exists in amblyopic eyes, mainly those that have failed to show an improvement in visual acuity despite compliance with treatment.

Lempert's initial study(Lempert, 2000) was however criticised for not taking into account the refractive error of the participants, in particular the level of hypermetropia present. The presence of hypermetropia which will be reflected in the smaller size of an eye is likely to be a confounding factor with the potential to influence the measurement of the disc size (Archer, 2000).In order to address this criticism the method of measuring disc size was altered in subsequent research. In the follow-up study (Lempert, 2003) relative disc size is reported as an axial-length to disc area ratio (AXL/DA). This indicator was chosen to provide a more accurate assessment of disproportionate reduction in disc size.

In amblyopes the presence of small disc size could be the result of hypermetropia, influencing the condition and confounding the result. Lempert (2003) suggests that the axial-length to disc area ratio amongst the general population is 8.66 to 9.5 mm^{-1}. However, this normative range of data is derived from a number of differing studies, measuring subjects of different ages and including ophthalmic conditions such as glaucoma and cataract. A recent study measuring the optic disc area in a group of adolescents has demonstrated a significant variability in the size of the

optic disc area in the normal population, the disc area varying by over 100%
(Figure 4.13) (Huynh et al., 2008). Using the measurements from Lempert's study
(Lempert, 2003), both normals and amblyopes would fit into this normative
distribution, with the mean disc area of the normative group measuring 2.57mm^2
and the amblyopes on the edge of the normative curve at 1.55 mm^2.
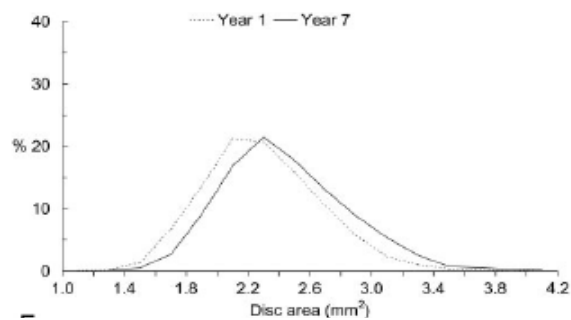
Figure 4.13: Comparative distribution of Optic Disc Area (mm^2) for two
groups of school children, year 1 (6 years of age) and year 7 (12 years of
age). Adapted from Huynh et al 2008.

As a result of the findings of the 2003 study suggesting that the disc area is
reduced in amblyopic eyes, (Lempert, 2003) Lempert states that :

*"A paucity of nerve fibres may be a factor in the explanation for decreased
visual acuity in amblyopic eyes."*

The theory suggested by Lempert (Lempert, 2003) that there is a reduction of the retinal nerve fibre layer thickness in amblyopes has however, not been reflected in the findings reported by any of the published imaging studies investigating amblyopia.

4.7.1 Overview of Published Studies

Following the publication of the first detailed structural study of the retina utilising fundus photography and digital imaging to suggest the presence of subtle optic nerve hypoplasia in amblyopes (Lempert, 2000); the idea that there may be some underlying pathology, particularly in those cases of amblyopia that does not respond well to treatment, has stimulated debate(Archer, 2000; Lempert, 2000). With the development of retinal imaging techniques further studies by a number of research teams have used the recent technologies to image the retina of amblyopes (Altintas et al., 2005; Bozkurt et al., 2003; Yen et al., 2004).However, far from producing a definitive answer to retinal structure in amblyopia the results have presented variable outcomes (Table 4.1). The reasons for this variability require to be further explored.

Table 4.1: Comparison of results for RNFL thickness and macular thickness from previously published imaging studies.

Author	Date	Journal	Imaging Technique	Area 1	Area 2	Area 3	No. subjects	Strab	Aniso	Mixed	Control group	Age (yrs)	Conclusion RNFL	Conclusion Macula
Altintas	2005	Paed Ophthal Strab	OCT	RNFL thk	Mac thk	Mac vol	14	Y	N	N	N	10.43 (5-18)	No significant diff between eyes	No significant difference between eyes
Baddini	2001	Journal of Aapos	GDx VCC	RNFL thk			21	Y	N	N	N	15 (7-35)	No significant diff between eyes	NA
Bozkurt	2003	Strabismus	GDx VCC	RNFL thk			24	Y	Y	Y	N	(7-66)	No significant diff between eyes	NA
Colen	2000	Binocul Vis Strab	GDx VCC	RNFL thk			20	Y	N	N	N	37.7 (15-60)	No significant diff between eyes	NA
Dickman	2009	Journal of Aapos	OCT	RNFL thk	Mac thk	Fov vol	40	Y	Y	N	N	15.2 (5-56)	No diff in RNFL	> Mac & Fov thk in strab amb
Huynh	2009	Ophthalmology	OCT	RNFL thk	Mac thk		4118	Y	Y		Y	6 & 12	No diff in RNFL	Mac thk >amb
Kee	2006	Korean J Ophth	OCT	RNFL thk	Fov thk		68	Y	Y	Y	Y	8	No significant diff between eyes	Mac thk >amb
Repka	2006	Am J Ophthalmol	OCT	RNFL thk			17	Y	Y	Y	N	10.7	No significant diff between eyes	NA
Repka	2009	Am J Ophthalmol	OCT	RNFL thk			37	Y	Y	Y	N	9.2 (7-12)	No significant diff between eyes	NA
Yen	2004	IOVS	OCT	RNFL thk	RNFL thk (est int)		38	Y	Y	Y	Y	26.4 (6-75)	> in RNFL thk (est int) in aniso amb v fellow eye.	NA
Yoon	2005	Korean J Ophthalmol	OCT	RNFL thk	Mac thk		31	N	Y	N	N	NR	> RNFL thk in aniso amb eye v fellow eye	No diff in Mac thk

To date there have been 11 published studies investigating retinal structure in amblyopia (Table 4.1). The earliest studies (Baddini-Caramelli et al., 2001; Bozkurt et al., 2003; Colen et al., 2000) have used the GDx VCC to investigate retinal nerve fibre layer (RNFL) thickness with no evidence found of any structural difference in amblyopic eyes. As OCT technology has developed and established itself in routine clinical practice researchers have begun to use the time domain OCT to investigate amblyopia and the number of published studies has begun to increase. With the increase in application of the OCT in this area of research the use of GDx VCC has diminished.

All the published studies (Table 4.1) investigating retinal structure in amblyopia have examined the retinal nerve fibre layer (RNFL) thickness in the circumpapillary area around the disc and only a small number have examined macular thickness (5/11). Generally the findings appear to suggest that there is no difference in the retinal nerve fibre layer (RNFL) thickness in amblyopic eyes. Only two studies have found a significant difference (Yen et al., 2004; Yoon et al., 2005) and both of these studies found significant differences between retinal nerve fibre layer (RNFL) thickness in the amblyopic eye in comparison to the fellow eye in anisometropic amblyopes.

Out of the five studies that examined macular thickness, three of the studies found an increase in the macular thickness of the amblyopic eye in strabismic amblyopes.

4.7.2 Control Groups

The majority of the studies investigating retinal structure have used the fellow eye as the control with which to compare measurements from the amblyopic eye (Altintas et al., 2005; Dickmann et al., 2009; Repka et al., 2006; Yoon et al., 2005). In research studies investigating visual function in amblyopes the fellow eye has been shown to demonstrate subtle effects in the presence of amblyopia (Kandel et al., 1980; Leguire et al., 1990). In order to establish the individual variation between right and left eyes in the general population it would be helpful to have normative data for comparison. The lack of control groups means that any subtle differences that may exist in the normal population cannot be compared.

Studies by Kee (2006) and Yen (2004) included control groups. The control group in Yen's study of strabismic and anisometropic amblyopes (Yen et al., 2004) comprised of a cohort of anisometropes, without the presence of amblyopia. No difference was found between the groups and no difference was found between the amblyopic and the fellow eye of the strabismic groups. However, a significant difference between the amblyopic and the fellow eye of the anisometropic amblyopes was found, with their parameter, RNFLT $_{estimated\ integrals}$. This difference was found only in refractive amblyopes and not in the strabismic amblyopes.

Kee (2006) investigated both the thickness of the fovea and the retinal nerve fibre layer in children with strabismic and anisometropic amblyopia; a normative control group of children without amblyopia was included for comparison. No difference was found between any of the cohorts (strabismic amblyopia, anisometropic

131

amblyopia, combined strabismic and anisometropic amblyopia and normals).
However, a significant difference was found between the amblyopic eye and the
fellow eye of the strabismic amblyopes and the anisometropic amblyopes. In the
strabismic amblyopes the average foveal thickness was found to be greater
(p=0.046) and in the anisometropic amblyopes the retinal nerve fibre layer (RNFL)
was found to be greater (p=0.034).

In the studies where the fellow eye is used as the control and there is no specific
control group, results varied (Altintas et al., 2005; Repka et al., 2006; Yoon et al.,
2005). Alintas (2005) found no difference between the amblyopic eye and the
fellow eye of a group of strabismic amblyopes; although the macular thickness and
volume was slightly increased it did not achieve statistical significance.

Yoon (2005) investigated anisometropic amblyopes and found no difference in
macular thickness between the eyes but did find a significant difference in the
mean retinal nerve fibre layer (RNFL) thickness, with the retinal nerve fibre layer
(RNFL) demonstrating a thicker measurement in the amblyopic eye (p=0.019).

Repka (2006) investigated retinal nerve fibre layer (RNFL) thickness in a small
number of combined amblyopes (strabismus and anisometropia). No difference
was found between the amblyopic and the fellow eye in this study.

Dickmann (2009) found no difference in the mean retinal nerve fibre layer (RNFL)
thickness between the amblyopic and fellow eyes in anisometropic or strabismic
amblyopia. However, the study showed a significant increase in the thickness of

the macula and foveal thickness in the amblyopic eye, but only in strabismic amblyopia.

The studies by Baddini-Caramelli et al.(2001), Bozkurt et al (2003) and Colen et al (2000) utilising the GDx VCC all compare the retinal nerve fibre layer (RNFL) thickness around the disc in the amblyopic eye to that of the non-amblyopic eye. No normative control groups were used in any of the studies, this may be due to the fact that the GDx has its own internal database with which measurements are compared and reported. The investigators using this technique may have considered that a normative control group was not required.

4.7.3 Scan Protocol

The rationale for the determination of scan selection appears to be determined by the availability of the technology and not by any rationale considering the most appropriate anatomical site. Therefore in studies using the OCT the investigators have used the standard scans provided by their instrument to image the macula and fovea (Altintas et al., 2005; Kee et al., 2006) or the retinal nerve fibre layer(RNFL) thickness in the circumpapillary area around the disc (Repka et al., 2006; Yen et al., 2004). In studies using the GDx VCC, which is designed to measure the retinal nerve fibre layer thickness around the disc area in glaucoma patients (Medeiros et al., 2004) the investigators have used the standard GDx format for measuring the retinal nerve fibre layer (RNFL) thickness (Baddini-Caramelli et al., 2001; Bozkurt et al., 2003; Colen et al., 2000). No significant

difference was found between the amblyopic eye and the fellow eye in any of the GDx studies measuring the optic disc parameters of amblyopes (Baddini-Caramelli et al., 2001; Bozkurt et al., 2003; Colen et al., 2000). This is perhaps not surprising as there is significant variation in optic disc parameters within the normal population (Huynh et al., 2007; Huynh et al., 2008; Jonas et al., 1999) and the GDx operates by comparing the measured data to its normative adult database of disc parameters.

4.7.4 Exclusion Criteria – Eccentric Fixation

In the majority of studies of retinal structure using imaging technology there are high exclusion rates. A number of studies have excluded amblyopes due to poor or eccentric fixation (Baddini-Caramelli et al., 2001; Colen et al., 2000; Dickmann et al., 2009; Repka et al., 2006; Yoon et al., 2005). Two of the studies (Baddini-Caramelli et al., 2001; Colen et al., 2000) had significantly high exclusion rates amongst the amblyopic cohorts, with 50% and 52% of recruits respectively being excluded due to eccentric fixation and difficulty maintaining fixation. The studies all demonstrated difficulty obtaining accurately centred scans. The presence of poor or eccentric fixation in the amblyopic cohorts resulted in the inability to centre the scan, an essential criterion for imaging using both the radial (Figure 4.6) and circumpapillary scan protocols used with time domain OCT technology. Where scans were obtainable the scan quality was reduced and exclusion from the studies was therefore high. The high rate of exclusion of amblyopes from the

studies is likely to affect the outcomes of the studies, as a significant number of amblyopes have the presence of eccentric fixation affecting their visual performance (Brock and Givner, 1952; Burian and Cortimiglia, 1962; Stewart et al., 2005). In essence the power of the study is reduced with the increase in exclusion rates of the amblyopes.

4.7.5 Type of Amblyopia

Although there is variation between the studies an overall commonality shows in the results. Where a difference in retinal structure is identified, this is an increase in the thickness of the retinal structures within the amblyopic eye, in comparison to the fellow eye. (It must be noted that the majority of studies have only carried out comparisons between the amblyopic and the fellow eye). In particular in strabismic amblyopia there appears to be an increase in the macular and foveal thickness, whilst in anisometropic amblyopia the increased thickness is found in the retinal nerve fibre layer (RNFL) around the optic disc. None of the studies, with the exception of (Huynh et al., 2009) have presented statistics of the difference between the mean thickness measurements between the amblyopic and fellow eyes, along with confidence intervals; this information would be helpful in establishing a plausible range of values for the true difference between the cohorts. Huynh (2009) found a significant difference in foveal and macular thickness in amblyopic eyes (combined amblyopia) in comparison to "normal" eyes from his control group. This difference is statistically significant, the foveal thickness of the

135

amblyopic group being 170.7 µm (95% CI 161.5 -179.9) and that of the non-amblyopic eyes 158.6 µm (95% CI 157.1 – 160.1). The study also investigated the macular thickness difference between treated and untreated amblyopes and although there was a difference in thickness, the treated amblyopic eye having slightly greater macular thickness, there is a lesser degree of significance and a greater degree of variation.

4.7.6 Age of Participants

More than 50% of the studies have recruited participants of a wide age range, incorporating adults and children. Only two studies have specifically recruited children. In population studies establishing normal profiles of retinal structure it has been shown that there is no significant change to disc dimensions or to foveal thickness with age (Chan et al., 2006; Huynh et al., 2006a; Salchow et al., 2006). However, this cannot be assumed to be the same for the amblyopic population. The effect of age, particularly on the foveal thickness needs to be investigated. Increased foveal thickness has been associated with reduced visual acuity in adult eyes (Hee et al., 1998) and it is important to establish the association between foveal thickness, age, retinal development and amblyopia.

4.7.7 Hypotheses

Yen (2004) in his study of anisometropic amblyopes speculates that an impediment in the mechanism of ganglion cell apoptosis during foetal development may contribute to a thicker retinal nerve fibre layer (RNFL) in anisometropic amblyopes and hypothesises that if amblyopia affects the process of the reduction of the ganglion cells postnatally the retinal nerve fibre layer will be thicker in the amblyopic eye (Yen et al., 2004). However, the effect of amblyopia on the retina, if any, is not certain and the involvement of the retina and in particular the retinal nerve fibre layer (RNFL) is not clear. Histological studies of the human retina (Georges et al., 1999; Provis, 1987) have demonstrated that the process of apoptosis is mainly confined to the bipolar cells, and is complete by 30 weeks gestation; no signs of cell death were found after this. It therefore cannot be assumed that apoptosis postnatally will affect retinal nerve fibre layer (RNFL) thickness and if there is an effect on the thickness in the peripapillary area of the retinal nerve fibre layer, that there will be any change in the macular area or indeed that any changes in the macular area will be reflected by changes in the peripapillary area. Huynh (2009) suggests that the findings from his study; an increase in foveal thickness in amblyopic eyes, supports the theory of apoptosis presented by Yen (2004). However, although both studies report an increased thickness the thickening is in different retinal areas. Yen found an increase in the retinal nerve fibre layer (RNFL) thickness and Huynh reported an increase in foveal and macular thickness but indeed did not find any increased thickness in retinal nerve fibre layer (RNFL) in his study (Huynh et al., 2009). The type of amblyopia

137

may contribute to the difference in the findings between the studies. Yen's study only investigated anisometropic amblyopia whilst Huynh included all types of amblyopia in his study group. Interestingly another study (Yoon et al., 2005) solely investigating anisometropic amblyopia also found increased thickness in the retinal nerve fibre layer (RNFL) but no difference in the macular thickness. This difference in the area of retinal thickening may be an indication that the two types of amblyopia have separate developmental processes.

Huynh further hypothesises that the increase in foveal thickness is associated with reduction in the level of visual acuity, although from his large population study, it is not possible to conclude this association, as the untreated group of amblyopes is small (n=12) in comparison to the recruited total (n=4118). There is also no indication that the treated group of amblyopes were part of a prospective study, ensuring compliance and providing evidence of different thickness measurements being linked to levels of visual acuity. A previous study has reported a link between foveal thickness and visual acuity in adults (Hee et al., 1998). This study however, was investigating diabetic oedema and therefore the presence of overt pathology could account for the reduction in visual acuity, further research is required prior to assuming there is a direct link between macular thickness and the level of visual acuity. None of the presented studies provide enough evidence to link the level of visual acuity with increased foveal thickness and further studies are required to clarify if foveal thickening precedes the development of amblyopia or indeed if it is a developmental response to the presence of amblyopia. This question can only be addressed by studying structure in fully developed adult eyes, both with and

138

without amblyopia, developing children's eyes, both with and without amblyopia and also treated amblyopes who are monitored prospectively in order to establish the natural development of the fovea. The design of this current research is intended to address this point and contribute to the understanding of retinal structure in amblyopia.

4.8 Calculation of Magnification – 3D-1000 OCT (Topcon)

4.8.1 Introduction

Previous studies using OCT have shown that the retinal nerve fibre layer (RNFL) thickness measurement is not significantly affected by ocular magnification (Schuman et al., 1996). However, lateral measurements e.g. optic disc diameter, are affected and the appropriate correction must occur in order to properly compare measurements in different eyes (Hee et al., 1998; Sanchez-Cano et al., 2008; Wang et al., 2007). In order to determine the magnification effect of the 3D OCT-1000 and appropriately interpret the acquired retinal images an axial length measurement is therefore required.

Axial length measurements are essential to the calculation of image magnification and the ability to both image and measure axial length simultaneously is an invaluable tool, reducing the number of procedures required for the observers. With the increasing advances and popularity of OCT in ophthalmic investigations this facility benefits both the practitioner and the observer. The image size produced by fundus photography or by other imaging techniques employing a camera is dependant on a number of factors. Variation in image size occurs due to the magnification effect both from the camera and also from the optics of the eye itself (Garway-Heath et al., 1998); (Littmann, 1982, 1992). It is impossible to obtain exact in vivo measurements directly from the eye; therefore information must be obtained by measuring the image produced by the imaging system. Littman (1982) developed a widely used (Ansari-Shahrezaei et al., 2001; Arnold et al., 1993;

Garway-Heath et al., 1998; Langenbucher et al., 2003) formula which determines

the effect from magnification, calculating the actual size of retinal features from the

measured image size (Equation 4.1). The use of this equation allows the true

retinal measurement to be established.

$$t = p \, . \, q \, . \, s$$

Equation 4.1: Littmanns equation used to establish actual retinal size, taking into account optical magnification from both the eye and the imaging system. t=true retinal size, p=magnification factor of the camera, q=magnification factor from the optics of the eye and s=measured image size.

In ophthalmic research and disease management, characteristic changes to the

optic disc and optic nerve head, reflecting disease progression are routinely

measured and monitored. It is important to accurately determine optic disc size to

distinguish pathological from physiological change. The collection of accurate

lateral measurements is therefore required (Bengtsson and Krakau, 1992; Quigley

and Dube, 2003).

141

4.8.2 Magnification Factor from the Optics of the Camera - "p"

The calculation of the camera factor p (°/mm) relates to the angle of the light rays emerging from the eye (U°) (Figure 4.1) in relation to the size of the image produced (mm). The factor "p" is therefore calculated by U°/s (s = image (mm). The equation (Equation 4.1) can be applied in principle to any fundus camera; however the numerical factor Littmann calculated, $p = 1.37$ (Littmann, 1982) applies only to the Zeiss fundus camera used by Littmann in his research. As magnification varies with each camera model, the magnification factor (p) needs to be established for each specific camera used for an individual study (Rudnicka et al., 1998).
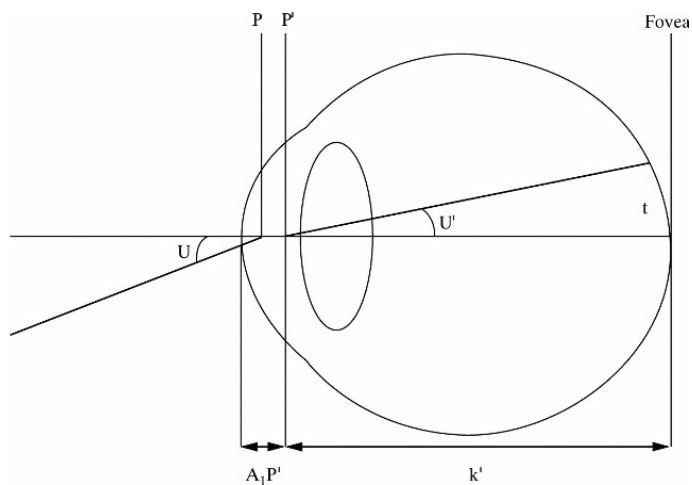
Figure 4.1: Chief rays from a parafoveal retinal feature forming the external angular difference (U). U' = angle subtended at second principal point (P') by retinal feature with height "t"; k' = distance from second principal point (P') to fovea; A1P' = distance from apex of cornea to second principal point; U = external angular difference (= U'.(1.336)). From (Garway-Heath et al., 1998).

4.8.3 Magnification Factor from the Optics of the Eye - "q"

The calculation of the ocular factor q (mm/°) relates to the size of the retinal characteristic being imaged (t) in relation to the angle (U') subtended at the second principal point (P') (Figure 4.1). The angle U' is assumed to equal the angle of the emerging light rays emanating from the retinal characteristic, divided by the refractive index of the ocular medium (1.336) (Bennett et al., 1994). The amount of ocular magnification produced by the eye is dependent on the internal axis of the eye (K') which is generally taken as the refractive index divided by the measurement from the second principle point (P') to the fovea i.e. K'= 1.336/k' (Figure 4.1). The objective of all the differing methods of calculating the magnification factor of the eye "q" is to provide an estimation of K'. This estimation can be formed by collecting measurements of the optical properties of an eye such as corneal curvature and thickness, the degree of ametropia, anterior chamber depth, axial length etc (Bengtsson and Krakau, 1992; Garway-Heath et al., 1998). Based on the investigations carried out by Littmann ((Littmann, 1977, 1979, 1982, 1988) a number of studies have considered methods for determining 'q', related to the optical dimensions of the eye (Bengtsson and Krakau, 1992; Bennett et al., 1994; Garway-Heath et al., 1998). The method of calculating "q" devised by Littman requires knowledge of the degree of ametropia and the keratometry measurement (Littmann, 1982). In a study comparing a variety of different methods, using a range of biometric data; ametropia, axial length, corneal curvature, and anterior chamber depth (Garway-Heath et al., 1998) it was found that methods using axial length to calculate "q" were most accurate, and in particular the

abbreviated axial length method published by Bennett (Bennett et al., 1994) who, simply by reducing the axial length measurement by a constant factor of 1.82 mm (which takes into account A1P') (Figure 4.1) improved on the accuracy of the original Littmann formula. This method of calculation demonstrated good agreement with Littmann's procedure (Garway-Heath et al., 1998).

4.9 The use of the z-score in calculation of ocular magnification

Optical Coherence Tomography (OCT) utilises the reflective properties of light to produce an in vivo image of the retina closely resembling histological sections (Blumenthal et al., 2009). OCT is employed clinically, to detect and measure changes in macular thickness and evaluate both qualitatively and quantitatively the thickness of the nerve fibre layer around the optic disc in glaucoma (Chen and Lee, 2007; Sakata et al., 2009) providing detailed information about retinal architecture and associated disease processes. In the process of image collection and measurement lateral dimensions as well as thickness measurements are commonly produced, with lateral dimensions being used to calculate optic disc area and volume. It is important that the effect of magnification is taken into account in this process (Leung et al., 2007; Sanchez-Cano et al., 2008; Wang et al., 2007).

4.9.1 3D OCT-1000: Z-Score

The 3D OCT-1000 (Topcon, Tokyo, Japan) used in this study includes a 'z-score' setting which can either be set manually or automatically to ensure the optimum positioning of B-scan image prior to capture of the complete 3D scan. The z-score facility is designed to ensure a complete 3D data set is captured and that none of the multiple B scans is missed or clipped due to being out of the measurement range. Prior to the imaging process taking place the observer fixates the internal fixation target in readiness for the scan to be taken. The OCT light source is reflected from the intraocular retinal layers producing a tomographic B scan image, viewed on the monitor by the examiner and adjusted in the longitudinal plane (z score adjustment) to ensure optimal positioning so that a complete 3D scan is captured. It is the eye's axial length that appears to determine this longitudinal adjustment and hence the z score.

The z-score has no recorded quantification of nomenclature and there is little information provided in the technical notes for the instrument. From clinical practice it had been noted that the z-score appeared to be an indicator of the axial length measurement. The ability to use the z-score from the 3D OCT to directly collect axial length data would reduce the number of procedures required to calculate the true measurement of retinal landmarks. This would be particularly helpful in data collection and magnification calculation, as only one procedure would be required to both capture the image and measure the axial length, providing the information necessary to allow calculation of image size magnification and accurate computational interpretation of the true size of retinal landmarks e.g. optic disc.

145

4.9.2 Materials and Methods

To establish the association between the z score and axial length system data was collected from 46 normal volunteers (21men, 25 women) aged 20 - 56 years (mean 32 yrs) in this prospective study. Participants were recruited from the staff, relatives of staff and patients from the Optometry Clinic at the University of Bradford. Only participants without a history or evidence of ophthalmic disease (including cataract), pathology or surgery were recruited. Refractive error ranged from - 13.00 DS to + 5.00 DS (MSE, ≤ 3D astigmatism) and visual acuities of 0.2 Log Mar (6/9 Snellen) or better were included. All participants gave informed consent and the study was conducted according to the tenets of the Declaration of Helsinki.

4.9.3 Optical Coherence Tomography (OCT) Imaging

OCT was performed with the 3D OCT-1000 (Topcon). The instruments light source is a super luminescence diode (SLD) (840nm) and utilises a Fourier domain system incorporating a spectrometer to produce cross-sectional B scans and 3-D volumetric images at a speed of 18,000 A scans /sec. The parameters for all scans in this study were a 3D macula scan covering 6 x 6 mm area, resolution 256 x 256 (65,536) axial scans. The B scan image, viewed on the monitor, prior to image capture was positioned manually using the systems z-score facility, allowing the full retinal thickness to be observed; two consecutive macular scans were taken, the OCT being reset to default between each scan. The z-score was recorded for each individual scan.

146

4.9.4 Ocular Biometry

The IOL Master (Carl Zeiss Meditec AG, Germany) was used to collect axial length measurement data. This commercially available optical biometry equipment is in common clinical use and has been shown to produce accurate repeatable measurement of axial length (Drexler et al., 1998; Kiss et al., 2002; Rajan et al., 2002) it is regarded in clinical practice as being the "gold standard" test (Parravano et al., 2007; Wang et al., 2009). The IOL Master uses the technique of partial coherence interferometry (PCI) (Fercher et al., 1995). This is a variation of optical coherence tomography (OCT) and is based on the same optical measurement technique using low or partial coherence interferometry (Hitzenberger, 1991). In contrast to OCT where a single light source is employed (Drexler and Fujimoto, 2008; Huang et al., 1991), partial coherence interferometry (PCI) uses a dual-beam infrared light source (780nm) of a short coherence length (160µm) to measure axial length; both the beams are reflected from the ocular surfaces of the cornea and the retinal pigment epithelium (RPE), producing a single A-scan measurement. The cornea is employed as a reference surface eliminating the effect of longitudinal eye movement during examination (Drexler et al., 1998; Kiss et al., 2002).

Data was collected from the volunteers at the same visit using the IOL Master to measure axial length, corneal curvature, and anterior chamber depth. Three consecutive axial length measurements were acquired and the mean reading used for calculation.

4.10 Statistical Analysis

Statistical Analysis was performed with commercial software STATA 10. The association between the z-score measurements and the axial length measurements were calculated with linear regression analysis; $p < 0.05$ was the criterion adopted for statistical significance. Bland-Altman plots were used to assess both the repeatability of the z-score measurement and the agreement between the predicted axial length measurement calculated from the OCT z-scores and the axial length measurements as measured by the IOL Master (Bland, 1995).

The optical magnification factor (q) was calculated using the abbreviated method of Bennett (Bennett et al., 1994) and the camera magnification (p) was calculated using the formula devised by (Littmann, 1982, 1988) and modified for use with OCT (Leung et al., 2007).

4.11 Results

92 eyes of 46 subjects were analysed, the measurements from both eyes were used to provide as wide a range of axial length measurements as possible. The mean axial length as measured by the IOL Master was 24.05 mm (SD 1.46), range = 21.76 mm to 28.4 mm. The OCT z-score measurements ranged from 660 to 1490 (these measurements are unitless). Repeatability of the consecutive z-scores was analysed using Bland-Altman analysis. No significant difference was found

between repeat z-score measurements (p = 0.6). The mean difference was 0.76 (CI -2.01 to 3.5) 95% limits of agreement - 26.00 to 27.53 (Figure 4.2). The z -score measurements obtained from the tomographic scans from the 3D OCT were compared to the axial length measurement data obtained from the IOL Master. Linear regression analysis demonstrated a high predictive association between the z-score and the axial length as measured by the IOL Master (R^2 = 0.981 p= <0.001). For each unit increase in the z-score the axial length increased by 0.007mm (95% CI 0.0075 to 0.0079) (Figure 4.3).The estimation of the effect of the z score in calculating the axial length can be best described by the equation:

Axial length = 0.0077 x z-score + 16.90

The above equation was used to predict the axial length from each z-score, a Bland-Altman plot of the predicted axial length and the IOL Master axial length measurements demonstrates a mean difference of 0.036 mm (CI -0.006 to 0.078) the 95% limits of agreement ranged from - 0.367 to 0.438 (Figure 4.4).

149
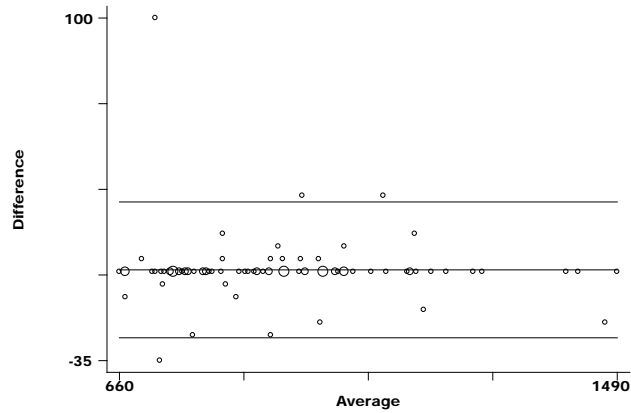
Figure 4.2: Bland-Altman plot of the consecutive OCT z-scores (n=92) with 95% limits of agreement indicated. Increased circle size indicates more than one reading on the same point. The central line = zero difference.
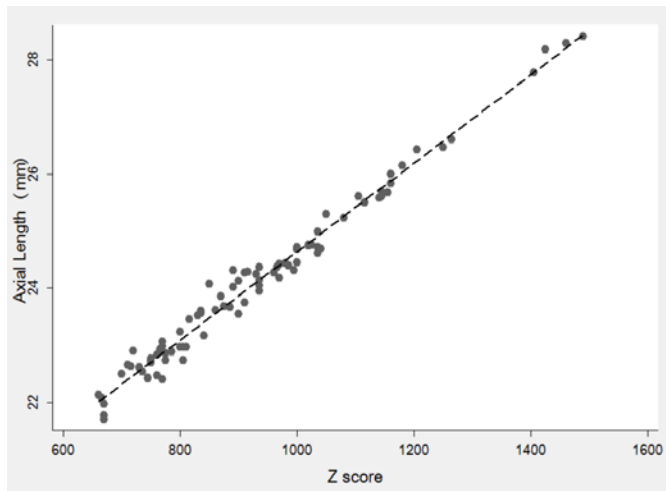
Figure 4.3: Linear regression of the Z-score recorded from the 3D-1000 OCT (Topcon) v axial length measurements (mm) recorded from the IOL Master. The equation for the regression line is y = 0.0077x + 16.90 (95% CI for slope, 0.0075 to 0.0079). R^2=0.98 p<0.001.
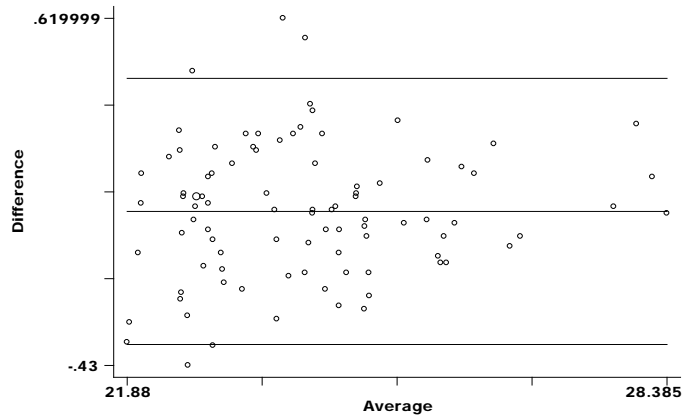
Figure 4.4: Bland-Altman plot of the predicted axial length and the IOL Master axial length measurements (n=92) with 95% limits of agreement indicated.
The central line = zero difference.

4.12 Calculation of Magnification of the Imaging System (p)

In order to calculate the total magnification produced by the eye and the imaging system, the factor relating to the camera "p" is also required. The establishment of the camera factor in this study however was illusive. The "p" factor calculated by Littmann (p=1.37) (Littmann, 1982) was developed using a Zeiss fundus camera and therefore was not applicable to the 3D OCT-1000 (Topcon) system.

An exploratory experiment was set up to calculate the factor "p" using the slit lamp to produce a constant beam in combination with a Super 66 Volk lens (Volk Opticals) (Ansari-Shahrezaei et al., 2001; Lim et al., 1996). This method utilises the

slit lamp beam, which is of a known length to measure the inverted image of the optic disc (Figure 4.5). The size of the image, measured by the length of the beam is dependant on the optical magnification produced by the eye and the magnification produced by the condensing lens. The image of the beam of known length was captured after passing through the eye and projected onto the subject's disc. The image length of the beam on the optic disc was then measured. The axial length of the recruited subjects was first measured using the IOL Master (Carl Zeiss Meditec AG, Germany), therefore factor "q" was calculated using the abbreviated axial length method (axial length – 1.82mm) (Bennett et al., 1994). The actual size of the slit beam (t), combined with the measurement of the image size (s), and the factor "q" should have allowed for calculation of factor "p". The results from this preliminary experiment were however inconsistent and did not produce data allowing the identification of a consistent stable value. This may be due to a variation in the position of the condensing lens in respect to the eye position, which although the procedure was carried out by the same examiner may have varied between individual procedures. The results may also have been affected by the imaging system of the camera used to take the image. This however would have been constant for all the individuals imaged and should not have produced the variable results obtained. The preliminary results from this procedure, however, were variable and not found to be reliable enough to estimate the camera factor "p".

Figure 4.5: Image of slit lamp beam of known length, projected onto optic disc image.

On communication with Topcon information was provided as to the default axial length and refraction setting of the 3D-1000 OCT imaging system. This is set to 24.39 mm at 0 D (personal communication from Topcon) with the default z-score set at 1000. Based on a previously published method of calculation (Dubis et al., 2009; Leung et al., 2007) the magnification factor "p" was calculated using the default measurement.

Using the 3D-1000 OCT system, the magnification factor in an eye with an axial length of 24.39mm will be 1 (actual retinal size [t] = image size [s]). The magnification calculation can therefore be reformulated taking into account that both the actual retinal size (t) and the image size (s) will cancel each other and the formula will change from, $t = p \cdot q \cdot s$ to $p = 1/q$.

Combing the revised formula with the abbreviated axial length method published

by Bennett (Bennett et al., 1994) allows "p" to be calculated,

$$p = 1/0.01306 (24.39 - 1.82)$$

$$p = 3.392$$

The value of the camera magnification factor "p" remains constant irrespective of

any change to the optical factor "q". Therefore, in order to directly calculate the

total magnification for the 3D OCT-1000 (Topcon) used in this study the following

formula was used.

$$t = 3.392 [0.01306 (0.0077 \cdot z\text{-score} + 16.90) - 1.82] \cdot s$$

4.13 Discussion

The results of this study demonstrate a strong level of prediction between the z-

score and the axial length (R^2 = 0.981 p =<0.001) with minimal variation. The

essential difference between the OCT and the IOL-Master is the use of the dual

beam light source by the IOL-Master and in particular the use of the cornea as a

reference beam to eliminate the influence of longitudinal eye motion. It is likely that

it is this factor that influences the difference between the axial length

measurements of the OCT and the IOL-Master. This difference is, however, small,

indicating that the z-score is suitable for use in the calculation of the magnification

154

factor "q". Repeated testing showed no significant difference in the z-scores when using the manual calibration (p=0.6) (Figure 4.2) and repeatability of the 3D OCT has been shown to have minimal variability (Bruce et al., 2009).

The z-score recorded from the 3D OCT system associates well to the axial length of the eye being imaged. Therefore, by recording the z-score reading and applying the prediction formula **Y = 0.0077 x + 16.90** the axial length can be determined. Using the abbreviated axial length method, q = 0.01306 (axial length – 1.82mm), (Bennett et al., 1994), the optical factor "q" can therefore be established.

This study has demonstrated the strong predictive relationship between the 3D OCT-1000 systems z-score setting and axial length, allowing accurate calculation of an individual axial length measurement. By applying the predictive calculation as found in this study to the z-score measurement an accurate axial length measurement can by achieved and the magnification factor for individual retinal landmarks calculated from the images. This is the approach that was used when lateral measures of optic disc and retinal structure e.g. foveal diameter and disc diameter were calculated (Chapter 7, Chapter 10 and Chapter 11).

Chapter 5. Repeatability and Reproducibility of Macular Thickness Measurements using Fourier Domain Optical Coherence Tomography.

5.1 Introduction

Prior to commencing the investigation of retinal structure in amblyopia using the 3D OCT-1000 (Topcon) the evaluation of the repeatability and reproducibility of macular thickness measurements in visually normal eyes was undertaken. This section of the study has been published in a peer review journal (Bruce et al., 2009).

The development of Optical Coherence Tomography (OCT) to produce high resolution tomographs has allowed detailed investigation of retinal structure (Huang et al., 1991). It is a routine, non-invasive method of imaging used to detect and measure retinal changes (Hee et al., 1995). Time Domain OCT (e.g. Stratus OCT, Carl Zeiss Meditec, Dublin, CA) utilises a low coherent light source to penetrate retinal tissue. The differential between the echo time delay of light from a reference beam is compared to that from a sample beam, allowing the reflectivity between intraocular microstructures to be measured (Medeiros et al., 2004).The measurement of reflectivity versus depth produces an axial scan (A-scan) and consecutive A-scans set side by side produce a two-dimensional B-scan (Costa et al., 2006). Acquiring approximately 400 axial scans per second, a standard 512 A-scan image is obtained in approximately 1.3 seconds (Wojtkowski et al., 2005).

Previous studies have investigated the reproducibility of first (Blumenthal et al., 2000), second (Schuman et al., 2003) and third generation (Budenz et al., 2005; Paunescu et al., 2004; Polito et al., 2005) OCT instruments. Paunescu et al. (2004) reported an interclass correlation coefficient (ICC) of 94% and Polito et al. (2005) reported ICC of 80-98% for macular scans.

The recent OCT development of Fourier domain/ spectral detection techniques has lead to dramatic improvements in image quality and acquisition speed (Wojtkowski et al., 2004). The spatially resolved tissue reflectance of the A-scan is obtained and the interference pattern measured simultaneously by the spectrometer increasing speed, reducing motion artefacts, and improving image quality (Huang, 2006). The development of Fourier-domain OCT offers considerable scope for improved detection and management of ophthalmic disease (Drexler and Fujimoto, 2008; Van Velthoven et al., 2007). However, in order for this new technology to be introduced into routine practice, replacing the existing time domain OCT, repeatability and reproducibility must be established. The results of studies comparing time- and Fourier domain OCT instruments are just beginning to emerge (Leung et al., 2008). The present study has been designed to prospectively examine factors that may affect repeatability and reproducibility of a Fourier-domain OCT.

5.2 Methods

In the context of the present study, repeatability is the variability of measurements by the same operator measuring the same entity, under the same conditions within a short period of time. It is a measure of the precision of the instrument. The standard deviation (SD) of the repeated measurements is a measure of repeatability. Reproducibility is the variability of measurements obtained under different conditions e.g. by a different operator or different visit (Bland, 1995; Gold and International Union of Pure and Applied Chemistry., 1987). The evaluation formed two phases; Phase 1 investigated scan repeatability, the effect of age and pupil dilation. Two groups; 6 younger and 6 older participants had one eye scanned 5 times pre and post- dilation by 1 operator. Phase 2 of the study investigated between-operator, within and between-visit reproducibility. 10 participants had 1 un-dilated eye scanned 3 times on 2 separate visits by 2 operators.

The instrument evaluated was the commercially available 3D OCT-1000 (Topcon, Tokyo, Japan) with version 2.00 software, which the manufacturers claim measures to a resolution of 6 µm. The instrument utilises a Fourier domain spectrometer producing cross-sectional B scans and 3-D volumetric images at a speed of 25,000 A scans /sec. The parameters for all scans in this study were a 3D macula scan covering 6 x 6 mm, resolution 256 x 256 (65,536 axial scans) imaging the complete macular area and ensuring equal transverse and axial spacing . The Early Treatment of Diabetic Retinopathy Study (ETDRS) 9 region map was used

for quantitative evaluation (Earl.Treatment.Diabetic.Retinopathy.Study., 1985)

(Figure 5.1).
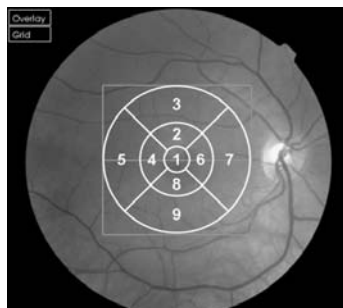
Figure 5.1: Fundus image of right eye with overlaid ETDRS 9 Region Map. Regions numbered for use in data analysis. For left eyes the region numbers were horizontally mirrored to maintain naso-temporal classification.

Instrument calculations (algorithms) are based on the reflections obtained from the individual A-scans, with the distance between two highly reflective layers (inner limiting membrane and retinal pigment epithelium) representing the thickness of the retina at that point. Scans were judged to be of acceptable quality when the algorithms correctly delineated the retinal layers, as judged by one operator (AB) where no significant motion or blink artefacts prevented acquisition of data. Participants were recruited from the staff, relatives of staff and patients from the Optometry Clinic at the University of Bradford. Only participants without a history or evidence of ophthalmic disease (including cataract), pathology or surgery, refractive error of less than ±8 D (MSE, ≤ 3D astigmatism) and visual acuities of

0.2 Log Mar (6/9 Snellen) or better were included. None of the participants had previously taken part in imaging studies and therefore the sample can be considered to be representative of the general population. Whilst this sample may not reflect the population who would typically undergo OCT assessment (i.e. patients with known or suspected pathology), in order to investigate the optimal repeatability and reproducibility of the Topcon OCT, healthy participants first need to be studied. All participants gave informed consent and the study was conducted according to the tenets of the Declaration of Helsinki.

5.2.1 Phase 1

Phase 1 was designed to identify the minimum number of scans required to ensure measurement repeatability and to assess the effect of age and pupil dilation. Twelve healthy volunteers (7 men, 5 women) formed two groups of 6 subjects, one younger group 30 - 43 years (mean 35.5) and one older group 57 - 78 years (mean 69.5). Each subject had one eye randomly selected (6 RE, 6 LE) and was scanned pre and post pupil dilation (1% Tropicamide) by one of two operators. In total 10 sequential scans (5 pre and 5 post-dilation) were analysed. A small number of scans were discarded mainly due to blinks or eye movement. The number of scans taken ranged from 11-18 (mean ~14 scans).

5.2.2 Phase 2

This second phase was designed to investigate between-operator, within and between-visit reproducibility. Ten healthy volunteers (7 men, 3 women) aged 25 - 44 years (mean 32) had 1 eye randomly selected (4 RE, 6 LE). Participants were scanned on 2 separate visits 1-10 days apart (mean 3). At each visit, 3 scans were carried out by 2 different operators. The order of operator was randomised and remained constant for both visits. After each scan the subject was repositioned and the instrument realigned. In previous scan repetition studies (Blumenthal et al., 2000; Chen and Lee, 2007; Stein et al., 2006b) reduced image quality has been reported. Pilot data indicated reduced image quality after multiple scans and a number of participants complained of dry eyes. Artificial tears (Minims Hydroxyethylcellulose 0.44%) were therefore used as necessary to maintain image quality or for participant comfort.

5.2.3 Statistical Analysis

Phase 1: A repeated measures random-effects regression model (STATA 9.2) was used to determine the effect of repeat scans (1-5) and pupil dilation. The standard deviation (SD) of the differences between participants 10 scans was used to estimate repeatability for each group. For Phase 1 the effective sample size reflected the total number of measurements (12 participants x 10 scans x 9 retinal regions).

Phase 2: Results were analysed using a linear mixed model ('xtmixed' command in STATA 9.2) to estimate variance components. This model takes account of the

nesting of measurements within visit, observer, and subject (Table 1). For Phase 2 the effective sample size also reflected the total number of measurements (10 participants, 12 scans and 9 retinal regions).

5.3 Results

5.3.1 Phase 1

No significant difference was found between each repeat scan (scan 1 vs. scan 2, p=0.75; scan 1 vs. scan 3, p= 0.8; scan 1 vs. scan 4, p= 0.76; scan 1 vs. scan 5, p= 0.76) or between non-dilated and dilated scans (p=0.54). In order to establish variability across the 10 scans obtained for each participant, the mean of the OCT measures was determined for each participant at each of the 9 retinal EDTRS sectors (Figure 5.1). Then, for each sector, the difference between the mean thickness for that participant and the thickness obtained in their first, second, third etc. scans was determined. Figure 5.2 shows a box and whisker plot of the differences of individual scans relative to the mean across the 9 sectors in the younger and older groups. In the younger group there was little variation (max difference: 6.8 µm) in repeat scans across all 9 EDTRS sectors; the standard deviation was only 1.81µm (approximate 95% prediction interval ± 3.62 µm). The older group showed greater variation, with a standard deviation of 3.73 µm (approximate 95% prediction interval ± 7.5 µm). However, the data for the older group must be viewed with some caution as the sample is not normally distributed

and the histogram of differences (max difference: 36 μm) demonstrates a large

kurtosis.
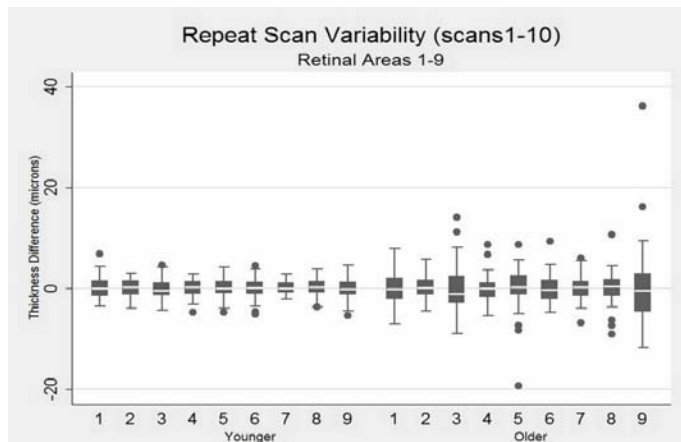
Figure 5.2: Box and whisper plots for older and younger groups at each of the 9 EDTRS (Figure 1) sectors.To establish variability across the 10 scans obtained for each participant, the mean of the OCT measures was determined for each participant at each of the 9 retinal EDTRS sectors (Figure 1). Then, for each sector, the difference between the mean thickness for that participant and the thickness obtained in their first, second, third etc. scans was determined. Hence, for each box in the plot above a total of 60 differences have been calculated (i.e. based upon 6 participants x 10 scans each). The middle horizontal bar in the box indicates the median difference, and the top and bottom horizontal boundaries of the box represents the third and first quartiles. The top and bottom bars represent the maximum and minimum differences in the absence of outliers. Single scans which are outliers are represented by dots.

5.3.2 Phase 2

Table 5.1 shows the results of the repeated measures regression model in which operator, visit and retinal area were random effects and pupil diameter was a fixed effect. Pupil size had a non-significant effect (p=0.545) upon macular thickness measurements, with 1mm increases in pupil diameter being associated with a reduction of 0.3 μm in measured thickness.

Table 5.1. Repeated Measures – Linear Mixed Model (STATA 9.2).

	Coef	Std err	z	P>|z|	95% CI	
Pupil	-0.318	0.526	-0.61	0.545	-1.349	0.712
_cons	281.900	4.205	67.04	0.000	273.658	290.141

Random effects parameters	Estimate	Std err	95% CI	
Retinal-area variability (SD)	29.935	2.250	25.835	34.686
Within-operator, within-visit (SD)	2.634	0.060	2.519	2.755
Between-visit (SD)	1.059	0.500	0.420	2.671
Between-operator (SD)	1.376	0.252	0.961	1.970

Table 5.2: Macular thickness values (µm) for all OCT Scans (Dilated and Undilated) at each EDTRS Region.

Retinal Region (Figure 5.1)	Younger Mean(SD)	Older Mean(SD)	Combined Mean(SD)
1	239.13 (16.25)	250.52 (17.65)	244.83 (17.84)
2	310.62 (12.83)	299.63 (10.57)	305.13 (12.94)
3	267.33 (12.75)	260.03 (13.57)	263.68 (13.61)
4	297.87 (14.12)	291.10 (10.98)	294.48 (13.04)
5	247.53 (17.43)	244.10 (10.58)	245.81 (14.46)
6	310.78 (11.67)	302.65 (11.58)	306.71 (12.27)
7	286.77 (15.45)	279.61 (4.42)	283.19 (11.87)
8	308.35 (13.96)	298.90 (9.93)	303.63 (12.96)
9	257.75 (13.58)	260.88 (13.01)	259.32 (13.33)

As expected there is a significant variation in macular thickness with EDTRS region (Table 5.2) consistent with known anatomical features of the human retina (Chan et al., 2006; Massin et al., 2001). The mean thickness reflecting all measures found in this study for EDTRS sector 1 was 244.83 ±17.84 µm; this is comparable to previous studies (Leung et al., 2005; Paunescu et al., 2004). Table 5.2 shows mean thicknesses for all 9 sectors. For a given retinal location, and an operator examining a given patient on repeated occasions within a single visit, 95% of measurements would be expected to fall within 5.16 µm (i.e. 1.96 x 2.634) of one another. This value increases to 5.56 µm for a given operator testing the same retinal area of the same patient but on separate occasions (combining variances for within and between-visit) (Equation 5.1).

$$\hat{\sigma}_{tot} = \sqrt{\hat{\sigma}_{within\_operator\&visit}^{2} + \hat{\sigma}_{between\_visit}^{2}}$$

Equation 5.1: Formula for combined within and between visits variance.

When different operators are considered over two separate visits, 95% of measures would be expected to fall within 6.18 µm (combining variances for within and between visits) within operator, and between-operator variance. This is determined from the following expression:

$$\hat{\sigma}_{tot} = \sqrt{\hat{\sigma}_{within\_operator\&visit}^{2} + \hat{\sigma}_{between\_visit}^{2} + \hat{\sigma}_{between\_operator}^{2}}$$

Equation 5.2: Formula for combined within and between operator variance.

5.4 Discussion

No significant variation between repeat scans (p=0.75) was established, indicating no benefit in precision from multiple scans. This is in contrast, to a study evaluating retinal nerve fibre layer (RNFL) measurements using the time-domain OCT 2000 (Humphrey Instruments) which indicated that 5 scans may be needed to produce optimum repeatability (Mok et al., 2004). This present study therefore confirms an improved precision for macular thickness measurements for Fourier-domain 3D OCT-1000 over time-domain OCT in support of recent findings (Leung et al., 2008). This present study also supports previous findings that pupil dilation does not affect scan repeatability (Paunescu et al., 2004; Polito et al., 2005) since no significant difference in retinal thickness measurement was noted pre- and post-dilation (p=0.50). In this study participants were free from pathology. In studies where participants have known lens opacities, dilation is indicated to ensure a reliable image (Chen and Lee, 2007; Smith et al., 2007; Van Velthoven et al., 2006). In the younger group 95% of measurements were within 3.62 µm, and variation was similar across all 9 retinal sectors. The older group showed greater variation (95% limits ± 7.6µm) with an increased number of outliers mainly in peripheral retina (areas 5 and 9). The error distribution was reasonably normal in the younger group. In the older age group the same did not apply. In this group we provide the caveat that distribution of the errors was wider, and non-normal - a finding that in itself is of interest because it suggests that the technique's reliability is age-dependent. Thus when imaging older individuals we suggest that a series of scans may be necessary. This will enable outliers to be more easily identified.

Previous time domain studies encompassing older groups with pathology e.g. glaucoma and diabetes reported greater variability (Blumenthal et al., 2000; Polito et al., 2005; Stein et al., 2006a). However, these studies could not distinguish between the effect of the pathology or age on variation. In this study all participants were free from pathology providing evidence that age or a combination of factors related to age, affects the variability of the OCT scan. Wu et al. (Wu et al., 2007) suggest that factors such as media opacity, pupil dilation and area measured have an effect on the overall scan quality, and Smith et al. (Smith et al., 2007) found that pupillary dilation was needed in 25% of their patients aged 39-88 years attending a glaucoma clinic in order to obtain an image with their time-domain OCT instrument. Fixational instability represents another possible reason why OCT results are more variable in older subjects (Birt et al., 1997).

The 95% confidence limits were larger for between-visit than within-visit reproducibility (5.56 µm v 5.16 µm). These results show better reproducibility for this Fourier-domain instrument compared to Stratus OCT e.g. inter-visit standard deviation = 12µm and intra-visit standard deviation = 6µm. The results indicate repeatability using the 3D OCT-1000 for measuring macular thickness within 6 µm for a single scan. Measured differences in macular thickness exceeding 6 µm in younger volunteers are therefore likely to reflect actual structural change. In older individuals measurements from occasional single scans differed from the remaining series and therefore it is advisable to take a series of scans in older individuals to enable outliers to be identified.

Chapter 6. General Methods

6.1 Summary of study

Amblyopia is the leading cause of monocular visual impairment in children (Attebo et al., 1998). The treatment for amblyopia, mainly that of occlusion therapy in combination with optical correction, is extremely beneficial in some children but ineffective in others with approximately 30% of amblyopes making no improvement(Clarke et al., 2003; Cleary, 2007; Cotter et al., 2003; Stewart et al., 2005) it is critical therefore that we understand the reasons for this incongruity. There is increasing evidence emerging to support an explanation for this finding, namely that subtle, undetected structural defects exist in many eyes diagnosed with amblyopia(Lempert, 2000; Lempert, 2003). Presently, the magnitude of this problem is unknown. If the problem is widespread, as the evidence suggests, it is unsurprising that treatment failures are common. Clinically, it is important that these individuals are identified early so that alternate management strategies can be developed, avoiding undue distress to the child and administration of any unnecessary treatment. In these cases the fundamental visual deficit is due to the structural anomaly rather than amblyopia and for this reason amblyopia treatment is highly unlikely to be beneficial. The purpose of this research is to establish the extent to which subtle structural anomalies, account for treatment failures and to evaluate both the clinical and scientific implications.

169

6.2 Research Hypothesis

Amblyopia can be defined as a form of reversible cerebral visual impairment (typically visual acuity) despite optimal optical correction. It is caused by a disturbance in visual development during the sensitive period of development and is never found in isolation, generally being associated with strabismus and or anisometropia (Holmes and Clarke, 2006).The prevalence of amblyopia in humans is ~2-3% (Attebo et al., 1998; Huynh et al., 2009). In childhood, no other condition is responsible for monocular visual impairment on this scale; indeed it has been estimated that it accounts for around 90% of children's eye appointments in the UK (Stewart et al., 2002). With the continued search for a greater understanding of the neurophysiological processes underlying amblyopia and better treatment of the condition, there is also a realisation by researchers that amblyopia may provide an invaluable insight into the role of early experience on the structure and function of the human brain; the neural basis of amblyopia has been the subject of a recent review (Barrett et al., 2004).

Current consensus is that the primary site of neural loss in amblyopia is the primary visual cortex (V1) (Barrett et al., 2004; Blakemore and Price, 1987; Hess, 2001; Hubel and Wiesel, 1998). However, the widely accepted view of the underlying neurology of human amblyopia (normal retina & lateral geniculate nucleus, anomalous V1) has recently been challenged by studies that have found retinal defects in eyes diagnosed with amblyopia (Lempert, 2000; Lempert, 2003) and deficient lateral geniculate nucleus function in amblyopes (Hess et al., 2009) (Chapter 2). In Lempert's studies the optic disc area was found to be significantly

smaller in amblyopic eyes with hypermetropic anisometropia when compared to the better eye and to non-amblyopic eyes, even when differences in axial length were taken into account (Lempert, 2003).

Although the association of amblyopia with pathology (e.g. congenital cataract) is well established, the vast majority of human cases are thought to develop in patients with normal, healthy eyes, except for the presence of anisometropia or strabismus. Recent studies using retinal imaging techniques (Huynh et al., 2009; Yen et al., 2004) have reported the presence of subtle structural abnormalities in the retina of some eyes diagnosed with amblyopia. Yen's study using OCT found increased thickness in the retinal nerve fibre layer around the optic disc in eyes with amblyopia and Huynh found an increase in foveal and macular thickness in amblyopic eyes. However as yet there is still little consensus on this issue (Bozkurt et al., 2003; Repka et al., 2009b; Yoon et al., 2005) (Chapter 4).

Human electrophysiological research also paints a rather contradictory picture of retinal function. There is considerable evidence that the electroretinogram (ERG) is normal in amblyopia (Gottlob and Welge-Lussen, 1987; Hess et al., 1985), conversely, other reports have presented evidence of the existence of subtle anomalies in electroretinograms (ERG) from amblyopic eyes(Arden et al., 1980; Arden and Wooding, 1985; Slyshalova and Shamshinova, 2008).

The presence of structural abnormalities in eyes diagnosed with amblyopia poses key questions concerning the aetiology of these abnormalities and the implications of their presence for the success of amblyopia therapy. In relation to aetiology,

three possible explanations exist for the presence of retinal abnormalities in eyes diagnosed with amblyopia:

The first is that subtle retinal defects arise directly as a result of the visual deprivation (usually anisometropia and/or strabismus) that has, in turn, caused the amblyopia. These retinal defects have been previously undetectable as the technology for detailed examination of retinal structure has not been possible. There is considerable support for this possibility in the published experimental animal literature. Recent studies have revealed anomalous retinal development in animals rendered amblyopic by depriving them of light and retrograde degenerations have been found in the retina and lateral geniculate nucleus of macaques after damage to the striate cortex (Cowey et al., 1989).

A second possible explanation for the existence of subtle retinal abnormalities is that, rather than arising as a response to anomalous visual input, they represent the primary, underlying cause of the visual loss that has been inadvertently labeled as amblyopia. In this latter case, individuals are effectively being misdiagnosed with amblyopia. If this is true, it is reasonable to consider the existence of the recognised link with anisometropia and strabismus. Anisometropia and strabismus are known amblyogenic factors; yet there is evidence that their presence in humans can *follow* the onset of a visual deficit such as amblyopia (Almeder et al., 1990; Ingram et al., 2003; Lepard, 1975). However, as the vast majority of amblyopes exhibit either strabismus or anisometropia but show no demonstrable pathology the proposal that they follow rather than initiate amblyopia has had little support (Barrett et al., 2005).

The third potential explanation is that there is some other, as yet unknown, defect perhaps at the level of the visual cortex, leading to the secondary occurrence of strabismus, anisometropia and retinal structure defects.

The prevalence of subtle retinal defects in eyes diagnosed with amblyopia is not currently known and it is this question that this study seeks to investigate. Initially the research is concerned with measuring normal retinal structure and quantifying the prevalence of retinal defects in amblyopic adults and children, respectively (Aim 1). Secondly the research aims to distinguish between the first two possible explanations, outlined above, by scrutinising the presence of retinal defects in eyes that have been diagnosed with amblyopia. It is necessary therefore to quantify the prevalence of retinal defects in children and adults with amblyopia in order that a comparison can be made. The two groups of amblyopes cannot be assumed to be the same; a difference in prevalence could arise, for example, if slow, retrograde retinal changes take place in the visual system of adult amblyopes. If this is the case, the prevalence of retinal abnormalities will be greater in the adult amblyopic population in comparison to the child population of amblyopes. If the prevalence is similar in both the amblyopic groups then this could indicate that the retinal anomaly is either the precipitating cause of the amblyopia or that the anomaly develops rapidly in the early stages of retinal maturation (Aim 2). In order to establish the extent to which the presence of retinal defects limit visual improvement achieved from the treatment of amblyopia, a group of children undertaking occlusion therapy for amblyopia will be prospectively monitored and their retinal structure measured (Aim 3).

6.2.2 Aims of the project

(i)   To establish the prevalence of subtle retinal defects in eyes diagnosed with amblyopia.

(ii)   To distinguish between two possible explanations for the origin of such defects.

(iii)   To investigate the relationship between quantitative measures of the retina; fovea, optic disc and papillomacular bundle, in children prior to amblyopia therapy, and relate this to the post-therapy visual outcome.

6.2.3 Rationale for OCT Scan Criterion

There have been a number of studies imaging the retina of amblyopes, these have used differing techniques particularly OCT and GDx (Altintas et al., 2005; Bozkurt et al., 2003) (Chapter 4). In these studies the rationale for the determination of the scan criterion appears to be determined by the technology of choice and not by any rationale considering the most appropriate anatomical site. Therefore in studies using the OCT the investigators have used the standard scans provided by their instrument to image the macula and fovea (Altintas et al., 2005; Kee et al., 2006) or the retinal nerve fibre layer (RNFL) thickness in the peripapillary area around the disc (Repka et al., 2006; Yen et al., 2004). In studies using the GDx which is designed to measure the RNFL around the disc area in glaucoma patients (Medeiros et al., 2004) the investigators have used the standard GDx format for

measuring the RNFL thickness (Baddini-Caramelli et al., 2001; Bozkurt et al., 2003; Colen et al., 2000). In the series of studies by Lempert (Lempert, 2000; Lempert, 2003, 2004, 2008) investigating the hypothesis that optic nerve hypoplasia (ONH) is present in amblyopes, then the specific anatomical structure, i.e. the optic disc area and dimensions, are targeted for measurement along with the axial length and retinal area. In this research study investigating the structural integrity of eyes diagnosed with amblyopia it was appropriate to image and measure the areas of the retina that would be most likely to be affected by the presence of amblyopia. Ambyopia is predominantly defined and measured as a loss in central visual acuity (Barrett et al., 2005) it was therefore appropriate to image the retinal areas particularly related to central visual acuity, i.e. the fovea, macula, and papillomacular bundle leading to the optic disc. Optical coherence tomography was therefore conducted on each eye using the macular scan, the centre scan and the optic disc scan parameters covering 6 mm x 6mm, resolution 250x250 (65,536 axial scans).

With regard to the series of studies by Lempert (Lempert, 2000; Lempert, 2003, 2004, 2008) imaging and measurement of the optic disc dimensions was instigated in order to investigate the theory that amblyopes, particularly those who do not demonstrate an improvement in visual acuity, despite successfully completing their occlusion therapy, are likely to show mild degrees of optic nerve hypoplasia (Lempert, 2008).Optic nerve hypoplasia is a developmental abnormality resulting in a reduced number of axons. There is a considerable variation in the degree of severity and the disc can in some cases have an almost normal appearance (De

175

Silva et al., 2006). Due to this substantial variation and the subjectivity of measuring the disc alone, in the investigation of optic nerve hypoplasia (Barr et al., 1999; De Silva et al., 2006; Taylor, 2005) measurement of the disc-macula distance to disc diameter ratio (DM:DD ratio) has been advocated as the most appropriate measurement method. De Silva (De Silva et al., 2006) found that there is substantial growth of the optic disc (51%) between infant and adulthood, but only minimal growth (11%) in the optic disc to foveal distance and presents the hypothesis that the DM:DD ratio is normally high in the neonatal period. However, if normal growth fails to occur a high DM:DD ratio will remain, this is consistent with optic nerve hypoplasia. Taylor (Taylor, 2005) suggests that this mechanism could explain the appearance of mild optic disc hypoplasia but it is unlikely to result in moderate or severe cases, which are probably the result of an insult to the developing visual system early in gestation. The presence of optic disc hypoplasia in amblyopic eyes is likely to be of a mild degree and therefore the measurement of the DM:DD ratio will provide evidence for this finding.

In order to address the previous points the following retinal areas will be considered for detailed measurement (adults & children):

- Macula   Foveal pit topography
- Papillomacular bundle   RNFL thickness
- Optic disc   RNFL thickness at edge of disc
- Optic disc   Optic disc dimensions

6.2.4 Study Design and Methodology

The methodology of this research study combines both a case-control with a longitudinal cohort design. The case control design of adults and children with and without amblyopia provides a comparison of the retinal topography between the groups allowing the identification of differences between the amblyopic and the normative groups. In order to further substantiate the natural history of retinal development in the presence of amblyopia and clarify the prevalence of retinal structural defects a prospective longitudinal cohort provides evidence of links between the structural defect and the final visual outcome of the treatment.

The research study has six distinct groups recruited to the investigation, including the longitudinal cohort of amblyopic children undertaking prospective monitoring of occlusion therapy (Table 6.1). Ethical approval was granted prior to the collection of data for this research study.

Table 6.1: Research Cohorts Recruited to the Study.

Adults	Children
Normal	Normal
Amblyopia	Amblyopia
Strabismus/Anisometropia Non-Amblyopic	Longitudinal treatment for Amblyopia

Initially adults both with and without amblyopia were investigated, followed by children both with and without amblyopia. The primary recruitment of the adult cohorts allowed competence and expertise to be developed with the optical coherence tomography technique prior to the challenge of imaging young children. The longitudinal cohort of children recruited prior to commencing therapy for amblyopia were examined at the outset of treatment and followed for a period of time until treatment was completed. The monitoring of this longitudinal cohort ran concurrently with the collection of the data from the other five cohorts.

There is evidence that measures of visual function other than visual acuity can continue to improve with amblyopia therapy even when visual acuity has ceased to improve. However, improvements in visual acuity remain the clinical gold standard for the assessment of treatment progress and success and, for this reason this clinical measure was utilised as the basis for evaluating treatment outcome. For the purposes of this study amblyopia was defined as a reduction in best corrected visual acuity in the amblyopic eye of $\geq$ 0.2 logmar with at least 2 lines difference between the amblyopic eye and the fellow eye (Awan et al., 2005; Holmes and Clarke, 2006; Stewart et al., 2003) and anisometropia defined as a difference of > 1.00 DS (see Chapter 3).

The requirement for steady fixation during the imaging process posed a challenge in both amblyopic subjects and in children where the quality of fixation was poor and eccentric fixation was commonly present. However, prior to commencing the research it was known that imaging data could be obtained in paediatric subjects, even in children aged 1 year or less (Kelly et al., 2003) and preliminary testing at

the university with children had demonstrated the ability to employ the technology for the purpose of imaging young children. The ocular imaging technique employed in this project, Fourier Domain Optical Coherence Tomography (OCT) was used to determine retinal topography and detailed structure of the fovea, papillomacular bundle and the optic disc.

6.2.4.1 Visual Acuity Measurement

The Bailey-Lovie LogMAR acuity chart (adults) and the Keeler LogMAR acuity cards (children) were used to measure the level of visual acuity in this study. The visual acuity for both LogMAR charts is expressed in terms of log of the minimum angle of resolution. Each row of the visual acuity tests has 5 letters with each letter having an acuity value of 0.02, giving a score of 0.1 for each row. The Bailie-Lovie chart (Bailie and Lovie, 1976) is designed to be used at 4m and the Keeler cards (Mc Graw 1993) at 3m.

All participants recruited via the University of Bradford were tested in the same consulting room where luminance was constant. The visually normal children recruited via local schools had their visual acuity tested in school where the luminance varied.

The children recruited to phase 2 of the study had their visual acuity tested in one consulting room in the hospital out-patient department. The luminance was consistent between visits.

6.2.4.2 Retinoscopy

All adults were refracted without cycloplegia, to ensure the appropriate refractive correction was being worn and any visual acuity reduction was due to the presence of amblyopia and not refractive error. The procedure was carried out by the same individual throughout the study (AB). The visually normal children were refracted without cyclopegia by one of two individuals (BTB or IP). This procedure was carried out in the school either before or after the OCT imaging.

All amblyopic children recruited to the study had a cycloplegic (cyclopentolate hydrochloride 1%) refraction carried out combined with a fundus and media examination. This was carried out by the consultant ophthalmologist or the hospital optometrist prior to being recruited into the study.

6.2.4.3 Occlusion

Prior to commencement of occlusion therapy a period of refractive adaptation was undertaken by each child. This consisted of wearing the prescription constantly until there was no further improvement in the visual acuity level (Chapter 3). This varied from 2-4 months.

Occlusion was only instigated after the period of refractive adaptation. Each child was prescribed 4 hours of occlusion to the fellow eye for 4 hours daily. A diary was provided to the parent/carer in order to record the amount of occlusion worn daily and it was requested that this was brought to each visit. The child was reviewed every 4-6 weeks to monitor the improvement in the visual acuity level.

6.2.5 Selection Criteria

Adult – visually normal cohort

Subjects were recruited from the staff and student populations at the University of Bradford, via the University's Eye Clinic, via local optometry practices and via a press release. Subjects attended the University of Bradford for either a single (1.5 hours) or double visit (2 x 1.5 hours - in a subset of individuals to assess the repeatability of the techniques - see Chapter 5). During each session, subjects received a full eye examination that included recording ocular history, subjective refraction, visual acuity measurement (logmar), cover test (at distance and near, with and without full refractive correction) and pupil evaluation. Binocular function was assessed using measurement of prism fusion and stereoacuity. Subjects with a known history of eye disease or ocular surgery were excluded from this cohort. Optical coherence tomography was conducted on each eye using the macular scan, the centre scan and the optic disc scan parameters covering 6 mm x 6mm, resolution 250x250 (65,536 axial scans).

Adult - amblyopia cohort

Subjects were recruited from the staff and student populations at the University of Bradford, via the University's Eye Clinic, via local optometry practices, via the Ophthalmology and orthoptic clinics at Bradford hospitals NHS Trust and Airedale NHS Trust and from the local community via a press release. Subjects attended either the University of Bradford or the Ophthalmology clinic at the local hospital.

During each session, subjects received a full eye examination that included recording ocular history, subjective refraction, visual acuity measurement (logmar), cover test (at distance and near, with and without full refractive correction), pupil evaluation and visuscopic assessment for eccentric fixation. Binocular function was also assessed using measurement of prism fusion and stereoacuity, where appropriate. Subjects with a known history of eye disease were excluded. Optical coherence tomography was conducted on each eye using the macular scan, the centre scan and the optic disc scan protocols 6 mm x 6mm, resolution 250x250 (65,536 axial scans).

At the outset there was no published normative data for the 3D-1000 OCT (Topcon) used in the study, therefore normative data was first collected, and the amblyopic data compared against the collected normative values. The results of this initial data collection will clearly provide an indication of the prevalence and extent of retinal defects in adults diagnosed with amblyopia.

Adult - non-amblyopic cohort with strabismus and/or anisometropia

In addition to a normal versus amblyopic comparison, a number of adults were recruited to a third group containing individuals with significant anisometropia or strabismus but no amblyopia. The results from this third group enable the evaluation of whether retinal anomalies are associated with amblyopic visual loss or indeed with the factors that are thought to lead to anisometropia or strabismus in humans.

182

Justification of Sample Size

Based upon initial data taken at the university, sample size calculations were employed to estimate the number of amblyopes and normal subjects required. The calculations indicated that a sample size of approximately 40 normal subjects and 40 amblyopes were required to detect a mean difference of 0.05 mm^2 in the temporal Neural Retinal Rim (NRR) area, with 85% power. The statistical analysis to justify the sample size was carried out under the guidance of a medical statistician from the Institute for Health Research, the University of Bradford.

Children – visually normal and amblyopic cohorts

The same visual examination procedures described above applied to both children and adults. OCT procedures are not frequently carried out in paediatric populations therefore; in the initial stages of collecting data from the children arrangements for obtaining OCT measures in the paediatric population were optimised. This consisted of changing the fixation target from a small square to a large cross which was easier for the children to maintain fixation with, positioning cartoon posters behind the examiner which helped in accurate positioning of the disc scans, and introducing a "counting" strategy which helped in maintaining the children's attention. A combination of all these different strategies was used in order to maximise fixation steadiness. Due to the difficulties for these young children in maintaining steady fixation, particularly for the optic disc scans where fixation needs to be maintained in an eccentric position during the scan, only 2 rather than

3 scan procedures were imaged, these were the macula and the disc scans. Central scans were not collected in any of the groups of children.

Bradford is the fifth largest metropolitan district in the UK and the city is the eighth most deprived health community. 20% of the overall population of 380,000 people are of South Asian origin. In order to reflect the diversity of the ethnic make up of the local population schools located in both inner city Bradford and in the suburban area of Bradford Metropolitan District were recruited to participate in the research study.

Normative data was gathered from children recruited from three local schools. The equipment was set up in the schools for short periods of intense data collection. Data was collected from children whose age profile matched (4 -5 years) that of children who were recruited to the longitudinal cohort to undergo occlusion therapy for their amblyopia. Children with amblyopia were drawn from the paediatric population attending Bradford hospitals NHS Trust and Airedale NHS Trust, referred via the local area school screening programme of reception class children, subject to written parental/guardian consent.

Justification of sample size
With the increased variability of OCT measures in children relative to adults (Kelly et al., 2003), calculations suggested that a sample size of approximately 50-60

visually normal children was required. Written consent was obtained from
parents/guardians before children participated in the study.

Children – Longitudinal Amblyopic Treatment Cohort

Although the association of reduced visual acuity in adult amblyopes with retinal
anomalies provides retrospective evidence for their influence on the treatment
outcome (since almost all the adult amblyopes had undergone therapy), the data
cannot provide a critical test of the hypothesis that such anomalies limit the
success of therapy. This can only be determined conclusively with a prospective
study. In this research cohort the success or failure of occlusion therapy in children
who were about to undergo initial occlusion therapy for their amblyopia was
examined. It is important to emphasise that all participating children were offered
conventional occlusion therapy in the normal manner and advised to wear the
occlusion patch for 4 hours every day (see Chapter 3). Although the precise nature
of the relationship between ocular structure and visual function is yet to be
determined, it is highly probable that structural defects impose an upper limit on the
level of visual performance which can be achieved after amblyopia treatment. By
relating the pre-therapy, quantitative measures obtained using the OCT imaging to
the visual outcome achieved following standardised treatment protocols, the
research examines whether the OCT measurement can identify children in whom a
poor final visual result can be expected. In addition to being able to avoid

unnecessary amblyopia treatment in these children, the opportunity to develop alternative treatment strategies is presented.

Both strabismic and anisometropic amblyopia has been shown to improve with glasses wear alone (Awan et al., 2005; Clarke et al., 2003; Moseley et al., 2002; Steele et al., 2006). Therefore the recommendation for a period of refractive adaptation prior to commencing occlusion therapy was instigated (Cleary, 2007; Holmes and Clarke, 2006; Moseley et al., 2002). All the children were subjected to a routine cycloplegic refraction and ophthalmologic examination prior to commencing occlusion. Where a refractive correction was prescribed the child was observed routinely whilst visual acuity was continuing to improve. Occlusion was only instigated when there was no improvement over two consecutive visits or after 4 months of wearing the prescribed glasses.

The benefits of amblyopia therapy have been shown to be evident within the first 400 hours or 4 months of treatment (Cleary, 2000; Stewart et al., 2004b; Stewart et al., 2007; Wallace et al., 2006). Based on these findings success was evaluated either at the completion of treatment, within the time frame of the research study, or after a 4 month time interval if treatment had not concluded by the end of the research study. It was therefore possible to relate the improvement in visual acuity after the completion of therapy to the captured OCT measurements. Since treatment compliance exerts a major influence on visual outcome (Stewart et al., 2004b), it is necessary to know the volume of occlusion therapy undertaken. To this end, participating children were provided with a parental diary to log their daily wear of the occlusion patch (Chapter 3).

Justification of sample size

Within the time frame and logistical constraints of the study it was desirable to obtain the largest sample size possible for this prospective longitudinal phase. Based upon recent research results (Clarke et al., 2003), a sample size of 40 for the longitudinal part of the study would be expected to produce ~27 children for whom treatment was effective and a poor visual outcome would result in around 13 children.

6.3 Data Sets

Normative Data – Adults

Data was collected as described from 54 adults with no ophthalmic history, of these, 4 adults were excluded due to the presence of ocular pathology during routine examination; two adults had the presence of cataracts detected during their examination, one adult was shown to have tilted discs and one was shown to have the presence of optic disc swelling on OCT examination. The age range was from 20- 59 years (mean = 32 years).The refractive error ranged from - 7.25 DS to + 5.00 DS (mean = - 1.5 DS) and visual acuity ranged from – 0.18 to 0.12 log units (mean = - 0.05). The demographic and ocular data for these 48 adults is presented in Data Set 6.1.

Adult Amblyopes

Data was collected from 43 adult amblyopes with a diagnosis of strabismus and or anisometropia, of these 7 amblyopes were excluded, 2 due to the absence of

saved scans, 4 due to poor quality scans and 1 due to the presence of nystagmus. 18 adult amblyopes had strabismus, 2 anisometropia and 16 combined strabismus and anisometropia. 26 of the 36 adult amblyopes (72%) had eccentric fixation. The age range was from 16- 76 years (mean = 47.5 years). The refractive error ranged from   - 8.5 DS to + 7.00 DS (mean = + 1.75 DS) and visual acuity ranged from 0.2 to1.0 log units (mean = 0.64) in the amblyopic eyes and – 0.10 to 0.3 log units (mean = 0.03) in the fellow eyes. The demographic and ocular data for these 36 amblyopic adults are presented in Data Set 6.2.

Non-amblyopic Strabismic & Anisometropic Adults (S/A)

Data was collected from 14 adults with either the presence of strabismus and/ or anisometropia but without the presence of amblyopia: 5 strabismus, 4 anisometropia and 5 combined strabismus and anisometropia. 2 subjects had eccentric fixation, both had the presence of a microtropia. The age range was from 21- 64 years (mean = 39 years). The refractive error ranged from - 9.0 DS to + 4.25 DS (mean = + 1.25 DS) and visual acuity ranged from - 0.14 to 0.24 log units (mean = 0.00).The demographic and ocular data is presented in Data Set 6.3.

Normative Data – Children

Data was collected by attending the reception classes of 3 local schools; one situated in inner city Bradford with a significantly high Asian (A) and lower socioeconomic population than the other two schools which are situated in the suburbs of Bradford Metropolitan District with a mainly white British (WBR)

population . All the children recruited from the reception classes were aged either 4 years (50%) or 5 years old (50%) the ethnic profile reflected that of the local community (30% Asian). Complete data sets were unable to be collected from 3 children due to their absence from school at the refraction session, 1 child refused to have the OCT scans and 12 were unable to sit still and maintain fixation during the OCT examination. Data was collected from a total of 73 children, however the data sets were not complete in all cases; 73 had macular scan sets completed and 49 had disc scan sets completed. The children found it difficult to maintain fixation particularly during disc imaging where an off centre fixation position requires to be maintained. This, along with the presence of blinking was the main cause of poor quality scans leading to exclusion. The refractive error of these children ranged from - 0.25 DS to + 2.50 DS (mean = + 0.75 DS) and visual acuity ranged from 0.00 to 0.18 log units (mean = 0.1). The demographic and ocular data of the children is presented in Data Set 6.4.

Amblyopic Data – Children

Data was collected from 27 children with the presence of amblyopia, despite having had treatment for the condition. The children's age ranged from 4 – 13 years (mean = 7.5 years). All the children either had the presence of strabismus and / or anisometropia: 9 strabismus, 5 anisometropia and 13 combined strabismus and anisometropia. 16 of the 27 (59%) children had eccentric fixation. These children were recruited into the study after their occlusion treatment for the amblyopia had been completed. The refractive error ranged from – 1.75 DS to +

9.75 DS (mean = + 3.5 DS) and visual acuity ranged from 0.2 to1.0 log units (mean = 0.40) in the amblyopic eyes and – 0.05 to 0.2 log units (mean = 0.0) in the fellow eyes. The demographic and ocular data of the children is presented in Data Set 6.5.

Amblyopic Data - Prospective Longitudinal Treatment Cohort (Children)

All the children recruited to the prospective longitudinal treatment cohort, except one, were referred to the Hospital Eye Service via the local school screening programme with the presence of amblyopia. The one child not recruited via the school screening programme was 7 years old and referred via his own GP. All the children were recruited prior to commencing their treatment. The children's age ranged from 4 – 7 years (mean = 5 years). 34 children were recruited to the longitudinal cohort, two wished to withdraw after the commencement of treatment, two were excluded as they were unable to carryout the OCT scanning procedure, one due to photophobia and one unable to maintain fixation for the OCT scans. 24 children completed their treatment; 5 had strabismus only, 11 had anisometropia only, and 7 had combined strabismus and anisometropia. 1 child was unusual in that he consistently demonstrated amblyopia without the presence of either strabismus or anisometropia. 11 out of 20 children had eccentric fixation (50%). The demographic and ocular data of the children is presented in Data Set 6.6.

Cohort Profiles

It must be noted that there are differences between the recruited groups with a difference in the mean age of the visually normal adults (32 yrs) and the amblyopic adults (47.5yrs) and also the visually normal children (5.1yrs) and the amblyopic children (7.5 yrs) in phase one of the study. There is also a difference in the refractive error between the groups with the visually normal adults (-1.5DS) being more myopic than the amblyopic adults (+1.75DS) and the visually normal children (+0.75DS) being less hypermetropic than the amblyopic children (+3.5DS). The potential effects from the differences of age and refractive error are addressed where appropriate in the experimental chapters.

Data Set 6.1 – Normal Adults (n=48)

Age	M/F	Ethn	RE Pupil	LE Pupil	RE Sph	RE cyl	RE axis	LE sph	LE cyl	LE axis	RE Log	LE Log	Diag	Sec Arc
31	M	WBR	6	6	0.25	-1.5	90	-0.25	-0.75	85	0	-0.02	EXP	55
22	F	WBR	5.5	5	0	0	0	0	0	0	-0.1	-0.12	NAD	55
31	F	WBR	5.5	5.5	-0.75	-0.25	144	-1	-0.25	61	0.1	0.12	NAD	55
22	F	WBR	5.5	5.5	0	0	0	0	0	0	0	0	NAD	55
56	F	WBR	4.5	5	-1	0.5	10	-1	0.5	180	-0.1	-0.1	NAD	55
59	M	INDBR	3	3	1	0	0	0	0	0	-0.1	-0.1	NAD	110
51	F	WBR	6	5	-0.25	0.25	35	0.25	0	0	-0.04	-0.1	NAD	55
30	F	WBR	6	4	0	0	0	0	0	0	0.08	0	NAD	55
49	F	WBR	3.5	3.5	0	0	0	0	0	0	0.02	0	NAD	55
38	M	WBR	6	5.5	-1	-1	100	-1	-1	80	-0.1	0	NAD	55
40	F	WBR	5	5	0	0	0	0	0	0	-0.08	-0.08	NAD	55
30	F	WBR	5	6	-1	0	0	-0.25	0	0	-0.08	-0.08	EXP	110
29	F	WBR	5.5	5.5	0	0	0	0	0	0	0	0	NAD	55
41	F	WBR	5.5	5	-3.25	0.5	152	-3.5	0	0	0	-0.1	NAD	55
20	M	IND	6.5	6.5	-3	-1.25	160	-1	-1	110	0.06	0	EXP	110
25	F	WBR	5	5	0	0	0	0	0	0	0	0.08	NAD	55
20	F	WBR	5	5	0.75	-0.5	10	1	-0.5	110	-0.02	0	NAD	55
27	M	WBR	5.5	5.5	-13	-1	180	-13	-1	180	0.02	-0.08	NAD	55
20	M	WBR	5.5	5.5	0	0	0	0	0	0	-0.01	-0.01	NAD	55
51	M	WBR	5.5	5.5	-1.5	0	0	-1	0	0	-0.2	-0.2	NAD	55
25	M	ASN	5	5	-5.75	-1.5	175	-6.75	-1.25	180	0	0	NAD	55
41	M	WBR	4.5	4.5	-6.75	-1	18	-7	-1	160	-0.02	-0.02	NAD	55
43	F	WBR	4.5	4.5	0.75	0	0	0.75	0	0	-0.2	-0.2	NAD	55
39	F	WBR	6	6	0	0	0	0	0	0	-0.1	-0.1	NAD	55
36	M	WBR	7	7							-0.16	-0.14	NAD	55

33	M	WOB	5.5	5	0	0	0	0	0	0	-0.1	-0.18	NAD	55
43	M	WBR	5	5	0.5	0	0	-0.5	0	0	-0.08	-0.06	NAD	55
20	M	APKN	4	4	0	0	0	0	0	0	-0.06	0	NAD	55
28	M	AIND	6.5	6.5	0	0	0	0	0	0	-0.08	-0.08	NAD	55
27	F	OTH	6	6	-1.25	-0.75	100	-2.25	-0.75	105	-0.1	-0.08	NAD	55
33	F	WBR	4	4	-7.5	-1.5	35	-6.25	-0.5	93	-0.1	-0.14	NAD	55
22	F	WBR	5.5	5	-0.75	-0.5	100	-0.5	-0.5	75	-0.08	0	NAD	55
20	F	WOB	6.5	7	-0.75	0	0	-0.75	0	0	0	0	NAD	55
43	M	WBR	5.5	4	-2.5	-0.25	60	-1.25	-0.5	128	-0.14	-0.18	NAD	55
27	F	WOB	5.5	5	-4.5	-0.75	180	-5.5	-0.75	180	0	0	NAD	55
30	M	WBR	6	6	-2.75	-0.5	175	-2.75	-0.5	15	-0.06	-0.1	NAD	55
22	F	AIND	6	6	0	0	0	0	0	0	-0.08	0	NAD	55
20	F	AIND	6.5	7	0	0	0	0	0	0	0.1	0.12	NAD	55
28	M	WOB	6	6	-3.75	0	0	-3.75	-0.25	180	-0.1	0	NAD	55
24	M	WBR	6.5	6.5	-5	0	0	-5.75	-0.25	92	0	-0.1	NAD	55
31	M	WBR	5	5	-4	-1.25	140	-3.75	-1	30	-0.1	-0.1	NAD	55
25	F	WBR	5	5	-5.5	-0.25	90	-5.5	-0.5	90	0	-0.1	NAD	55
33	M	WBR	6	5.5	-6.25	-0.25	80	-7.25	0	0	-0.1	-0.08	NAD	55
20	F	ABAN	5	5	-1	0	0	-0.75	0	0	-0.08	-0.06	NAD	55
38	M	WBR	5	4	-2.75	-1.25	145	-2.5	-1	70	-0.18	-0.18	NAD	55
32	F	WOB	6	6	0.75	0	0	0.75	0	0	-0.08	-0.1	NAD	55
25	M	WBR	6	6.5	5	-2	30	5	-2	145	-0.14	-0.04	NAD	55
35	F	WBR	6	6	0	0	0	0	0	0	0	0	ESP	55

Data Set 6.2 – Adult Amblyopes (n= 36)

Age	M/F	Ethnicity	RE pupil	LE pupil	RE Sph	RE cyl	RE axis	LE Sph	LE cyl	LE axis	RE Log	LE Log	Diagnosis	ANI	Eye	Fixation
48	M	WBR	5	5	2.75	0	0	2.75	0	0	0.80	0.00	Eso	N	RE	E
46	M	WBR	NR	NR	0.5	-5.5	180	1.25	-0.3	91	0.72	0.08	Micro	Y	RE	E
17	F	WBR	5	6	0	0	0	-1.5	0	0	0.00	0.30	Micro	Y	LE	E
40	M	WBR	3.5	3.5	0	0	0	0	0	0	-0.10	1.00	Exo	N	LE	E
42	F	WBR	6	6	6	1.25	10	6	1.25	175	0.30	-0.10	ESA	N	RE	F
32	F	WBR	4.5	5	4	0	0	-0.75	0	0	0.60	-0.10	Eso	Y	RE	E
32	F	WBR	6	5.5	5.5	1	75	4.5	2.5	90	0.10	0.70	Exo	Y	LE	E
66	M	WBR	3	3	1.75	-0.25	70	1	0	0	0.80	0.08	Micro	N	RE	E
53	M	WBR	3	3	-8.5	-0.75	175	-8.5	-0.8	175	0.86	0.08	Eso	N	RE	E
52	F	WBR	4	4	3	0.5	160	3	0	0	0.06	1.00	Eso	N	LE	E
60	F	WBR	3	3	4.5	2	110	5	1.5	105	0.08	0.60	ESA	Y	LE	F
37	F	WBR	4	3.5	-1.5	2	107	-0.25	1.75	95	-0.10	0.36	Micro	Y	LE	F
57	F	WBR	7	7	4.25	0.5	140	6.25	0.5	140	0.08	0.36	Micro	Y	LE	F
35	F	WBR	4.5	4	3.25	2.25	90	4.25	2.25	90	0.40	0.04	Micro	Y	RE	E
60	M	WBR	4.5	5.5	0.75	1.75	110	1.5	-0.5	180	0.00	1.00	Vert	N	LE	E
61	F	WBR	4	4	6.75	0.5	8	6.5	0	0	0.04	1.00	Exo	N	LE	E
51	F	WBR	5	5	0	0	0	4	0	0	-0.10	0.30	Micro	Y	LE	E
20	M	APK	4.5	4.5	4.25	-2.50	55	1.00	-1.00	120	0.25	0.00	ANI	Y	RE	F
48	F	WBR	5.5	5.5	1.75	-0.5	21	2.25	-0.5	160	0.10	0.30	Micro	N	LE	E
45	F	WBR	3.5	3.5	-0.5	-1	160	1	-1.5	15	0.00	0.84	Exo	Y	LE	F
76	M	WBR	3	3	5	0	0	5.5	-0.8	165	0.80	0.00	Exo	N	RE	E
73	M	WBR	4	4.5	3.25	1.25	15	4.25	0	0	0.10	0.50	Exo	Y	LE	E

194

71	F	WBR	NR	NR	0	0	0	0	0	0	1.00	0.20	Exo	N	RE	E
59	F	WBR	4	4	0	0	0	0	0	0	1.00	-0.02	Exo	N	RE	E
36	F	WBR	6.5	5	7	2	115	5.75	2.25	90	0.10	0.84	ESA	Y	LE	E
27	F	APK	5.5	6	0.25	-2.75	30	-2.5	-0.8	160	0.26	0.08	ANI	Y	RE	F
16	F	ABR	NR	NR	0	0	0	0	-0.5	90	0.00	1.00	Eso	N	LE	E
42	F	WBR	6	6	-2.25	2	14	-1.75	1	141	0.20	0.05	Exo	Y	RE	E
17	F	ABR	6	6	3.75	0.25	172	4	0.5	82	-0.01	0.23	ESA	N	LE	F
50	M	ASN	NR	NR	3.75	-1.25	56	2.5	0	0	0.05	0.80	Exo	Y	LE	E
63	M	WBR	NR	NR	-3.5	-1	100	-2.5	-0.3	30	0.08	0.40	Eso	Y	LE	E
64	F	WBR	4	4	0	0	0	0	0	0	0.05	0.80	Exo	N	LE	E
42	F	WBR	4.5	5	0	0	0	0	0	0	0.66	-0.01	Exo	N	RE	E
71	M	WBR	3	3	0	0	0	0	0	0	1.00	0.30	Eso	N	RE	E
64	F	WBR	3.5	3.5	1	5	180	1	2	35	0.48	0.02	Micro X	Y	RE	F
38	F	WBR	5	5	7	-2.25	15	6.5	-2.5	165	0.25	-0.10	ESA	N	RE	F

Data Set 6.3 –Strabismic & Anisometropic Adults – No Amblyopia (n= 14)

Age	M/F	Ethnicity	RE Pupil	LE Pupil	RE Sph	RE cyl	RE axis	LE Sph	LE cyl	LE axis	RE Log	LE Log	Diagnosis	Eye	Fixation	Sec of Arc
43	M	WBR	4	4	-1	0	0	-1.75	0.5	90	0.025	-1	Eso	RE	F	0
45	M	APK	4	4	0	0	0	0	0	0	0	0	Exo	LE	F	0
29	M	WBR	3.5	4	-5.5	-0.5	25	-3	-0.5	180	-0.1	-0.1	Eso & Ani	Alt	F	0
26	F	WBR	5	5	0	0	0	0	0	0	0	0.1	Eso	LE	E	0
21	F	WBR	6	6.5	-2	0	0	-0.75	0	0	0.01	-0.08	Dexo & Ani	LE	F	35
48	F	WBR	3	3	0	0	0	0	0	0	0.06	0.2	Eso	LE	F	0
50	F	WBR	4	3.5	0	0	0	-2	0	0	0	0.2	Ani		F	110
64	M	WBR	4	3	0.75	1.5	140	0.25	1	30	0.24	0.08	Micro	RE	F	110
22	F	AIND	5	5	1.5	0	0	0	0.5	90	0.16	0	Micro & Ani	RE	E	110
41	F	WBR	5	5	2.25	2	90	-1	3.25	90	0.1	0.1	Ani		F	55
53	F	WBR	4	4	4.25	-0.75	63	1.5	0.25	38	0	-0.15	Ani		F	110
33	F	WBR	4	4	-7.5	-1.5	35	-6.25	-0.5	93	-0.1	-0.14	Ani		F	55
47	F	WBR	5	5	-9	-0.5	15	-4.25	-3	180	0.175	0.2	Vert & Ani	Alt	F	0
29	F	ABR	4.5	4.5	2	-0.25	60	-1	0	0	0.18	0.08	Micro & Ani	RE	F	0

196

Data Set 6.4 – Normal Children (n= 73)

Age	M/F	Ethn	RE Sph	RE cyl	RE axis	LE sph	LE cyl	LE axis	RE Log	LE Log	Sec Arc
4	F	WBR	1.00	-1.00	180	0.50	-0.25	180	0.15	0.15	110
5	F	WBR	0.75	0.00	0	0.75	0.00	0	0.13	0.10	110
5	M	WBR	0.75	0.00	0	0.75	0.00	0	0.15	0.18	55
4	M	WBR	0.75	0.00	0	0.75	0.00	0	0.15	0.15	110
5	M	WBR	0.75	0.00	0	0.75	0.00	0	0.08	0.08	55
5	M	WBR	0.25	-0.50	180	0.25	-0.50	180	0.03	0.05	55
5	M	WBR	0.50	0.00	0	0.50	0.00	0	0.15	0.15	55
4	F	WBR	1.00	0.00	0	0.50	0.00	0	0.13	0.10	55
4	F	WBR	0.50	0.00	0	0.50	0.00	0	0.15	0.13	110
5	M	WBR	0.50	0.00	0	0.50	0.00	0	0.05	0.05	55
4	F	WBR	0.50	0.00	0	0.50	0.00	0	0.15	0.15	110
4	M	WBR	0.75	-0.50	180	0.75	-0.50	180	0.08	0.08	55
4	F	BRCB	1.25	-1.00	30	1.00	-1.00	180	0.18	0.18	55
4	F	BRCB	1.00	-0.50	180	1.00	-0.75	180	0.18	0.18	110
4	F	BRCB	1.00	0.00	0	0.50	0.00	0	0.15	0.15	110
4	F	WBR	1.00	0.00	0	1.00	0.00	0	0.05	0.05	340
4	M	WBR	0.75	0.00	0	0.50	-0.50	180	0.10	0.08	55
5	M	WBR	0.75	0.00	0	0.75	0.00	0	0.15	0.15	55
5	M	WBR	1.00	0.00	0	0.50	0.00	0	0.08	0.05	55
5	M	WBR	1.00	-0.50	180	0.75	0.00	0	0.10	0.10	
	M	WBR	1.00	0.00	0	1.00	0.00	0	0.15	0.15	55
4	M	WBR	0.50	0.00	0	0.50	0.00	0	0.10	0.10	55
4	F	WBR	1.00	-1.50	160	1.50	-1.50	180	0.13	0.15	55
5	M	WBR	1.00	0.00	0	1.00	0.00	0	0.13	0.13	55
5	M	WBR	1.50	0.00	0	1.50	-0.50	90	0.10	0.10	110
4	F	WBR	1.00	0.00	0	1.25	0.00	0	0.05	0.03	110
4	F	WBR	1.00	0.00	0	1.00	0.00	0	0.08	0.05	55
5	M	WBR	1.25	0.00	0	1.00	0.00	0	0.05	0.05	55
4	F	WBR	1.25	0.00	0	1.00	0.00	0	0.10	0.05	110
5	F	WBR	1.25	-0.25	25	1.00	-0.50	160	0.05	0.05	110
4	M	WBR	1.00	0.00	0	1.00	0.00	0	0.15	0.18	55
4	F	WBR	0.75	0.00	0	0.75	0.00	0	0.13	0.13	55
4	F	WBR	1.00	0.00	0	0.75	0.00	0	0.10	0.05	55
5	F	WBR	1.00	0.00	0	1.00	0.00	0	0.00	0.00	110
5	M	WBR	0.50	0.00	0	1.00	0.00	0	0.18	0.18	110
5	F	WBR	2.50	0.00	0	1.75	0.00	0	0.10	0.08	55
4	F	WBR	1.00	0.00	0	1.00	0.00	0	0.15	0.15	55
4	M	WBR	1.00	0.00	0	0.75	0.00	0	0.15	0.18	55
4	M	WBR	0.00	0.00	0	0.25	0.00	0	0.13	0.10	55
5	M	WBR	0.50	0.00	0	1.00	0.00	0	0.13	0.13	55
5	F	WBR	1.00	0.00	0	0.50	0.00	0	0.03	0.00	55
4	M	WBR	2.00	-1.00	180	2.00	-0.50	180	0.10	0.10	340
4	M	WBR	1.00	0.00	0	1.00	0.00	0	0.05	0.05	55
4	M	WBR	1.50	-1.00	160	1.00	0.00	0	0.15	0.13	
4	M	WBR	0.75	0.00	0	0.50	0.00	0	0.05	0.00	55
5	M	WBR	1.00	0.00	0	1.00	0.00	0	0.10	0.13	340
5	F	A	1.00	0.00	0	0.75	0.00	0	0.10	0.10	55

197

4	M	A	0.00	-1.00	180	0.00	-0.50	180	0.13	0.13	110
5	M	A	1.00	0.00	0	0.75	0.00	0	0.13	0.13	55
5	F	A	0.50	0.00	0	0.50	-0.50	180	0.10	0.10	55
4	M	A	0.50	0.00	0	0.50	0.00	0	0.15	0.13	110
5	M	A	0.50	-0.25	180	0.50	0.00	0	0.13	0.10	110
4	F	A	0.50	-0.75	160	0.50	-0.50	20	0.10	0.10	55
4	F	A	0.50	0.00	0	0.00	0.00	0	0.13	0.13	55
4	M	A	0.00	0.00	0	0.00	0.00	0	0.15	0.10	55
5	M	A	0.50	-0.50	180	0.50	-0.50	180	0.10	0.10	55
4	M	A	0.00	0.00	0	0.00	0.00	0	0.10	0.13	55
5	M	A	0.00	0.00	0	-0.25	0.00	0	0.13	0.13	55
5	M	A	0.00	-0.50	180	0.50	-0.50	180	0.10	0.13	55
4	M	A	1.50	-0.75	180	2.00	-0.50	180	0.10	0.18	55
5	F	A	0.25	0.00	0	0.25	0.00	0	0.10	0.10	55
4	F	A	0.25	0.00	0	0.50	0.00	0	0.13	0.13	55
5	F	A	0.75	0.00	0	0.75	-0.50	180	0.15	0.15	340
5	M	A	0.75	-0.25	180	0.50	-0.25	180	0.10	0.13	55
4	M	A	0.50	0.00	0	0.50	0.00	0	0.10	0.13	55
4	M	A	1.50	0.00	0	1.00	0.00	0	0.15	0.15	110
5	M	A	0.00	-0.50	180	0.00	0.00	0	0.15	0.15	110
5	F	A	1.00	0.00	0	1.25	0.00	0	0.10	0.10	55
4	F	A	0.50	0.00	0	0.25	0.00	0	0.13	0.15	110
5	F	A	1.25	0.00	0	1.25	-0.50	180	0.10	0.15	110
5	F	A	0.50	-0.50	180	0.50	-0.25	180	0.10	0.10	110
5	F	A	2.00	-1.50	180	2.00	-1.50	180	0.13	0.13	340
5	F	A	1.00	0.00	0	1.00	0.00	0	0.15	0.10	110

Data Set 6.5 – Amblyopic Children (n = 27)

Age	M/F	Ethnicity	RE pupil	LE pupil	RE Sph	RE cyl	RE axis	LE Sph	LE cyl	LE axis	RE Log	LE Log	Diagnosis	ANI	Eye	Fixation
6	F	WBR	8	8	4.50	-0.25	180	3.50	-0.50	80	0.300	0.075	ESA	Y	RE	E
13	M	WBR	4	3.5	3.25	0.00	0	3.00	0.00	0	0.200	0.000	ESA	N	RE	F
7	F	WBR	6	6	5.00	0.00	0	2.50	1.00	75	0.250	0.000	ANI	Y	RE	F
6	M	WBR			4.00	0.25	5	5.75	0.25	175	0.000	0.850	ESO	Y	LE	E
5	M	WBR	5	4	2.50	0.75	90	1.25	1.00	90	0.675	0.100	MICRO	Y	RE	F
7	F	WBR	8	8	1.00	0.00	0	3.75	1.00	80	-0.050	0.200	ANI	Y	LE	E
8	M	WBR			3.00	0.00	0	7.00	-2.75	170	0.050	0.400	MICRO	Y	LE	NR
7	F	WBR	4	4	5.50	-1.25	135	6.25	-1.50	50	0.000	0.200	MICRO	N	LE	E
6	M	WBR			-1.00	0.00	0	-1.25	0.00	0	0.050	0.450	ESO	N	LE	E
13	M	WBR	4	4	0.00	0.00	0	3.00	-1.00	130	-0.100	0.500	ANI	Y	LE	E
4	F	WBR	6	6	4.50	1.00	60	3.50	0.50	70	1.000	0.050	ESO	Y	RE	E
8	F	WBR	5	5	1.50	0.50	90	3.50	1.50	110	0.050	0.525	ESA	Y	LE	E
5	M	WBR	6	6	-1.00	0.00	0	-1.75	0.00	0	0.025	0.725	ESO	N	LE	E
9	F	WBR	6	6	2.50	0.00	0	4.00	0.00	0	0.000	0.275	ANI	Y	LE	E
9	M	WBR	5	5	5.50	0.00	0	4.00	0.00	0	0.300	0.000	ESO	Y	RE	F
8	M	BR/C			4.25	0.00	0	4.75	0.00	0	0.200	0.325	ESO	N	LE	NR
6	F	WBR	7	7	4.75	2.00	80	5.25	2.50	112	0.000	0.375	ESA	N	LE	F
6	M	WBR	6	6	4.50	0.00	0	7.00	0.75	130	0.000	0.300	MICRO	Y	LE	E
11	M	BR/C	6	6	5.25	0.75	180	6.00	0.00	0	0.320	0.100	ESA	Y	RE	E
7	F	WBR	5	5	4.00	0.75	90	1.50	0.00	0	0.200	0.000	MICRO	Y	RE	E
8	M	WBR	4	4	1.50	0.50	50	2.00	0.50	135	0.000	0.275	ESA	N	LE	E
6	M	WBR	5	5	4.00	0.50	10	4.00	1.00	180	0.050	0.275	ESA	N	LE	F
7	F	WBR	5	5	4.00	0.00	0	9.75	-1.00	180	0.000	0.250	ANI	Y	LE	F

6	M	WBR	6	6	5.00	-1.25	152	5.00	-0.75	180	0.200	0.025	MICRO	N	RE	F
7	F	ABR	5	5	0.00	0.00	0	5.25	0.00	0	0.000	0.600	MICRO	Y	LE	E
5	M	WBR	5	5	3.75	0.25	95	5.00	1.00	90	0.000	0.725	ESA	Y	LE	E
12	M	WBR	6	6	2.50	-2.00	5	0.00	0.00	0	0.200	-0.100	MICRO X	Y	RE	F

Data Set 6.6 – Longitudinal Treatment Group - Amblyopic Children (n = 24)

PID	Age	M/F	Ethn	RE Sph	RE cyl	RE axis	LE Sph	LE cyl	LE axis	RE Log	LE Log	Diagn	ANI	Eye	Fix[n]	Sec Arc
AB0199	5	F	A	0.00	0.50	90	0.50	0.00	0	0.100	0.850	ESO	N	LE	E	0
AB0218	5	F	A	-2.00	-0.25	40	0.25	-0.50	20	0.325	0.100	MICRO	Y	RE	E	110
AB0184	5	F	A	3.25	0.00	0	5.00	0.00	0	0.200	0.675	MICRO	Y	LE	E	0
AB0215	5	M	A	1.00	-1.00	180	0.75	-1.25	180	0.200	0.000	ESO	N	RE	F	0
AB0225	5	M	WBR	6.00	1.00	30	5.00	0.00	0	0.4	0.1	ANI	Y	RE	F	110
AB0262	5	F	A	1.50	-0.75	10	3.50	0.00	0	0.075	0.300	MICRO X	Y	LE	E	0
AB0123	5	M	WBR	6.00	-1.00	90	1.00	0.00	0	0.800	0.075	ANI	Y	RE	F	55
AB0197	5	M	WBR	1.25	1.50	90	1.26	3.00	90	0.050	0.250	ANI	Y	LE	F	110
AB028	5	F	A	5.00	-2.00	15	6.00	-2.50	20	0.15	0.50	ANI	Y	LE	E	0
AB0255	5	F	A	-5.00	4.00	105	-3.00	4.00	85	0.4	0.0	ANI	Y	RE	F	55
AB0204	5	M	A	3.75	3.50	110	4.25	2.50	75	0.400	0.275	ESO	Y	RE	E	0
AB0214	6	M	A	1.00	-2.50	10	1.00	-1.75	175	0.275	0.075	AM	N	RE	F	110
AB0208	5	F	BR/C	2.25	-0.25	180	4.50	-1.00	180	0.050	0.250	ANI	Y	LE	F	55
AB0217	5	F	WBR	1.50	0.00	0	5.50	0.00	0	0.025	0.325	ANI	Y	LE	F	55

AB0212	5	F	WBR	1.50	-0.50	90	6.00	-0.50	90	0.000	0.425	MICRO X	Y	LE	E	110
AB0186	5	M	BR/C	-2.00	1.00	20	1.50	0.00	0	1.000	0.050	ESO	Y	RE	E	0
AB0074	5	M	WBR	1.25	1.00	90	1.25	0.50	90	0.575	0.050	MICRO	N	RE	E	0
AB0185	5	F	WBR	4.50	0.00	0	2.00	0.00	0	0.350	0.125	EXP	Y	RE	F	55
AB0200	7	M	WBR	4.50	0.00	0	1.75	0.00	0	0.850	0.025	MICRO	Y	RE	E	0
AB0207	5	M	WBR	0.75	-2.25	30	0.75	-2.25	170	0.275	0.550	ESO	N	LE	F	0
AB0252	4	M	A	2.75	-2.75	10	1.00	-1.00	175	0.475	0.175	ANI	Y	RE	F	0
AB0244	5	F	WBR	2.50	0.00	0	3.00	0.50	180	0.00	0.20	MICRO	Y	LE	E	110
AB0241	5	F	A	2.25	-0.75	180	4.50	-1.50	5	0.10	0.40	ANI	Y	LE	E	340
AB0219	6	F	A	-1.75	3.00	90	-1.25	3.00	90	0.275	0.05	AM	N	RE	F	0

Legend for Data Sets: RE = right eye LE = left eye ANI = anisometropia DEXO = distance exotropia ESA = accommodative esotropia ESO = esotropia EXP = exophoria MICRO = microtropia MICRO X = microexotropia Vert = vertical deviation WBR = white British A = Asian BR/C = British Caribbean F = female M = male E = eccentric F = foveal

Chapter 7. Foveal Pit Topography in Amblyopia

7.1 Introduction

The configuration of the fovea is distinctive; it is characterised by being an avascular, rod-free zone of approximately 1.5 mm in diameter. In the centre of the pit is located the foveola (diameter 0.35 mm), a smaller central area where only cones and glial cells are situated (see Chapter 1, Figure 1.4). It is in this area the highest density of cones is found (Provis and Hendrickson, 2008). The unique feature of the fovea is the displacement of the connecting cells onto the foveal rim. This formation is believed to prevent light scatter, enabling high spatial resolution (Rowe and Dreher, 1982). The concentration of cones reduces exponentially away from the fovea and outside of the macular region there are few cones, the retina being dominated by rods (Miller, 2005) (see Chapter 1, Figure 1.4).

Information regarding the topography of the human foveal pit is limited. An histological study investigating foveal structure measured the slope of the foveal pit of an excised human retina and found it to be 20º (Polyak, 1941). An attempt to mathematically model the slope of the foveal pit using two differing entoptic phenomena, the Stiles-Crawford effect and fundal scatter, estimated the slope to be 43°(Williams, 1980). Recently, two studies utilising OCT technology combined with mathematical modelling of the foveal metrics have investigated foveal pit morphology in visually normal adult subjects (Dubis et al., 2009) and in subjects

diagnosed with retinopathy of prematurity (Hammer et al., 2008). Dubis et al found the foveal slope to be 12 ± 0.32 º (± sem). The study noted significant variation in pit structure (depth, diameter, and slope) in visually normal individuals, although not between the right and left eyes where a high degree of symmetry was observed (Foveal pit depth - Pearson r = 0.9185 p<0.0001). Hammer et al described the fine structure of the fovea in both visually normal adult subjects (n=5) and those with a history of mild retinopathy of prematurity (ROP) (n=5) using adaptive optics-Fourier domain optical coherence tomography (AO-FDOCT). The foveal pit was found to be wider and shallower in ROP participants than in control subjects and an avascular zone was not identified in the subjects with ROP but was present in all of the control subjects (normal mean pit depth = 121μm, ROP subjects = 53μm).

Foveal thickness measures ,mean retinal thickness measured with the macular grid from the inner limiting membrane (ILM) to the retinal pigment epithelium (RPE), (Figure 7.1) using OCT have been obtained in amblyopia (Huynh et al., 2009). However, the standard OCT image analysis software only provides limited information on foveal structure, quoting mean thickness measurements in the foveal and macular areas (Figure 7.1). Without an indication of the detailed topography (e.g. width, depth and slope) the usefulness of the measures are limited, this detailed quantitative description of the structure of the architecture of foveal pit in amblyopia is only just beginning to emerge with the development and improvement in imaging techniques.

Amblyopia is a condition where there is reduction in visual acuity despite optimal optical correction and the absence of any pathology (see Chapter 3). The aetiology of amblyopia is currently believed to be cortical in origin (Hess, 2001; Hubel, 1963; Hubel and Wiesel, 1968, 1998), although retinal involvement in amblyopia has been the subject of long-standing controversy. Recently, the hypothesis that amblyopia is of cortical origin(Hess, 2001) has been challenged and some research studies suggest that retinal structure may be affected in amblyopia (Huynh et al., 2009; Lempert, 2003; Yen et al., 2004) (see Chapter 6). Unfortunately these results are by no means clear cut and for every study that has claimed retinal involvement (Huynh et al., 2009; Lempert, 2003; Yen et al., 2004) many more have found no evidence (Altintas et al., 2005; Bozkurt et al., 2003; Repka et al., 2006; Repka et al., 2009b). Given that visual acuity is reduced in amblyopia it is logical to investigate foveal structure. As well as foveal structure, retinal structures likely to affect visual acuity include the papillomacular bundle, where the retinal nerve fibres from the fovea travel to the optic disc and also the areas at the disc where these fibres are received. By examining the structure of the central visual pathway, the question of whether there is retinal involvement in amblyopia can thus be examined.

Given the 3 ways in which retinal structural defects could be interpreted in relation to the presence of amblyopia described earlier the aim of this experimental chapter is to topographically map the structure of the fovea, so as to produce detailed measurements on foveal thickness, foveal diameters, foveal pit depth and slope of the pit walls. In chapters 8 and 9, respectively, the structure of the papillomacular bundle and disc structure in amblyopes will also be compared to visual normals.

7.2 Methods

7.2.1 Subjects

A total of five subject groups were recruited to the study; two groups of amblyopes (36 adult amblyopes and 27 amblyopic children), two groups of control subjects (47 visually normal adults and 73 visually normal children) plus a group of adults without amblyopia (n= 14) but with strabismus (n= 5), anisometropia (n=4) or both strabismus and anisometropia (n= 5). The participants were recruited from the staff and student populations at the University of Bradford (via the University's Eye Clinic) via local optometry practices, via the Ophthalmology and Orthoptic clinics at local hospitals and from the local community via a press release. The visually normal children (4-5 years) were recruited from the reception classes of three local schools. A complete description of the participants in each category and the procedures undertaken are detailed in Chapter 6.

7.2.2 Fourier Domain Optical Coherence Tomography (OCT)

Fourier-domain OCT provides 3D images of the retina (Drexler and Fujimoto, 2008; Van Velthoven et al., 2007) producing high resolution scans (see chapter 4). However, the current technological configuration of both time-domain and Fourier-domain OCT, which provides the mean thickness measurement of the fovea, does not provide detailed quantitative dimensional measurements of the structure of the foveal pit. In this study, a mathematical algorithm was applied to B-scans that directly cross the centre of the foveal pit providing topographic mapping and accurate measurement of foveal structure. The topography of the foveal pit is of interest here because it will allow the diameter, depth, area, and slopes of the pit sides to be determined.
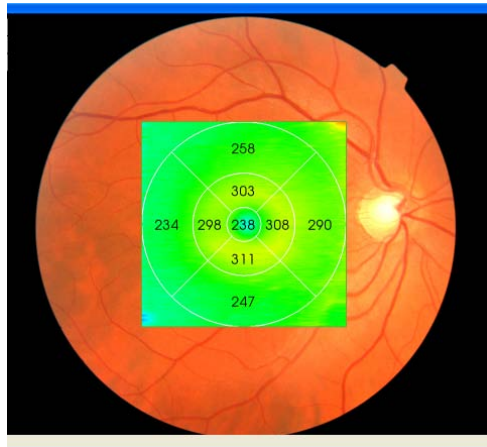
Figure 7.1: Topcon Macular OCT 3D-1000 scan from a RE providing mean retinal thickness measurements (µm) for the 9 macular areas depicted. The pale central circle represents the fovea. This is where retinal thickness is at its thinnest, reflecting the position of the foveal pit.

All participants were imaged using the 3D OCT-1000 (Topcon, Tokyo, Japan) with version 2.00 software. The parameters for all scans in this study were a 3D - macula scan covering 6 x 6 mm, resolution 256 x 256 (65,536 axial scans) imaging the complete macular area (see Chapter 4). In the majority of studies of retinal structure using imaging technology there are high exclusion rates. A number of studies using time-domain OCT (see Chapter 4) have excluded amblyopes due to poor of eccentric fixation (Baddini-Caramelli et al., 2001; Colen et al., 2000; Dickmann et al., 2009; Repka et al., 2006; Yoon et al., 2005). Two studies (Baddini-Caramelli et al., 2001; Colen et al., 2000) had very high exclusion rates amongst the amblyopic cohorts, with 50% and 52% of recruits, respectively, being excluded due to the presence of eccentric fixation and / or difficulty maintaining fixation, resulting in the inability to obtain accurately centred scans. The high exclusion rates found with time-domain OCT can be attributed to the method of obtaining the macular scan. In order for the scan to be accurate 6 radial B-scans are required to be centred on the fovea (see Chapter 4). The inability to centre the scan, in the presence of eccentric fixation, an essential criterion for imaging using time-domain OCT technology, leads to an un-useable image with a low score. The high exclusion rate is likely to affect the outcome of the studies in amblyopes as it estimated that around 80% of amblyopes have eccentric fixation (Brock and Givner, 1952; Burian and Cortimiglia, 1962; Stewart et al., 2005).

In order to address this issue in the present study, the centre of the fovea was identified manually and an individual B-scan which traversed the fovea was

selected for both the horizontal and the vertical scan meridians. Foveal
identification was indicated by the presence of the bright foveal reflex, present in all
but 7 of the scans, (1 horizontal and 1 vertical scan in the adult normal group and 3
horizontal and 2 vertical in the amblyopic adult group). Where the reflex could not
be identified the area of greatest separation between the inner and outer segments
of the photoreceptors was used to identify the centre of the fovea. The ability to
select and measure individual B-scans allowed the inclusion of all the recruited
amblyopes, even in cases where there was poor visual acuity, unsteady fixation
and / or eccentric fixation.

7.2.3 Magnification

Differences in axial length between eyes was taken into account using a
magnification factor established for the OCT Topcon 3D-1000 based on the
recognized formulae determined by Littman (Littmann, 1982) and Bennett (Bennett
et al., 1994) and modified for the OCT by Leung (Leung et al., 2007) (see Chapter
4).

7.3 Gaussian Function

7.3.1 Modelling the Shape of the Foveal Pit.

The shape of the human fovea has been shown to fit well with the mathematical
model of the Gaussian curve (Figure 7.2); this was initially described by Williams
(1980) when, by means of psychophysical methods he modelled the shape of the

foveal pit, suggesting the use of an inverted Gaussian curve. In mathematical

terms a Gaussian function can be written as the formula given by Equation 1.
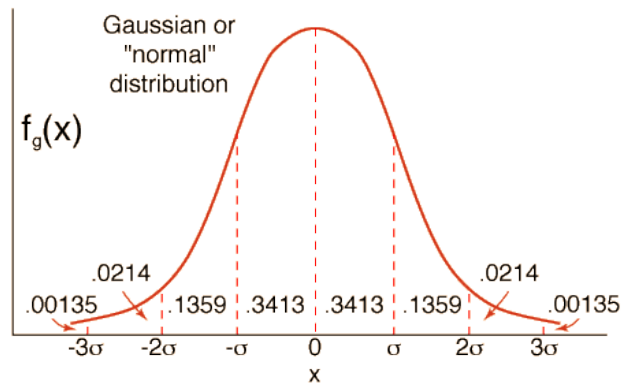
Figure 7.2: Bell curve or Gaussian function depicting the shape of the normal distribution. X =mean value, ō = standard deviation.

$$(x) = a. exp\left(\frac{-(x - \mu)^2}{2\sigma^2}\right)$$

Equation 7.1: a= height of curve peak, μ = position of the centre of the peak, σ = width of the bell curve (standard deviation of the guassian function), exp = Euler's number (exponential constant).

7.3.2 Difference of Gaussian (DoG)

More recently Dubis *et al* (2009) used a Difference of Gaussian (DoG) function
(Equation 7.2) to model the shape of the foveal pit including the foveal rim. The
DoG provides a good mathematical fit as it captures the contour of the foveal pit
and the foveal rim, key areas to measure both the diameter and depth from. The
retinal data thickness measurements are fitted to the DoG using least squares
analysis.

When calculating the difference of Gaussian (DoG), six parameters of the curve fit
are taken into account; the mean height of curve 1 and 2 (a) the standard deviation
(σ) of curve 1 and 2, the positions at the centre of the peaks (μ), plus a constant.
The difference of Gaussian is calculated by subtracting one curve or waveform
from another (Equation 7.2).

<div style="float:right; border:1px solid #c0c; padding:4px;">Comment [I1]: Absolute best?</div>

<div style="float:right; border:1px solid #c0c; padding:4px;">Comment [I2]: Mention 7 parameters to curve fit</div>

$$F(x) = a_1 x\left(exp\left(\frac{-(x-\mu_1)^2}{-2\sigma_1^2}\right)\right) - a_2 x\left(exp\left(\frac{-(x-\mu_2)^2}{-2\sigma_2^2}\right)\right) + constant$$

Equation 7.2: μ_1 and μ_2 = means of the Gaussian curves, σ_1, σ_2 = standard deviations of curve 1 and curve, a_1 and a_2 = heights of curve 1 and 2. Parameters of first and second Gaussians respectively.

7.3.3 Processing of Images

After acquisition and processing of the 3D OCT scan using the standard Topcon procedure , two individual B-scans, one bisecting the fovea horizontally and one crossing it vertically were selected (Figure 7.3). The callipers of the OCT 3D-1000 (software version 2) were used to delineate an artificial x and y axis on the B scans. The individual B-scans were then exported into a shareware software package known as Data Thief III (B. Tummers, DataThief III. 2006 http://datathief.org/) where the inner limiting membrane (ILM) and retinal pigment epithelium (RPE) layers were delineated manually (Figure 7.4). DataThief III is a program designed to extract x and y co-ordinates from a graph or figure. In this study it was utilised to provide x, y co-ordinates for the points manually marked on the internal limiting membrane layer (ILM) and the retinal pigment epithelium (RPE). The ILM-RPE values derived from Data Thief III were then exported into Matlab (Mathworks, Natick, MA, USA) and the data used to provide retinal thickness measures (Figure 7.5). By calculating the difference between the ILM y value (blue circles) and the polynomial fit to the RPE data (dashed red line superimposed to red circles) at the ILM x value, an absolute retinal thickness value is determined.

In Matlab, the foveal pit was subjected to mathematical reconstruction using a Difference of Gaussian (DoG) as previously explained. A customised Matlab programme was designed emulating the procedure advocated by Dubis et al (2009) to automatically identify the thinnest and thickest points of the foveal pit. After the data was initially run through Matlab a number of scans were identified with a poor fit. These scans tended to curve at the periphery, towards the edge of the 6 mm

211

Comment [13]: Raise discussion with BTB/IP

Comment [14]: Mention calliper use in Topcon to provide artificial axes

Comment [15]: Here used to get x/y co-ords of various points on layers, RPE &ILM

Comment [16]: And used to derive retinal thickness values by calculating the difference b/w ILM y value and y value of polynomial fit to RPE data at the ILM x value.

Comment [17]: Lowest/highest = thinnest & thickest

scan and although this was well away from the foveal pit it influenced the curve fitting required to reconstruct the shape of the foveal pit. In order to minimise the number of scans with a poor fit, the processed B-scan images were cropped at either side of the foveal pit centre to a maximum of 2mm to eliminate extraneous data in the periphery of the scan which could affect the centring of the curve, ensuring best fit. Once the foveal pit was cropped to a maximum of 2mm either side the DOG was fitted again to obtain the bottom of the foveal pit, the thickest points on the foveal pit rim, and the steepest points on either side of the pit slope (nasal/temporal for horizontal meridian scans and superior/ inferior for vertical scans).
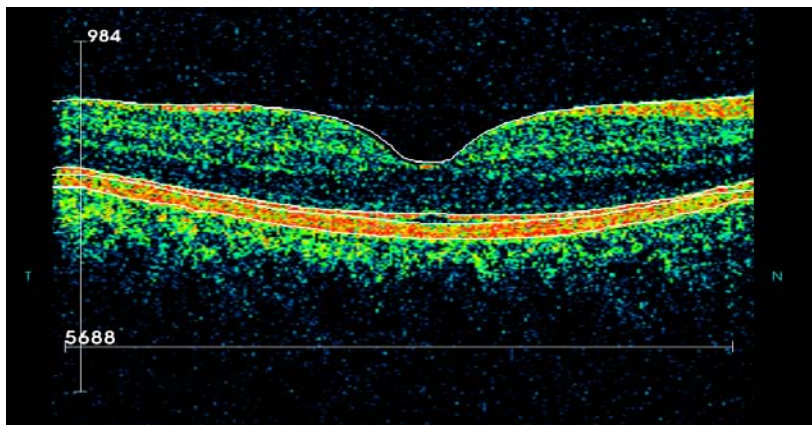
Figure 7.3: Step1 of image processing **-** Horizontal B-scan scan 0001PD635129RH from the OCT 3D-1000 bisecting the fovea (central red reflex).The white lines are the retinal layers identified by the OCT processing prior to export into Data Thief III. The x-axis 5688μm and the y-axis 984μm were manually added during OCT processing prior to export into Data Thief III.
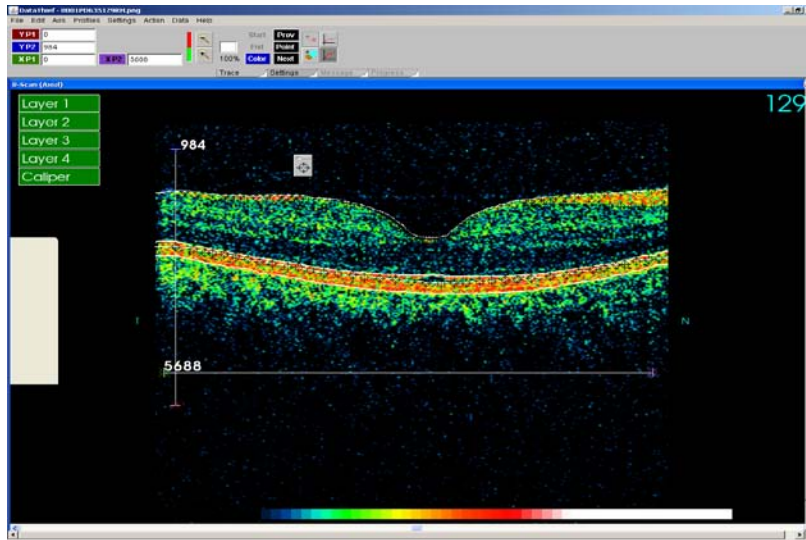
Figure 7.4: Step 2 of image processing **-** Horizontal B-scan scan 0001PD635129RH from the OCT 3D-1000 bisecting the fovea (central red reflex) exported into Data Thief III. The x-axis 5688μm and the y-axis 984μm manually added during OCT processing prior to export into Data Thief III are utilised as the measure for the x and y axis in Data Thief. The retinal layers were delineated manually (black circles) and the measurements saved as a data text file prior to export into Matlab.

0001PD635129RH.txt

XL   sl_L   Xo   Sl_R   XR
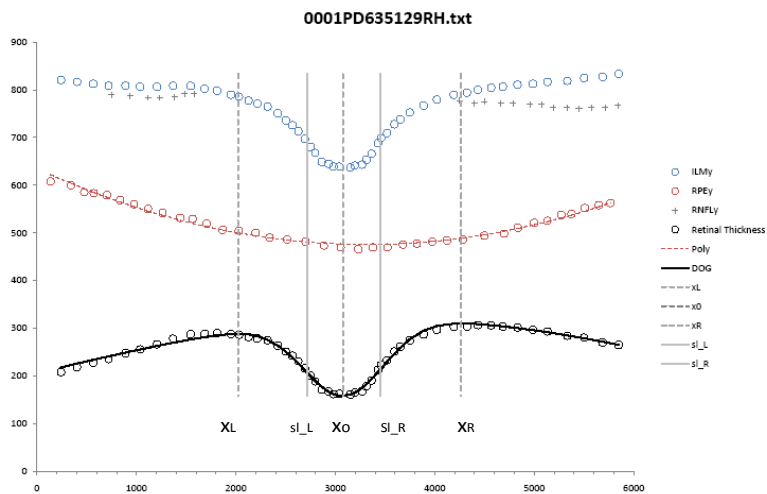
Figure 7.5: Step 3 of the image processing. The Data Thief co-ordinates of the same horizontal scan 0001PD635129RH (Figure 7.3 and Figure 7.4) are imported into Matlab. The mathematical fit of a Gaussian function allows the highest point of the fovea at both the nasal and temporal sides (dotted vertical lines xR and xL), the lowest point in the pit (central vertical dotted line x0) and the pit slope at its steepest points (solid lines sl_R and sl_L) to be identified. The raw thickness data for the B-scan is presented, blue circles indicate internal limiting membrane (ILM), red circles indicate retinal pigment epithelium (RPE). The DoG fit (solid black line) to the data is presented overlaid on the absolute retinal thickness (difference between the ILM_y and RPE_y black circles).

In this study, where the 6mm OCT B-scan is used; the initial assumption of the

curve fit assumes that the fovea is central in the scan (3000μm). After running the

Matlab programme to fit the DoG, if the fit did not pick up the centre of the scan

then the initial values of the six parameters were adjusted to try to improve the

goodness of fit. There are two aspects to the DOG curve fit; the central Gaussian

214

fit and the carrier fit, which takes into account the edges of the scan. In the case of the foveal B-scan it becomes narrower towards the edge. If there is a difference between the centre of the Gaussian curve and the centre of the carrier then there is a "poor fit". When this occurred, in B-scans which narrow slightly towards the periphery, the process was adjusted to take into account the actual centre of the scan (Figure 7.6). This process allowed asymmetrical fitting of the centre and the carrier to account for differences found between the retinal thickness of the nasal and temporal sides; the nasal side is generally thicker than that of the temporal side of the fovea (Polyak, 1941). This process differs from that of Dubis et al (2009) who constrained their curve parameters to having the same central position (μ). The root mean error score of the difference of Gaussian fit ranged from 143.09 – 11452.07 with a mean error score of 1083.76 (SD 931.14).

Comment [I10]: Allowed asymmetrical fitting of centre and carrier to account for asymmetry of ret thick on nas and temp sides of fovea. [Dubis constrained both to have same mu]
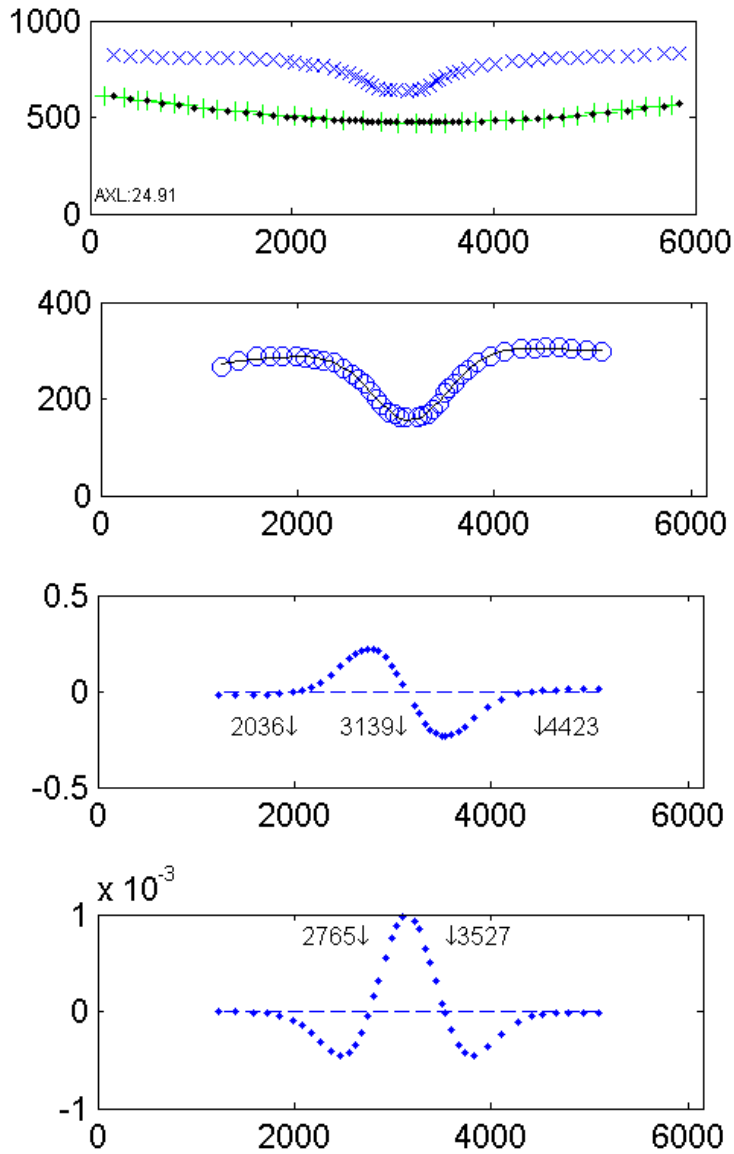
Figure 7.6: Horizontal B-scan 0001PD635129 processed in Matlab. The upper panel shows the raw thickness data produced via the Data Thief Process imported as a text file into Matlab (blue crosses=ILM, green crosses = RPE).The second panel shows the DoG (black line)fitted to the thickness data (blue circles). The third panel depicts the first derivative of the DoG fit. The first derivative identifies the locations of the foveal pit and nasal and temporal peak thickness. The second derivative defines the locations of the steepest slope of the foveal pit (sl_L and sl_R depicted in Figure 7.5).

All participants in the study had a minimum of 4 scans taken, two per eye, one horizontal, one vertical. Thus around a total of 714 scans were included in the study; 151 were from adult amblyopes, 60 from non-amblyopic strabismic or anisometropic adults, 172 from visually normal adults, 235 from child normals and 86 from amblyopic children. Thirty-eight (5%) scans were excluded; 12 from adult amblyopes, 1from a visually normal adult, 20 from visually normal children and 5 from amblyopic children. Three scans were excluded as they were unable to be fitted to the Gaussian curve in Matlab. Thirty-five scans were excluded due to a poor OCT scan that was not able to be processed; this was generally due to movement artefacts caused by unstable and or eccentric fixation which particularly affected the vertical scans of the children and the amblyopes.

The 3-D scans produced by the Topcon 3-D OCT-1000 are made up from the 256 horizontal A-scans that are captured in the horizontal linear raster pattern repeated in vertical steps 256 times producing a 256 x 256 grid of scans. The horizontal B-scan chosen for analysis is one of the horizontal linear raster scans produced from the multiple A-scans traversing the centre of the fovea. The vertical scan however, is not formed from a linear raster scan; it is a production of selected A-scans in vertical alignment and although the central scan was manually chosen to bisect the fovea the effect of horizontal movement produces some variability. The occurrence of eye movement whilst capturing the scan is predominantly in the horizontal meridian and therefore has the potential to affect the vertical alignment of the B-scans, leading to an increase in variation of the vertical scan. In the majority of the

217

adult scans this variation did not occur. However, in the scans of the children's

eyes and the scans of the amblyopic eyes where stable fixation is compromised

the vertical scan quality was reduced by increased motion artefacts.

7.3.4 Foveal Metrics

The measured parameters of the fovea are derived from specific locations within

the original B-scans. Figure 7.7 and Table 7.1 detail the foveal parameters that

were evaluated and describe how these have been defined in this study.
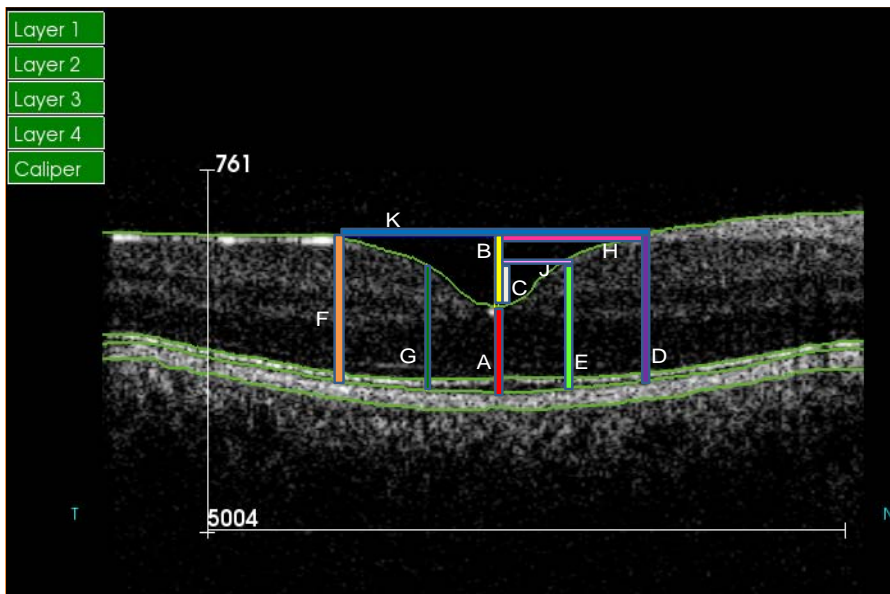
Figure 7.7: Horizontal macular B-scan AB00011578128RH bisecting the fovea (bright white central reflex at the bottom of the foveal pit), detailing the measured foveal parameters (coloured lines) described in Table 1. N = nasal and T = temporal.

Table 7.1: Details of the foveal metrics measured in this study. The foveal parameters are derived from the five locations detailed for the black curve in Figure 7.4 (x_L x_R; sl_L, sl_R and xO). In vertical scans nasal=superior, temporal = inferior.

Measured Parameter	Definition of Foveal Metric
Foveal Thickness (**A**)	Distance from ILM to RPE centred at the fovea (red line)
Pit Depth (max) (**B**)	Distance from the top height (mean of temporal & nasal heights) to the lowest point of the pit at the fovea (yellow line).
Pit Depth (mid) (C)	Distance from the mid height (steepest point on the nasal & temporal slopes) to the lowest point of the pit at the fovea (grayish/white line).
Nasal Thickness (max) (D)	Distance from the highest nasal point on the pit rim to the RPE (purple line).
Nasal Thickness (mid) (E)	Distance from the mid height (steepest point on the slope) to the RPE (bright green).
Temporal Thickness (max) (F)	Distance from the highest temporal point on the pit rim to the RPE (orange line).
Temporal Thickness (mid) (G)	Distance from the mid height (steepest point on the slope) to the RPE (turquoise line).
Nasal Width (max) (H)	Horizontal distance between highest nasal point on the pit rim to central foveal point x0 (Fig.1) (bright pink line).
Nasal Width (mid) (J)	Horizontal distance from the mid height (steepest point on the slope) to central foveal point x0 (Fig.1) (lilac line).
Nasal Retinal Triangle (Figure 7.8)	Area of the retinal triangle: ½ x Height from highest nasal point on the pit rim to ILM centred at the fovea x width from central foveal point x0 to point x_R or x_L (nasal point).
Nasal Retinal Base (Figure 7.8)	Area of the rectangle at the base: Height from ILM to RPE centred at the fovea x width from central foveal point x0 to point x_R or x_L (nasal point).
Foveal Slope Nasal	Angle at the steepest point on the nasal slope of the horizontal B scan.
Foveal Slope Temporal	Angle at the steepest point on the temporal slope of the horizontal B scan.
Horizontal Diameter (max) (K)	Diameter across the foveal pit from the highest nasal point to the highest temporal point (bright blue line).
Vertical Diameter (max) (K)	Diameter across the foveal pit from the highest superior point to the highest inferior point.
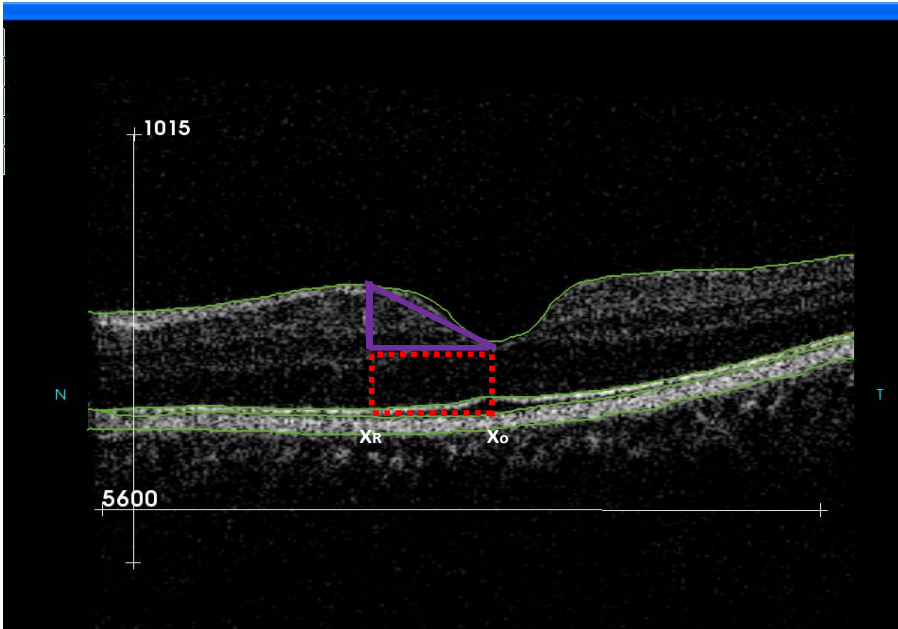
Figure 7.8: Horizontal macular B-scan 0009PD707127LH bisecting the fovea , detailing the measured foveal parameters Nasal Retinal Triangle (purple triangle) and Nasal Retinal Base (red dotted line) described in Table1. N = nasal and T = temporal.

7.4 Statistical Analysis

Statistical analysis was carried out using commercially available Stata SE version 10.0. Paired t-tests were used to directly compare the inter-ocular symmetry between eyes for each group (Table 7.2) for adults and children for all measured foveal parameters (Figure 7.7 and Table 7.1). ANOVA of the differences between each group was used to evaluate the group differences. 2 sided t-tests were used to explore the difference between visually normal and amblyopic children and ANOVA was used to explore the differences between visually normal adults, amblyopic adults and non-amblyopic adults with strabismus and/or anisometropia, for all measured foveal parameters. All ANOVA's were carried out using the Bonferroni correction.

The Bonferroni correction is a common statistical technique to account for multiple group comparisons (Bland, 1995). Conventionally the statistically significant probability value is taken to be p <0.05 i.e. a 1in 20 chance of finding a difference where none exists and a 19 out of 20 chance or 0.95 probability of finding no difference. However if a further comparison is undertaken and the two results are compared the probability of finding no difference is reduced 0.95 x 0.95 = 0.90. The greater the number of comparisons undertaken the greater the chance that a significant result may be found, producing a false positive result (Type I error). Bonferroni's correction adjusts the probability level in order to compensate for the repeated tests. The adjustment is made to the probability level by multiplying it by the number of comparisons made.

221

Table 7.2: Categorisation of the groups and eye categories used for statistical analysis.

Groups	Eye Categories (five)
Visual Normals (adults & children)	One randomly chosen Visually Normal Eye
Amblyopes (adults & children)	Amblyopic Eye
	Fellow Eye
Non-amblyopic participants (adults)	Strabismic and/or eye with the highest refractive error (S/A eye)
	S/A Fellow Eye

7.5 Results

7.5.1 Normal Foveal Topography – Adults

Foveal parameters (Figures 7.7, 7.8 and Table 7.1) were measured in both the horizontal and vertical meridians from scans that bisected the centre of the fovea (Figure 7.3). A summary of the results of all the foveal parameters in adult normals for both the horizontal (nasal – temporal meridian) and the vertical (superior – inferior meridian) scans is provided in Table 7.3.

The foveal thickness was found to be similar when measured both in the horizontal (184.18μm ± 20.73) and vertical meridians (184.94μm ± 19.42), paired t-test: p=0.861 CI: -9.37 to 7.85). The retinal thickness (highest point from the top of the pit (max) to the Retinal Pigment Epithelium); (Figure 7.7 and Table 1) was found to be of similar thickness in the nasal (321.67μm ±17.40), superior (320.53μm ±17.18)

and inferior (316.46µm ± 16.48) meridians but was significantly thinner in the temporal meridian (295.38µm ± 17.67), paired t-test temporal thickness v inferior thickness; p=0.000, diff= -21.09, CI: -28.41 to -13.76). (Table 7.3).

The pit depth (max) (Figure 7.7 and Table 7.1) for visually normal adults was 124.34µm (SD 19.50µm) in the horizontal meridian and 133.56µm (SD 18.87) in the vertical meridian, this difference was significant (paired t-test p=0.028, diff = -9.21 CI: -17.44 to -0.98). The difference between the horizontal and vertical pit depth (max) is likely to be related to the reduced thickness measurement on the temporal side, which will effectively reduce the overall pit depth measurement in the horizontal meridian, since it is calculated from the mean of the nasal and temporal thickness, as opposed to the vertical pit depth (max), as the parameter is calculated from the mean of the superior and inferior thickness measurements. (Table 7.1).

The nasal pit slope was 12.67º (SD 2.2) and the temporal slope was 11.18º (SD 2.1). This difference between the nasal slope and the temporal slope was significant (paired t-test: diff = 1.48º p = <0.001; CI: 1.3º to 1.7º). The slope of the foveal pit in the vertical meridians was steeper, with the superior slope measuring 14.75º (SD 2.3) and the inferior slope measuring 14.49º (SD 2.4). A summary of the results of parameters in adult normals for both the horizontal foveal scans and the vertical foveal scans is provided in Table 7.3.

7.5.2 Horizontal and Vertical Foveal Pit Diameter

A significant difference was found between the pit diameters along the horizontal and vertical meridians. This indicates that the foveal pit is slightly oval in shape. It has an increased width horizontally. The mean normal adult horizontal diameter was 2109.9µm (SD 225.9), and mean normal adult vertical diameter was 1773.6µm (SD 181.96). The mean pit horizontal diameter/vertical diameter ratio was therefore 1.19 and this ratio is broadly similar to that reported by (Hammer et al., 2008) who reported a value of 1.1.

Table 7.3: Mean foveal topography measurements ± SD for visually normal adults both in the horizontal and vertical scan meridians taken from the parameters detailed in Figure 7.5. The results of paired t-tests between horizontal scans v vertical scans in for each foveal parameter are shown.

Foveal Parameter	Adult Visually Normal Eye, Horizontal Scan(mean μm ± SD)	Adult Visually Normal Eye, Vertical Scan(mean μm ± SD)	Horiz v Vert Scan Paired T-Test (μm)
Foveal Thickness	184.18μm (20.73)	184.94μm (19.42)	diff= -0.76 p=0.861 CI: -9.37 to 7.85
Thickness (Max)	**Nasal** 321.67μm (17.40)	**Superior** 320.53 μm (17.18)	diff=1.14 p=0.76 CI: -6.27 to 8.56
Thickness (Mid)	**Nasal** 240.54 μm (16.98)	**Superior** 242.71 μm (15.56)	diff= -2.16 p=0.54 CI:-9.15 to 4.82
Thickness (Max)	**Temporal** 295.38 μm (17.67)	**Inferior** 316.46 μm (16.48)	diff= -21.09 **p<0.001** CI: -28.41 to -13.76
Thickness (Mid)	**Temporal** 231.13 μm (16.87)	**Inferior** 242.13 μm (14.75)	diff= -10.99 **p=0.002** CI:-17.79 to - 4.20
Retinal Base Area	**Nasal** 206614 μm^2 (28447)	**Superior** 164025 μm^2 (20404)	diff= 42589 **p<0.001** CI: 31972 to 53205
Retinal Triangle Area	**Nasal** 77772 μm^2 (16104)	**Superior** 60573 μm^2 (11986)	diff= 17199 **p <0.001** CI: 11111 to 23287
Pit Depth (max)	124.34 μm (19.50)	133.56 μm (18.87)	diff = -9.21 p=0.029 CI: -17.44 to -0.98
Pit Depth (mid)	51.66 μm (7.97)	57.48 μm (8.64)	diff = -5.82 **p= 0.0017** CI: -9.38 to -2.25
Pit Diameter (max)	2109.9 μm (225.9)	1773.6 μm (181.96)	diff = 336.32 **p<0.001** CI:248.35 to 424.29
Pit Diameter (mid)	762.26 μm (95.55)	684.24 μm (85.12)	diff = 78.02 **p<0.001** CI:39.21 to 116.82
Max Width	**Nasal** 1126 μm (130.08)	**Superior** 890.14 μm (93.85)	diff= 235.91 **p<0.001** CI:187.27 to 84.56
Mid Width	**Nasal** 394.97 μm (51.74)	**Superior** 342.99 μm (43.23)	diff = 51.98 **p<0.001** CI: 31.53 to 72.43
Foveal Slope	**Nasal**:12.67º (2.2)	**Superior**:14.75º (2.3)	diff = -2.09º **p<0.001** CI: -3.04 to -1.13
Foveal Slope	**Temporal**:11.18º (2.1)	**Inferior**:14.49º (2.4)	diff=-3.30º **p <0.001** CI:-4.27 to -2.34

7.5.3 Inter-ocular Symmetry (IOS)

Visually normal eyes were first examined in order to establish the degree of inter-ocular asymmetry that can exist in normals. If foveal structure is linked to the visual deficit in the amblyopic eye then inter-ocular asymmetry between the eyes in amblyopes would need to exceed that which can be expected in visual normals. There are claims that the fellow eye of amblyopes show subtle structural differences in size and shape of the optic disc (Pineles and Demer, 2009). If this is the case then both eyes in amblyopes may show differences in foveal structure relative to normals and it is thus necessary to examine inter-ocular symmetry as well as differences in absolute foveal structural parameters between amblyopic and normal eyes.

7.5.3.1 Adult Visually Normal Eyes

A high degree of symmetry between the right and left eyes was found in all measured foveal parameters, both in the horizontal and the vertical meridians. Although no significant difference was found between the right and left eyes, a degree of variation exists within the visually normal eyes. The foveal thickness parameter (RE = 185.51 ± 23.10 and LE = 182.80 ± 18.40 p= 0.67) has a confidence interval from -15.62 to 10.17µm indicating some individual variation within the normal expected range. Similarly, the nasal thickness (max) parameter (RE = 295.16 ± 19.91and LE = 295.60 ± 15.47 p= 0.937) has a confidence interval from -10.58 to 11.45µm indicating some individual variation. This variation of

around 5% is reflected across all the parameters. The results are presented in Table 7.4.

7.5.3.2 Visually Normal Children

The degree of inter-ocular symmetry in the eyes of visually normal children was also analysed. A high degree of symmetry between the right and left eyes was found in all measured foveal parameters, both in the horizontal and the vertical meridians. Again although no significant difference was found between the right and left eyes, a degree of variation exists within the visually normal eyes. The foveal thickness parameter (RE = 166.13 ± 14.08 and LE = 165.71 ± 16.50 p= 0.912) has a confidence interval from -8.04 to 7.19µm indicating some individual variation within the normal expected range. This variation was reflected across all the parameters. The results are presented in Table 7.5.

Foveal Parameter	Visually Normal Adult RE Horizontal (mean ± SD)	Visually Normal Adult LE Horizontal (mean ± SD)	Paired T-test	Visually Normal Adult RE Vertical (mean ± SD)	Visually Normal Adult LE Vertical (mean ± SD)	Paired T-test
Foveal Thickness	185.51µm (23.10)	182.80 µm (18.40)	p=0.67 CI:-15.62 to 10.17	184.30 µm (21.16)	185.62 µm (17.91)	p= 0.826 CI:-10.78 to 13.43
Nasal/Superior Thickness (max)	321.06 µm (17.73)	322.33 µm (17.48)	p=0.815 CI: -9.58 to 12.12	318.42 µm (17.91)	322.74 µm (16.51)	p=0.416 CI: -6.30 to 14.94
Nasal/Superior Thickness (mid)	241.59 µm (19.90)	239.45 µm (13.68)	p=0.685 CI: -12.71 to 8.43	241.59 µm (17.16)	243.79 µm (14.04)	p=0.660 CI: -7.56 to 11.80
Temporal/Inferior Thickness (max)	295.16 µm (19.91)	295.60 µm (15.47)	p=0.937 CI: -10.58 to 11.45	316.09 µm (17.58)	316.86 µm (15.66)	p=0.88 CI: -9.50 to 11.04
Temporal/Inferior Thickness (mid)	232.14 µm (20.09)	230.08 µm (13.09)	p=0.694 CI: -12.56 to 8.44	241.95 µm (16.99)	242.32 µm (12.40)	p=0.936 CI: -6.86 to 10.23
Nasal/Superior Retinal Base Area	206022 µm^2 (28629)	207234 µm^2 (28949)	p=0.891 CI: -16524 to 18947	160953 µm^2 (19479)	167244 µm^2 (21322)	p=0.318 CI: -6276 to 18860
Nasal/Superior Retinal Triangle Area	76022 µm^2 (14697)	79606 µm^2 (17632)	p=0.472 CI: -6395 to 13562	59317 µm^2 (12640)	61889 µm^2 (11418)	p=0.488 CI:-4858 to 10003
Pit Depth (max)	122.60 µm (16.62)	126.17 µm (22.40)	p=0.554 CI: -8.54 to 15.69	132.96 µm (17.15)	134.18 µm (20.93)	p=0.835 CI:-10.54 to 12.98
Pit Depth (mid)	51.35 µm (6.90)	51.98 µm (9.12)	p=0.801 CI: -4.34 to 5.59	57.52 µm (8.24)	57.43 µm (9.25)	p=0.976 CI: -5.47 to 5.31
Pit Diameter (max)	2098 µm (228)	2122 µm (228)	p=0.730 CI:-116.49 to164.84	1753.91 µm (180.80)	1794.19 µm (185.32)	p=0.475 CI:-72.48 to 153.04
Pit Diameter (mid)	765.35 µm (93.99)	759.03 µm (99.37)	p=0.831 CI: -65.87 to 53.23	683.63 µm (94.55)	684.88 µm (76.34)	p=0.962 CI: -51.83 to 54.33
Nasal/Superior Width (max)	1116 µm (128.80)	1137 µm (133.75)	p= 0.609 CI: -60.26 to 101.45	877.77 µm (92.94)	903.10 µm (95.29)	p=0.383 CI: -32.65 to 83.30
Nasal/Superior Width (mid)	396.74 µm (50.63)	393.11 µm (54.06)	p= 0.821 CI: -35.87 to 28.61	341.70 µm (47.32)	344.34 µm (39.62)	p= 0.844 CI: -24.30 to 29.59
Nasal/Superior Foveal Slope	12.51º (1.73)	12.83º (2.58)	p= 0.6352 CI: -1.03 to 1.67	14.68º (1.78)	14.84º (2.77)	p= 0.821 CI: -1.26 to 1.59
Temporal/Inferior Foveal Slope	11.04º (1.84)	11.33º (2.41)	p= 0.660 CI: -1.03 to 1.61	14.53º (1.81)	14.44º (2.90)	p= 0.910 CI: -1.57 to 1.40

Table 7.4: Foveal topography measurements ± SD of the RE and LE in visually normal adults. Paired t-tests for each foveal parameter are shown.

Foveal Parameter	Visually Normal Child RE, Horizontal (mean ± SD)	Visually Normal Child LE, Horizontal (mean ± SD)	Paired T-test	Visually Normal Child RE, Vertical (mean ± SD)	Visually Normal Child LE, Vertical (mean ± SD)	Paired T-test
Foveal Thickness	166.13 µm (14.08)	165.71 µm (16.50)	p=0.912 CI: -8.04 to 7.19	167.99 µm (18.20)	170.92 µm (15.65)	p=0.54 CI: -6.60 to 12.45
Nasal/Superior Thickness (max)	309.79 µm (17.90)	307.53 µm (17.94)	p=0.614 CI: -11.14 to 6.63	311.48 µm (20.68)	308.43 µm (33.48)	p=0.70 CI: -19.14 to 13.04
Nasal/Superior Thickness (mid)	225.22 µm (12.65)	224.09 µm (14.19)	p=0.737 CI: -7.79 to 5.55	229.24 µm (17.52)	230.93 µm (12.82)	p=0.694 CI: -6.86 to 10.23
Temporal/Inferior Thickness (max)	286.71 µm (19.18)	286.74 µm (20.58)	p=0.996 CI: -9.84 to 9.89	304.51 µm (17.79)	300.69 µm (40.14)	p=0.674 CI: -21.98 to 14.32
Temporal/Inferior Thickness (mid)	217.28 µm (12.13)	216.81 µm (15.62)	p=0.894 CI: -7.41 to 6.48	227.59 µm (16.53)	228.15 µm (16.60)	p=0.905 CI: -8.81 to 9.93
Nasal/Superior Retinal Base Area	182402 µm (27636)	177502 µm (28756)	p=0.487 CI: -18886 to 9087	156282 µm (29093)	159876 µm (15686)	p=0.582 CI: -9432 to 16618
Nasal/Superior Retinal Triangle Area	78345 µm (10491)	76591 µm (17574)	p=0.628 CI: -8956 to 5448	66454 µm (11663)	67483 µm (15232)	p=0.793 CI: -6795 to 8852
Pit Depth (max)	132.12 µm (19.69)	131.43 µm (19.80)	p=0.888 CI: -10.48 to 9.10	140.00 µm (17.68)	133.64 µm (35.51)	p=0.438 CI: -22.71 to 9.98
Pit Depth (mid)	55.12 µm (8.46)	54.75 µm (8.19)	p=0.858 CI: -4.49 to 3.76	60.42 µm (7.33)	58.62 µm (10.04)	p=0.476 CI: -6.85 to 3.25
Pit Diameter (max)	2064 µm (249.91)	2034.65 µm (280.9)	p=0.656 CI:-161.5 to 102.34	1847.69 µm (252.76)	1868.38 µm (240.61)	p=0.767 CI:-118.5 to 159.88
Pit Diameter (mid)	734.77 µm (120.16)	721.15 µm (102.73)	p=0.625 CI: -68.98 to 41.73	718.84 µm (153.74)	700.83 µm (103.72)	p=0.621 CI: -90.74 to 54.72
Nasal/Superior Width (max)	1097 µm (129.14)	1076 µm (171.04)	p= 0.578 CI: -96.38 to 54.22	928.65 µm (130.42)	905.80 µm (205.94)	p=0.647 CI: -122.43 to 76.73
Nasal/Superior Width (mid)	361.63 µm (79.11)	353.72 µm (50.95)	p= 0.572 CI: -35.68 to 19.89	361.63 µm (79.11)	353.72 µm (50.95)	p= 0.668 CI: -44.73 to 28.92
Nasal/Superior Foveal Slope	13.94º (2.88)	13.94º (2.41)	p= 0.999 CI: -1.31 to 1.32	15.22º (3.32)	14.74º (2.27)	p= 0.546 CI: -2.06 to 1.10
Temporal/Inferior Foveal Slope	12.58º (2.81)	12.73º (2.31)	p= 0.812 CI: -1.12 to 1.42	14.68º (3.38)	14.28º (2.23)	p= 0.607 CI: -1.99 to 1.18

Table 7.5: Foveal topography measurements ± SD of the RE and LE in visually normal children. Paired t-tests for each foveal parameter are shown.

7.5.3.3 Adult Amlyopes

As with visual normals, a high degree of symmetry was found between the amblyopic eyes and fellow eyes, both in the horizontal and the vertical meridians. (Table7.6).

7.5.3.4 Non-Amblyopic Adults

A high degree of symmetry was demonstrated between the strabismic eye and/or the eye with the highest refractive error (S/A eye) and its fellow in the non-amblyopic group. (Table 7.7).

7.5.3.5 Amblyopic Children

A high degree of symmetry was found between the amblyopic eye and the amblyopic fellow eyes, both in the horizontal and the vertical meridians in amblyopic children. Only one parameter came close to reaching statistical significance between the amblyopic and the fellow eye. The inferior thickness (max) was greater in the amblyopic eye than the fellow eye and this difference came close to significance (p=0.054 CI: -0.26 to 26.70). The confidence interval is however wide and examination of the data shows a number of outliers in the inferior measurements of the fellow eye group skewing the data. (Figure 7.9). No

difference was found in the horizontal meridian (nasal and temporal heights) or in the superior height measurement of the vertical meridian. (Table 7.8).

Foveal Parameter	Amblyopic Eye Horizontal (mean ± SD)	Amblyopic Fellow Eye Horizontal (mean ± SD)	Paired T-test	Amblyopic Eye Vertical (mean ± SD)	Amblyopic Fellow Eye Vertical (mean ± SD)	Paired T-test
Foveal Thickness	192.95µm (24.82)	191.79 µm (27.51)	p=0.854 CI: -11.35 to 13.65	194.54 µm (22.54)	193.18 µm (25.17)	p=0.815 CI: -10.14 to 12.85
Nasal/Superior Thickness (max)	319.16µm (19.04)	318.52 µm (23.13)	p=0.899 CI: -9.47 to 10.74	316.26 µm (20.19)	319.40 µm (18.65)	p=0.505 CI: -12.47 to 6.20
Nasal/Superior Thickness (mid)	245.63µm(17.41)	244.66µm (19.40)	p=0.828 CI: -7.83 to 9.75	246.44 µm (18.88)	246.83 µm (17.93)	p=0.929 CI: -9.24 to 8.46
Temporal/Inferior Thickness (max)	289.35 µm (16.32)	293.22 µm (17.14)	p=0.337 CI: -11.85 to 4.11	305.79 µm (16.28)	306.1 µm (17.79)	p=0.934 CI: -8.55 to 7.86
Temporal/Inferior Thickness (mid)	234.14 µm (17.68)	234.90 µm (19.43)	p=0.864 CI: -9.62 to 8.10	242.41 µm (16.97)	242.13 µm (17.50)	p=0.945 CI: -7.99 to 8.58
Nasal/Superior Retinal Base Area	211596 µm^2 (37997)	206633 µm^2 (38361)	p=0.588 CI: -13249 to 23175	172992 µm^2 (24882)	172813 µm^2 (27353)	p=0.977 CI: -12397 to 12755
Nasal/Superior Retinal Triangle Area	70048 µm^2 (21818)	69551 µm^2 (23128)	p=0.927 CI:-10227 to 11222	54411 µm^2 (13785)	56754 µm^2 (14934)	p=0.501 CI: -9254 to 4569
Pit Depth (max)	111.30 µm (26.49)	114.08 µm (29.45)	p=0.680 CI: -16.13 to 10.59	116.49 µm (23.47)	119.58 µm (26.75)	p=0.612 CI: -15.20 to 9.01
Pit Depth (mid)	46.93 µm (11.62)	47.99 µm (12.24)	p=0.713 CI: -6.75 to 4.64	49.89 µm (9.80)	51.29 µm (11.56)	p=0.588 CI: -6.56 to 3.75
Pit Diameter (max)	2061 µm (283)	2041 µm (245)	p=0.754 CI: -106.28 to 146	1759 µm (196)	1755 µm (211)	p=0.918 CI: -92.74 to 102.81
Pit Diameter (mid)	762.45 µm (120.62)	767.46 µm (117.56)	p=0.861 CI: -61.83 to 51.79	687.20 µm (101.11)	684.08 µm (101.58)	p= 0.899 CI: -45.59 to 51.83
Nasal/Superior Width (max)	1100 µm (157.53)	1080 µm (149.60)	p= 0.600 CI: -53.93 to 92.62	891.80 µm (99.11)	897.31 µm (107.34)	p=0.825 CI: -55.20 to 44.16
Nasal/Superior Width (mid)	400.63 µm (69.04)	400.41 µm (70.97)	p= 0.989 CI: -33.17 to 33.62	348.91 µm (53.42)	348.57 µm (52.64)	p=0.979 CI: -25.15 to 25.83
Nasal/Superior Foveal Slope	11.75º (2.85)	11.73º (2.68)	p= 0.9801 CI: 11.08 to 12.39	13.21º (3.06)	13.76º (3.85)	p=0.514 CI: -2.23 to 1.12
Temporal/Inferior Foveal Slope	10.01º (2.85)	10.37º (2.75)	p= 0.593 CI: -1.69 to 0.975	12.46º (2.98)	12.81º (3.86)	p=0.672 CI: -2.01 to 1.31

Table 7.6: Foveal topography measurements ± SD of both eyes in amblyopic adults. The results of paired t-tests between the amblyopic eye and amblyopic fellow eye for each foveal parameter are shown.

Foveal Parameter	Strabismic/High Ref Error Eye Horizontal (mean ± SD)	Fellow Eye Horizontal (mean ± SD)	Paired T-test	Strabismic/High Ref Error Eye Vertical (mean ± SD)	Fellow Eye Vertical (mean ± SD)	Paired T-test
Foveal Thickness	179.94 µm (18.31)	183.72 µm (17.81)	p=0.572 CI: -17.28 to 9.73	184.22 µm (22.01)	182.04 µm (16.89)	p=0.762 CI: -12.49 to 16.86
Nasal/Superior Thickness (max)	311.29 µm (15.29)	318.23 µm (18.19)	p=0.267 CI: -19.51 to 5.62	309.93 µm (15.20)	312.35 µm (14.36)	p=0.657 CI: -13.48 to 8.64
Nasal/Superior Thickness (mid)	232.96 µm (12.31)	239.38 µm (10.49)	p=0.135 CI: -14.98 to 2.13	237.73 µm (14.18)	237.14 µm (8.67)	p=0.891 CI: -8.20 to 9.38
Temporal/Inferior Thickness (max)	287.55 µm (16.75)	292.61 µm (20.99)	p=0.472 CI: -19.26 to 9.14	301.22 µm (15.98)	305.74 µm (15.82)	p=0.443 CI: -16.41 to 7.37
Temporal/Inferior Thickness (mid)	223.94 µm (12.91)	230.07 (11.43)	p=0.179 CI: -15.25 to 2.99	235.01 (13.26)	236.71 (9.10)	p=0.685 CI: -10.21 to 6.81
Nasal/Superior Retinal Base Area	198968 µm^2 (30248)	200888 µm^2 (31907)	p=0.867 CI:-25174 to 21334	159866 µm^2 (12805)	161421 µm^2 (17445)	p=0.783 CI: -13000 to 9891
Nasal/Superior Retinal Triangle Area	73520 µm^2 (18574)	73992 µm^2 (18933)	p=0.946 CI:-14500 to 13555	55792 µm^2 (15046)	58298 µm^2 (14271)	p=0.643 CI: -13474 to 8462
Pit Depth (max)	119.48 µm (22.25)	121.71 µm (28.52)	p=0.813 CI: -21.36 to 16.91	121.35 µm (26.26)	127.01 µm (26.47)	p=0.562 CI: -25.38 to 14.07
Pit Depth (mid)	48.51 µm (10.26)	51.01 µm (12.35)	p=0.551 CI: -10.99 to 5.99	52.15 µm (11.60)	54.89 µm (11.19)	p=0.515 CI: -11.27 to 5.78
Pit Diameter (max)	2082 µm (256.77)	2054 µm (233.13)	p=0.758 CI:-155.59 to 211.3	1723 µm (219.51)	1766 µm (176.73)	p=0.552 CI:-192.83 to105.27
Pit Diameter (mid)	749.32 µm (108.85)	753.65 µm (95.15)	p=0.908 CI: -80.79 to 72.13	665.33 µm (105.32)	686.27 µm (76.84)	p=0.539 CI: -89.90 to 48.01
Nasal/Superior Width (max)	1111 µm (157.53)	1093 µm (136.57)	p=0.750 CI:-92.96 to 127.58	876.16 µm (100.28)	888.98 µm (84.10)	p=0.707 CI: -82.04 to 56.41
Nasal/Superior Width (mid)	388.57 µm (61.78)	391.63 µm (51.82)	p=0.884 CI:	336.13 µm (50.20)	343.78 µm (35.89)	p=0.635 CI: -40.29 to 24.99
Nasal/Superior Foveal Slope	12º (2.31)	12.57º (2.92)	p=0.559 CI: -2.54 to 1.40	13.85º (2.53)	14.08º (2.99)	p=0.826 CI: -2.29 to 1.85
Temporal/Inferior Foveal Slope	10.67º (2.63)	11.09º (3.12)	p=0.690 CI: -2.58 to 1.73	13.28º (2.57)	13.67º (2.97)	p=0.704 CI: -2.47 to 1.69

Table 7.7: Foveal topography measurements ± SD of both eyes in anisometropic or strabismic adults without amblyopia. The results of paired t-tests between the strabismic/anisometropic eye (S/A eye) and the S/A fellow eye for each foveal parameter are shown.

233

Foveal Parameter	Amblyopic Eye, Horizontal (mean ± SD)	Fellow Eye, Horizontal (mean ± SD)	Paired T-test	Amblyopic Eye, Vertical (mean ± SD)	Fellow Eye, Vertical (mean ± SD)	Paired T-test
Foveal Thickness	176.52 µm (23.16)	176.74 µm (23.85)	p=0.972 CI: -13.07 to 12.61	178.27 µm (21.94)	181.63 µm (24.36)	p=0.640 CI: -17.80 to 11.07
Nasal/Superior Thickness (max)	320.00 µm (13.33)	318.66 µm (12.39)	p=0.702 CI: -5.68 to 8.38	325.89 µm (13.96)	324.71 µm (18.05)	p=0.814 CI: -8.84 to 11.19
Nasal/Superior Thickness (mid)	234.59 µm (16.90)	235.30 µm (15.85)	p=0.875 CI: -9.65 to 8.24	240.93 µm (16.27)	241.49 µm (17.17)	p=0.914 CI: -10.99 to 9.87
Temporal/Inferior Thickness (max)	294.16 µm (14.18)	293.86 µm (15.52)	p=0.943 CI: -7.83 to 8.41	319.40 µm (15.74)	306.18 µm (26.58)	p=0.054 CI: -0.26 to 26.70
Temporal/Inferior Thickness (mid)	225.67 µm (17.39)	226.34 µm (16.18)	p=0.884 CI: -9.84 to 8.50	238.73 µm (16.42)	236.16 µm (20.77)	p=0.658 CI: -9.06 to 14.19
Nasal/Superior Retinal Base Area	198862 µm^2 (37085)	193188 µm^2 (37217)	p=0.577 CI:-14616 to 25964	167729 µm^2 (29193)	176766 µm^2 (34342)	p=0.362 CI: -28857 to 10785
Nasal/Superior Retinal Triangle Area	81920 µm^2 (21377)	77433 µm^2 (15490)	p=0.381 CI: -5708 to 14682	69437 µm^2 (13376)	69693 µm^2 (18336)	p=0.959 CI: -10200 to 9689
Pit Depth (max)	130.56 µm (22.17)	129.52 µm (23.97)	p=0.868 CI: -11.56 to 13.66	144.38 µm (20.54)	133.82 µm (26.49)	p=0.155 CI: -4.15 to 25.27
Pit Depth (mid)	53.62 µm (9.67)	54.08 µm (10.27)	p=0.866 CI: -5.91 to 4.99	61.56 µm (8.81)	57.20 µm (11.81)	p=0.178 CI: -2.09 to 10.82
Pit Diameter (max)	2093 µm (337)	2055 µm (279)	p=0.651 CI:-130.51 to 207.2	1895 µm (283)	1907 µm (304)	p=0.889 CI: -196 to 170
Pit Diameter (mid)	715.76 µm (128.62)	737.84 µm (141.68)	p=0.552 CI: -95.97 to 51.82	714.08 µm (150.07)	716.70 µm (146.31)	p=0.955 CI: -95.22 to 89.98
Nasal/Superior Width (max)	1136 µm (207.32)	1095 µm (150.21)	p=0.408 CI:-57.80 to 139.93	942.87 µm (132.78)	973.61 µm (139.80)	p=0.469 CI: -115.76 to 54.28
Nasal/Superior Width (mid)	370.22 µm (68.23)	382.27 µm (77.25)	p=0.546 CI: -51.86 to 27.75	359.43 µm (75.65)	364.83 µm (72.89)	p=0.815 CI: -51.82 to 41.03
Nasal/Superior Foveal Slope	14.01º (2.80)	13.78º (3.22)	p=0.787 CI: -1.43 to 1.87	15.62º (3.46)	14.76º (12.91)	p=0.459 CI: -1.46 to 3.16
Temporal/Inferior Foveal Slope	12.52º (2.94)	12.39º (3.28)	p=0.879 CI: -1.57 to 1.83	15.16º (3.41)	13.59º (3.79)	p=0.167 CI: -0.68 to 3.81

Table 7.8: Foveal topography measurements ± SD of both eyes in amblyopic children. The results of paired t-tests between the amblyopic eye and the amblyopic fellow eye for each foveal parameter are shown.
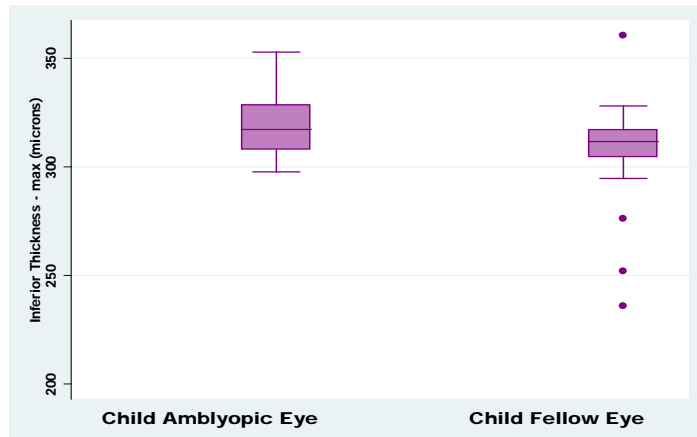
Figure 7.9: Box plots of inferior thickness (max) measurements in the amblyopic and fellow eyes of amblyopic children. A number of outliers can be seen in the inferior meridian measurements taken from the vertical scan (paired t-test of amblyopic v fellow eye inferior height: diff =13μm, p=0.054 CI: -0.26 to 26.70).

7.5.3.6 ANOVA of Differences

In order to identify if the degree of asymmetry differed, the inter-ocular difference found in each group (normal adults, amblyopic adults, amblyopic children and normal children) was analysed to identify any significance between the groups. Only one group difference was identified. (Table 7.9).The scan analysis showed the parameter demonstrating significance was the superior foveal width (max) difference (p= 0.034). On examination of the interactions between the groups the normal adults v the normal children demonstrated significance (p=0.047). On scrutinizing the data a number of outliers can be seen in the group of normal

children (Figure 7.10). It is these outliers that account for the skewed data. The
results of the ANOVA of differences are presented in Table 7.9.
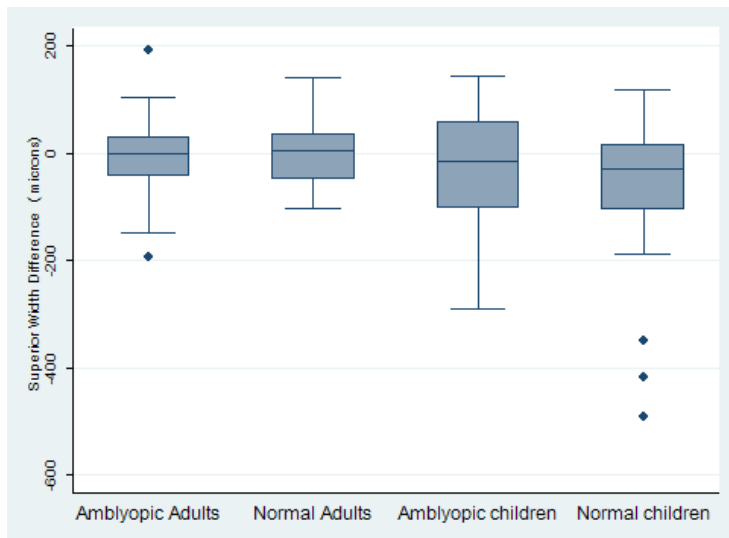
Figure 7.10: Box plots of superior width (max) difference measurements in
normal adults and children and amblyopic adults and children. A number of
outliers can be seen in the measurements taken from the vertical foveal scans
of normal children (superior width difference between visually normal adults v
children p=0.047).

Further analysis of the data did not identify any group differences and inter-ocular
symmetry was consistently demonstrated. This presence of symmetry justifies the
further analysis of foveal structure using direct comparison of the amblyopic eyes
to the visually normal eyes, along with the strabismic/highest refractive error eye
(S/A eye) in adults.

Table 7.9: Results of One-way ANOVA for the comparison of **differences** between the visually normal adults, the visually normal children, the amblyopic adults and the amblyopic children (4 groups). Post-hoc analysis are shown. Adult Norm = normal adult eyes, Adult Amb = adult amblyopic eyes, Child Norm = visually normal child eyes and Child Amb = child amblyopic eyes.

Foveal Parameter *Differences*	Source of variation	Degrees of freedom	Sum of squares	Variance Ratio (F)	Probability	Post-hoc Significance	Post-hoc Non-Significance
Foveal Thickness *Horizontal*	Between groups Within groups	3 166	34.65 14082.72	0.14	0.938		
Foveal Thickness *Vertical*	Between groups Within groups	3 136	331.15 32797.91	0.46	0.712		
Nasal Retinal Thickness *(max)*	Between groups Within groups	3 166	64.58 24507.47	0.15	0.932		
Superior Retinal Thickness *(max)*	Between groups Within groups	3 136	349.21 40205.05	0.39	0.758		
Temporal Retinal Thickness *(max)*	Between groups Within groups	3 166	650.31 15494.71	2.27	0.083		
Inferior Retinal Thickness *(max)*	Between groups Within groups	3 136	1893.37 73186.27	1.17	0.323		
Nasal Retinal Thickness *(mid)*	Between groups Within groups	3 166	64.33 11436.69	0.31	0.817		
Nasal Retinal Base Area	Between groups Within groups	3 166	1.12×10^{09} 7.33×10^{10}	0.84	0.472		
Nasal Retinal Triangle	Between groups Within groups	3 166	597957020 2.184×10^{10}	1.52	0.213		

.

Foveal Parameter *Differences*	Source of variation	Degrees of freedom	Sum of squares	Variance Ratio (F)	Probability	Post-hoc Significance	Post-hoc Non-Significance
Pit Depth (max) *Horizontal*	Between groups Within groups	3 166	387.48 15451.56	1.39	0.248		
Pit Depth (max) *Vertical*	Between groups Within groups	3 136	169.78 62416.83	0.12	0.946		
Pit Depth (mid) *Horizontal*	Between groups Within groups	3 166	48.86 3130.07	0.86	0.461		
Pit Diameter (max) *Horizontal*	Between groups Within groups	3 166	111972.78 4017064.59	1.54	0.206		
Pit Diameter (mid) *Horizontal*	Between groups Within groups	3 166	13546.58 652130.43	1.15	0.331		
Nasal Width *(max)*	Between groups Within groups	3 166	54604.89 1983013.12	1.52	0.210		
Superior Width *(max)*	Between groups Within groups	3 136	146857.51 2239496	2.97	**0.034**	**Child Norm v Adult Norm p=0.047**	**Child Norm v Adult Amb p=0.122 Child Amb v Adult Amb p=1.00 Adult Norm v Adult Amb p=1.00 Child Amb v Adult Norm p=1.00 Child Norm v Child Amb p=1.00**
Foveal Slope *Nasal*	Between groups Within groups	3 166	1.24 323.12	0.21	0.887		
Foveal Slope *Temporal*	Between groups Within groups	3 166	9.57 302.91	1.75	0.159		

238

7.5.4 Foveal Topography in Visual Normals: Adults v Children

This study documents in detail foveal topography of the visually normal eye in the human adult and the visually normal child eye (age range 4 years to 13.5 years). Significant differences were found between the visually normal adult eyes and the visually normal eyes of children in many of the measured thickness parameters; foveal thickness (p<0.001), nasal thickness (max) (p<0.001), temporal thickness (max) (p=0.02), nasal retinal base area (p=0.002) with the adult measurements mainly being significantly thicker than the child measurements. (Figures 7.11 to 7.14). The exception to this was pit depth measurements; measured from the top of the pit (max) (Figure 7.15) and from the mid point (mid) (Figure 7.16) both in the horizontal and vertical meridians, where the values for the visually normal child were greater than the visually normal adult (t-test top pit depth: diff= -7.43μm p=0.056, CI:-15.05 to 0.197; t-test mid pit depth: diff = -3.27μm, p=0.04, CI:-6.45 to -0.098). (Table 7.10). No significant difference was found in any of the diameter measurements, although the vertical pit diameter (max) came close to statistical significance (t-test vertical pit diameter: diff = -85.5μm, p=0.06, CI: -175 to 4.09).
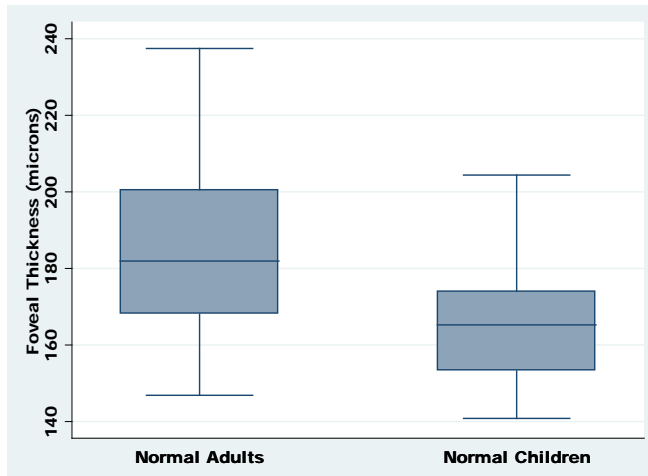
Figure 7.11: Box plots of Foveal Thickness Measurement (microns) demonstrating the mean and spread of results from horizontal scans in Normal Adults and Normal Children (p<0.001).
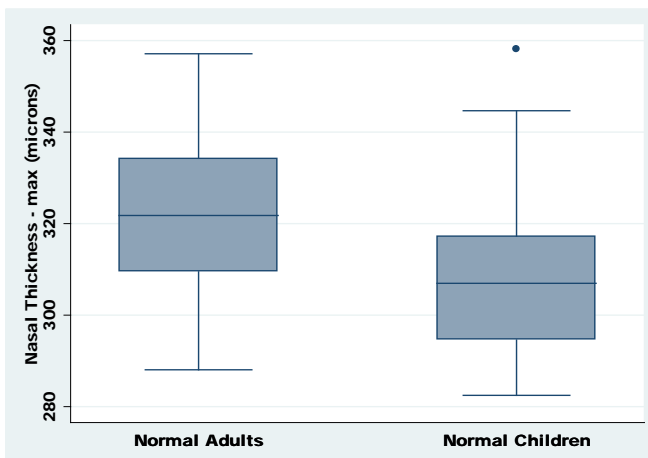
Figure 7.12: Box plots of Nasal Thickness (max) measurements (microns) (figure 7.5 and table1) demonstrating the mean and spread of results in Normal Adults and Normal Children (p<0.001).
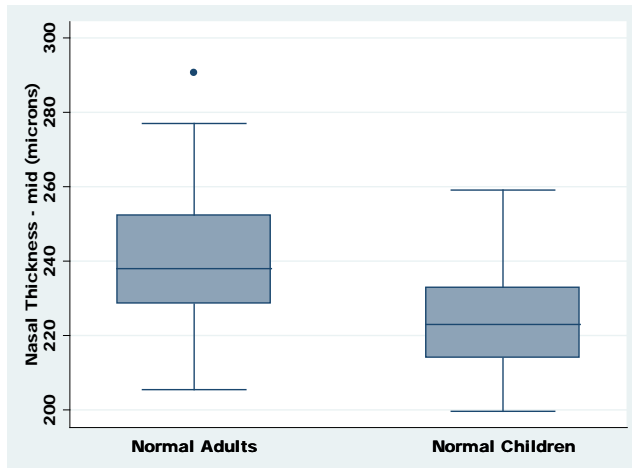
Figure 7.13: Box plots of Nasal Thickness (mid) measurements (microns) demonstrating the mean and spread of results in Visually Normal Adults and Visually Normal Children (p<0.001).
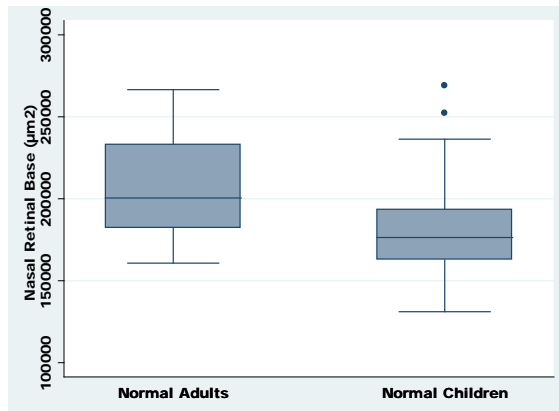
Figure 7.14: Box plots of the Nasal Retinal Base Area Measurement (μm^2) demonstrating the mean and spread of results in Normal Adults and Normal Children (p=0.002).
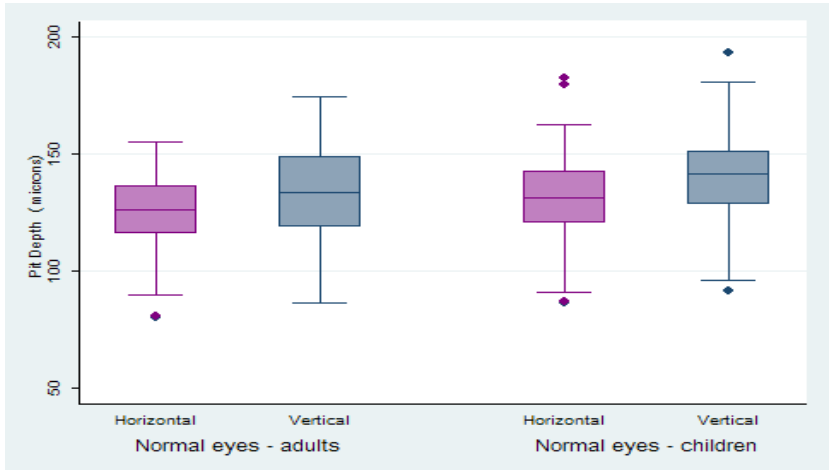
Figure 7.15: Box plots of Pit Depth (max) measurements in microns (µm) for visually normal adults v visually normal children: horizontal scans, p=0.056 and vertical scans p=0.57.
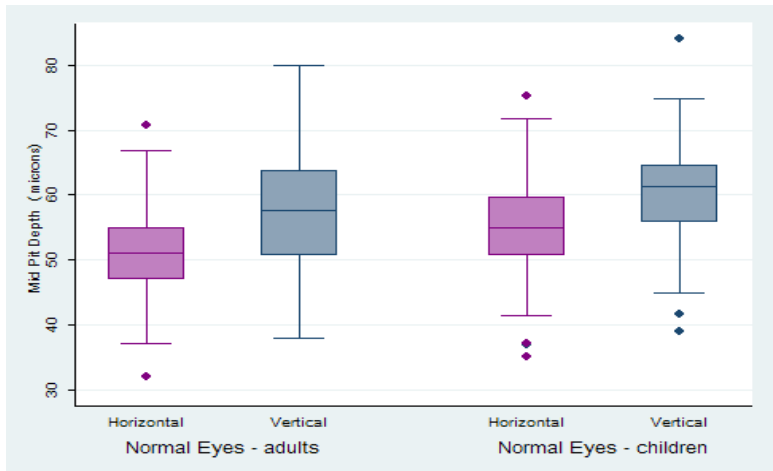
Figure 7.16: Box plots of Pit Depth (mid) measurements in microns (µm) for visually normal adults v visually normal children: horizontal scans, p=0.04 and vertical scans p=0.28.

Table 7.10: Foveal topography measurements ± SD for normal adults and children. The results of 2 sided t-tests between normal adults v normal children for each foveal parameter are shown.

Foveal Parameter	Adult (norms) Measurements (mean ± SD)	Child (norms) Measurements (mean ± SD)	Adult v Child Normal Eyes 2 tail t-test
Foveal Thickness *Horizontal*	184.18µm (20.73)	165.91 µm (15.24)	**p<0.001 CI: 11.4 to 25.14**
Foveal Thickness *Vertical*	184.94µm (19.42)	169.59 µm (16.74)	**p<0.001 CI: 7.94 to 22.75**
Nasal Thickness (max)	321.67 µm (17.40)	308.64 µm (17.82)	**p<0.001 CI: 6.15 to 19.91**
Superior Thickness (max)	320.53 µm (17.17)	309.81 µm (28.21)	**p=0.032 CI: 0.931 to 20.52**
Nasal Thickness (mid)	240.54 µm (16.98)	224.64 µm (13.36)	**p<0.001 CI: 10.08 to 21.70**
Superior Thickness (mid)	242.71 µm (15.56)	230.17 µm (14.98)	**p<0.001 CI: 6.26 to 18.81**
Temporal Thickness (max)	295.38 µm (17.67)	286.73 µm (19.75)	**p=0.022 CI: 1.26 to 16.04**
Inferior Thickness (max)	316.46 µm (16.47)	302.42 µm (31.83)	**p=0.011 CI: 3.37 to 24.73**
Nasal Retinal Base Area	206614 µm^2 (28447)	179915 µm^2 (28097)	**p=0.002 CI:15695 to 37704**
Superior Retinal Base Area	164025 µm^2 (20404)	158223 µm^2 (22668)	p=0.201 CI: -3143 to 14748
Nasal Retinal Triangle Area	77772 µm^2 (16104)	77455 µm^2 (14440)	p=0.92 CI: -5575 to 6210
Superior Retinal Triangle Area	60573 µm^2 (11986)	67009 µm^2 (13582)	**p=0.018 CI:-11753 to -1120**
Pit Depth (max) *Horizontal*	124.34 µm (19.50)	131.77 µm (19.60)	p=0.056 CI: -15.05 to 0.197
Pit Depth (max) *Vertical*	133.55 µm (18.87)	136.51 µm (28.78)	p=0.565 CI: -13.14 to 7.221
Pit Depth (mid) *Horizontal*	51.66 µm (7.97)	54.93 µm (8.26)	**p=0.04 CI: -6.45 to -0.098**
Pit Depth (mid) *Vertical*	57.48 µm (8.64)	59.43 µm (8.89)	p=0.28 CI: -5.57 to 1.65
Horizontal Pit Diam.	2109.9 µm (225.9)	2049.2 µm (264.4)	p=0.22 CI: -36.70 to 158
Vertical Pit Diam.	1773.6 µm (181.96)	1859 µm (243.89)	p=0.06 CI: -175 to 4.09
Nasal Width (max)	1126 µm (130.08)	1086.6 µm (151.10)	p=0.16 CI: -16.28 to 95.27
Superior Width (max)	890.13 µm (93.85)	916.10 µm (174.69)	p=0.38 CI: -85 to 33.06
Foveal Slope Nasal	12.67º (2.2)	13.94º (2.6)	**p=0.01 CI: -2.23 to -0.31**
Foveal Slope Superior	14.75° (2.3)	14.96° (2.8)	p=0.70 CI: -1.26 to 0.85
Foveal Slope Temporal	11.18º (2.1)	12.65º (2.5)	**p=0.002 CI: -2.4 to -0.54**
Foveal Slope Inferior	14.48° (2.38)243	14.46° (2.79)	p=0.96 CI: -1.04 to 1.10

7.5.5 Foveal Topography in Amblyopia: Adults v Children

Significant differences were found between the amblyopic adult eye and the amblyopic child eye. As with the visually normal eyes, the foveal thickness was found to be significantly greater in adults than children (p=0.010) (Table 7.11). A number of the thickness parameters (nasal thickness p=0.84, superior thickness, p=0.27, and temporal thickness p=0.23) demonstrated no difference between the amblyopic adult and the amblyopic child eyes.

The pit depth, measured from both the top (max) (Figure 7.17) and the mid point (Figure 7.18) was found to be significantly greater in the amblyopic child eye (t-test top pit depth: diff = -19.26 µm, p=0.0035, CI: -31.92 to -6.60). The topographic measurements of all the foveal parameters in adult and child amblyopes are presented in Table 7.11.

The complete pattern of differences found between the visually normal adults and children, is not replicated between the amblyopic adults and children. However, although the increase across all thickness parameters was not present in the amblyopic groups there was an increase in the foveal thickness between the adult (192.95µm ± 24.82) and child (176.52 µm ± 23.16) amblyopic eyes. Similarly a reduction in the foveal pit depth was found in both the visually normal and the amblyopic groups, with the amblyopic child pit (130.56 µm ± 22.17), being deeper than the amblyopic adult pit (111.30µm ± 26.48). The normal adult foveal pit =184.18µm ± 20.73 and normal child foveal pit = 165.91µm ± 15.24 were both deeper still.

Table 7.11: Foveal topography measurements ± SD for amblyopic eyes of adults and children. The results of 2 sided t-tests for each foveal parameter are shown.

Foveal Parameter	Adult (amblyopes) Measurements (mean ± SD)	Child (amblyopes) Measurements (mean ± SD)	Adult v Child Amblyopic Eyes 2 tailed t-test
Foveal Thickness *Horizontal*	192.95µm (24.82)	176.52 µm (23.16)	**p=0.01** **CI: 4.07 to 28.79**
Foveal Thickness *Vertical*	194.53 µm (22.54)	178.27 µm (21.94)	**p=0.01** **CI: 4.03 to 28.51**
Nasal Thickness (max)	319.16 µm (19.04)	320.00 µm (13.33)	p=0.84 CI: -9.45 to 7.76
Superior Thickness (max)	316.26 µm (20.19)	325.89 µm (13.96)	p=0.056 CI: -19.51 to 0.26
Nasal Thickness (mid)	245.62 µm (17.40)	234.59 µm (16.90)	p=0.015 CI: 2.22 to 19.84
Superior Thickness (mid)	246.44 µm (18.88)	240.93 µm (16.27)	p=0.27 CI: -4.32 to 15.34
Temporal Thickness (max)	289.35 µm (16.32)	294.16 µm (14.18)	p=0.23 CI: -12.71 to 3.10
Inferior Thickness (max)	305.79 µm (16.28)	319.40 µm (15.74)	**p=0.003** **CI: -22.43 to -4.80**
Nasal Retinal Base Area	211596 µm^2 (37997)	198862 µm^2 (37085)	p=0.19 CI: -6533 to 32001
Superior Retinal Base Area	172992 µm^2 (24882)	167729 µm^2 (29193)	p=0.47 CI: -9352 to 19877
Nasal Retinal Triangle Area	70048 µm^2 (21818)	81920 µm^2 (21377)	**p=0.036** **CI: -22953 to -790**
Superior Retinal Triangle Area	54411 µm^2 (13785)	69437 µm^2 (13376)	**p<0.001** **CI: -22502 to -7550**
Pit Depth (max) *Horizontal*	111.30 µm (26.48)	130.56 µm (22.17)	**p=0.004** **CI: -31.92 to -6.60**
Pit Depth (max) *Vertical*	116.49 µm (23.47)	144.38 µm (20.54)	**p<0.001** **CI: -40.16 to -15.62**
Pit Depth (mid) *Horizontal*	46.93 µm (11.62)	53.62 µm (9.67)	**p=0.019** **CI: -12.23 to -1.14**
Pit Depth (mid) *Vertical*	49.89 µm (9.8)	61.56 µm (8.81)	**p<0.001** **CI: -16.84 to -6.50**
Horizontal Pit Diam.	2061 µm (283)	2093 µm (337)	p=0.68 CI: -190 to 125
Vertical Pit Diam.	1759 µm (196)	1895 µm (241)	**p=0.039** **CI: -263 to -6.92**
Nasal Width (max)	1100 µm (158)	1136 µm (180)	p=0.44 CI: -129 to 56.43
Superior Width (max)	891.80 µm (99.11)	942.87 µm (132.78)	p=0.106 CI: -113.3 to 11.13
Foveal Slope Nasal	11.75º (2.85)	14.00º (2.80)	**p=0.003** **CI: -3.70 to -0.81**
Foveal Slope Superior	13.21º (3.06)	15.62º (3.46)	**p=0.009** **CI: -4.17 to -0.64**
Foveal Slope Temporal	10.01º (2.85)	12.52º (2.94)	**p=0.001** **CI: -3.98 to -1.03**
Foveal Slope Inferior	12.46º (2.98)	15.16º (3.42)	**p=0.003** **CI: -4.44 to -0.97**
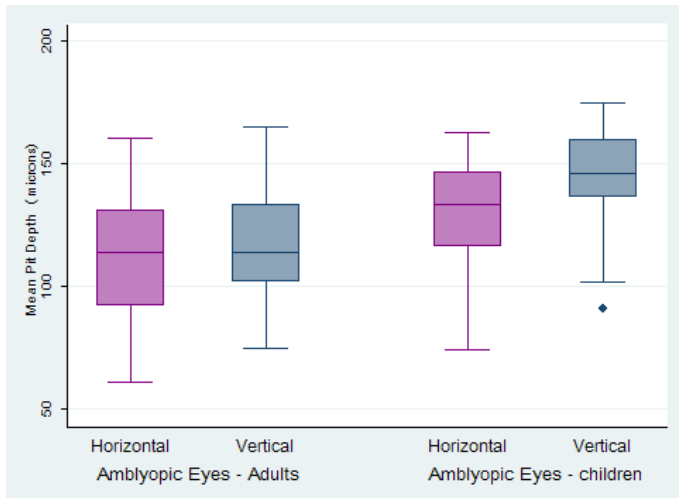
**Figure 7.17:** Box plots of Pit Depth (max) measurements in microns (µm) for amblyopic adults v amblyopic children: horizontal scans, p=0.004 and vertical scans p<0.001.
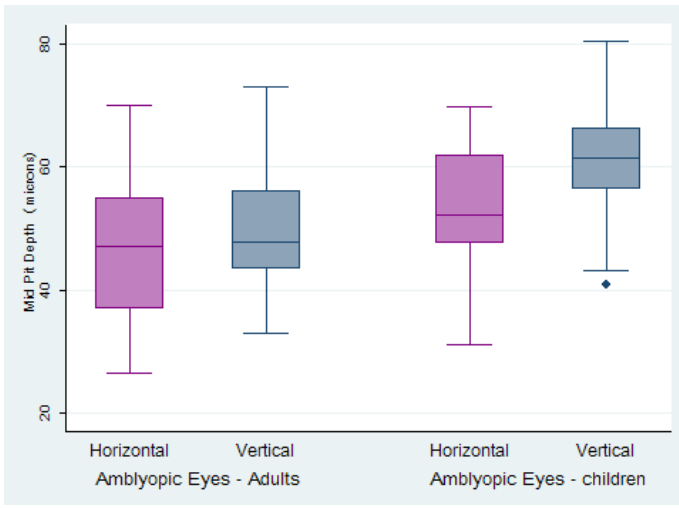
**Figure 7.18:** Box plots of Pit Depth (mid) measurements in microns (µm) for amblyopic adults v amblyopic children: horizontal scans, p=0.019 and vertical scans p<0.001.

7.5.6 Foveal Topography in Adults: Normals v Amblyopes

Given that adult v child differences exist in visual normals it was decided that the results need to be separately compared for adults and children.

The visually normal eyes of adults, adult amblyopic eyes and the strabismic and/or eye with the highest refractive error (S/A eye) were compared in an ANOVA of all foveal parameters. The majority of measured parameters showed no significant difference between these three groups. (Table 7.12). However, the pit depth (max) (p=0.003) and the pit depth (mid) (p=0.003) in the vertical meridian showed a significant difference between the amblyopic and the normal eyes and was close to statistical significance in the horizontal meridian (max) (p=0.084). (Figure 7.19). The inferior thickness was significantly reduced in the amblyopic eyes in comparison to the normal eyes (p=0.016) and in the non-amblyopic eyes compared to the normal eyes (p=0.007). (Figure 7.20).

The foveal slope was found to be greater in the normal eyes in comparison to the amblyopic eyes in both the superior (p=0.038) and inferior (p=0.004) meridians (Figure 7.21 and Table 7.12).

Given the visual acuity deficit in amblyopia the nasal parameters, thickness, width and slope of the fovea, where the paramacular bundle arises, is of key interest. However, on examination of the data no significance was found in these parameters between the amblyopic eyes and the visually normal eyes or the strabismic/anisometropic eyes.
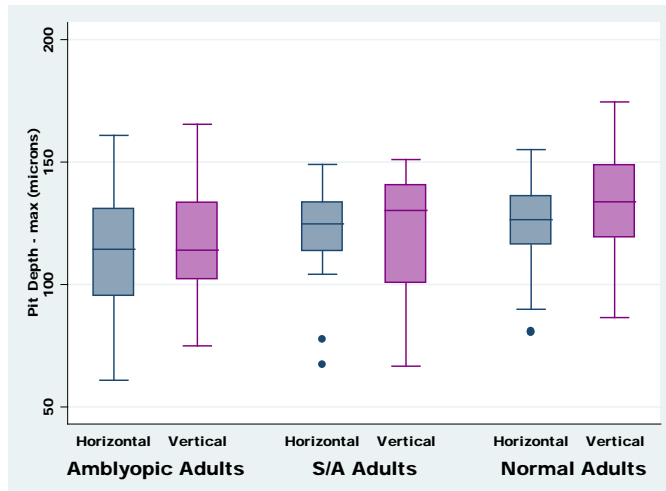
Figure 7.19: Box plots depicting the pit depth measurements (max) in microns (μm) measured in the horizontal (amblyopic v normal eyes p=0.08) and vertical (amblyopic v normal eyes p=0.003) meridians for the three adult eye categories. No significant difference was found between the eyes in the strabismic/anisometropic group (S/A) and the other two categories.
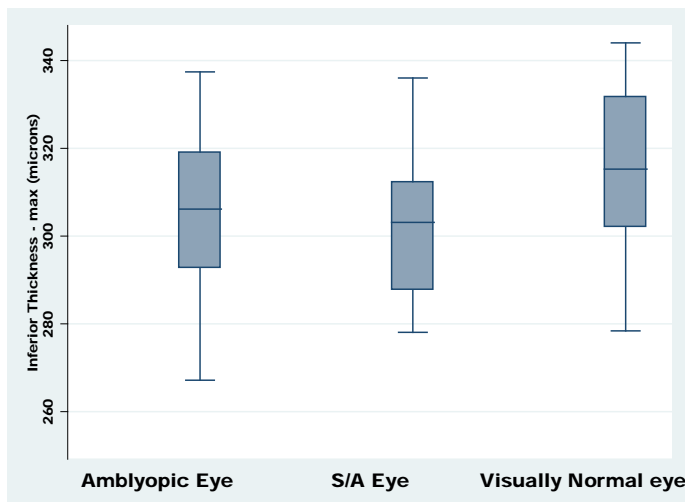
Figure 7.20: Box plots depicting the inferior thickness measurements in microns (μm), amblyopic v normal eyes p=0.016 and normal v strabismic/anisometropic eyes, p=0.007).
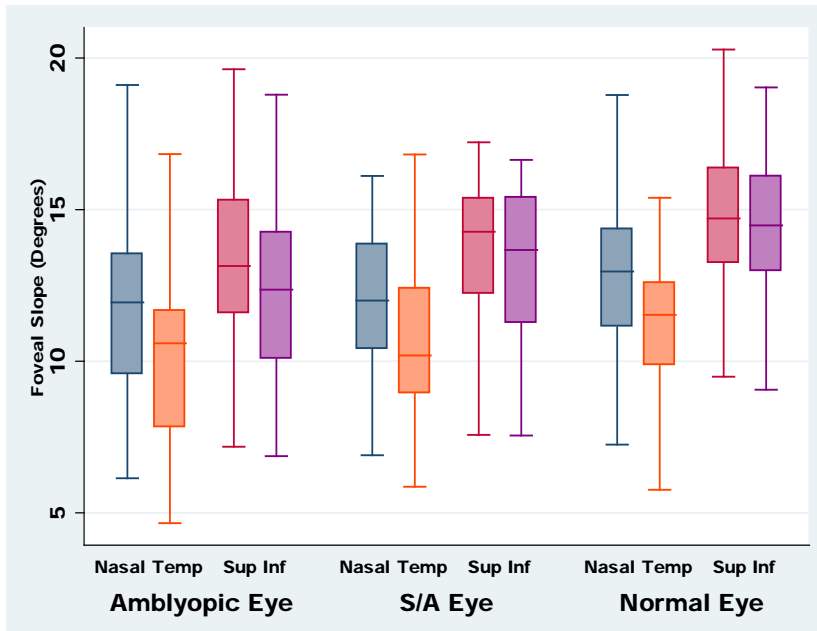
Figure 7.21: Box plots of the foveal slope measurements in degrees (°) for the nasal, temporal, superior and inferior slopes in all three adult eye categories. A significant difference was found between the amblyopic eyes and the normal eyes in the superior (p=0.038) and the inferior slopes (p=0.004). No other significant differences were found.

Table 7.12: Results of One-way ANOVA for the comparison of mean foveal parameters between the three adult groups. Post-hoc analysis are shown. Norm = normal adult eyes, Amb = amblyopic eyes, S/A = selected eye of strabismic &/or anisometropic group.

Foveal Parameter	Source of variation	Degrees of freedom	Sum of squares	Variance Ratio (F)	Probability	Post-hoc Significance	Post-hoc Non-Significance
Foveal Thickness *Horizontal*	Between groups Within groups	2 88	1820.96 42461	1.89	0.158		
Foveal Thickness *Vertical*	Between groups Within groups	2 89	2055.7 39394	2.32	0.104		
Nasal Retinal Thickness *(max)*	Between groups Within groups	2 88	1209 27960	1.9	0.155		
Superior Retinal Thickness *(max)*	Between groups Within groups	2 89	1300.06 29076.62	1.99	0.143		
Temporal Retinal Thickness *(max)*	Between groups Within groups	2 88	1080.34 26011.31	1.83	0.167		
Inferior Retinal Thickness *(max)*	Between groups Within groups	2 89	3554.45 23718.17	6.67	**0.002**	**Norm v Amb p=0.016 Norm v S/A p=0.007**	**Amb v S/A p=1.00**
Nasal Retinal Thickness *(mid)*	Between groups Within groups	2 88	1540.43 23950.37	2.83	0.064		
Superior Retinal Thickness *(mid)*	Between groups Within groups	2 89	815.15 24755.39	1.47	0.236		
Temporal Retinal Thickness *(mid)*	Between groups Within groups	2 88	912.67 24271.26	1.65	0.197		
Inferior Retinal Thickness *(mid)*	Between groups Within groups	2 89	659.92 21108.62	1.39	0.254		
Nasal Retinal Base Area	Between groups Within groups	2 88	1.689×10^{09} 8.951×10^{10}	0.83	0.439		
Superior Retinal Base Area	Between groups Within groups	2 89	2.354×10^{09} 4.021×10^{10}	2.61	0.079		
Nasal Retinal Triangle	Between groups Within groups	2 88	801702331 3.087×10^{10}	1.14	0.323		
Superior Retinal Triangle	Between groups Within groups	2 89	774173166 1.547×10^{10}	2.23	0.114		

Foveal Parameter	Source of variation	Degrees of freedom	Sum of squares	Variance Ratio (F)	Probability	Post-hoc Significance	Post-hoc Non-Significance
Pit Depth (max) *Horizontal*	Between groups Within groups	2 88	2646.78 45805	2.54	0.084		
Pit Depth (max) *Vertical*	Between groups Within groups	2 89	5803.72 42784.06	6.04	**0.004**	**Norm v Amb p=0.003**	**Norm v S/A p=0.20** **Amb v S/A p=1.00**
Pit Depth (mid) *Horizontal*	Between groups Within groups	2 88	368.84 8604.19	1.89	0.158		
Pit Depth (mid) *Vertical*	Between groups Within groups	2 89	1142.05 8192.39	6.20	**0.003**	**Norm v Amb p=0.003**	**Norm v S/A p=0.20** **Amb v S/A p=1.00**
Pit Diameter (max) *Horizontal*	Between groups Within groups	2 88	29523.90 5525644	0.24	0.791		
Pit Diameter (max) *Vertical*	Between groups Within groups	2 89	28810 3328549	0.39	0.681		
Pit Diameter (mid) *Horizontal*	Between groups Within groups	2 88	2353 986459	0.10	0.901		
Pit Diameter (mid) *Vertical*	Between groups Within groups	2 89	5298 796993	0.30	0.745		
Nasal Width *(max)*	Between groups Within groups	2 88	7495 1800674	0.18	0.833		
Superior Width *(max)*	Between groups Within groups	2 89	2767.69 834865	0.15	0.863		
Nasal Width *(mid)*	Between groups Within groups	2 88	1926.29 309082	0.27	0.761		
Superior Width *(mid)*	Between groups Within groups	2 89	1793.35 207981.96	0.38	0.683		
Foveal Slope *Nasal*	Between groups Within groups	2 88	14.62 527.73	1.22	0.301		
Foveal Slope *Temporal*	Between groups Within groups	2 88	24.97 539.14	2.04	0.136		
Foveal Slope *Superior*	Between groups Within groups	2 88	45.67 617.66	3.29	**0.042**	**Norm v Amb p=0.038**	**Norm v S/A p=0.774** **Amb v S/A p=1.00**
Foveal Slope *Inferior*	Between groups Within groups	2 88	79.39 623.19	5.67	**0.005**	**Norm v Amb p=0.004**	**Norm v S/A p=0.395** **Amb v S/A p=0.957**

Table 7.12 (Continued): Results of One-way ANOVA for the comparison of mean foveal parameters between the three adult groups.

251

7.5.7 Foveal Topography in Children: Normals v Amblyopes

In children there were significant differences between amblyopic and visually normal eyes in a large number of the measured parameters; these were the foveal thickness from the horizontal scans (p=0.011) (Figure 7.22), nasal thickness (max) (p=0.004), superior thickness (max) (p=0.013) inferior thickness (max) (p=0.02) (Figure 7.23), nasal thickness (mid) (p=0.003), temporal thickness (mid) (p=0.013), superior thickness (mid) (p=0.008), inferior thickness (mid) (p=0.012), (Figure 7.24) and nasal retinal base (p=0.007). A summary of the results of parameters in amblyopic and normal eyes in children is provided in Table 13. All nine parameters showing differences measured significantly thicker in the amblyopic eyes, however, the nine parameters are all influenced by the foveal thickness measurement and it may be that this sole parameter is influencing the thickness measurements (two-tail t-test of foveal thickness (horizontal scan): diff = 10.71μm, p = 0.003; CI: 3.68 to 17.76).

252
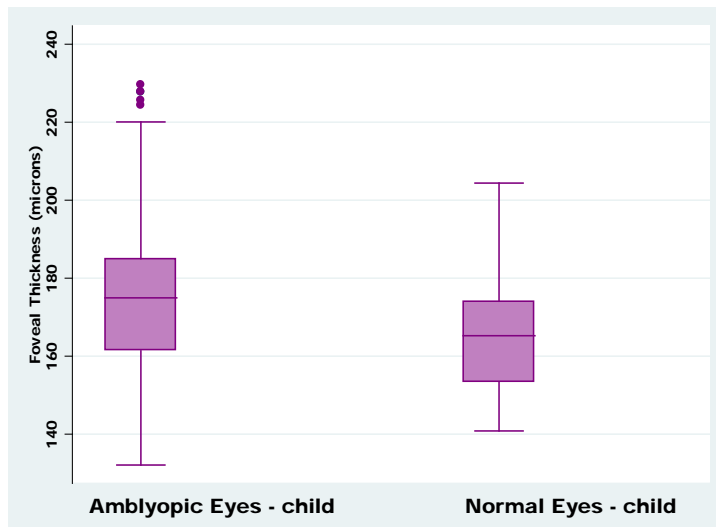
Figure 7.22: Box plots depicting the foveal thickness measurements in microns (μm) (horizontal) of children (2 sided t-test of amblyopic v normal eyes, diff: +10.83, p=0.011, CI: 2.54 to 19.12). A number of outliers are present in the amblyopic eye data.

Table 7.13: Foveal topography measurements ± SD and 2 sided t-tests of each parameter for normal eyes v amblyopic eyes in children.

Foveal Parameter	Child (normals) (mean ± SD)	Child (amblyopes) (mean ± SD)	Amblyopic Eyes v Normals (2 tail t-test)
Foveal Thickness *Horizontal*	165.91µm (15.24)	176.63 µm (23.29)	**p=0.011** **CI: 2.54 to 19.12**
Foveal Thickness *Vertical*	169.60 µm (16.74)	179.87 µm (22.90)	p=0.069 CI: -0.71 to 18.04
Nasal Thickness *(max)*	308.64 µm (17.82)	319.33 µm (12.76)	**p=0.004** **CI: 3.92 to 19.34**
Superior Thickness *(max)*	309.81 µm (28.21)	325.33 µm (15.85)	**p= 0.0134** **CI: 3.43 to 28.72**
Nasal Thickness *(mid)*	224.65 µm (13.36)	234.94 µm (16.22)	**p=0.003** **CI: 3.67 to 17.05**
Superior Thickness *(mid)*	230.17 µm (14.98)	241.19 µm (16.50)	**p= 0.008** **CI: 2.94 to 18.58**
Temporal Thickness *(mid)*	217.04 µm (13.90)	226.01 µm (16.64)	**p= 0.013** **CI: 1.96 to 15.84**
Inferior Thickness *(mid)*	228.40 µm (16.17)	237.50 µm (18.44)	**p= 0.012** **CI: 2.48 to 19.17**
Temporal Thickness *(max)*	286.73 µm (19.75)	294.01 µm (14.72)	p= 0.087 CI: 0.85 to 13.72
Inferior Thickness *(max)*	305.74 µm (21.37)	313.11 µm (22.34)	**p= 0.020** **CI: 2.72 to 31.25**
Nasal Retinal Base Area	179915 µm^2 (28098)	196025 µm^2 (36910)	**p= 0.007** **CI: 5496 to 34122**
Superior Retinal Base Area	158223 µm^2 (22668)	172032 µm^2 (31684)	p=0.139 CI: -3150.84 to 2164.38
Nasal Retinal Triangle	77455 µm^2 (14440)	79676 µm^2 (18628)	p= 0.224 CI: -4471.37 to 9326.4
Pit Depth (max) *Horizontal*	131.77 µm (19.60)	130.04 µm (22.87)	p= 0.783 CI: -10.76 to 8.13
Pit Depth (max) *Vertical*	139.51 µm (19.42)	139.35 µm (23.87)	p= 0.251 CI: -5.67 to 21.40
Pit Depth (mid) *Horizontal*	54.93 µm (8.26)	53.85 µm (9.88)	p= 0.52 CI: -4.37 to 2.21
Pit Depth (mid) *Vertical*	59.72 µm (8.74)	59.48 µm (10.45)	p= 0.350 CI: -2.38 to 6.63
Pit Diameter (max) *Horizontal*	2049 µm (264.44)	2074 µm (306.85)	p= 0.451 CI: -82.23 to 183.58
Pit Diameter (max) *Vertical*	1859 µm (243.88)	1901 µm (290)	p= 0.58 CI: -94.67 to 165.80
Nasal Width *(max)*	1087 µm (151)	1115 µm (180.5)	p=0.180 CI: -24.99 to 131.62
Superior Width *(max)*	934.4 µm (116.92)	957.5 µm (135.38)	p= 0.523 CI: -56.35 to 109.88
Foveal Slope *Nasal*	13.94º (2.63)	13.89º (2.99)	p= 0.949 CI: -1.20 to 1.28
Foveal Slope *Superior*	15.02º (2.77)	15.21º (3.68)	p= 0.391 CI: -0.86 to 2.18
Foveal Slope *Temporal*	12.65º (2.54)	12.45º (3.09)	p= 0.759 CI: -1.43 to 1.04
Foveal Slope *Inferior*	14.54º (2.79)	14.41º (3.64)	p= 0.361 CI: -0.818 to 2.22
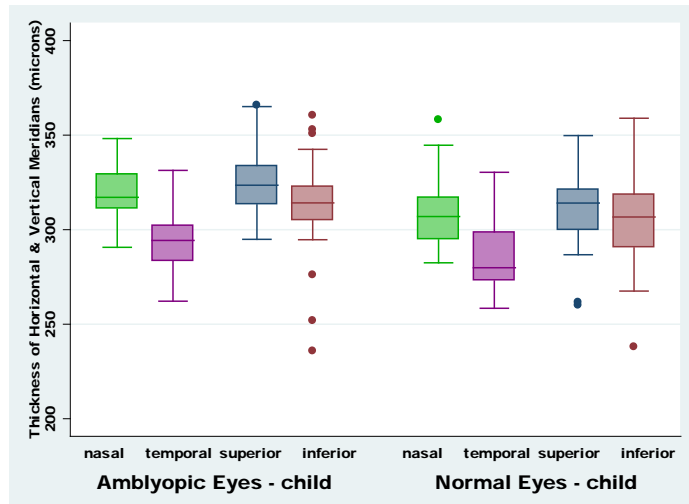
Figure 7.23: Box plots of thickness measurements (max) in microns (μm) for nasal, temporal, superior and inferior meridians (2 sided t-test of amblyopic v normal eyes nasal thickness, diff: 11.63, p=0.004, CI: 3.92 to 19.34). A number of outliers can be seen particularly in the amblyopic eyes in the inferior meridian.
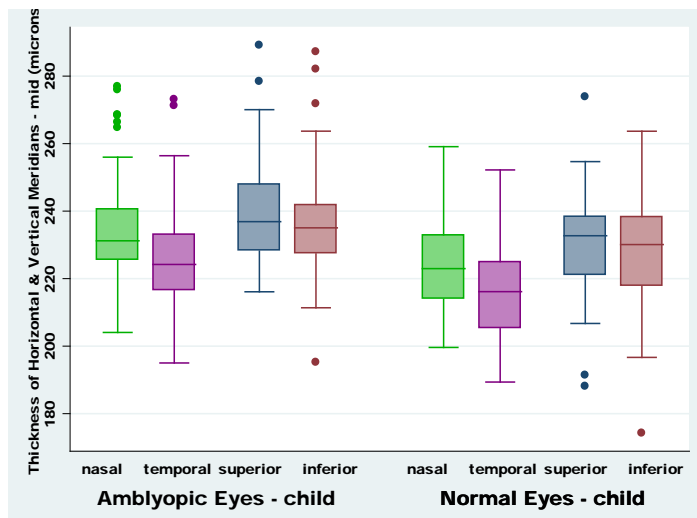
Figure 7.24: Box plots of thickness measurements in microns (μm) for mid nasal, temporal, superior and inferior meridians (2 sided t-test of amblyopic v normal eyes mid nasal thickness, diff: 10.36, p=0.003, CI: 3.67 to 17.05). A number of outliers can be seen particularly in the amblyopic eyes.

7.6 Foveal Thickness: Association of Visual Acuity

The foveal thickness (µm) was compared to the level of visual acuity in the amblyopic eye and/or the non-dominant eye of visually normal individuals, both adults and children were included (Figure 7.25). The foveal thickness (µm) thickness varies across all levels of visual acuity in the 5 presented cohorts.
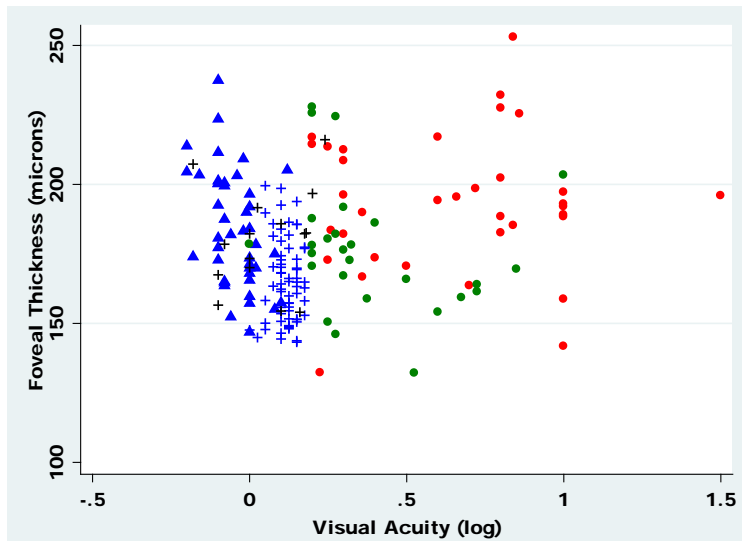
Figure 7.25: Foveal thickness (µm) compared to the amblyopic or non-dominant eye visual acuity (logMAR) for amblyopic adults ● amblyopic children ● visually normal adults ▲ visually normal children ✛ and non-amblyopic adults ✛.

7.6.1 Foveal Thickness: Association of Axial Length and Age

Studies of the retinal nerve fibre layer around the peripapillary area of the optic disc using OCT in adults and children (Alamouti and Funk, 2003; Parikh 2007, Huynh 2006; Salchow et al.,2006) have demonstrated a link between RNFL thickness, age and axial length. The effect of these two factors was therefore examined against the current data investigating foveal structure. A regression analysis including all five cohorts; visually normal adults, amblyopic adults, non-amblyopic adults with S/A, visually normal children and amblyopic children was undertaken using foveal thickness as the dependant variable and axial length and age as the predictor variables (Figure 7.26 and Figure 7.27).

The analysis of the effect of axial length on foveal thickness shows the regression coefficient is positive, indicating that there is a slight trend for foveal thickness to increase with increasing axial length, this however was not shown to be significant (p=0.32). In amblyopia the mean axial length measurements are shorter in comparison to the other cohorts and the foveal thickness value was found to be thicker, this finding suggests that the group differences could be even greater and may actually be masked by the effect of the axial length.

257
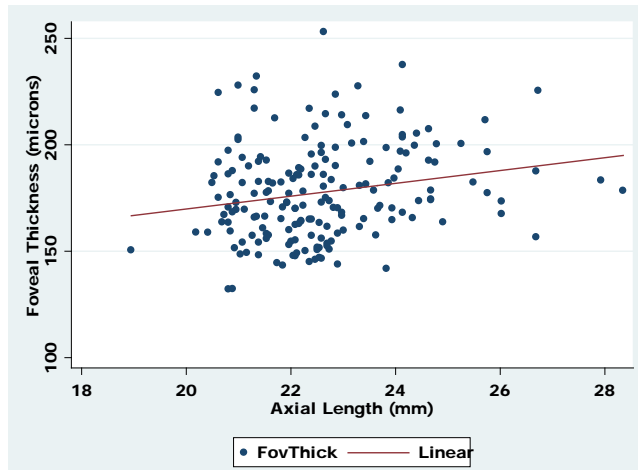
Figure 7.26: Linear regression of Foveal Thickness (µm) v axial length (mm) in visually normal adults and children, amblyopic adults and children and non-amblyopic adults with S/A. Equation for the regression line is y =0.97x + 143.26 (95% CI for coefficient, -0.95 to 2.89). R^2=0.04.

The effect of age (p<0.001) is significant and its coefficient is positive indicating that there is an increase in foveal thickness by 0.58µm for every one year (Figure 7.27). This result confirms the findings reported previously of increased foveal thickness found in adults compared to children (Table 7.10).
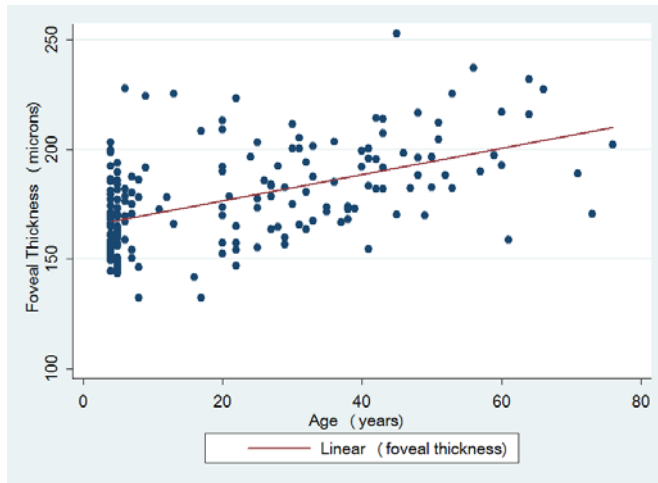
Figure 7.27: Linear regression of Foveal Thickness (µm) v age (years) in visually normal adults and children, amblyopic adults and children and non-amblyopic adults with S/A. Equation for the regression line is y =0.58x + 143.26 (95% CI for coefficient, 0.42 to 0.73). R^2=0.26

7.7 Discussion

7.7.1 Normal Foveal Topography – Adults

The foveal topography measurements of the visually normal adults were consistent with those reported by previous studies using optical coherence tomography combined with image analysis of foveal metrics (Dubis et al., 2009; Hammer et al., 2008) (Table 7.14). However, they differ from the single histopathology study (Polyak, 1941) and the modelling study using entoptic phenomena (Williams, 1980). The difference between the studies is perhaps not surprising. In the histological study the form of the foveal pit from the excised retina, which will have been sectioned and fixed, is likely to have been subject to some degree of distortion (Polyak, 1941) and the study utilising the entoptic phenomena is an indirect technique of measurement which is subject to observer variation (Williams, 1980).

Table 7.15: Comparison of normal adult foveal topography measurements from this current study with previously published studies.

Study	Depth of Foveal Pit (µm)	Slope (º)	Method of measurement
Polyak, 1941	240 (n=1)	20	Histology (excised human retina)
Williams, 1980	220 (n=4)	43	Entoptic Phenomena Techniques
Hammer, 2008	121 (sem 4.3) (n=5)	Not recorded	OCT with foveal metric analysis
Dubis, 2009	122 (SD 20.2) (n=39)	12	OCT with foveal metric analysis
Bruce, 2010	124 (SD 19.5) (n=48)	12.67 (nasal) 11.18 (temporal)	OCT with foveal metric analysis

7.7.1.1 Horizontal and Vertical Meridians

The imaging technique in the study by Dubis (2009) measured the values from six radial B-scans set at 30° intervals; the definitive measurement was produced by averaging the absolute values of each scan. In this study, the horizontal and vertical B-scan measurements are presented separately providing detailed topographic information on the foveal pit in the nasal, temporal, superior and inferior meridians. The results depict a fovea that is not of equal peak thickness in all meridians and indeed depicts a consistent diminution in thickness on the temporal side. This reduction of temporal thickness has been noted in previous studies (Dubis, 2009; Polyak, 1941; Huynh, 2006). This is generally attributed to the location of the paramacular bundle, between the fovea and the optic disc (Dubis et al., 2009). However, the data from the present study, from the horizontal and vertical meridian scans, demonstrate that the nasal, superior and inferior meridians are of a similar thickness to each other and it is solely the temporal side that is reduced. This would indicate that the retinal fibres from the fovea contributing to the paramacular bundle do not simply exit the fovea from the nasal side but arise from the superior and inferior meridians in addition to the nasal meridian.

In this study the foveal pit depth measurement is a mean value derived from the measurements in the horizontal meridian of the nasal and the temporal thickness from the horizontal scan and in the vertical meridian of the superior and inferior thickness (Figure 7.7 and Table 7.1). The reduced temporal thickness

measurement therefore leads to a difference in the pit depth (max) (Figure 7.7) value when measured in the horizontal meridian (124.34µm±20) and the vertical meridian (133.56µm±19) and the pit depth (mid) when measured in the horizontal meridian (51.66µm±8) compared to the vertical meridian (57.48µm±9).

The quantification of the foveal thickness measure is the distance from the inner limiting membrane (ILM) to the retinal pigment epithelium (RPE) centred at the fovea (Figure 7.7 and Table 7.1). With the foveal thickness parameter, the horizontal and the vertical scans are essentially measuring the exact same retinal position. The measurements in the adult normal eye derived from the horizontal scan (184.18µm±21) and the vertical scan (184.94µm±19), demonstrating very little difference. The horizontal B-scan traversing the centre of the fovea is one of the horizontal linear raster scans produced from multiple A-scans. The vertical scan however, is not formed from a linear raster scan; it is a production of selected A-scans in vertical alignment and although the central scan was manually chosen to bisect the fovea the effect of horizontal movement produces some variability (see section 7.4 Processing of Images). The occurrence of eye movements whilst capturing the scan is predominantly in the horizontal meridian and potentially could affect the vertical alignment of the B-scans, leading to increased variation of the vertical scan. In the majority of the adult scans this variation did not occur. However, in the scans of the children's eyes and the scans of the amblyopic eyes, where stable fixation is compromised, an increased number of outliers are seen (Figures 7.9, 7.22 and 7.23.). This must be borne in mind when interpreting the vertical data.

7.7.2 Visually Normal Children

The vast majority of studies reporting retinal structure using imaging techniques have reported the results of topographic results from adults (Dubis et al., 2009; Hammer et al., 2008; Leung et al., 2008).The exception is a series of comprehensive population based studies by Huynh between 2003 and 2005, compiling the Sydney Childhood Eye Study. In these studies the time domain Stratus OCT (Carl Zeiss, Dublin, California, USA) has been employed to image the eyes of 6 year-old and 12 year-old children both visual normals and amblyopes(Huynh et al., 2009; Huynh et al., 2007; Huynh et al., 2006b) . The difference in the instrumentation used for the Huynh study and this present study limits the comparisons that can be made but the foveal minimum thickness (161.1µm ± 19.4) presented (Huynh et al., 2006a) is comparable to the foveal thickness parameter (165.91µm ± 15.24) found in the visually normal child control group in this study.

7.7.2.1 Foveal Topography in Visual Normals: Adults v Children

The findings of this study show a change in normal retinal structure between the child retina and the adult retina, with increased thickness measurements found in the adult fovea in the nasal (321.67 µm v 308.64 µm), superior (320.53 µm v 309.81 µm) temporal (295.38 µm v 286.73 µm) and inferior (316.46 µm v 302.42 µm) meridians (Table 7.10). The foveal thickness parameters in the nasal, superior, temporal and inferior meridians are all greater in the adult eye. The reduced

263

thickness reported in the temporal meridian is also found to be present in children, with the nasal, superior and inferior meridians being of a similar thickness. The foveal pit depth (max), however, is deeper in the child eye (131.77µm ±19.60) compared to the adult eye (124.34µm ±19.50), although this difference fell just short of being statistically significant (p=0.056). The difference does, however, reach statistical significance when measured from the midpoint of the pit (p=0.004). The pit depth parameter, derived from the mean height measurements, which are thicker in the nasal, temporal, superior and inferior meridians in adults compared to children, must therefore be influenced by the foveal thickness parameter which was found to be reduced in the child eye compared to the adult eye (Figure 7.28).
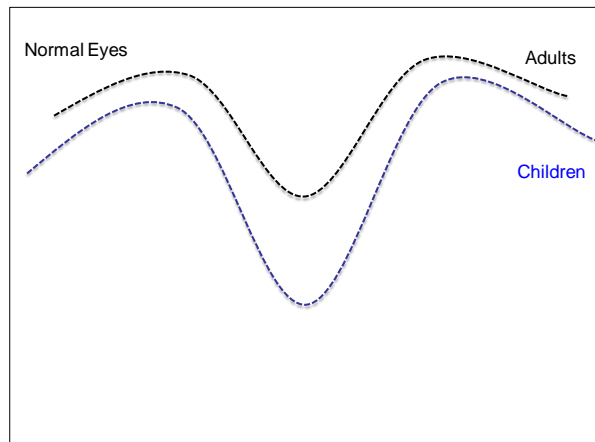
Figure 7.28: Schematic representation of the topographic findings in adults and children in visually normal eyes.

264

7.8 Inter-Ocular Symmetry (IOS)

A high degree of symmetry was found in all the measured foveal parameters. The presence of inter-ocular symmetry in visual normals is important to establish as it provides a benchmark for comparison. Inter-ocular symmetry has been noted in studies of both the adult and child macula using OCT (Dubis et al., 2009; Huynh et al., 2007) although in both studies a potential for individual variation was noted. In the investigation of retinal structure in amblyopia a recent study of optic nerve size and eye shape using magnetic resonance imaging (MRI) compared the amblyopic eye with the fellow eye along with a normal control group. The study found inter-ocular symmetry in the eyes of the amblyopic subjects (Pineles and Demer, 2009). In the present study presenting detailed foveal topography the presence of inter-ocular symmetry has been shown to be present in all groups; adults, children, amblyopes, non-amblyopes i.e. individuals with strabismus and or anisometropia and visually normal controls. This consistent finding of inter-ocular symmetry may explain the equivocal results found in previous studies of retinal structure in amblyopia. If amblyopic eyes are compared to their fellow then the presence of inter-ocular symmetry explains why no significant differences have been found (Altintas et al., 2005; Colen et al., 2000; Repka et al., 2009b; Yen et al., 2004; Yoon et al., 2005). Where as studies that compare visually normal eyes to amblyopic eyes are likely to show differences (Huynh et al., 2009).

7.9 Foveal Topography in Children: Normals v Amblyopes

In children there were significant differences between amblyopic and visually normal eyes; foveal thickness from the horizontal scans (p=0.011) (Figure 7.22), nasal thickness (max) (p=0.004), superior thickness (max) (p=0.013) inferior thickness (max) (p=0.02) (Figure 7.23), nasal thickness (mid) (p=0.003), temporal thickness (mid) (p=0.013), superior thickness (mid) (p=0.008), inferior thickness (mid) (p=0.012), (Figure 7.24) and nasal retinal base (p=0.007).

The nine foveal parameters demonstrating significant differences between the visually normal eyes and the amblyopic eyes in children were found to be significantly thicker. (Table 7.13).The factor influencing all nine parameters is the foveal thickness measurement (visually normal eyes = 165.91µm, amblyopic eyes = 176.63 µm, diff = 10.72µm, p = 0.011 CI: 2.54 to 19.12). The foveal thickness in this study is comparable to that reported by Huynh (Huynh et al., 2009) in a study of macular thickness in amblyopia using the Straus OCT. Huyhn reported an increased minimum foveal thickness between amblyopic eyes (170.7µm) and visually normal eyes (158.6µm) in children (diff = 11µm). The Huyhn study also found a difference of 5µm (p<0.05) between the amblyopic and amblyopic fellow eyes, although this was not as marked.

It has to be considered that the age difference between the visually normal group of children (mean age = 4.5 years) and the amblyopic group of children (mean age = 7.5 years) could affect the foveal thickness measurement. Both groups are within the age range where adult–like cone density is believed to be achieved, 4 –7 years

(Provis et al., 1998; Yuodelis and Hendrickson, 1986). However, the mean visual acuity in the group of normal children was +0.1 logMar and the amblyopic children presented with a mean visual acuity in the fellow eyes of 0.0 logMar, indicating that the fovea of the visually normal children may not have achieved full development at the age of 4-5 years, in contrast to that of the slightly older amblyopic group who may have achieved foveal maturity thus allowing a better level of visual acuity. The presence of an age difference between the two groups may limit the comparisons to some extent, however, in the study by Huynh (2009), increased foveal thickness measurements are presented in both the group of 6 year-old amblyopic children (difference of 6.9μm) and in the group of 12 year-old children (difference of 4.2μm) with amblyopia, although the difference was not as marked in the older group the findings demonstrate structural differences in amblyopes, irrespective of age.

7.9.1 Foveal Topography in Adults: Normals v Amblyopes

The foveal structure of the adult amblyopes also demonstrated an increase in the foveal thickness (192.95μm) in comparison to the visually normal adult eyes (184.18μm) (ANOVA post-hoc analysis: diff = 7.68μm, p=0.40) and the non-amblyopic eyes (179.94μm) (ANOVA post-hoc analysis: diff = 13μm, p=0.26) these differences were not however statistically significant.

A reduction of the foveal pit depth in adult amblyopic eyes was found in comparison to the visually normal eyes, but not when compared to the non-amblyopic eyes with strabismus and/or anisometropia. This difference was

particularly significant in the vertical meridian (p= 0.003) (Figure 7.19 and Table 7.12). The inferior foveal thickness in the amblyopic eyes was found to be reduced when compared to the visually normal eyes (p=0.016) (Figure 7.20 and Table 7.12) and also reduced in the non-amblyopic eyes with strabismus and/or anisometropia when compared to the normal eyes (p=0.007) (Figure 7.20 and Table 7.12). It is this inferior thickness measurement that is most probably contributing to the reduction in the pit depth measurement as it is calculated from the mean of the superior and inferior thickness measurements. The inferior foveal slope is also shown to be significantly statistically reduced in the amblyopic eyes (12.46°) compared to the normal eyes (14.48°) p=0.004(Figure 7.21 and Table 7.12).

7.9.2 Non-amblyopes with Strabismus and/or Anisometropia - Adults

Examination of the data for the group of non-amblyopic adults with the presence of strabismus and/or anisometropia (S/A) found little difference in any of the measured foveal parameters when compared to either the visually normal group or the amblyopic group. Only the inferior thickness measurement of the fovea, when compared to the normal eyes, reached significance (p = 0.007) (Figure 7.20 and Table 7.12), with the selected S/A eye demonstrating a reduced thickness, this was the sole parameter in this group to reach significance. It is difficult to explain why this sole parameter would be affected and it may be a spurious result. It could be related to the variability of the vertical scan, particularly on the inferior margin towards the end of the scan where fixation may be affected to a greater degree by

eye movements. However, no outliers are present in this data set (Figure 7.20), which suggests that eye movements alone are not the reason for this difference. The majority of the S/A non-amblyopic group (10 out of 14) had previously had treatment for their amblyopia, producing a successful visual outcome and it may be that this factor is influencing the results in this study. Both the groups of amblyopes, adults and children, had also received treatment for their amblyopia, but this had not been successful, leaving residual amblyopia. Whether the instigation of treatment affects the retinal structure cannot be concluded from this study but the results of the longitudinal study in this thesis may shed light on this important issue (Chapter 11).

7.10 Results from Histological Studies

The increase in foveal thickness between the child (165.91μm ±15.24) and the adult visually normal eye (184.18μm ± 20.73) may be explained in terms of the process of normal foveal pit formation during retinal development. As the foveal pit develops the cones change in orientation and length, the inner and outer segments forming elongated appendages, with an associated increase in cone density, changing the single cell photoreceptor layer to a multi-cell layer in the fovea (Polyak, 1941; Provis et al., 1998; Yuodelis and Hendrickson, 1986). In the development of the human eye, cone density has been shown to achieve adult proportions between the age of 4-7 years (Provis et al., 1998; Yuodelis and Hendrickson, 1986). Yuodelis and Hendrickson (1986) examined the anatomical development of the human fovea, sampling cadavers from 22 weeks gestation to

adulthood. The study found that the foveal cone diameter changes markedly after birth, going from 7.5µm at 5 days postnatally to 2µm microns by 45 months. During this time, the cones were shown to develop, with both the outer segment (60µm) and inner segments (20-35µm) increasing in length. This combination of elongation and increasing cone density produces significant change at the fovea, from18 cones/100µm at 1 week postnatally to 42 cones/100 µm in the adult. Yuodelis and Hendrickson (1986) found that the measure of cone diameter reached the adult stage of development at 45 months of age. The latter authors also noted importantly that the outer segment length and the cone packing density were still only half the adult values at 45 months of age, suggesting that foveal development is far from complete at this age. The foveal thickness parameter, a measure of the distance from the ILM to the RPE, is a measure of the cone photoreceptors along with their emerging elongated appendages of the Fibres of Henlé and therefore the foveal thickness measurement would be expected to reflect foveal development.

7.11 Results from Animal Studies

There is evidence from monocular deprivation and studies in animals that structural adaptation to deprivation can occur, leading to changes in retinal structure. This structural change, arising from the presence of monocular deprivation in chickens, resulting in increased axial length, has been shown to produce elongation of the outer segment of the photoreceptors, both rods and cones (Liang et al., 1995; Rucker and Wallman, 2008).Liang found that eyes subjected to occlusion and examined at one, two and four weeks showed a general thinning of the retina but

conversely also found that the photoreceptors responded by thickening of the inner segments and elongation of the outer segments. Interestingly, in both of the aforementioned animal studies the retinal changes were found to produce similar responses in the fellow eye. This reflects the findings of the present study, showing differences in both eyes of amblyopes, in comparison to the visually normal eyes

It is possible that the pit depth is reduced due to a reduction in the numbers of fibres emerging from the photoreceptors. Studies of foveal development have shown that as the foveal pit develops, the elongated axons emerging from the cone photoreceptors connect to the bipolar cells on the rim of the fovea, these then further connect to the ganglion cells. Bipolar cells transfer the impulses from photoreceptors to ganglion cells, matching specific photoreceptor cells (Provis and Hendrickson, 2008). Research has shown that the elimination of bipolar cells during retinal synaptogenesis could be a mechanism for obtaining appropriate connections between specific photoreceptors and ganglion cells; a synaptic mismatch between photoreceptor type and ganglion cell type may result in the death (apoptosis) of the intervening bipolar cell (Georges et al., 1999). In animal studies the process of apoptosis has been shown to occur in response to disease processes such as glaucoma and altered visual experiences such as monocular deprivation (Nucci et al., 2000; Quigley et al., 2000). In particular, studies in rats where a sustained elevation in intraocular pressure was induced found the retrograde transport of neurotrophic factor was obstructed, resulting in the deprivation of the neurotrophins required for retinal ganglion cell support, triggering apoptosis (Johnson et al., 2009; Quigley et al., 2000). It is therefore possible that

the occurrence of a visual assault by way of unequal visual input associated with amblyopia triggers the process of apoptosis, leading to reduction of the pit depth in the adult amblyope.

However, when examining the combined foveal thickness : pit ratio, the overall combined measurement (303µm) of the foveal thickness (192µm) and pit depth (111µm) in adult amblyopes is close to the combined measurement (308µm) of foveal thickness (184µm) and pit depth (124µm) of the normal adult. This would indicate that the reduction in pit depth is most likely to be produced by the thickening of the fovea, produced by elongation of the cone photoreceptors rather than the reduction of the pit height by the process of apoptosis (Figure 7.29).

Normal adult foveal thickness to pit depth ratio

Amblyopic foveal thickness to pit depth ratio
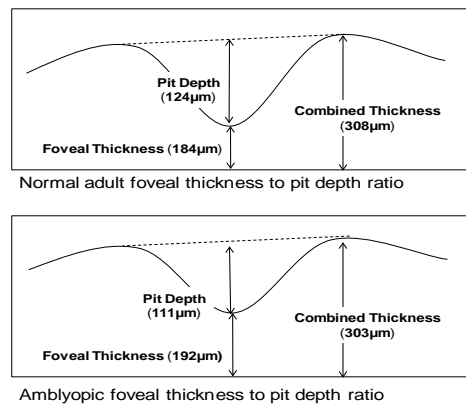
Figure 7.29: Schematic of foveal thickness to pit depth ratio for adult visually normal eyes and adult amblyopic eyes.

7.12 Conclusion

The essential supposition influencing the current clinical treatment of amblyopia is the principle that there is no structural anomaly in the amblyopic eye and that any change in structure is at the level of the visual cortex (Horton and Hocking, 1996c; Hubel and Wiesel, 1965). The results of this present study investigating foveal topography have demonstrated that not only is there a change in retinal structure in amblyopic eyes but that this change is both bilateral and symmetrical. This symmetry is consistent with the structural study detailing the optic nerve size and eye shape in amblyopia (Pineles and Demer, 2009). The finding of structural symmetry between the eyes indicates that it is not the change in retinal structure per se that is the cause of the visual deficit in amblyopia. As suggested in the introduction, there are 3 ways in which these structural defects could be interpreted in relation to the presence of amblyopia.

1. The structural defects could be the primary cause of the visual deficit and the occurrence of strabismus and anisometropia are secondary to this, possibly contributing to the initial visual deficit.

2. The structural defects are caused by the visual insult, primarily produced by the presence of strabismus and/ or anisometropia.

3. The structural defects could be caused by some as yet unknown defect, other than strabismus and/ or anisometropia, perhaps at the level of the

visual cortex, which leads to the secondary occurrence of strabismus, anisometropia and retinal structural defects.

The structural differences found in the amblyopic eyes were also found to be present in the fellow eyes. Therefore the structural changes are unlikely to be the primary cause of the visual deficit in the amblyopic eye (option 1). The structural changes could however be secondary changes produced by a developmental response to the visual insult produced by the presence of amblyopic factors such as strabismus and or anisometropia (option 2) leading to visual loss. This in turn could produce structural change. This second option is supported by both the results from this study and from animal studies in which deprivation of one eye caused anatomical changes in both eyes. It is also possible that the structural differences, along with strabismus and anisometropia are caused by some, as yet undiscovered defect, perhaps at the level of the visual cortex, however, further studies are required to either rule out or substantiate this option (3). The results of this study make option 1 less likely but currently cannot distinguish between option 2 and option 3.

Chapter 8. Peripapillary Retinal Nerve Fibre Layer Thickness

8.1 Introduction

The retinal nerve fibre layer (RNFL) is formed from the axons of the retinal ganglion cells gathered together in bundles, located between the inner limiting membrane (ILM) and the retinal ganglion cell layer. The RNFL consists of retinal ganglion cell axons embedded in astrocytes, retinal vessels and Müller cell processes (Jonas and Dichtl, 1996; Pollock and Miller, 1986),Chapter 1 Figure1.1 RNFL = Stratum opticum). Histological studies have shown that, although the RNFL thickness is subject to individual variation, the thickness of the superior and inferior peripapillary disc regions are thicker than the temporal and nasal regions and the RNFL thickness decreases towards peripheral retina, away from the disc margin (Frenkel et al., 2005; Quigley and Addicks, 1982). The greater thickness in the superior and inferior regions is due to the increased number of retinal ganglion axons converging onto the optic disc from the superior and inferior arcuate bundles, relative to the numbers of axons from the papillomacular bundle and nasal retina. In all diseases of the optic nerve there is reduction in the thickness of the RNFL; observation and measurement of the RNFL is therefore key to identifying abnormalities. Considering visual acuity is reduced in amblyopia it is logical to investigate RNFL thickness in the peripapillary area surrounding the optic disc. This represents an additional way in which the retina may differ from normal in amblyopia.

275

A number of imaging studies of RNFL thickness in amblyopia have now been published with varying results (Chapter 4). In a study using time domain OCT to image amblyopic eyes (Yen et al., 2004) a difference was demonstrated between amblyopic eyes and their fellow eyes with anisometropia, with the amblyopic eyes having thicker RNFL measurements than the fellow eye. Yen et al (2004) hypothesised that the mechanism of ganglion cell apoptosis during development may be reduced in amblyopia producing a thicker RNFL.

However other imaging studies using both OCT and GDx (Colen et al., 2000) found no difference between the amblyopic eye and the fellow eye.

The aim of this section of the study is to assess the RNFL thickness in the peripapillary sectors around the optic disc in amblyopic adults and children.

8.2 Methods

The participants recruited to this stage of the study are comprised of the same individuals recruited to the foveal topography stage (Chapter 7) of the study. (Refer to Chapter 7 for detailed description of the groups and methods of recruitment).

8.3 Optic Disc Measurement – Retinal Nerve Fibre Thickness

The retinal nerve fibre thickness (RNFL) was measured using the 3D OCT-1000 (Topcon, Tokyo, Japan) standard disc scan, made up of 256 x 256 A-scans covering a 6mm x 6mm area across the disc (Figure 8.1). A circular grid 3.4mm in diameter located in the centre of the scan is used to obtain the RNFL

276

measurements. The grid is made up of 6 sectors nasal, upper nasal, upper temporal, temporal, lower temporal, and lower nasal. The scans in each sector are used to calculate a mean RNFL measurement for each of the 6 sectors within the RNFL scan grid (Figure 8.2 and Table 8.1). The RNFL thickness for each sector was recorded. The procedure for obtaining an optic disc scan requires the observer to fix a small target viewed off centre to the nasal side. The target used for the adults was a single small square. However, with the children the target size was generally increased to a target made up of 4 of the small squares. This increase of size was made to aid fixation.
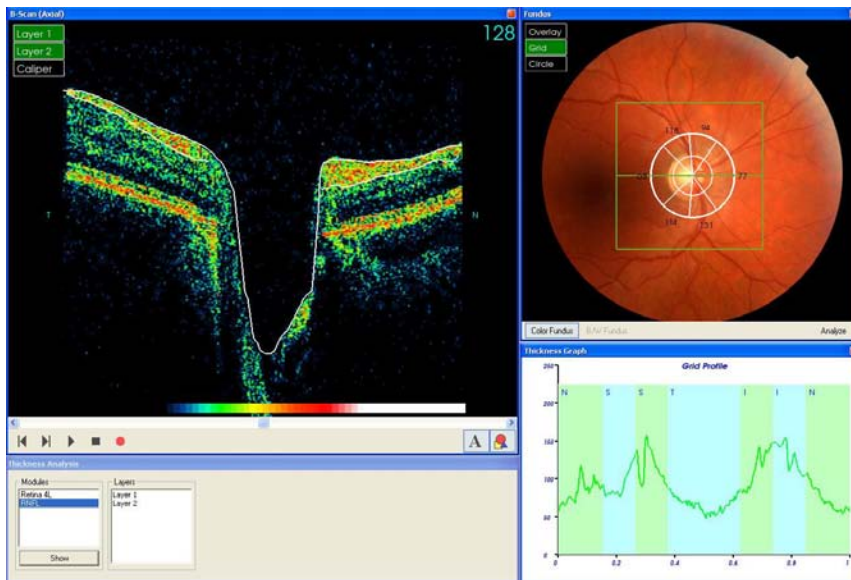
Figure 8.1: Screen shot from 3D Topcon 1000 optic disc scan 0013PD1032128 (visually normal adult) detailing the B- scan measuring the RNFL thickness, the disc grid overlaid on the fundus photograph, the measured sectors and presenting a graphic profile of the RNFL thickness sectors. N = nasal and T = temporal

In total two hundred and ninety two of the 394 (74%) disc scans imaged were included for analysis. The scan inclusion rate in the adult groups was high, visually normal adults 92%, amblyopic adults 72% and non-amblyopic adults with strabismus and/or anisometropia 93%. The amblyopic children had an inclusion rate of 74% however the visually normal children had a low inclusion rate of only 52%. The rejected scans were not included as they contained insufficient data to produce a mean measurement in all the required sectors, even with repositioning. In thirty-one scans the quality was poor i.e. included blinks, or movement; the measurements however, were included in the data set as they were considered to contain sufficient data. Twenty-four of these scans were from normal children and 5 were from amblyopic adults. In six cases the disc grid was not centred over the optic disc due to poorly maintained fixation. In these cases the grid was manually repositioned to ensure centration of the grid over the disc (Figure 8.3). In cases where there was a blink or movement that completely split the scan, the grid was repositioned and the measurements recorded from separate grid positions in order to obtain measurements for all of the 6 sectors (Figure 8.4). The low inclusion rate (52%) of the visually normal children is most probably due to the age of the visually normal group (5 years), as they found it very difficult to maintain the eccentric viewing position required to image the disc. The slightly older amblyopic children (7.5 years) found it easier to maintain the fixation required. The inclusion rate for our child amblyopic group (74%) is similar to that reported by the Australian population based study (78%) of disc RNFL thickness in normal 6 year olds (Huynh et al., 2006a).
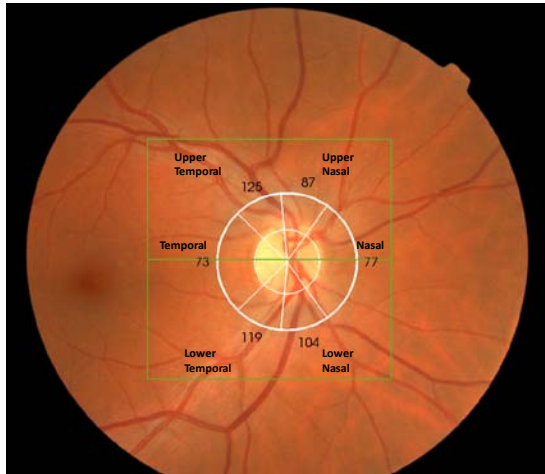
Figure 8.2: Screen shot from 3D-1000 Topcon optic disc scan AB01373346 (visually normal adult) detailing the disc grid sectors measuring RNFL thickness (μm) overlaid on the disc photograph

Figure 8.3: Screen shot from 3D-1000 Topcon disc photograph AB02003975 (amblyopic child) detailing the RNFL thickness measurements (μm). The grid has been manually moved to ensure centration over the optic disc.

279
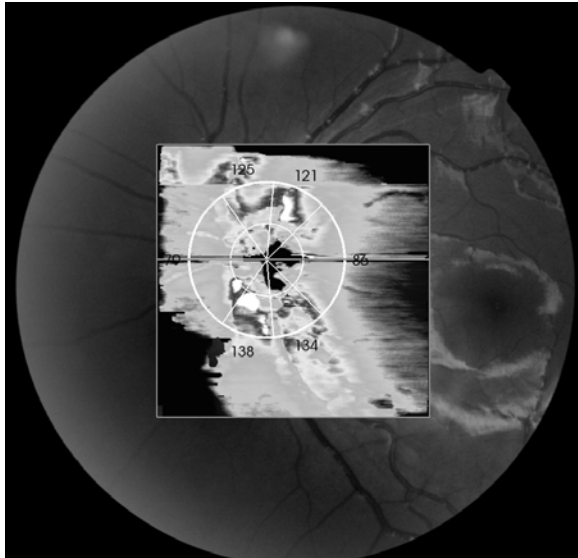
Figure 8.4: Example of a "poor" optic disc scan AB0172 (normal child) overlaid on the fundus photograph, detailing the RNFL thickness grid measurements. The grid has been manually repositioned to account for the blink (horizontal line across the optic disc).

8.4 Statistical Analysis

Statistical analysis was carried out using commercially available Stata SE version 10.0. Paired t-tests were used to compare the inter-ocular symmetry between eyes for each group, adults and children were analysed separately for all measured optic disc sectors. ANOVA of the differences between each group was used to evaluate the group differences, the Bonferroni correction was applied to the analysis (Chapter 7, statistical analysis). Linear regression analysis was used to investigate the effect of axial length, age and the presence of amblyopia on RNFL thickness.

8.5 Results

8.5.1 Retinal Nerve Fibre Layer Thickness in Visually Normal Adults

The retinal nerve fibre layer (RNFL) thickness around the optic disc was imaged and measurements obtained for the six sectors of the disc. In visually normal adults the traditional pattern of thicker RNFL in the superior and inferior sectors in comparison to the nasal and temporal sectors was demonstrated. Upper nasal (103.96±22.14µm), upper temporal (113.49±22.87µm), lower nasal (109.53±20.48µm), lower temporal (115.4±18.86µm), nasal (75.98±12.12µm) and temporal sectors (60.82±10.31µm) (Figure 8.5). A summary of the results of all the RNFL measurements in visually normal adults is provided in Table 8.1 and Figure 8.5.
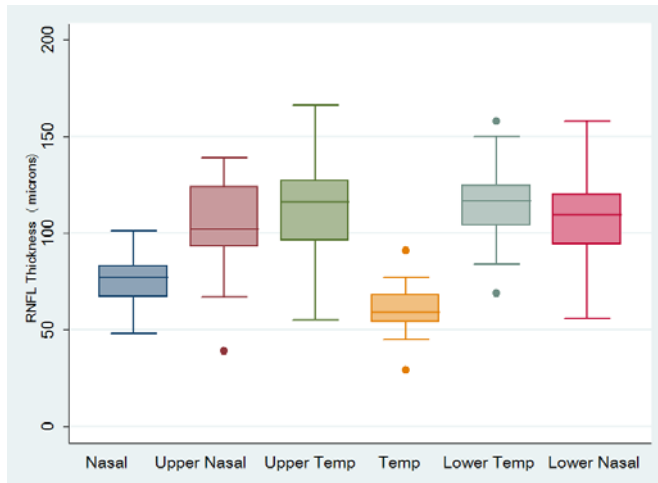
Figure 8.5: Box plots of RNFL thickness (µm) measurements in visually normal adults depicting the six sectors around the optic disc. The dots represent outliers.

8.5.2 Inter-ocular Symmetry (IOS)

Visually normal eyes were first examined in order to establish the degree of inter-ocular asymmetry that is present around the optic disc. There are claims that the fellow eye of amblyopes show subtle structural differences in size and shape of the optic disc similar to that of the amblyopic eye (Pineles and Demer, 2009). If this is the case then both eyes in amblyopes may show differences in RNFL thickness measurements relative to visual normals in order to establish if this is the case then it is necessary to examine inter-ocular symmetry, as well as differences in absolute RNFL thickness measurements between amblyopic and normal eyes (Table 8.1).

The dominant eyes in the visually normal adults and children were chosen
randomly with a random number generator programme in Excel.

Table 8.1: Disc RNFL (µm) measurements ± SD of the non-dominant and dominant eye in visually normal adults. Paired t-tests for each disc sector are shown.

Disc Sector	Adult Non-dom Eye (mean ± SD)	Adult Dominant Eye (mean ± SD)	Dom v Non-dom Eye Paired t-test
Nasal	76.53 µm (11.69)	75.98 µm (12.12)	p=0.66 CI:-3.08 to 1.98
Upper Nasal	105.71 µm (19.21)	103.96 µm (22.14)	p=0.52 CI:-7.24 to 3.73
Upper Temporal	112.51 µm (16.51)	113.49 µm (22.87)	p=0.80 CI:-6.57 to 8.53
Temporal	59.78 µm (10.03)	60.82 µm (10.31)	p=0.36 CI:-1.24 to 3.33
Lower Temporal	117.02 µm (21.43)	115.4 µm (18.86)	p=0.59 CI:-7.62 to 4.37
Lower Nasal	111.4 µm (23.20)	109.53 µm (20.48)	p=0.45 CI:-6.80 to 3.07

8.5.2.1 Visually Normal Eyes - Adults

A high degree of symmetry between the eyes was found in all measured RNFL
disc sectors. Although no significant difference was found, a degree of variation
exists within visually normal eyes. For example the lower nasal sector RNFL
thickness non-dominant = 111.4±23.20µm, dominant = 109.53±20.48µm, p=0.45
has a confidence interval from -6.8 to 3.07µm indicating some individual variation
within the normal expected range (Table 8.1).

Table 8.1 presents the differences between the mean measurements in visually
normal adults; individually no subject had an inter-ocular difference in the nasal

sector of greater than 18μm with a mean individual difference of 2μm, in the upper nasal sector the greatest individual difference was 55μm and the mean individual difference was 0.9μm. In the upper temporal sector 74μm was the greatest difference with a mean individual difference of 0.49μm, the greatest temporal sector difference was 18μm with a mean individual difference of 0.5μm, the greatest lower temporal sector difference was 50μm with a mean individual difference of 0.8μm and in the lower nasal sector the greatest individual difference was 38μm with a mean individual difference of 0.9μm. The statistics present a picture of a high degree of inter-ocular symmetry but with considerable individual variation in RNFL thickness in the peripapillary area in visually normal adults.

8.5.2.2 Visually Normal Eyes - Children

The degree of inter-ocular symmetry in the eyes of visually normal children was also analysed and again a high degree of symmetry between the eyes was found in all measured RNFL disc sectors. Again although no significant difference was found between the eyes, a degree of variation exists within the visually normal eyes; this variation is greater in the visually normal children in comparison to the visually normal adults. For example the upper nasal sector RNFL thickness (non-dominant = 114.97±18.66μm and dominant =109.67±25.29μm, p=0.20) has a confidence interval from -13.58 to 2.96μm indicating considerable individual variation between visually normal eyes. This variation in RNFL thickness was greatest in the lower nasal, lower temporal, upper nasal and upper temporal sectors. The results are presented in Table 8.2.

Table 8.2: Disc RNFL (µm) measurements ± SD of the non-dominant and dominant eyes in visually normal children. Paired t-tests for each disc sector are shown.

Disc Sector	Child Non-dom Eye (mean ± SD)	Child Dominant Eye (mean ± SD)	Dom v Non-dom Eye Paired t-test
Nasal	75.38 µm (9.48)	74.31 µm (11.01)	p=0.45 CI:-3.90 to 1.75
Upper Nasal	114.97 µm (18.66)	109.67 µm (25.29)	p=0.20 CI:-13.58 to 2.96
Upper Temporal	107.10 µm (21.72)	106.67 µm (24.44)	p=0.82 CI:-15.92 to 19.55
Temporal	62.97 µm (8.73)	61.10 µm (8.93)	p=0.23 CI:-4.95 to 1.21
Lower Temporal	115.92 µm (24.35)	111.2 µm (24.96)	p=0.39 CI:-15.70 to 6.25
Lower Nasal	114.95 µm (23.42)	116.87 µm (32.00)	p=0.50 CI:-16.81 to 12.39

Table 8.2 presents the differences between the mean measurements in visually normal children; individually no subject had an inter-ocular difference in the nasal sector of greater than 28µm with a mean individual difference of 0.5µm, in the upper nasal sector the greatest individual difference was 51µm and the mean individual difference was 0.88µm. In the upper temporal sector 62µm was the greatest difference with a mean individual difference of 0.2µm, the greatest temporal sector difference was 28µm with a mean individual difference of 0.9µm, the greatest lower temporal sector difference was 70µm with a mean individual difference of 4.85µm and in the lower nasal sector the greatest individual difference was 72µm with a mean individual difference of 2.2µm. The statistics present a picture of a high degree of inter-ocular symmetry, however, the visually normal children demonstrated greater individual variation in RNFL thickness in the peripapillary area than the visually normal adults, particularly in the lower sectors.

8.5.2.3 Adult Amlyopes

As with visual normals, a high degree of symmetry was found between the amblyopic eyes and amblyopic fellow eyes in all sectors (Table 8.3).

Table 8.3: Disc RNFL (µm) measurements ± SD of both eyes in amblyopic adults. The results of paired t-tests between the amblyopic eye and amblyopic fellow eye for each disc sector are shown.

Disc Sector	Adult Amblyopic Eye (mean ± SD)	Adult Amblyopic Fellow Eye (mean ± SD)	Fellow v Amblyopic Eye Paired t-test
Nasal	78.81 µm (14.83)	77.45 µm (17.67)	p=0.53 CI:-5.75 to 3.04
Upper Nasal	97.74 µm (19.36)	96.90 µm (19.32)	p=0.84 CI:-9.25 to 7.57
Upper Temporal	103.55 µm (18.10)	104.45 µm (16.02)	p=0.81 CI:-6.67 to 8.48
Temporal	57.16 µm (13.86)	56.19 µm (10.55)	p=0.72 CI:-6.49 to 4.56
Lower Temporal	115.55 µm (20.29)	111.90 µm (19.26)	p=0.38 CI:-12.05 to 4.76
Lower Nasal	108.16 µm (23.86)	107.16 µm (25.61)	p=0.79 CI:-8.78 to 6.78

Table 8.3 presents the differences between the mean measurements in amblyopic adults; individually no subject had an inter-ocular difference in the nasal sector of greater than 27µm with a mean individual difference of 0.7µm, in the upper nasal sector the greatest individual difference was 99µm and the mean individual difference was 0.4µm. In the upper temporal sector 48µm was the greatest difference with a mean individual difference of 0.46µm, the greatest temporal sector difference was 39µm with a mean individual difference of 0.49µm, the greatest lower temporal sector difference was 81µm with a mean individual

difference of 1.85μm and in the lower nasal sector the greatest individual difference was 50μm with a mean individual difference of 0.5μm. Again the statistics present a picture of a high degree of inter-ocular symmetry but with considerable individual variation in RNFL thickness in the peripapillary area in amblyopic adults.

8.5.2.4 Non-Amblyopic Adults with Strabismus and/or Anisometropia (S/A)

A high degree of symmetry was also demonstrated between the strabismic eye and / or the eye with the highest refractive error (S/A) eye and its fellow eye in non-amblyopic subjects. The difference between the strabismic/ anisometropic eye in the nasal sector approached but did not reach statistical significance (p=0.07) (Table 8.4).

Table 8.4: Disc RNFL (μm) measurements ± SD of both eyes in anisometropic or strabismic adults without amblyopia. The results of paired t-tests between the strabismic/anisometropic eye (S/A eye) and the S/A fellow eye for each disc sector are shown.

Disc Sector	Strabismic/High Ref Error Eye (mean ± SD)	Fellow Eye (mean ± SD)	Fellow v S/A Eye Paired t-test
Nasal	78.73 μm (19.76)	72.55 μm (17.58)	p=0.07 CI:-12.99 to 0.62
Upper Nasal	101.09 μm (17.00)	111.18 μm (24.88)	p=0.126 CI:-3.37 to 23.55
Upper Temporal	102 μm (17.46)	103.82 μm (26.94)	p=0.82 CI:-15.92 to 19.55
Temporal	57.18 μm (15.14)	55.27 μm (9.84)	p=0.61 CI:-10.07 to 6.26
Lower Temporal	106.91 μm (21.45)	105.82 μm (21.82)	p=0.86 CI:-14.88 to 12.70
Lower Nasal	117.18 μm (37.03)	109.82 μm (23.18)	p=0.28 CI:-21.80 to 7.07

Table 8.4 presents the differences between the mean measurements in non-amblyopic adults with S/A; individually no subject had an inter-ocular difference in the nasal sector of greater than 25μm with a mean individual difference of 3.1μm, in the upper nasal sector the greatest individual difference was 38μm and the mean individual difference was 5.0μm. In the upper temporal sector 47μm was the greatest difference with a mean individual difference of 0.91μm, the greatest temporal sector difference was 19μm with a mean individual difference of 0.95μm, the greatest lower temporal sector difference was 34μm with a mean individual difference of 0.55μm and in the lower nasal sector the greatest individual difference was 35μm with a mean individual difference of 3.7μm.

8.5.5.5 Amblyopic Children

Once again, a high degree of symmetry was found between the amblyopic eyes and the amblyopic fellow eyes in children (Table 8.5).

Table 8.5: Disc RNFL (μm) measurements ± SD of both eyes in amblyopic children. The results of paired t-tests between the amblyopic eye and the fellow eye for each disc sector are shown.

Disc Sector	Child Amblyopic Eye (mean ± SD)	Child Fellow Eye (mean ± SD)	Fellow v Amblyopic Eye Paired t-test
Nasal	86.11 μm (14.27)	82.05 μm (15.35)	p=0.10 CI:-8.92 to 0.82
Upper Nasal	117.58 μm (18.77)	115 μm (22.83)	p=0.61 CI:-12.93 to 7.77
Upper Temporal	110.63 μm (21.50)	108.11 μm (22.35)	p=0.75 CI:-18.95 to 13.90
Temporal	63.53 μm (13.42)	61.74 μm (7.30)	p=0.34 CI:-5.64 to 2.06
Lower Temporal	112 μm (28.81)	111.84 μm (17.79)	p=0.99 CI:-18.34 to 18.03
Lower Nasal	124.63 μm (26.40)	122.42 μm (23.91)	p=0.28 CI:-21.80 to 7.07

Table 8.5 presents the differences between the mean measurements in amblyopic children; individually no subject had an inter-ocular difference in the nasal sector of greater than 21µm with a mean individual difference of 2.0µm, in the upper nasal sector the greatest individual difference was 54µm and the mean individual difference was 1.9µm. In the upper temporal sector 63µm was the greatest difference with a mean individual difference of 1.3µm, the greatest temporal sector difference was 17µm with a mean individual difference of 0.9µm, the greatest lower temporal sector difference was 71µm with a mean individual difference of 0.08µm and in the lower nasal sector the greatest individual difference was 64µm with a mean individual difference of 1.1µm.

8.5.5.6 ANOVA of Differences

In order to identify if the degree of symmetry differed between the groups, the inter-ocular difference found in each group (normal adults, amblyopic adults, amblyopic children and normal children) was analysed using an ANOVA. No significant difference was found between the inter-ocular differences across the various participant groups. The results of the ANOVA of differences are presented in Table 8.6.

Disc Sector *Differences*	Source of variation	Degrees of freedom	Sum of squares	Variance Ratio (F)	Probability
Nasal *Differences*	Between groups Within groups	3 265	85.33 12384.06	0.61	0.61
Upper Nasal *Differences*	Between groups Within groups	3 265	194.76 68191.78	0.27	0.85
Upper Temporal *Differences*	Between groups Within groups	3 265	98.43 93714.39	0.09	0.96
Temporal *Differences*	Between groups Within groups	3 265	106.22 14067.67	0.67	0.57
Lower Temporal *Differences*	Between groups Within groups	3 265	912.92 88484.42	0.91	0.44
Lower Nasal *Differences*	Between groups Within groups	3 265	513.74 76039.31	0.60	0.62

An overview of the RNFL thickness measurements for each group is provided in

Table 8.7.

Table 8.7: Disc RNFL (µm) measurements ± SD for all 5 categories, visually normal adults, amblyopic adults, non-amblyopic adults with S/A, visually normal children and amblyopic children.

Disc Sector	Adult Visual Normal (mean ± SD)	Adult Amblyopes (mean ± SD)	Strabismic/High Ref Error Eye (mean ± SD)	Child Visual Normal (mean ± SD)	Child Amblyopes (mean ± SD)
Nasal	75.97µm (12.12)	79.2µm (14.92)	78.73µm (19.76)	74.31µm (11.00)	86.11µm (14.27)
Upper nasal	103.96µm (22.14)	98.53µm (19.17)	101.09µm (17.00)	109.67µm (25.29)	117.58µm (18.77)
Upper Temporal	113.49µm (22.87)	103.67µm (18.40)	102µm (17.46)	106.67µm (24.44)	110.63µm (21.50)
Temporal	60.82µm (10.31)	57.23µm (14.09)	57.18µm (15.14)	61.10µm (8.93)	63.53µm (13.42)
Lower Temporal	115.4µm (18.86)	115.77µm (20.6)	106.91µm (21.45)	108.33µm (27.37)	112µm (28.81)
Lower Nasal	109.53µm (20.48)	109.63µm (22.79)	117.18µm (37.03)	116.87µm (32.01)	124.63µm (26.39)

8.6 RNFL Thickness: The effect of axial length and age.

Previous studies investigating the peripapillary RNFL thickness using OCT in adults (Alamouti and Funk, 2003; Parikh et al., 2007) and children (El-Dairi et al., 2009; Huynh et al., 2006c; Salchow et al., 2006) have demonstrated that mean RNFL thickness is frequently affected by the variables of axial length and age. In order to account for the effect produced by these variables, multivariate regression analysis was performed. As there are only a small number of non-amblyopic adults (n=14) with the presence and/or absence of strabismus, in comparison to the other groups (visually normal adults n=47, visually normal children n=73, amblyopic adults =36 and amblyopic children = 27) and little notable significance has been demonstrated in this group (Chapter 7and Chapter 8, Table 8.8) they were not included in the analysis. The RNFL thickness value was the dependant variable and analysed separately for each peripapillary sector, axial length and age were included in the model as continuous variables and a categorical variable of the presence/ absence of amblyopia was also included. The majority of studies (Budenz et al., 2007, Huynh et al., 2006b, Pakravan et al., 2009) report the mean RNFL thickness measurement in relation to axial length. In order to allow comparison to other peer reviewed studies, the 6 peripapillary sectors were therefore combined to produce a mean RNFL thickness measurement in addition to the 6 individual sector measurements. Regression analysis with adjustment for axial length and age (for details of axial length and age for all participants see Chapter 6, data sets 1- 4) indicated a significant effect on the mean RNFL thickness from axial length (p=0.023) (Table 8.8). This was also significant in the

nasal sector (p=0.004) (Table 8.9), and upper nasal sector (p=0.002) (Table 8.10), but not in any of the temporal sectors or lower nasal sector (Tables 8.11 – 8.14).The mean RNFL thickness reduced by 1.94µm for every 1mm increase in axial length. In the nasal sector, RNFL thickness reduced by 2.48µm for every 1mm increase in axial length and in the upper nasal sector, RNFL thickness reduced by 4.73µm for every 1mm increase in axial length (Tables 8.8 - 8.10, Figures 8.6 and 8.7). Age was not found to have a statistical effect for any RNFL thickness measurements, with the exception of the temporal sector (p=0.02). The RNFL in the temporal sector was shown to reduce by 0.15µm for every 1 year increase in age (Table 8.12 and Figure 8.8). The presence of amblyopia was not found to have a significant effect on the RNFL thickness in any of the sectors (Tables 8.8 – 8.14).

Table 8.8: Multiple linear regression analysis of **mean RNFL** (µm) thickness including independent variables for the axial length, age and the presence of amblyopia.

Variable	Regression Coefficient	Standard error	P-value	95% CI (µm)
Axial length	-1.93	0.85	**0.02**	-3.61 to -0.27
Age	-0.04	0.07	0.53	-0.18 to 0.09
Amblyopia	-1.06	19.1	0.70	-6.52 to 4.39

Table 8.9: Multiple linear regression analysis of **nasal RNFL** (µm) thickness including independent variables for the axial length, age and the presence of amblyopia.

Variable	Regression Coefficient	Standard error	P-value	95% CI (µm)
Axial length	-2.48	0.85	**0.004**	-4.16 to -0.79
Age	0.03	0.07	0.63	-0.10 to 0.17
Amblyopia	2.87	2.77	0.30	-2.61 to 8.35

Table 8.10: Multiple linear regression analysis of **upper nasal RNFL** (µm) thickness including independent variables for the axial length, age and the presence of amblyopia.

Variable	Regression Coefficient	Standard error	P-value	95% CI (µm)
Axial length	-4.73	1.46	**0.002**	-7.62 to -1.85
Age	-0.08	0.12	0.5	-0.31 to 0.15
Amblyopia	-6.27	4.76	0.19	-15.68 to 3.15

Table 8.11: Multiple linear regression analysis of **upper temporal RNFL** (µm) thickness including independent variables for the axial length, age and the presence of amblyopia.

Variable	Regression Coefficient	Standard error	P-value	95% CI (µm)
Axial length	-1.27	1.52	0.41	-4.27 to 1.73
Age	-0.01	0.12	0.96	0.25 to 0.24
Amblyopia	-5.07	4.94	0.31	-14.85 to 4.70

Table 8.12: Multiple linear regression analysis of **temporal RNFL** (µm) thickness including independent variables for the axial length, age and the presence of amblyopia.

Variable	Regression Coefficient	Standard error	P-value	95% CI (µm)
Axial length	0.03	0.76	0.97	-1.48 to 1.54
Age	-0.15	0.06	**0.02**	-0.27 to -0.03
Amblyopia	0.87	2.49	0.73	-4.06 to 5.79

Table 8.13: Multiple linear regression analysis of **lower temporal RNFL** (μm) thickness including independent variables for the axial length, age and the presence of amblyopia.

Variable	Regression Coefficient	Standard error	P-value	95% CI (μm)
Axial length	-0.58	1.60	0.72	-3.76 to 2.59
Age	0.144	0.13	0.27	-0.11 to 0.39
Amblyopia	-0.29	5.23	0.96	-10.64 to 10.06

Table 8.14: Multiple linear regression analysis of **lower nasal RNFL** (μm) thickness including independent variables for the axial length, age and the presence of amblyopia.

Variable	Regression Coefficient	Standard error	P-value	95% CI (μm)
Axial length	-2.70	1.75	0.13	-6.16 to 0.76
Age	-0.19	0.14	0.17	-0.47 to 0.08
Amblyopia	1.16	5.70	0.84	-10.12 to 12.44
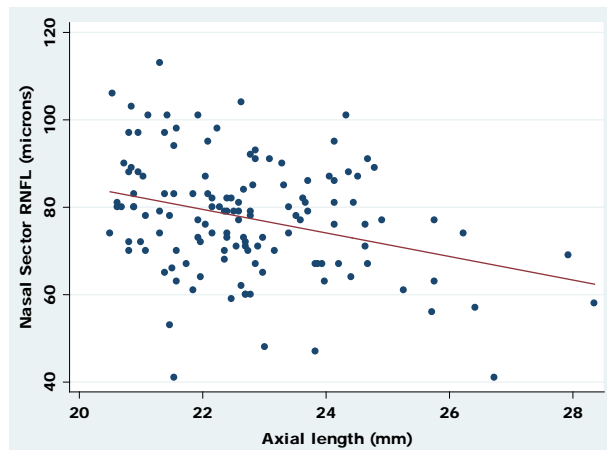
Figure 8.6: Linear regression of **nasal** RNFL thickness (μm) v axial length (mm) in visually normal adults and children, amblyopic adults and children. The equation for the regression line (red) is $y = -2.48x + 131.99$ (95% CI for slope, -4.16 to -0.79).
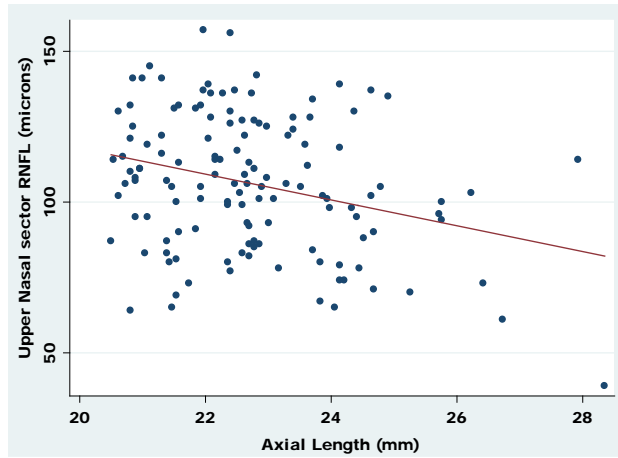
Figure 8.7: Linear regression of **upper nasal** RNFL thickness (µm) v axial length (mm) in visually normal adults and children, amblyopic adults and children. The equation for the regression line (red) is $y = -4.73x + 217.9$ (95% CI for slope, -7.62 to -1.84).
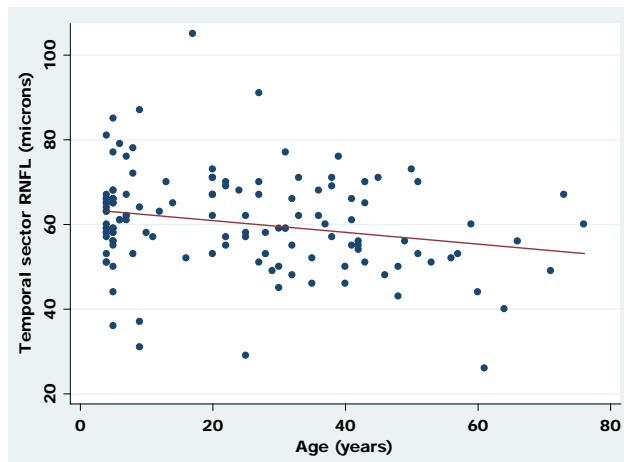
Figure 8.8: Linear regression of **temporal** RNFL thickness (µm) v age (years) in visually normal adults and children, amblyopic adults and children. The equation for the regression line (red) is $y = -0.15x + 62.9$ (95% CI for slope, -0.27 to -0.03).

8.6.1 RNFL Thickness: Association of Visual Acuity

The RNFL thickness (μm) in the nasal sector was one of the closest sectors to demonstrating an effect from the presence of amblyopia (p=0.30), therefore the relationship between RNFL thickness in this sector and visual acuity was further investigated (Figure 8.9). The RNFL thickness varies across all levels of visual acuity presented.
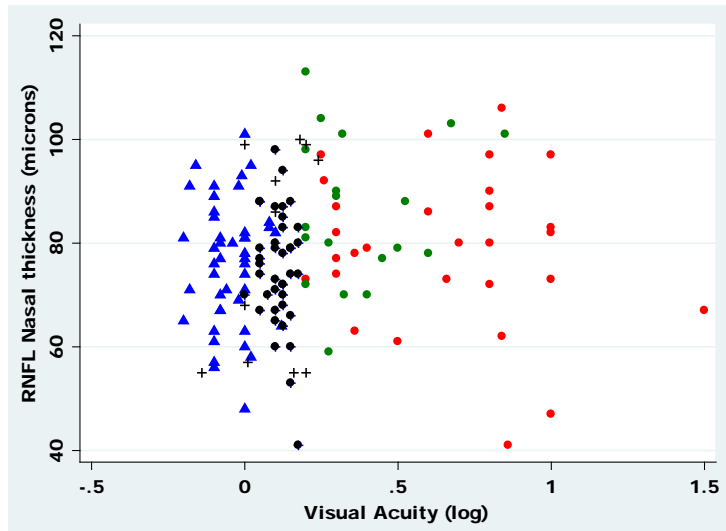
Figure 8.9: RNFL Nasal thickness (μm) compared to the amblyopic or non-dominant eye visual acuity (logMAR) for amblyopic adults ● amblyopic children ● visually normal adults ▲ visually normal children ● and non-amblyopic adults + .

8.7 Discussion

8.7.1 Retinal Nerve Fibre Layer Thickness - Visually Normal Adults

The RNFL thickness measured in visually normal adults produced the typical "double hump" pattern described in previous studies (Blumenthal et al., 2009; Frenkel et al., 2005) with the superior (upper nasal = 103.96±22.14μm, upper temporal = 113.49±22.87μm) and inferior (lower nasal = 109.53±20.48 μm, lower temporal = 115.4 ± 18.86μm) sectors being thicker than the nasal (75.98±12.12μm) and temporal (60.82±10.31μm) sectors. The majority of commercially available OCT's produce RNFL measurements in the format of quadrants, superior, inferior, nasal and temporal; the RNFL measurement grid used in the 3D-1000 Topcon splits the superior and inferior quadrants into upper nasal and upper temporal and lower nasal and lower temporal sectors. This format limits direct comparison with other studies. However, by combining both upper and both lower sectors comparisons can be made. As OCT technology has developed the volume of published studies have also grown, with the earliest published studies using time-domain OCT, but the more recent studies using Fourier Domain OCT. Comparisons between current study results and previously published values are provided in Table 8.15.

Table 8.15: Comparison of normal adult RNFL (µm) thickness measurements for each quadrant from this current study with three previously published studies.

Study	Inferior (mean ± SD)	Superior (mean ± SD)	Nasal (mean ± SD)	Temporal (mean ± SD)
Bruce 2010 (3D OCT-1000)	112.47 ± 19.79µm	108.72 ± 22.88µm	75.98 ± 12.12µm	60.82 ± 10.31µm
Pakravan 2009 (3D OCT-1000)	80.5 ± 10.5µm	78.5 ± 10.1µm	77.1 ± 13.9µm	63.2 ± 9.7µm
Leung 2009 (Cirrus HD-OCT)	127.48 ± 14.51µm	122.49 ± 14.18µm	66.05 ±10.79µm	71.20 ± 11.70µm
Budenz 2005 (Stratus OCT)	131.5 ± 18.1µm	125.5 ± 15.8µm	76.3 ± 14.7µm	72.7 ± 13.1µm

All of these studies demonstrate the pattern of increased thickness in the superior and inferior quadrants, and present similar thickness measurements in nasal and temporal quadrants. However, in the inferior and superior sectors there is a higher degree of variation between the studies with the superior sector measurements ranging from 78.5±10.1µm (Pakravan et al.,2009) to 125.5±15.8µm (Budenz et al.,2005). The measurements produced by the time-domain OCT systems (Budenz et al., 2005) are generally thicker than the Fourier-domain OCT systems (Leung et al., 2009; Pakravan et al., 2009). This may be due to the differing techniques obtaining the A-scans. With the Topcon system, a raster grid pattern covers a 6mm x 6mm area over the disc and the circular grid (diameter = 3.4mm) is superimposed. The scans from within the circle are then identified and the thickness measurement calculated. With the time-domain systems the measurement circle is manually placed and 3 circular scans (diameter 3.4mm) are taken around the optic disc and the average thickness for each quadrant is then determined. This difference in thickness between the OCT modalities has recently

been reported (Huang et al., 2010; Knight et al., 2009) and, although the different systems correlate well, there are systematic differences between the measurements of RNFL thickness making direct comparison problematic. There is limited evidence from histological studies to allow comparison; one study has compared histological measurements to OCT and GDx results (Blumenthal et al., 2009) and found peripapillary RNFL thickness measurements from histology, OCT and GDx to be comparable. However, as the published histological study was carried out on a single eye many more measurements would be required before confirmation that each method produces similar measures for a given eye.

8.7.2 Visually Normal Eyes – Children

The RNFL thickness measured in the visually normal children also produced the typical "double hump" pattern described (Blumenthal et al., 2009; Frenkel et al., 2005) with the superior (upper nasal = 109.67±25.29µm, upper temporal = 106.67±24.44 µm) and inferior (lower nasal = 116.87±32.01 µm, lower temporal = 108.33±27.37µm) sectors being thicker than the nasal (74.31±11.0µm) and temporal (61.10±8.93µm) sectors. The thickness measurements are reported along with those from previous studies of RNFL thickness in children in Table 8.16. The measurements in this study using Fourier domain OCT are, as with the adult data, reduced in comparison to those reported with the time domain OCT technology (El-Dairi et al., 2009; Huynh et al., 2006a; Salchow et al., 2006) (Table 8.16).

Table 8.16: Comparison of RNFL (μm) thickness measurements in visually normal children for each quadrant from four different studies. No standard deviation is quoted in the El-Dairi (2009) study.

Study	Inferior (mean ± SD)	Superior (mean ± SD)	Nasal (mean ± SD)	Temporal (mean ± SD)
Bruce 2010 (3D OCT-1000)	112.6 ± 29.9μm	108.16 ± 24.76μm	74.31 ± 11μm	61.1 ± 8.93μm
Salchow 2006 (Stratus OCT)	136.9 ± 16.9μm	135.4 ± 19.3μm	83.0 ± 18.0μm	72.5 ± 13.4μm
Huynh 2006 (Stratus OCT)	127.8 ± 20.5μm	129.5 ± 20.6μm	81.7 ±19.6μm	75.7 ± 14.7μm
El-Dairi 2009 (Stratus OCT)	129 μm	143 μm	83 μm	78 μm

8.7.3 Inter-Ocular Symmetry (IOS)

A high degree of symmetry was found in all the measured RNFL sectors. As with foveal topography, RNFL thickness in the peripapillary area is important to establish in visual normals as it provides a standard comparison. Inter-ocular symmetry of the RNFL has been noted in studies of both adults and children using OCT (Budenz, 2008; Dubis et al., 2009; Huynh et al., 2007) although in these studies considerable individual variation was noted. In this study of RNFL thickness inter-ocular symmetry has been shown to be present in all recruited cohorts; adults, children, amblyopes, non-amblyopic individuals (S/A) and visually normal controls.

8.7.4 Retinal Nerve Fibre Thickness – Amblyopia

Imaging studies of RNFL thickness in amblyopia have produced equivocal results. In a study using time domain OCT to image amblyopic eyes (Yen et al., 2004) a difference was demonstrated between amblyopic eyes and their fellow eyes with anisometropia, with the amblyopic eyes having thicker RNFL measurements than the fellow eye. Yen et al (2004) also found the amblyopic eyes to have a thicker RNFL than a group of control eyes with anisometropia but without amblyopia. No inter-ocular difference was found in strabismic amblyopes. Similarly in a study using GDx (Colen et al., 2000) no difference was found between the amblyopic eye and the fellow eye. The majority of the studies, with the exception of Yen et al (2004) have used the fellow eye as the comparator to the amblyopic eye. In the present study a consistent degree of intra-ocular symmetry has been demonstrated in each cohort. The presence of inter-ocular symmetry is therefore likely to contribute to the results showing no significant difference in RNFL thickness produced in the previous published studies where the amblyopic and the fellow eye have been directly compared. That said, in this study no significant difference was found in the RNFL thickness in any of the sectors in the peripapillary region of the optic disc in the presence of amblyopia compared to visual normals. It could be expected, in particular, that the temporal sector, where the papillomacular bundle enters the optic disc, has the potential to be affected by the presence of amblyopia. This was not found.

The nasal RNFL thickness (86.11μm) and upper nasal thickness (117.58μm) in amblyopic children appear to be thicker than the other groups, the presence of

amblyopia, however, does not significantly affect RNFL thickness in either of these sectors. These two sectors are particularly influenced by axial length, with the RNFL reducing by 2.48µm and 4.73µm for every 1mm increase in axial length respectively in the nasal and upper nasal sectors. The mean axial length in the amblyopic children (21.38mm) (Chapter 8- RNFL Thickness: axial length) is lower than the other groups and it is likely that it is the effect of a shorter axial length rather than the presence of amblyopia that is contributing to the thicker RNFL measurements in amblyopic children in these sectors.

The majority of studies measuring RNFL thickness with amblyopia have failed to find any thickness difference in amblyopic eyes relative to their fellow eye. In two separate studies using time domain OCT in children (Repka et al., 2006; Repka et al., 2009b), no significant difference in RNFL thickness between the amblyopic and the fellow eye was found. In an imaging study of RNFL thickness in children with strabismus, no significant difference was found between visually normal children or amblyopic children with either esotropia or exotropia (Reche-Sainz et al., 2006). The latter study, however, only examined children with mild reduction in visual acuity, this could have accounted for the lack of difference found. In the series of publications from a large scale Australian population based study (Huynh et al., 2006c) no difference was found between the RNFL thickness in amblyopic eyes compared to visually normal eyes. Only two studies have found a significant difference (Yen et al., 2004; Yoon et al., 2005) and both of these studies found significant differences between retinal nerve fibre layer (RNFL) thickness in the amblyopic eye in comparison to the fellow eye in anisometropic amblyopes only,

with the amblyopic eyes demonstrating increased RNFL thickness. This finding is not corroborated by the present study.

8.7.5 RNFL Thickness in Visually Normal Eyes: Age

On analysis of the data for the majority of the sectors, age was not found to be a significant contributing factor. However, an effect was found in the temporal sector. In the temporal sector the RNFL thickness was shown to reduce with age by 0.15µm per year (p=0.02) (Table 8.12 and Figure 8.8). This finding needs to be considered in comparison to previous imaging studies which report that age is a factor affecting RNFL thickness (Alamouti and Funk, 2003; El-Dairi et al., 2009; Parikh et al., 2007; Poinoosawmy et al., 1997). These studies have all reported the effect of age on the **mean** RNFL thickness and have generally reported on older adult subjects. In order to allow comparison with these other studies the mean RNFL thickness value was calculated from the 6 peripapillary sectors for each participant. The regression analysis did not show any effect of age on the mean RNFL thickness (p=0.53). The mean age of the adults in this study was 32 years and the children's mean age 5 years. In the study presented by Parikh et al (2007) RNFL thickness was reported to reduce with age, especially over the age of 50 years. The current study includes only 4 participants over 50 years which may account for the lack of an age effect. However, similar to this study, other published studies have also failed to find a significant correlation with age, (Leung et al., 2010; Pakravan et al., 2009). Pakravan et al (2009) imaged 96 visually normal adults, mean age 33 years (range 20 – 53 years) and found no significant

303

effect of age on RNFL thickness (p=0.95). A study using scanning laser polarimetry in children (Filous et al., 2008) also found no correlation between RNFL and age, and in a histological study of the RNFL (Repka and Quigley, 1989) no decrease in the number of retinal nerve fibre axons with age was found, although a large variability of axon numbers amongst individuals existed and this could have masked the effect of age. This variability may account for the findings in the temporal sector; however, it should be considered that if the RNFL reduction with age is restricted to the temporal sector the effect of age could also have been masked in the mean measurement commonly reported in other studies.

8.7.6 RNFL Thickness: Axial Length

In this study axial length was found to be correlated with RNFL thickness, with the mean RNFL thickness reducing by 1.94µm for every 1mm increase in axial length (Table 8.8). In a study of visually normal children (Huynh et al., 2006c) an average RNFL thickness decrease of 2.2µm for every 1 mm increase in axial length was reported and a study of adult normal eyes (Budenz et al., 2007) found a decrease of 2.2µm (95% CI, 1.1 -3.4) for every 1mm increase in axial length. In a study comparing the 3D-100 Topcon OCT with the OCT II (Humphrey-Zeiss Meditec Inc, Dublin) (Pakravan et al., 2009) no significant correlation between axial length and RNFL thickness was found (p=0.32). The majority of studies have highlighted the mean RNFL thickness measurement in relation to axial length. The present study demonstrates that although the mean RNFL does indeed reduce with an increase in axial length, this is limited to the nasal and upper nasal sectors (Tables 8.9 and

8.10 and Figures 8.6 and 8.7). This finding is similar to Leung et al (2006) who noted in their study that although there was a high correlation between axial length and RNFL thickness in the nasal sectors (nasal sector p=0.027), there was no correlation in the temporal sectors (temporal sector p=0.46). In the study reported by Leung (2006) of RNFL thickness in myopia (Leung et al., 2006), it was noted that a high proportion of myopes demonstrated RNFL thickness outside the expected normal limits in the nasal sectors (10% in low myopia to 20% in high myopia); this was particularly evident in the supero-nasal sector. In the present study both axial length and age were taken into account during the analysis of the RNFL thickness and therefore the results should not be unduly influenced by any increase in myopia/ axial length that naturally occurs with age with the potential to confound the results.

8.7.7 Stability of Fixation

The ability to maintain steady fixation and hence the quality of the scans was not as good in the children as in the adults and this may have affected the results, giving a spurious result in the nasal sector. A study examining the effect of the improper alignment of the scan circle around the optic nerve head whilst measuring RNFL thickness with the Stratus OCT (time-domain) (Vizzeri et al., 2008) found a significant difference in scan results if the scan was not centrally aligned over the disc and was in fact displaced temporally (p=<0.001). In the present study, nineteen out of the 34 (56%) adult amblyopes with analysed optic disc scans had a convergent deviation and 72% had eccentric fixation and twenty-two (81%)

children had a convergent deviation and 59% had eccentric fixation, this could have led to the position of the scan grid being displaced temporally thus producing a thinner nasal RNFL thickness measurement. However, the axial length of the amblyopes (mean = 22.01µm, range 20.5µm to 24.52µm) was less than the visual normals (mean = 23.16µm, range 20.89µm to 26.42µm). If the RNFL thickness measurement in the nasal sector was influenced by the convergent position of the amblyopic eyes it would be expected that with a shorter axial length the RNFL measurement would be thinner; however, the opposite was found (Table 8.9 and 8.10 and Figure 8.6 and 8.7). The quality of fixation would, therefore, not appear to explain the findings of this study.

8.8 Conclusion

The investigation of the peripapillary RNFL thickness has found no significant difference in thickness in the presence of amblyopia. RNFL thickness however does seem to be affected by axial length, particularly in the nasal (p=0.004) and upper nasal sectors (p=0.002) and by age in the temporal sector (p=0.02). This is difficult to explain in terms of retinal anatomy and retinal development. These effects may be due to the variation found in the thickness in the peripapillary area around the disc; variation around the disc has been previously attributed to the blood vessels entering the orbit, (Hood et al., 2008; Hood et al., 2009). However, the vessels are mainly located in the nasal and temporal, upper and lower sectors and only the upper nasal sector demonstrated differences in RNFL thickness. Where differences have been found between amblyopic and normal or fellow eyes

306

in other studies (Repka et al., 2009b; Yen et al., 2004) although not always significant, a picture of increased thickness in amblyopic eyes has been reported, this differs from the current findings. Although foveal thickness (Chapter 7) was found to be increased in amblyopes, the peripapillary retinal nerve fibre layer appears similar in normals and amblyopes. If the increased foveal thickness found in Chapter 7 is indeed from the lengthening of the photoreceptors, with subsequent reduction of the foveal pit depth, then it may not necessarily translate into an effect on the peripapillary area around the optic disc. The retinal ganglion cell axons travel from the macula via the papillomacular bundle to the optic disc (Chapter 1). As they travel, they are situated deep within the paillomacular bundle surrounded by the fibres from more peripheral retina. The evidence from this study suggests amblyopia, or the conditions thought to cause amblyopia, are not associated with a change in peripapillary RNFL thickness.

Chapter 9. Papillomacular Bundle Structure in Amblyopia

9.1 Introduction

The papillomacular bundle runs between the macula and the optic disc (Figure 9.1).
It is comprised of the retinal ganglion cell axons from the macula which are
grouped together into bundles travelling towards the optic disc (Figure 9.2) (Ogden,
1984). Histological studies have shown that as the axon bundles approach the
optic disc they increase in size; this is due to lateral fusion with other bundles and
is reflected in the increased RNFL thickness that is reported around the optic disc
(Minckler, 1980; Ogden, 1983). The papillomacular bundle has been the subject to
a small number of histological studies (Ogden, 1984; Varma et al., 1996) but
currently no published data was found from imaging studies detailing RNFL
thickness between the macula and the optic disc. The aim of this chapter is to
provide quantitative data detailing the RNFL thickness between the macula and the
optic disc in both visually normal adults and children and also in amblyopic adults
and children. Given that amblyopia is diagnosed when there is a reduction in visual
acuity, it is reasonable to ask whether there is a likely explanation for the visual
acuity deficit in the structure of the fibres carrying information from the fovea to the
optic disc en route to the cortex.
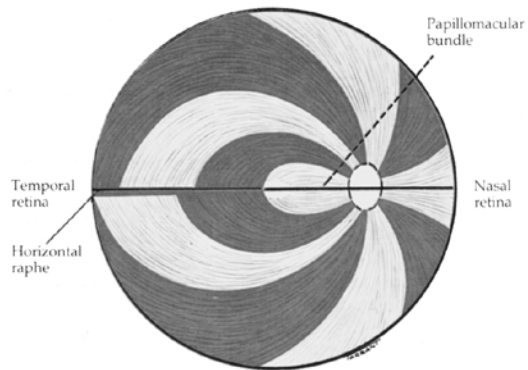
Figure 9.1: Illustration of retinal nerve fibre layer configuration the papillomacular bundle is positioned between the macula and the optic disc. (Adapted from Kanski 1999).

Figure 9.2: Illustration of retinal nerve fibre layer in the human eye using a green filter to define the axons of the RNFL. (Adapted from Kanski 1999).

9.2 Methods

The participants recruited to this stage of the study are comprised of the same individuals recruited to the foveal topography and RNFL thickness stages (Chapter 7 and Chapter 8) of the study. (Refer to Chapter 7 for detailed description of the groups and methods of recruitment).

9.23 Papillomacular Measurement – Retinal Nerve Fibre Thickness

Prior to the setting up of the study imaging of the papillomacular bundle using the "central scan" modality of the OCT was piloted. This mode of scan was collected easily with the adult participants but not with the children. The children did not have the concentration to sit for macular, disc and central scan images; a decision was therefore made to scan the children only using the macula and disc modes. However, in order to obtain data regarding the papillomacular bundle, the disc scan mode was adapted. The retinal nerve fibre thickness (RNFL) was measured using the 3D OCT-1000 (Topcon, Tokyo, Japan) standard disc scan, made up of 256 x 256 A-scans covering a putative 6mm x 6mm area across the disc (Figure 9.3) as described in Chapter 8. The 6mm x 6mm grid was then manually repositioned with the centre of the grid in the centre of the optic disc scan; this allowed RNFL measurements to be recorded from 6 areas of the papillomacular bundle, P1,P2, S1,S2,I1 and I2 (Figure 9.3 and Table 9.1).
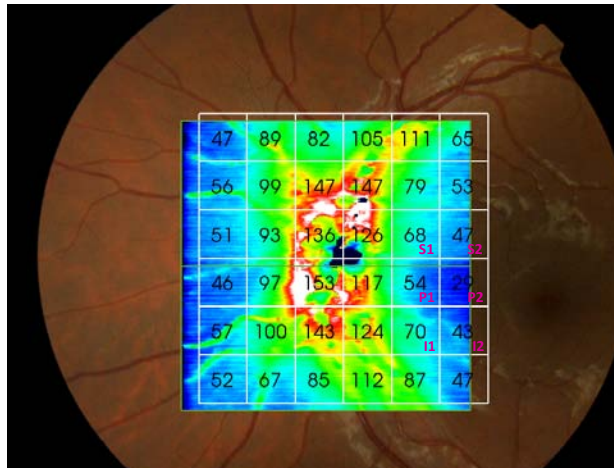
Figure 9.3: Disc scan of AB0133 LE with 6mmx6mm grid positioned to provide RNFL (µm) measurements of the papillomacular bundle. The 6 sectors measured were P1, P2, S1, S2, I1 and I2 as described in Table 10.1.

Table 9.1: Description of papillomacular sectors measured.

Description of Measured Sector	Papillomacular Area
Central area next to optic disc	P1
Central area nearest macula	P2
Superior area next to optic disc	S1
Superior area nearest macula	S2
Inferior area next to optic disc	I1
Inferior area nearest macula	I2

In total three hundred and twenty-four scans of the 394 (82%) disc scans imaged were included for analysis of papillomacular RNFL thickness. The scan inclusion rate in the adult groups was high; visually normal adults: 93.6%, amblyopic adults: 91.6%; non-amblyopic adults with strabismus and/or anisometropia: 100%. The amblyopic children had an inclusion rate of 81.5%. However, the visually normal children had a lower inclusion rate of 68.5%. In all groups the inclusion rate was higher than that of the peripapillary scans around the optic disc. This was mainly due to the fact that movements and blinks tended to occur at the superior and inferior sections of the 6 x 6mm raster scan affecting the peripapillary circular scan encompassing the optic disc but not disturbing the central area where the papillomacular bundle enters the optic disc. The papillomacular scans were therefore relatively unaffected. The excluded scans did not differ from the included scans along the area of interest (papillomacular bundle) except for the lack of data due to movement or blink.

9.3 Statistical Analysis

Statistical analysis was carried out using commercially available Stata SE version 10.0. Paired t-tests were used to compare the inter-ocular symmetry between eyes for each group, adults and children were analysed separately for all measured sectors of the papillomacular bundle. ANOVA of the differences between each group was used to evaluate the group differences, the Bonferroni correction was applied to the analysis (Chapter 7, statistical analysis). Linear regression analysis was used to investigate the effect of axial length, age and the presence of

amblyopia on papillomacular bundle RNFL thickness. The dominant eyes in the visually normal adults and children were chosen randomly with a random number generator programme in Excel.

9.4 Results

9.4.1 Papillomacular RNFL Thickness in Visually Normal Adults

The retinal nerve fibre layer (RNFL) thickness extending between the macula and the optic disc was imaged and measurements produced for the six sectors described in Table 9.1. The papillomacular bundle in visually normal adults was found to have a pattern of thicker RNFL in the superior and inferior sectors in comparison to the central sectors and the sectors closest to the optic disc (P1, S1 and I1) were thicker than the sectors closest to the macula (P2, S2, I2), mean RNFL thickness measures of the randomly chosen dominant eyes were as follows: P1= 42.27±14.74μm, P2= 20.09±12.15μm, S1 = 54.97±12.64μm, S2 = 33.09±10.21μm, I1= 60.97±19.19μm and I2 = 29.61±13.77μm (Figure 10.4). A summary of the results of all the papillomacular RNFL measurements in visually normal adults is provided in Table 9.2 and Figure 9.4.

Table 9.2: Papillomacular RNFL measurements (µm) ± SD of the 6 sectors in dominant and non-dominant eyes of visually normal adults. Paired t-tests for each disc sector are shown.

Papillomacular Sector	Adult Dom Eye (mean ± SD)	Adult Non-Dom Eye (mean ± SD)	Dom v Non-dom Eye Paired t-test
P1	51.30 µm (10.88)	50.95 µm (14.63)	p=0.78 CI: -2.15 to 2.83
P2	23.86 µm (10.09)	23.84 µm (9.00)	p=0.99 CI:-2.6 to 2.66
S1	62.80 µm (11.25)	63.59 µm (11.55)	p=0.52 CI:-3.27 to 1.68
S2	36.61 µm (8.69)	37.73 µm (8.20)	p=0.34 CI:-3.44 to 1.21
I1	71.93 µm (18.12)	71.07 µm (15.35)	p=0.57 CI:-2.16 to 3.89
I2	37.98 µm (10.19)	36.44 µm (9.25)	p=0.11 CI:-0.35 to 3.42
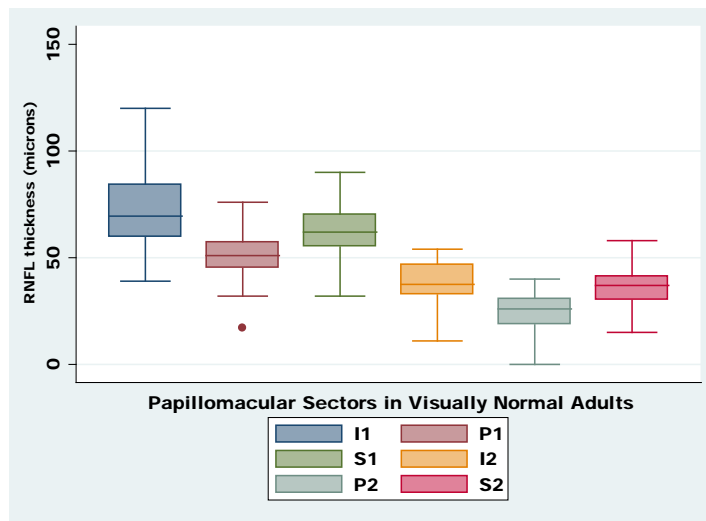
Figure 9.4: RNFL (µm) thickness measurements for the 6 papillomacular sectors in visually normal adult eyes.

314

9.4.2 Inter-ocular Symmetry (IOS)

Visually normal eyes were first examined in order to establish the degree of inter-ocular asymmetry that is present at the papillomacular bundle. The previous investigations of the fovea and the optic disc (Chapter 7 and Chapter 8) have demonstrated a high degree of inter-ocular structural symmetry. It is important to establish if inter-ocular symmetry is also present in the papillomacular bundle for the reasons outlined elsewhere (Chapter 7). It has been claimed that the fellow eye of amblyopes show subtle structural differences in size and shape of the optic disc similar to that of the amblyopic eye (Pineles and Demer, 2009). If this is the case then both eyes in amblyopes may show differences in RNFL thickness measurements relative to visual normals and it is thus necessary to examine inter-ocular symmetry, as well as differences in absolute RNFL thickness measurements between amblyopic and normal eyes.

9.4.2.1 Visually Normal Eyes – Adults

A high degree of symmetry between the eyes was found in all the papillomacular sectors. The degree of variation that exists within visually normal eyes in the papillomacular bundle sectors is less than in the peripapillary area around the disc. For example the sector with the greatest variation in papillomacular RNFL thickness is I1; non-dominant : 71.93±18.12µm; dominant : 71.07±15.35µm and this is still less than 1µm, indicating little individual variation (Table 9.2). Table 9.2 presents the differences between the mean measurements in visually normal adults; individually no subject had an inter-ocular difference in P1of greater than

31μm with a mean individual difference of 0.3μm, in P2 the greatest individual difference was 22μm and the mean individual difference was 0.2μm. In the S1 24μm was the greatest difference with a mean individual difference of 0.8μm, the greatest S2 difference was 22μm with a mean individual difference of 1.1μm, the greatest I1 difference was 31μm with a mean individual difference of 0.86μm and in I2 the greatest individual difference was 27μm with a mean individual difference of 2.1μm. The statistics present a picture of a high degree of inter-ocular symmetry but with considerable individual variation in RNFL thickness in the papillomacular bundle sectors in visually normal adults.

9.4.2.2 Visually Normal Eyes - Children

The degree of inter-ocular symmetry in the eyes of visually normal children was also analysed. A high degree of symmetry between the eyes was found in all measured RNFL papillomacular sectors. Again, although no significant difference was found between the eyes, a degree of variation exists within visually normal eyes; this variation is greater in the visually normal children in comparison to the visually normal adults. The RNFL thickness in sector I1 demonstrates the greatest variation; P1 (non-dominant : 62.14±19.44μm and dominant = 66.44±19.68μm). The results are presented in Table 9.3.

Table 9.3: Papillomacular RNFL (µm) measurements ± SD of the non-dominant and dominant eyes in visually normal children. Paired t-tests for each sector are shown.

Papillomacular Sector	Child Dominant Eye (mean ± SD)	Child Non-Dominant Eye (mean ± SD)	Dom v Non-Dom Eye Paired t-test
P1	50.56 µm (10.73)	50.72 µm (10.28)	p=0.90 CI: -2.8 to 2.48
P2	27.72 µm (8.69)	26.36 µm (9.69)	p=0.38 CI: -1.7 to 4.43
S1	63.26 µm (9.84)	59.84 µm (14.16)	p=0.09 CI: -0.53 to 7.37
S2	38 µm (8.79)	35.62 µm (11.06)	p=0.18 CI: -3.44 to 1.21
I1	62.14 µm (19.44)	66.44 µm (19.68)	p=0.17 CI: -10.55 to 1.95
I2	33.84 µm (12.55)	34.54 µm (12.62)	p=0.75 CI: -5.03 to 3.63

Table 9.3 presents the differences between the mean measurements in visually normal children; individually no subject had an inter-ocular difference in P1of greater than 37µm with a mean individual difference of 0.16µm, in P2 the greatest individual difference was 34µm and the mean individual difference was 1.4µm. In the S1 56µm was the greatest difference with a mean individual difference of 3.4µm, the greatest S2 difference was 39µm with a mean individual difference of 2.4µm, the greatest I1 difference was 66µm with a mean individual difference of 4.3µm and in I2 the greatest individual difference was 39µm with a mean individual difference of 0.7µm. Again the statistics present a picture of a high degree of inter-ocular symmetry but with considerable individual variation in RNFL thickness in the papillomacular bundle sectors in visually normal children.

317

9.4.2.3 Adult Amlyopes

As with the visually normal adults, a high degree of symmetry was found between the amblyopic eyes and their fellow eyes in all sectors (Table 9.4). Individually the maximum inter-ocular difference in P1 was 45µm with a mean individual difference of 2.29µm, in P2 the greatest individual difference was 33µm and the mean individual difference was 0.33µm. In the S1 68µm was the greatest difference with a mean individual difference of 1.5µm, the greatest S2 difference was 52µm with a mean individual difference of 0.1µm, the greatest I1 difference was 73µm with a mean individual difference of 1.4µm and in I2 the greatest individual difference was 41µm with a mean individual difference of 2.0µm.

Table 9.4: Papillomacular RNFL (µm) measurements ± SD of the amblyopic eye and the amblyopic fellow eye in adults. Paired t-tests for each sector are shown.

Papillomacular Sector	Adult Amblyopic Eye (mean ± SD)	Adult Amblyopic Fellow Eye (mean ± SD)	Fellow v Amblyopic Eye Paired t-test
P1	42.19 µm (14.63)	42.27 µm (14.74)	p=0.65 CI: -5.23 to 8.19
P2	20.32 µm (11.53)	20.83 µm (11.96)	p=0.86 CI:-5.23 to 6.26
S1	56.58 µm (13.92)	54.97 µm (12.61)	p=0.59 CI:-7.6 to 4.39
S2	34.52 µm (12.46)	32.77 µm (10.34)	p=0.51 CI:-7.08 to 3.60
I1	67.58 µm (18.49)	61.68 µm (18.68)	p=0.11 CI:-13.21 to 1.40
I2	33.55 µm (13.57)	30.35 µm (13.17)	p=0.35 CI:-10.02 to 3.63

9.4.2.4 Non-Amblyopic Adults

Again, a high degree of symmetry was demonstrated between the strabismic eye and / or the eye with the highest refractive error (S/A) eye and its fellow eye in the non-amblyopic group (Table 9.5).

Table 9.5: Papillomacular bundle RNFL (µm) measurements ± SD of both eyes in anisometropic or strabismic adults without amblyopia. The results of paired t-tests between the strabismic/anisometropic eye (S/A eye) and the S/A fellow eye for each sector are shown.

Papillomacular Sector	Strabismic/High Ref Error Eye (mean ± SD)	Fellow Eye (mean ± SD)	Fellow v S/A Eye Paired t-test
P1	45.71µm (15.41)	44.71µm (10.25)	p=0.90 CI:-11.49 to 9.49
P2	24.36µm (12.9)	18.92µm (9.91)	p=0.16 CI:-13.27 to 2.42
S1	58.93µm (14.50)	58.5µm (12.02)	p=0.89 CI:-7.17 to 6.31
S2	35.5µm (15.14)	31.86µm (8.98)	p=0.19 CI:-9.40 to 2.12
I1	61.36µm (19.88)	57.79µm (22.57)	p=0.66 CI:-20.82 to 13.68
I2	32.93µm (12.80)	28.93µm (16.38)	p=0.51 CI:-16.74 to 8.74

Table 9.5 presents the differences between the mean measurements in non-amblyopic adults with S/A; individually the maximum inter-ocular difference in P1 was 34µm with a mean individual difference of 1.0µm, in P2 the greatest individual difference was 31µm and the mean individual difference was 5.4µm. In the S1 18µm was the greatest difference with a mean individual difference of 0.4µm, the greatest S2 difference was 23µm with a mean individual difference of 3.6µm, the greatest I1 difference was 87µm with a mean individual difference of 3.57µm and in I2 the greatest individual difference was 41µm with a mean individual difference of 4.0µm.

9.4.2.5 Amblyopic Children

A high degree of symmetry of all the papillomacular sectors was also found between the amblyopic eyes and the amblyopic fellow eyes in children (Table 9.6). Table 9.6 presents the differences between the mean measurements in amblyopic children; individually the maximum inter-ocular difference in P1 was 31µm with a mean individual difference of 1.8µm, in P2 the greatest individual difference was 29µm and the mean individual difference was 2.3µm. In the S1 21µm was the greatest difference with a mean individual difference of 9.5µm, the greatest S2 difference was 18µm with a mean individual difference of 6.4µm, the greatest I1 difference was 43µm with a mean individual difference of 0.27µm and in I2 the greatest individual difference was 37µm with a mean individual difference of 2.4µm.

Table 9.6: Paramacular RNFL (µm) measurements ± SD of both eyes in amblyopic children. The results of paired t-tests between the amblyopic eye and the fellow eye for each sector are shown.

Papillomacular Sector	Child Amblyopic Eye (mean ± SD)	Child Fellow Eye (mean ± SD)	Fellow v Amblyopic Eye Paired t-test
P1	51.14 µm (3.17)	52.91 µm (9.27)	p= 0.45 CI: -3.06 to 6.6
P2	31 µm (18.01)	28.68 µm (14.54)	p=0.39 CI: -7.76 to 3.12 to
S1	63.72 µm (10.64)	64.68 µm (8.39)	p=0.70 CI: -4.05 to 5.96
S2	40.45 µm (11.20)	39.82 µm (11.41)	p=0.73 CI: -4.43 to 3.15
I1	64.64 µm (21.57)	64.91 µm (13.89)	p=0.95 CI: -9.32 to 9.88
I2	36.18 µm (18.83)	33.82 µm (13.25)	p=0.54 CI: -10.31 to 5.58

9.4.2.6 ANOVA of Differences

In order to identify if the degree of symmetry differed between the groups, the inter-ocular difference found in each group (normal adults, amblyopic adults, amblyopic children and normal children) was examined using an ANOVA to identify any statistical significance in the differences between the groups. No significance was found. The results of the ANOVA of differences are presented in Table 9.7.

Table 9.7: Results of one-way ANOVA, comparing the inter-ocular **differences** of papillomacular bundle sectors between visually normal adults, visually normal children, amblyopic adults and amblyopic children (4 groups).

Papillomacular Sector *Differences*	Source of variation	Degrees of freedom	Sum of squares	Variance Ratio (F)	Probability
P1 *Differences*	Between groups Within groups	3 217	243.76 27668.54	0.64	0.59
P2 *Differences*	Between groups Within groups	3 217	288.18 28786.90	0.72	0.54
S1 *Differences*	Between groups Within groups	3 217	579.89 41562.18	1.01	0.39
S2 *Differences*	Between groups Within groups	3 217	479.55 30295.92	1.14	0.33
I1 *Differences*	Between groups Within groups	3 217	1021.26 90309.75	0.82	0.49
I2 *Differences*	Between groups Within groups	3 217	515.10 50283.06	0.74	0.53

An overview of the papillomacular bundle RNFL thickness measurements for each group is provided in Table 9.8. The visually normal children demonstrated slightly greater variation in their results than the visually normal adults in all 6 sectors, as is depicted by the increased number of outliers (Figure 9.5).

Table 9.8: Papillomacular bundle RNFL (µm) measurements ± SD for all 5 participant categories, visually normal adults, amblyopic adults, non-amblyopic adults with S/A, visually normal children and amblyopic children.

Papillomacular Sector	Adult Visual Normal (mean ± SD)	Adult Amblyopes (mean ± SD)	Strabismic/High Ref Error Eye (mean ± SD)	Child Visual Normal (mean ± SD)	Child Amblyopes (mean ± SD)
P1	51.29µm (10.88)	42.19µm (14.63)	45.71µm (15.41)	50.56µm (10.73)	51.14µm (14.87)
P2	23.86µm (10.09)	20.32µm (11.53)	24.36µm (12.9)	27.72µm (8.69)	31µm (18.01)
S1	62.79µm (11.25)	56.58µm (13.92)	58.93µm (14.50)	63.26µm (9.84)	63.73µm (10.65)
S2	36.61µm (8.69)	34.52µm (12.46)	35.5µm (15.14)	38µm (8.79)	40.45µm (11.19)
I1	71.93µm (18.12)	67.58µm (18.49)	61.36µm (19.88)	62.14µm (19.44)	64.64µm (21.57)
I2	37.73µm (10.20)	33.55µm (13.57)	32.93µm (12.80)	33.84µm (12.55)	36.18µm (18.83)

Papillomacular Bundle Sectors in Visually Normal Eyes

Figure 9.5: Box & whisker plots of RNFL (µm) thickness measurements for the 6 papillomacular sectors in eyes of visually normal adults and children. The dots depict the outliers.

9.5 RNFL Thickness: The effect of axial length and age.

In this present study, investigation of foveal topography (Chapter 7) has shown that the foveal thickness and pit depth is not associated with axial length, but that there is an effect of age. RNFL thickness around the peripapillary area of the optic disc in this study (Chapter 8) has shown an association with axial length. Previous published studies investigating the peripapillary RNFL thickness using OCT in adults (Alamouti and Funk, 2003; Parikh et al., 2007) and children (El-Dairi et al., 2009; Huynh et al., 2006c; Salchow et al., 2006) have demonstrated that mean RNFL thickness is frequently affected by the variables of axial length and age. Since axial length increases with age, it could be that age is not independently associated with RNFL thickness. Therefore, as with the analysis for the RNFL measurements around the optic disc (Chapter 8), in order to predict the effect produced by axial length and age on the papillomacular bundle multivariate regression analysis was performed. The mean RNFL value was calculated, as well as the 6 individual papillomacular sectors, this value was then used as the dependant variable and the effects of axial length, age and amblyopia were evaluated. Axial length and age were included in the model as metric variables and along with a categorical variable concerning the presence/ absence of amblyopia. Regression analysis with adjustment for axial length and age (For details of all participants see Chapter 6, data sets 1- 4) indicated no significant effect on the mean or the individual sectors of the papillomacular bundle RNFL thickness from axial length (p=0.88) (Tables 9.9 to 9.15). Statistical significance was, however, found for the effect of age (p=0.04) on the mean RNFL thickness (Table 9.9 and

Figure 9.6) with the mean RNFL thickness of the papillomacular bundle reducing by 0.12µm for every 1 year increase in age; this is very similar to the findings at the temporal peripapillary disc sector where the papillomacular axon fibres join the disc (Chapter 8, Table 8.12). A statistically significant effect of age was also found in individual sectors P2 (p=0.004) and S1 (p=0.04) (Tables 9.11 and 9.12), but not in sectors P1, S2, I1 or I2 (Tables 9.10, 9.13, 9.14 and 9.15). The P2 sector RNFL thickness reduced by 0.18µm for every 1year increase in age and the S1 sector RNFL thickness reduced by 0.13µm per year. The presence of amblyopia was not found to have a significant effect on the RNFL thickness in any of the papillomacular sectors. However, the presence of amblyopia may be associated with reduced RNFL thickness in sector P1, the area where the retinal ganglion axons from the macula would enter the optic disc. In this sector the presence of amblyopia came close to, but did not reach,statistical significance (p=0.06) (Table 9.10).

Table 9.9: Multiple linear regression analysis of **mean papillomacular bundle RNFL** (µm) thickness including independent variables for the axial length, age and the presence of amblyopia.

Variable	Regression Coefficient	Standard error	P-value	95% CI (µm)
Axial length	0.11	0.73	0.88	-1.34 to 1.56
Age	-0.12	0.06	**0.04**	-0.23 to -0.003
Amblyopia	-2.04	2.30	0.38	-6.59 to 2.52
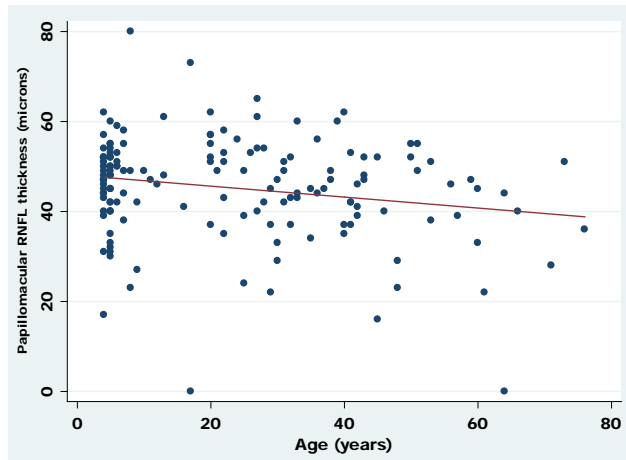
Figure 9.6: Linear regression of mean papillomacular bundle RNFL thickness (µm) v age (years) in visually normal adults and children, amblyopic adults and children. The equation for the regression line (red) is $y = -0.12x + 46.64$ (95% CI for coefficient, -0.24 to -0.004).

Table 9.10: Multiple linear regression analysis of **P1 papillomacular bundle RNFL** (µm) thickness including independent variables for the axial length, age and the presence of amblyopia.

Variable	Regression Coefficient	Standard error	P-value	95% CI (µm)
Axial length	-0.80	0.81	0.32	-2.41 to 0.80
Age	-0.11	0.07	0.09	-0.25 to -0.02
Amblyopia	-4.75	2.54	0.06	-9.77 to 0.27

Table 9.11: Multiple linear regression analysis of **P2 papillomacular bundle RNFL** (µm) thickness including independent variables for the axial length, age and the presence of amblyopia.

Variable	Regression Coefficient	Standard error	P-value	95% CI (µm)
Axial length	-1.08	0.77	0.161	-2.60 to 0.44
Age	-0.18	0.06	**0.004**	-0.31 to -0.06
Amblyopia	-0.08	2.40	0.97	-4.84 to 4.67

Table 9.12: Multiple linear regression analysis of **S1 papillomacular bundle RNFL** (µm) thickness including independent variables for the axial length, age and the presence of amblyopia.

Variable	Regression Coefficient	Standard error	P-value	95% CI (µm)
Axial length	-0.38	0.75	0.62	-1.87 to 1.11
Age	-0.13	0.06	**0.04**	-0.25 to -0.003
Amblyopia	-1.93	2.36	0.42	-6.59 to 2.73

Table 9.13: Multiple linear regression analysis of **S2 papillomacular bundle RNFL** (µm) thickness including independent variables for the axial length, age and the presence of amblyopia.

Variable	Regression Coefficient	Standard error	P-value	95% CI (µm)
Axial length	-1.08	0.66	0.11	-2.39 to 0.23
Age	-0.09	0.05	0.07	-0.20 to 0.01
Amblyopia	-0.18	2.07	0.93	-3.92 to 4.27

Table 9.14: Multiple linear regression analysis of **I1 papillomacular bundle RNFL** (µm) thickness including independent variables for the axial length, age and the presence of amblyopia.

Variable	Regression Coefficient	Standard error	P-value	95% CI (µm)
Axial length	0.77	1.31	0.56	-1.82 to 3.35
Age	0.07	0.10	0.49	-0.14 to 0.28
Amblyopia	-1.28	4.09	0.76	-9.37 to 6.81

Table 9.15: Multiple linear regression analysis of **I2 papillomacular bundle RNFL** (µm) thickness including independent variables for the axial length, age and the presence of amblyopia.

Variable	Regression Coefficient	Standard error	P-value	95% CI (µm)
Axial length	0.37	0.86	0.67	-1.33 to 2.07
Age	-0.07	0.07	0.29	-0.21 to 0.06
Amblyopia	0.13	2.69	0.96	-5.19 to 5.45

9.5.1 P1Thickness: Association of Visual Acuity

The RNFL thickness at P1 demonstrated a borderline (p=0.06) association with amblyopia, therefore the relationship between RNFL thickness at P1 and visual acuity was further explored (Figure 9.7).
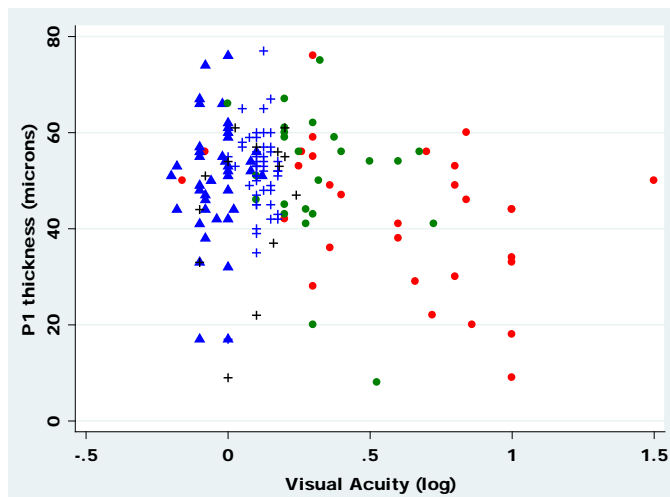
Figure 9.7: P1 RNFL thickness (µm) for visually normal adults ▲ adult amblyopes ● non-amblyopic adults with S/A ✚ visually normal children ✚ and child amblyopes ● .

9.6 Discussion

9.6.1 Papillomacular RNFL Thickness - Visually Normal Adults

The papillomacular RNFL demonstrates a consistent pattern in visually normal adults. The RNFL sectors closest to the optic disc (P1, S1, I1) are thicker than those closer to the macula (P2, S2, I2) (Figure 9.3). The structural pattern of the papillomacular bundle is one of thicker inferior (I1=71.93±18.2µm) and superior (S1=62±11.25µm) sectors in comparison to the central sectors (P1=51.30±10.88µm) (Table 9.8 Figure 9.8).

I1
(71.93µm)

P1
(51.30µm)

S1
(62.80µm)
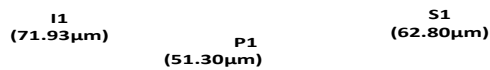
Figure 9.8: Schematic cross-section through the papillomacular bundle indicating that inferior sector I1 and superior sector S1 are thicker than central sector P1. Values from Table 10.2 of measurements in visually normal adults.

No published imaging studies reporting the structure of the papillomacular bundle were found during an extensive search of imaging literature, therefore comparisons of present results with existing literature are limited to histological studies. The axons from the central areas of the papillomacular bundle (P1 and P2) feed into the temporal quadrant of the peripapillary sector of the optic disc (Chapter 8,

Figure 8.2). The temporal area of the optic disc has been shown to have a thinner RNFL thickness (Chapter 8) than the superior and inferior quadrants, indicating that the RNFL structure and organisation maintains a consistent pattern crossing the retina from the papillomacular bundle to the optic disc. The degree of individual variation in the paramacular bundle is less than at the optic disc, with the RNFL thickness standard deviations generally smaller and the 95% confidence intervals closer, than that of the optic disc RNFL. The papillomacular bundle area displaying the greatest variation is the inferior sector, I1, closest to the optic disc which demonstrated the greatest variation in every group (I1 71.93±18.12µm) (Table 9.8).

9.6.2 Visually Normal Eyes – Children

The RNFL pattern produced at the papillomacular bundle in the visually normal children was similar to that of the adults with the inferior (I1 and I2) (I1=62.14±19.44µm, I2=33.84±12.55µm) and superior sectors (S1 and S2) (S1=63.26±9.84µm, S2=38±8.79µm) demonstrating thicker measurements than the central sectors (P1 and P2) (P1=50.56±10.73µm, P2=27±8.69µm) (Table 9.3).

9.6.3 Inter-ocular Symmetry (IOS)

A high degree of inter-ocular symmetry was found in all the measured papillomacular sectors. This was a consistent finding all the groups (adults and children, amblyopes and non-amblyopic individuals (S/A) and visually normal controls). It is also comparable with the findings of the foveal topography (Chapter 7) and the RNFL thickness around the optic disc (Chapter 8).

9.6.4 Retinal Nerve Fibre Thickness – Amblyopia

No previous study has reported the RNFL thickness of the papillomacular bundle in the presence of amblyopia. In this study no significant difference was found in the RNFL thickness across the papillomacular bundle (P1, P2, I1,I 2, S1 or S2) in the presence of amblyopia. A borderline effect of amblyopia was however shown in sector P1 where the papillomacular bundle retinal nerve fibre layer axons merge into the temporal quadrant of the optic disc. Here the RNFL was reduced in thickness, but did not achieve statistical significance (p=0.06) (Table 9.10). It is this sector in particular that could be expected to potentially demonstrate a difference in the presence of amblyopia. In the two published imaging studies reporting a difference in RNFL thickness around the optic disc (Yen et al., 2004; Yoon et al., 2005) thicker RNFL was reported. This finding was not corroborated by the present study which shows no effect or a borderline reduction in RNFL thickness.

9.6.5 Papillomacular RNFL Thickness: Age

On analysis of the data, age was found to be either a significant factor or close to achieving significance, affecting the mean RNFL thickness, in all but two individual sectors (I1 and I2) of the papillomacular bundle (Tables 10.10 to 10.15). The mean RNFL thickness was shown to reduce by 0.12μm per year (p=0.04) (Table 10.9). The effect of age was similar in all the sectors except for the inferior sectors (I1 and I2), neither of which demonstrated an effect with age (I1, p=0.49 and I2, p=0.29). The reduction of the papillomacular bundle RNFL thickness with age differs from the findings of foveal topography (Chapter7), which demonstrated an increase in foveal thickness with age. The increase in foveal thickness however, appears to be contributed to by an increase in the photoreceptor length (Chapter 7), whereas the papillomacular RNFL is likely to be affected by the number and/ or thickness of the ganglion cell axons.

9.6.6 Papillomacular RNFL Thickness : Axial Length

The RNFL thickness of the papillomacular bundle was not found to be affected by axial length. This was consistent across all sectors. This lack of effect was the same as at the fovea but differed to that found at the peripapillary area around the optic disc.

9.7 Conclusion

This investigation of the papillomacular bundle RNFL thickness has not shown any significant difference in thickness measurement in the presence of amblyopia. A small effect (-4.75µm) was shown in the presence of amblyopia (P1 sector, entering the temporal sector of the optic disc) but this did not reach statistical significance (p=0.06). The RNFL in the papillomacular bundle was not affected by axial length but was affected by age (p=0.04) with a reduction in thickness with increasing age. The evidence from both this part of the study and the results from the analysis of the RNFL thickness around the peripapillary area of the disc have not demonstrated any significant structural effect from the presence of amblyopia. The RNFL thickness at the disc and at the papillomacular area are not therefore, caused by or the cause of amblyopic visual loss or the cause of or caused by the factors that can lead to amblyopia.

Chapter 10. Optic Disc Characteristics in Amblyopia

10.1 Introduction

The optic disc (Figure 10.1) is located approximately 5mm nasal to the fovea (Miller, 2005; Williams and Wilkinson, 1992) and consists of the retinal ganglion axons which travel from the fovea via the papillomacular bundle to the optic disc, continuing via the optic foramen to the optic chiasm, the lateral geniculate nucleus (LGN) and beyond to the visual cortex (V1) (see Chapter 1). The number of axons travelling through the optic disc has been shown to influence the size of the optic disc (Jonas et al., 1992) with an increased number of axons found in larger optic discs. Any insult to the visual system that results in a reduction of the RNFL axons is likely to lead to a decrease in disc size. This has been well documented in chronic conditions such as glaucoma (Johnson et al., 2003; Klein et al., 2004; Medeiros et al., 2006). The optic disc is slightly oval in shape, with the vertical diameter generally greater than the horizontal. The disc area is defined as the area lying inside the inner circumference of the peripapillary sclera ring (Jonas,1999) (Figure 10.2). Optic disc dimensions have been shown to vary between visually normal individuals, with optic disc area reported to range from $0.8mm^2$ to $5.54mm^2$ in adults (Jonas et al., 1988).
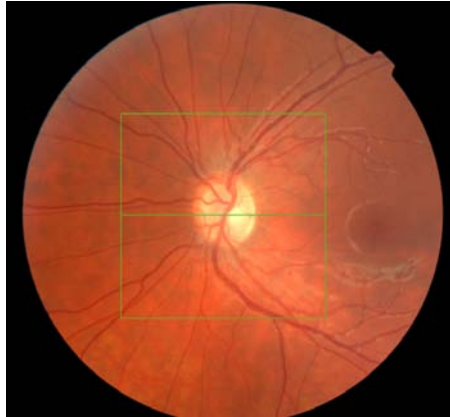
Figure 10.1: Screen shot from 3D-1000 Topcon disc photograph AB00572364 (non-amblyopic adult) detailing the optic disc (RE) and the fovea. The 6x6mm grid is depicted in green.
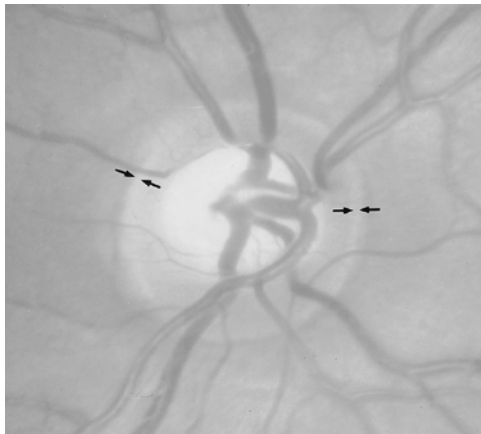
Figure 10.2: Slightly large, otherwise normal, optic disc. The black arrows point toward the peripapillary scleral ring. Adapted from (Jonas et al., 1999).

Amblyopia has been attributed to changes at the level of the visual cortex (see Chapter 2), however, this has recently been challenged by the work of Lempert (2000, 2003,2004) who has presented evidence of structural change at retinal level and, in particular, suggested that there is a degree of optic disc hypoplasia in 74% of amblyopic eyes (Lempert,2000). If the assertion that some amblyopic eyes have a subtle degree of optic disc hypoplasia is correct, then the function of amblyopic eyes would be limited by structural abnormalities. This would account for the percentage of amblyopes who do not respond to treatment and would therefore have implications on the current rationale for occlusion therapy in these individuals.

The development of imaging technology has allowed further investigation into the structure and size of the optic disc (see Chapter 4) but the vast majority of studies have failed to show any significant difference in the optic disc size or the RNFL thickness between amblyopic eyes and their fellow eyes (Altintas et al., 2005; Bozkurt et al., 2003; Colen et al., 2000; Repka et al., 2009b). The results from the investigation of retinal structure detailing foveal topography, paramacular bundle structure and peripapillary RNFL thickness in this study have indicated either no structural differences (Chapters 7, 8 and 9) or where differences have been shown, these have been bilateral and symmetrical (Chapter 7) indicating that they cannot be the primary cause of the reduction in visual acuity found in amblyopia. The aim of this chapter is to investigate the structure of the optic disc and provide detailed measurements of optic disc dimensions, in both visually normal adults and children and also in amblyopic adults and children. The information will allow us to discover if structural defects of the optic disc are present in amblyopia.

10.2 Methods

The participants recruited to this stage of the study are comprised of the same individuals recruited to the other stages; foveal topography, papillomacular bundle and RNFL thickness (Chapters 7, 8 and 9). (Refer to Chapter 7 for detailed description of the groups and methods of recruitment).

10.2.1 Optic Disc Measurement

The 3D OCT-1000 (Topcon, Tokyo, Japan) incorporates a digital fundus camera. After every set of disc scans taken (Chapter 8) a photograph was taken for each eye of each participant. After acquisition the image was exported into commercially available software GNU Image Manipulation Programe (GIMP). One individual (AB) then used GIMP to mark the optic disc vertical and horizontal meridians. The fovea was also marked (Figure 10.3). The optic disc parameters were reviewed by a second individual (IP) and any revisions of the marks undertaken. At the time of "marking up" the individuals were 'blind' as to which images were from the amblyopic eyes and which were from visually normal eyes. Agreement was made to the position of the marks prior to measurement. However, had there been a disagreement on the positioning of the marks then a third individual (BTB) would have been asked to make a final judgement, this was not required. Measurements of the horizontal diameter, vertical diameter and disc-centre to fovea distance were then taken using the GIMP software (Figure 10.4). The centre of the disc was taken as the intersection of the horizontal and vertical diameter axes. The

dimensions were initially measured in pixels and then converted into millimetres (mm) prior to analysis.
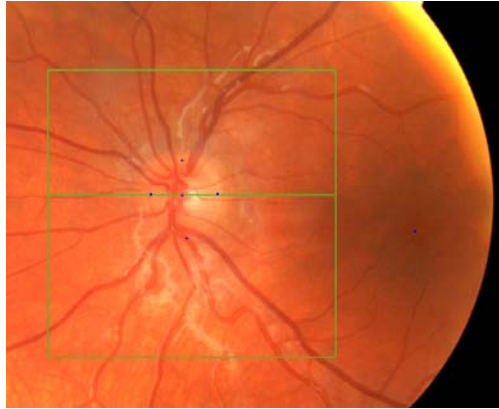
Figure 10.3: Screen shot from 3D-1000 Topcon disc photograph AB00744265 (amblyopic child) showing the optic disc (RE). The 6x6mm grid is depicted in green. The optic disc parameters are compiled from the marked blue dots, applied to define the horizontal and vertical diameters and the fovea using GIMP.

The measured optic disc dimensions were then used to calculate the optic disc area, the vertical to horizontal ratio, the axial length to disc area ratio and the disc-fovea to disc-diameter ratio. Disc area has been identified as being reduced in amblyopic eyes (Lempert, 2000), however, Lempert's measurements did not take into account the factors of axial length and refractive error, which could have influenced the findings. As both axial length and dioptric power are known to influence the magnification in image acquisition it is difficult to obtain absolute measurements of intraocular structures. However, calculated ratios provide an enhanced way of assessing relative difference between eyes, as the measurement of each structure is equally influenced by axial length and refractive error. Thus comparison of the optic disc diameter (DD) with the distance between the optic

disc and the fovea (DF:DD) (Zeki Alvarez 1988) and comparison of axial length to the disc area (AXL/DA) (Lempert, 2003) provide a useful evaluation of optic disc size.
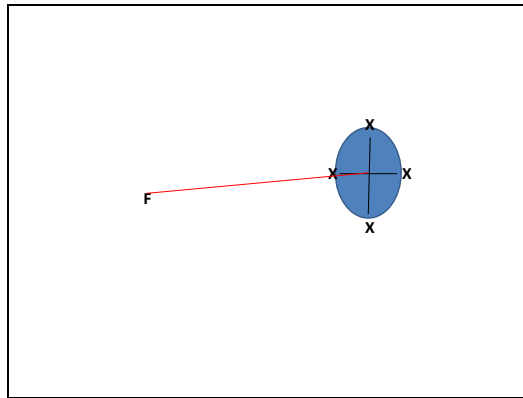
Figure 10.4: Schematic of disc parameter measurements in a hypothetical RE. The optic disc parameters are compiled from the marked crosses (x), applied to define the horizontal and vertical diameters. The centre of the disc is determined by the intersection of the vertical and horizontal diameters. The fovea (F) to disc centre measurement is marked in red.

Table 10.1: Description of measured optic disc parameters.

Optic Disc Parameter	Description of Measured Dimension
Horizontal diameter (mm)	Optic disc diameter in the horizontal meridian
Vertical diameter (mm)	Optic disc diameter in the vertical meridian
Disc to Fovea (mm)	Distance from the centre of the optic disc to the fovea
Disc Area (mm^2)	Area of optic disc (vert diam/2 *horizdiam/2 * π)
Vertical : Horizontal Ratio (no units)	Vertical diameter divided by horizontal diameter
Axial length : Disc Area Ratio (mm^{-1})	Axial length (mm) divided by disc area
Disc-Fovea : Disc diameter Ratio (no units)	Distance from the centre of the optic disc to the fovea divided by mean diameter of horizontal & vertical diameter

338

10.2.2 Magnification

As with the foveal topography (Chapter 7), differences in axial length between eyes were taken into account using a magnification factor established for the OCT 3D-1000 (Topcon). This is based on the recognized formulae determined by Littman (Littmann, 1982) and Bennett (Bennett et al., 1994) and modified for the OCT by Leung (Leung et al., 2007) (see Chapter 4). The axial length of each individual was calculated using the method described previously in Chapter 4.

In total three hundred and thirty-two (166 pairs of RE and LE images) optic disc images (84%) were included for analysis. The inclusion rate in all the groups was high, visually normal adults, (89%), amblyopic adults, (83%) and non-amblyopic adults with strabismus and/or anisometropia (93%). The amblyopic children had an inclusion rate of 93% and the visually normal children had an inclusion rate of 77%. The rejected images were not included as the quality was poor i.e. blinks, movement leading to a defocused image. In 6 cases the fovea was not visible preventing the measurement of the disc to fovea distance.

10.3 Statistical Analysis

Statistical analysis was carried out using commercially available Stata SE version 10.0. Paired t-tests were used to compare the inter-ocular symmetry between eyes for each group. Adults and children were analysed separately for all measured optic disc parameters. ANOVA of the differences between each group was used to investigate any group differences and the Bonferroni correction was applied to the

analysis (Chapter 7, statistical analysis). Two sided t-tests were used to directly compare groups and multiple regression analysis was used to investigate the effect of axial length, age, refractive error and the presence of amblyopia on the measured optic disc parameters.

10.4 Results

10.4.1 Optic Disc Parameters in Visually Normal Adults

The optic disc dimensions (Figure 10.3 and Table 10.1) for each individual were measured and analysed. The optic disc in visually normal adults was found to be oval in shape with the vertical diameter (mean=1.66mm, range 1.39 to 2.04mm) on average being greater than the horizontal diameter (mean=1.49mm, range 1.22 to 1.9mm).The average disc area was 1.95mm^2 but this showed significant variation within the visually normal adults, with a range of 1.35 to 3.05mm^2. A summary of the optic disc characteristics in visually normal adults is provided in Table 10.2.

10.4.2 Inter-ocular Symmetry (IOS)

Visually normal eyes were first examined in order to establish the degree of inter-ocular asymmetry that is present in relation to optic disc size. There are claims that the fellow eye of amblyopes show subtle structural differences in size and shape of the optic disc similar to that of the amblyopic eye (Pineles and Demer, 2009). If this is the case then both eyes in amblyopes may show differences in the measured

optic disc parameters relative to visual normals. In this study bilateral and symmetrical differences have been found in the investigation of foveal topography (Chapter 7). In order to establish if this is the case in optic disc structure it is necessary to examine inter-ocular symmetry between amblyopic and their fellow eyes, as well as differences in optic disc measurements between amblyopic and normal eyes (Table 10.2). The dominant eyes in the visually normal adults and children were chosen randomly with a random number generator programme in Excel at the start of this study.

Table 10.2: Optic Disc parameter measurements ± SD of the non-dominant and dominant eye in visually normal adults. Paired t-tests for each optic disc parameter are shown.

Optic Disc Parameter	Adult Non-dom Eye (mean ± SD)	Adult Dominant Eye (mean ± SD)	Dom v Non-dom Eye Paired t-test
Vertical diameter	1.66 mm (0.15)	1.66 mm (0.17)	p=0.93 CI:-0.03 to 0.03
Horizontal diameter	1.47 mm (0.15)	1.49 mm (0.15)	p=0.44 CI:-0.02 to 0.05
Disc to Fovea	4.35 mm (0.31)	4.36 mm (0.30)	p=0.78 CI:-0.20 to 0.15
Disc Area	1.93 mm^2 (0.35)	1.95 mm^2 (0.39)	p=0.59 CI:-0.06 to 0.10
Vertical to Horizontal Ratio	1.13 (0.07)	1.12 (0.06)	p=0.31 CI:-0.03 to 0.01
Axial length: Disc Area Ratio	12.86 mm^{-1} (2.31)	12.71 mm^{-1} (2.27)	p=0.54 CI:-0.65 to 0.34
Disc-Fovea: Disc Diameter Ratio	2.31 (0.32)	2.29 (0.27)	p=0.76 CI:-0.08 to 0.06

10.4.3 Visually Normal Eyes - Adults

A high degree of symmetry between the eyes was found in all measured optic disc parameters with little variation. The results are presented in Table 10.2. The vertical diameter (mean = 1.66±0.17mm, (dominant eye) ranged from 1.39 to 2.04mm. The horizontal diameter (mean = 1.49±0.15mm, (dominant eye) ranged from 1.22 to 1.9mm and the disc area (mean = 1.95±0.39mm^2, (dominant eye) ranged from 1.35 to 3.05mm^2. The individual with the largest disc area (3.05mm^2) in this group of visually normal adults had both the largest vertical diameter (2.04mm) and the largest horizontal diameter (1.9mm). This individual had an axial length measurement of 24.29mm (the group axial length mean= 23.98mm, range 21.35 to 28.08mm) and a MSE of 0.00DS.

Table 10.2 presents the differences between the mean measurements in visually normal adults; individually no subject had an inter-ocular difference in the vertical diameter of greater than 0.32mm with a mean individual difference of 0.08mm. In the horizontal diameter no individual had a difference greater than 0.31mm and the mean individual difference was 0.08mm. The greatest inter-ocular difference of the disc to fovea distance was 0.35mm with a mean individual difference of 0.14mm. The greatest inter-ocular difference of the disc area was 0.77mm^2 with a mean individual difference of 0.17mm^2. The statistics present a picture of a high degree of inter-ocular symmetry in visually normal adults in relation to optic disc size and location relative to the fovea.

10.4.4 Visually Normal Eyes - Children

The degree of inter-ocular symmetry in the eyes of visually normal children was also analysed and again a high degree of symmetry between the eyes was found of the measured optic disc parameters (Table 10.3). The vertical diameter: mean = 1.64±0.16mm (dominant eye) ranged from 1.16 to 2.02mm, the horizontal diameter (mean = 1.44±0.17mm, (dominant eye) ranged from 1.01 to 1.85mm and the disc area (mean = 1.87±0.37mm^2, (dominant eye) ranged from 0.92 to 2.69mm^2. The individual with the smallest disc area (0.92mm^2) in this group of normal children had both the smallest vertical diameter (1.16mm) and the smallest horizontal diameter (1.01mm). This individual had a low axial length measurement (20.73mm) although it was not the lowest measurement in this group (mean= 21.92mm, range 19.77 to 23.29mm).

Table 10.3: Optic Disc parameter measurements ± SD of the non-dominant and dominant eyes in visually normal children. Paired t-tests for each optic disc parameter are shown.

Optic Disc Parameter	Child Non-dom Eye (mean ± SD)	Child Dominant Eye (mean ± SD)	Dom v Non-dom Eye Paired t-test
Vertical diameter	1.64 mm (0.19)	1.64 mm (0.16)	p=0.98 CI:-0.03 to 0.03
Horizontal diameter	1.45 mm (0.16)	1.44 mm (0.17)	p=0.58 CI:-0.02 to 0.03
Disc to Fovea	4.35 mm (0.04)	4.38 mm (0.04)	p=0.43 CI:-0.09 to 0.04
Disc Area	1.88 mm^2 (0.38)	1.87 mm^2 (0.37)	p=0.79 CI:-0.05 to 0.07
Vertical to Horizontal Ratio	1.14 (0.10)	1.15 (0.11)	p=0.37 CI:-0.03 to 0.01
Axial length: Disc Area Ratio	12.13 mm^{-1} (2.49)	12.18 mm-1 (2.25)	p=0.79 CI:-0.44 to 0.33
Disc-Fovea: Disc Diameter Ratio	2.35 (0.30)	2.37 (0.29)	p=0.44 CI:-0.07 to 0.03

Table 10.3 presents the differences between the mean measurements in visually normal children; individually no subject had an inter-ocular difference in the vertical diameter greater than 0.39mm and the mean individual difference was 0.09mm. In the horizontal diameters no individual had a difference greater than 0.23mm and the mean individual difference was 0.07mm. The greatest inter-ocular difference of the disc to fovea distance was 0.56mm with a mean individual difference of 0.16mm. The greatest inter-ocular difference of the disc area was 0.76mm^2 with a mean individual difference of 0.17mm^2. Again these descriptive statistics present a picture of significant inter-ocular symmetry in visually normal children.

10.4.5 Adult Amlyopes

As with the visually normal adults, a high degree of symmetry was found between the amblyopic eyes and their fellow eyes in all sectors (Table 10.4). The vertical diameter (mean = 1.56±0.17mm (amblyopic eye) ranged from 1.24 to 1.96mm, the vertical diameter (mean = 1.56±0.15mm (fellow eye) ranged from 1.36 to 1.86mm, the horizontal diameter (mean = 1.39±0.18mm (amblyopic eye) ranged from 0.98 to 1.96mm, the horizontal diameter (mean = 1.39±0.15mm (fellow eye) ranged from 1.1 to 1.7mm and the disc area (mean = 1.73±0.38mm^2 (amblyopic eye) ranged from 1.01 to 2.77mm^2, the disc area (mean = 1.72±0.32mm^2 (fellow eye) ranged from 1.19 to 2.23mm^2 .The smallest disc area (1.01mm^2) in this group of amblyopic adults was in the amblyopic eye and had the smallest horizontal diameter (0.98mm).

Table 10.4: Optic Disc parameter measurements ± SD of both eyes in amblyopic adults. The results of paired t-tests between the amblyopic eye and amblyopic fellow eye for each disc parameter are shown.

Optic Disc Parameter	Adult Amblyopic Eye (mean ± SD)	Adult Amblyopic Fellow Eye (mean ± SD)	Fellow v Amblyopic Eye Paired t-test
Vertical diameter	1.56 mm (0.17)	1.56 mm (0.15)	p=0.96 CI:-0.04 to 0.04
Horizontal diameter	1.39 mm (0.18)	1.39 mm (0.15)	p=0.99 CI:-0.05 to 0.53
Disc to Fovea	4.28 mm (0.50)	4.26 mm (0.27)	p=0.78 CI:-0.20 to 0.15
Disc Area	1.73 mm^2 (0.38)	1.72 mm^2 (0.32)	p=0.92 CI:-0.10 to 0.09
Vertical to Horizontal Ratio	1.13 (0.10)	1.13 (0.09)	p=0.91 CI:-.04 to 0.04
Axial length: Disc Area Ratio	13.56 mm^{-1} (2.89)	13.62 mm^{-1} (2.44)	p=0.86 CI:-0.68 to 0.81
Disc-Fovea: Disc Diameter Ratio	2.41 (0.40)	2.39 (0.32)	p=0.68 CI:-0.14 to 0.09

Table 10.4 presents the differences between the mean measurements in amblyopic adults; individually no amblyopic subject had an inter-ocular difference in the vertical diameter greater than 0.25mm,with the mean individual difference of 0.08mm. In the horizontal diameter no individual had a difference greater than 0.39mm and the mean individual difference was 0.11mm. The greatest inter-ocular difference of the disc to fovea distance was 1.29mm with a mean individual difference of 0.34mm. The greatest inter-ocular difference of the disc area was 0.6mm^2 with a mean individual difference of 0.2mm^2.

10.4.6 Non-Amblyopic Adults with Strabismus and/or Anisometropia (S/A)

Again, a high degree of inter-ocular symmetry was demonstrated between the strabismic eye and / or the eye with the highest refractive error (S/A) and its fellow eye in the non-amblyopic group (Table 10.5). The vertical diameter (mean = 1.61±0.19mm, (S/A eye) ranged from 1.22 to 1.84mm, the vertical diameter (mean = 1.61±0.23mm, (fellow eye) ranged from 1.2 to 1.91mm, the horizontal diameter (mean = 1.44±0.18mm, (S/A eye) ranged from 1.14 to 1.74mm, the horizontal diameter (mean = 1.41±0.16mm, (fellow eye) ranged from 1.09 to 1.7mm and the disc area (mean = 1.83±0.39mm^2, (S/A eye) ranged from 1.16 to 2.4mm^2, the disc area (mean = 1.81±0.42mm^2, (fellow eye) ranged from 1.03 to 2.34mm^2 .The smallest disc area (1.03mm^2) in this group of non-amblyopic adults was in the fellow eye which also had the smallest horizontal diameter (1.09mm).

Table 10.5: Optic Disc parameter measurements ± SD of both eyes in anisometropic or strabismic adults without amblyopia. The results of paired t-tests between the strabismic/anisometropic eye (S/A eye) and the S/A fellow eye for each disc sector are shown.

Optic Disc Parameter	Strabismic/High Ref Error Eye (mean ± SD)	Fellow Eye (mean ± SD)	Fellow v S/A Eye Paired t-test
Vertical diameter	1.61 mm (0.19)	1.61 mm (0.23)	p=0.95 CI:-0.10 to 0.11
Horizontal diameter	1.44 mm (0.18)	1.41 mm (0.16)	p=0.56 CI:-0.12 to 0.07
Disc to Fovea	4.31 mm (0.48)	4.28 mm (0.38)	p=0.70 CI:-0.23 to 0.16
Disc Area	1.83 mm^2 (0.39)	1.81 mm^2 (0.42)	p=0.81 CI:-0.24 to 0.19
Vertical to Horizontal Ratio	1.13 (0.11)	1.14 (0.11)	p=0.62 CI:-0.05 to 0.08
Axial length: Disc Area Ratio	13.32 mm^{-1} (3.08)	13.7 mm^{-1} (3.37)	p=0.61 CI:-1.22 to 1.99
Disc-Fovea: Disc Diameter Ratio	2.35 (0.33)	2.35 (0.24)	p=0.94 CI:-0.14 to 0.13

Table 10.5 presents the differences between the mean measurements in non-amblyopic adults; individually no non-amblyopic subject had an inter-ocular difference between the S/A eye and the fellow eye in the vertical diameter greater than 0.39mm with a mean individual difference of 0.12mm, in the horizontal diameter no individual had a difference greater than 0.23mm with a mean individual difference of 0.11mm. The greatest inter-ocular difference of the disc to fovea distance was 0.68mm with a mean individual difference of 0.22mm. The greatest inter-ocular difference of the disc area was 0.76mm^2 with a mean individual difference of 0.25mm^2.

10.4.7 Amblyopic Children

A high degree of symmetry in all optic disc dimensions was also found between the amblyopic eyes and their fellow eyes in children (Table 10.6).The vertical diameter: mean = 1.60±0.18mm (amblyopic eye) ranged from 1.36 to 2.0mm, the vertical diameter (mean = 1.61±0.19mm, (fellow eye) ranged from 1.28 to 2.16mm, the horizontal diameter (mean = 1.35±0.17mm, (amblyopic eye) ranged from 1.14 to 1.68mm, the horizontal diameter (mean = 1.39±0.19mm (fellow eye) ranged from 1.08 to 1.96mm and the disc area (mean = 1.72±0.39mm^2 (amblyopic eye) ranged from 1.22 to 2.63mm^2, the disc area (mean = 1.78±0.32mm^2 (fellow eye) ranged from 1.16 to 3.32mm^2 .The smallest disc area (1.16mm^2) in this group was in a fellow eye.

Table 10.6: Optic Disc parameter measurements ± SD of both eyes in amblyopic children. The results of paired t-tests between the amblyopic eye and the fellow eye for each disc sector are shown.

Optic Disc Parameter	Child Amblyopic Eye (mean ± SD)	Child Amblyopic Fellow Eye (mean ± SD)	Fellow v Amblyopic Eye Paired t-test
Vertical diameter	1.60 mm (0.18)	1.61 mm (0.15)	p=0.69 CI:-0.05 to 0.07
Horizontal diameter	1.35 mm (0.17)	1.39 mm (0.19)	p=0.23 CI:-0.25 to 0.10
Disc to Fovea	4.31 mm (0.33)	4.34 mm (0.32)	p=0.44 CI:-0.48 to 0.11
Disc Area	1.72 mm^2 (0.40)	1.78 mm^2 (0.45)	p=0.33 CI:-0.07 to 0.21
Vertical to Horizontal Ratio	1.19 (0.10)	1.17 (0.09)	p=0.28 CI:-.06 to 0.02
Axial length: Disc Area Ratio	12.95 mm^{-1} (2.45)	12.81 mm^{-1} (2.48)	p=0.75 CI:-0.99 to 0.72
Disc-Fovea: Disc Diameter Ratio	2.45 (0.35)	2.42 (0.33)	p=0.54 CI:-0.13 to 0.69

Table 10.6 presents the differences between the mean measurements in amblyopic children; individually no amblyopic child had an inter-ocular difference in the vertical diameter greater than 0.34mm with a mean individual difference of 0.11mm, in the horizontal diameter no individual had a difference greater than 0.47mm with a mean individual difference of 0.12mm. The greatest inter-ocular difference of the disc to fovea distance was 0.45mm with a mean individual difference of 0.15mm. The greatest inter-ocular difference of the disc area was 0.77mm^2 with a mean individual difference of 0.26mm^2.

10.4.8 ANOVA of Differences

In order to identify if the degree of symmetry differed between the groups, the inter-ocular difference found in each group (normal adults, amblyopic adults, non-amblyopic adults, amblyopic children and normal children) was examined using an ANOVA to identify any statistical significance in the differences between the groups. No significance was found. The results of the ANOVA of differences are presented in Table 10.7.

Table 10.7: Results of one-way ANOVA, comparing the inter-ocular **differences** of optic disc parameters between visually normal adults, visually normal children, amblyopic adults, non-amblyopic adults with strabismus and/or anisometropia and amblyopic children (5 groups).

Optic Disc Parameter *Differences*	Source of variation	Degrees of freedom	Sum of squares	Variance Ratio (F)	Probability
Vertical diameter *Differences*	Between groups Within groups	4 160	0.14 2.34	0.24	0.92
Horizontal diameter *Differences*	Between groups Within groups	4 160	0.05 2.43	0.81	0.52
Disc to Fovea *Differences*	Between groups Within groups	4 160	0.20 11.61	0.67	0.62
Disc Area *Differences*	Between groups Within groups	4 160	0.10 11.25	0.35	0.85
Vertical to Horizontal Ratio *Differences*	Between groups Within groups	4 160	0.33 1.20	1.10	0.36
Axial length: Disc Area Ratio *Differences*	Between groups Within groups	4 160	3.39 515.83	0.26	0.90
Disc-Fovea: Disc Diameter Ratio *Differences*	Between groups Within groups	4 160	0.05 8.19	0.24	0.91

An overview of the Disc Parameter measurements for each group is provided in Table 10.8.

Table 10.8: Disc parameter measurements ± SD for all 5 categories, visually normal adults, amblyopic adults, non-amblyopic adults with S/A, visually normal children and amblyopic children.

Optic Disc Parameter	Adult Visual Normal (mean ± SD)	Adult Amblyopes (mean ± SD)	Strabismic/High Ref Error Eye (mean ± SD)	Child Visual Normal (mean ± SD)	Child Amblyopes (mean ± SD)
Vertical diameter	1.66 mm (0.17)	1.56 mm (0.17)	1.61 mm (0.19)	1.64 mm (0.16)	1.60 mm (0.18)
Horizontal diameter	1.49 mm (0.15)	1.39 mm (0.18)	1.44 mm (0.18)	1.44 mm (0.17)	1.35 mm (0.17)
Disc to Fovea	4.36 mm (0.30)	4.28 mm (0.50)	4.31 mm (0.48)	4.38 mm (0.04)	4.31 mm (0.33)
Disc Area	1.95 mm^2 (0.39)	1.73 mm^2 (0.38)	1.83 mm^2 (0.39)	1.87 mm^2 (0.37)	1.72 mm^2 (0.40)
Vertical to Horizontal Ratio	1.12 (0.06)	1.13 (0.10)	1.13 (0.11)	1.15 (0.11)	1.19 (0.10)
Axial length : Disc Area Ratio	12.71 mm^{-1} (2.27)	13.56 mm^{-1} (2.89)	13.32 mm^{-1} (3.08)	12.18 mm^{-1} (2.25)	12.95 mm^{-1} (2.45)
Disc-Fovea : Disc Diameter Ratio	2.29 (0.27)	2.41 (0.40)	2.35 (0.33)	2.37 (0.29)	2.45 (0.35)

10.5 The effect of axial length, refractive error and age.

Studies investigating the optic disc have demonstrated that the dimensions are frequently affected by the variables of axial length (Leung et al., 2007; Leung et al., 2006), refractive error (Barr et al., 1999; Huynh et al., 2006a) and age (Barr et al., 1999). The series of studies undertaken by Lempert (Lempert, 2000; Lempert, 2003, 2004, 2008) have highlighted the likely effect on the optic disc measurements from axial length and the presence of hypermetropia. In order to

account for the effect produced by these variables, multivariate regression analysis was performed. As there are only a small number of non-amblyopic adults (n=13) with the presence and/or absence of strabismus, in comparison to the other groups (visually normal adults n=42, visually normal children n=56, amblyopic adults =30 and amblyopic children = 25) and little notable significance has been demonstrated in this group during this study (Chapter 7 and Chapter 8, Table 8.8) they were not included in the analysis. Each optic disc parameter was selected as the dependant variable and analysed separately, axial length, refractive error, and age were included in the model as continuous variables and a categorical variable of the presence/ absence of amblyopia was also included.

Regression analysis with adjustment for axial length, refractive error (MSE) and age (for details of axial length, MSE and age for all participants see Chapter 6, data sets 1- 4) indicated that axial length has a significant effect on the vertical diameter ($p<0.001$), horizontal diameter ($p<0.001$), disc to fovea distance ($p=0.01$) and optic disc area ($p<0.001$) (Figure 10.5), with the parameters increasing with increasing axial length (mm) (Tables 10.9 – 10.12). A smaller but significant effect on the axial length: disc area ratio ($p=0.03$), and disc to fovea: disc diameter ratio ($p=0.05$), was also shown with the ratios decreasing with every mm increase in axial length (Table 10.14 and Table 10.15). Axial length did not have any significant effect on the vertical: horizontal ratio ($p=0.86$) (Table 10.13).

Age was found to have a weak but significant statistical effect on the vertical diameter ($p=0.01$), disc to fovea distance ($p=0.001$), optic disc area ($p=0.05$) with

each parameter demonstrating a decrease with an increase in age (years) (Tables 10.9, 10.11 and 10.12). Age did not have any significant effect on the horizontal diameter (p=0.33) and disc-fovea: disc diameter ratio (p=0.51) (Tables 10.10 and 10.15) and missed achieving statistical significance on the vertical: horizontal ratio (p=0.06) and the axial length: disc area ratio (p=0.07) (Tables 10.13 and 10.14).

Refractive error (MSE) was shown only to have a significant effect on the disc to fovea: disc diameter ratio (p=0.04) with a decrease in the ratio of 0.03 for every 1DS increase in the MSE. No significant effect on any of the other optic disc dimensions and MSE was found (Tables 10.9 to 10.15).

Amblyopia was shown to just have a significant effect on the disc to fovea: disc diameter ratio (p=0.054) with an increase in the ratio of 0.14 in the presence of amblyopia (Table 10.15 and Figure 10.6). The presence of amblyopia did not have a significant effect on any of the other optic disc dimensions (Tables 10.9 to 10.15). In order to further investigate the effect of amblyopia on the disc to fovea: disc diameter ratio a 2 sided t-test comparing the visually normal adult eyes and the amblyopic adult eyes was undertaken. This did not demonstrate a significant difference between the two groups; diff = 0.13, p=0.12, CI: -0.03 to 0.29. Similarly no significant difference was found between the visually normal eyes of children and the amblyopic eyes; diff = 0.08, p=0.32, CI: -0.08 to 0.23. The individual DF: DD measurements for visual normals and amblyopes are presented in Figure 10.7.

Table 10.9: Multiple linear regression analysis of the **vertical diameter (mm)** including independent variables for the axial length, age, refractive error and the presence of amblyopia.

Variable	Regression Coefficient	Standard error	P-value	95% CI
Axial length	0.06	0.16	**0.000**	0.03 to 0.09
Age	-0.002	0.001	**0.01**	-0.004 to -0.001
Refractive Error (MSE)	0.12	0.008	0.08	-0.002 to 0.03
Amblyopia	-0.03	0.037	0.55	-0.09 to 0.046

Table 10.10: Multiple linear regression analysis of the **horizontal diameter (mm)** including independent variables for the axial length, age, refractive error and the presence of amblyopia.

Variable	Regression Coefficient	Standard error	P-value	95% CI
Axial length	0.06	0.15	**0.000**	0.03 to 0.09
Age	-0.001	0.001	0.33	-0.003 to 0.001
Refractive Error (MSE)	0.007	0.01	0.37	-0.01 to 0.02
Amblyopia	-0.04	0.035	0.25	-0.11 to 0.03

Table 10.11: Multiple linear regression analysis of the **disc to fovea distance (mm)** including independent variables for the axial length, age, refractive error and the presence of amblyopia.

Variable	Regression Coefficient	Standard error	P-value	95% CI
Axial length	0.08	0.03	**0.01**	0.02 to 0.15
Age	-0.006	0.001	**0.001**	-0.01 to -0.003
Refractive Error (MSE)	-0.02	0.02	0.27	-0.05 to 0.01
Amblyopia	0.11	0.07	0.12	1.30 to 4.03

353

Table 10.12: Multiple linear regression analysis of the **Disc Area (mm^2)** including independent variables for the axial length, age, refractive error and the presence of amblyopia.

Variable	Regression Coefficient	Standard error	P-value	95% CI
Axial length	0.14	0.04	**0.000**	0.07 to 0.22
Age	-0.004	0.002	**0.05**	-0.008 to 0.00002
Refractive Error (MSE)	0.22	0.02	0.21	-0.13 to 0.06
Amblyopia	-0.07	0.08	0.38	-0.23 to 0.09
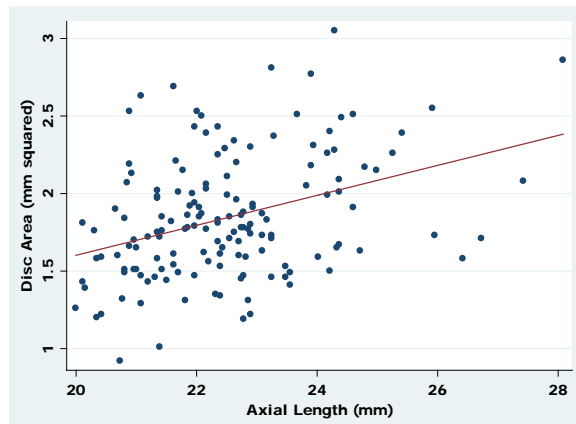
Figure 10.5: Linear regression of disc area (mm^2) v axial length (mm) in visually normal adults and children, amblyopic adults and children. The equation for the regression line (red) is $y = 0.14x + -1.32$ (95% CI for slope, 0.07 to 0.22).

Table 10.13: Multiple linear regression analysis of the **Vertical:Horizontal Ratio** including independent variables for the axial length, age, refractive error and the presence of amblyopia.

Variable	Regression Coefficient	Standard error	P-value	95% CI
Axial length	-0.002	0.01	0.86	-0.02 to 0.16
Age	-0.001	0.001	0.06	-0.002 to 0.0002
Refractive Error (MSE)	0.005	0.004	0.25	-0.004 to 0.014
Amblyopia	0.012	0.02	0.56	-0.03 to 0.05

Table 10.14: Multiple linear regression analysis of the **Axial Length:Disc Area Ratio** including independent variables for the axial length, age, refractive error and the presence of amblyopia.

Variable	Regression Coefficient	Standard error	P-value	95% CI
Axial length	-0.55	0.25	**0.03**	-1.0 to -0.06
Age	0.03	0.014	0.07	0.002 to 0.05
Refractive Error (MSE)	-0.24	0.12	0.06	-0.48 to 0.008
Amblyopia	0.75	0.56	0.19	-0.361 to 1.85

Table 10.15: Multiple linear regression analysis of the **Disc-Fovea: Disc Diameter Ratio** including independent variables for the axial length, age, refractive error and the presence of amblyopia.

Variable	Regression Coefficient	Standard error	P-value	95% CI
Axial length	-0.06	0.03	**0.05**	-0.13 to -0.001
Age	-0.001	0.002	0.51	-0.005 to 0.002
Refractive Error (MSE)	-0.03	0.16	**0.04**	-0.066 to -0.002
Amblyopia	0.14	0.07	**0.054**	-0.003 to 0.29
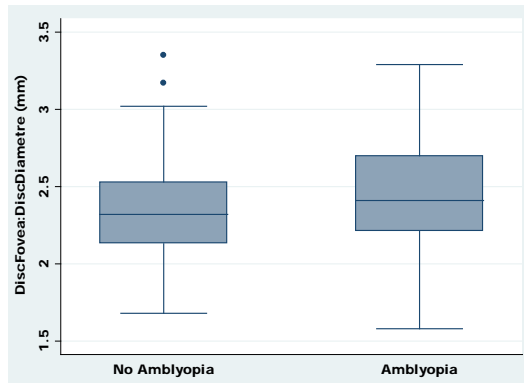
Figure 10.6: Box & whisker plots of Disc-Fovea: Disc Diameter Ratio measurements in visual normals and amblyopes. The dots represent outliers.
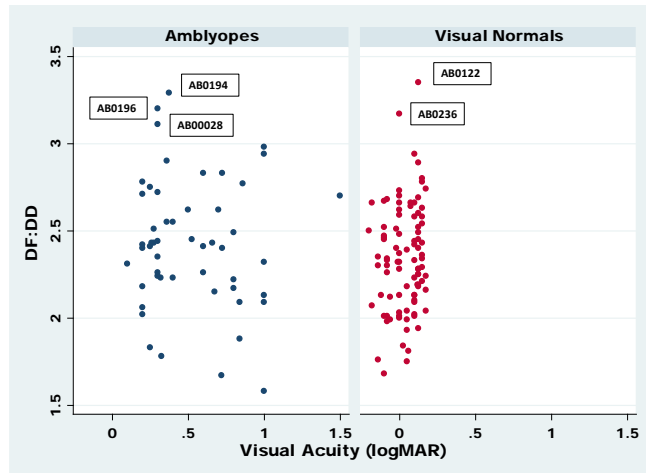
Figure 10.7: Scatter plots of Disc-Fovea: Disc Diameter Ratio measurements in visual normals and amblyopes. The individuals with the greatest DF:DD are indicated. AB0194, AB0196,and AB0122 are children, AB0236 and AB0028 are adults.

10.6 Discussion

10.6.1 Optic Disc Characteristics - Visually Normal Adults

The optic disc measurements found in visually normal adults produced the typical configuration described in previous studies (Blumenthal et al., 2009; Frenkel et al., 2005) with the disc being of increased diameter (1.66±0.17mm) in the vertical meridian in comparison to the horizontal meridian (1.49±0.15mm). The majority of studies documenting optic disc dimensions in visually normal adults have noted significant inter-individual variation in the normal dimensions with the optic disc area showing a mean of 2.69±0.70mm^2 and a range of 0.80mm^2 to 5.54mm^2

(Jonas et al., 1988). In this study although there was variability, the mean disc area was found to be less variable than that reported by Jonas et al 1988, with a mean disc area of 1.95±0.39mm^2 and a range of 1.35mm^2 to 3.05mm^2. The optic disc measurements in this study are closer to that reported by a study using scanning laser ophthalmoscopy and ocular biometry (Oliveira et al., 2007) where a mean disc area of 2.05±0.5mm^2, range 0.95 to 4.8mm^2 was reported. The methodology used in this study of evaluating magnification corrected measurements from optic disc photographs is similar to that undertaken by Jonas et al, 1988, it is therefore unlikely that it is the technique that has contributed to any difference found. Comparisons between current study results and previously published values are provided in Table 10.16.

Table 10.16: Comparison of normal adult optic disc characteristics from this current study with three previously published studies.

Study	Optic Disc Area in visually normal adults (mean ± SD)	Disc to Fovea:Disc Diameter Ratio (mean ± SD)
Bruce 2010	1.95 (0.39) mm^2	2.29 (0.27)
Barr 1999	n/a	2.82 (0.39)
Oliveira 2007	2.05 (0.5) mm^2	n/a
Jonas 1988	2.69 (0.70)mm^2	n/a

10.6.2 Optic Disc Characteristics - Visually Normal Children

The optic disc measurements found in visually normal children also produced the typical configuration described in previous studies (Blumenthal et al., 2009; Frenkel et al., 2005) with the disc being of increased diameter (1.64±0.16mm) in the vertical meridian in comparison to the horizontal meridian (1.44±0.17mm). The small number of studies documenting optic disc dimensions in visually normal children have also noted significant inter-individual variation. In a study of normal and preterm children using fundus photography (Hellstrom et al., 1997) the control group showed a mean optic disc area of 2.86±0.48mm^2 and a range of 2.04mm^2 to 4.02mm^2. In a study using OCT to identify disc margins (the disc margins are identified on the B-scan as the termination of the retinal pigment epithelium) (Huynh et al., 2006a) the mean disc area was found to be 2.20±0.39mm^2 with a range of 1.09 to 4.27mm^2. In this present study the mean disc area was found to be 1.87±0.37mm^2 with a range of 0.92mm^2 to 2.81mm^2. In the latter population based study of 6 year old children using OCT (Huynh et al., 2006a) the disc area was found to increase significantly with axial length (p<0.001) but was weakly associated with refractive error (p=0.02). This is similar to other studies examining discs in children (Hellstrom et al., 1997; Mansour, 1992; Samarawickrama et al., 2007) where no or only a weak association with refractive error was found. In this study refractive error (optic disc area coefficient: 0.22; p=0.21) was not shown to have a significant effect, however, axial length was shown to have a significant effect on all the optic disc dimensions, except the vertical to horizontal diameter ratio (optic disc area coefficient: 0.14; p<0.001) (Tables 10.9 – 10.15). The optic

disc parameter measurements are reported along with those from previous studies in children in Table 10.17.

Table 10.17: Comparison of normal optic disc characteristics in children from this current study with three previously published studies (**calculated from vertical and horizontal diameters, not reported in published paper).

Study	Optic Disc Area In visually normal children (mean ± SD)	Optic Disc Vertical diameter	Optic Disc Horizontal diameter	Disc to Fovea distance (mean ± SD)
Bruce 2010	1.87 (0.37)mm^2	1.64 (0.16)mm	1.44 (0.17)mm	4.38 (0.04)mm
De Silva 2006	1.48 mm^{2**}	1.41 (0.19)mm	1.05 (0.13)mm	4.4 (0.4)mm
Huynh 2006	2.20 (0.39)mm^2	1.79 (0.28)mm	1.53 (0.21)mm	n/a
Hellström 1997	2.86 (0.48)mm^2	n/a	n/a	n/a

10.6.3 Inter-Ocular Symmetry (IOS)

A high degree of symmetry was found in all the measured optic disc parameters. As with the foveal topography, RNFL thickness and papillomacular bundle structure (Chapters 7 to 9) it is important to establish the presence of inter-ocular symmetry in visual normals as it provides a standard comparison. Inter-ocular symmetry of the RNFL has been noted in studies of both adults and children using OCT (Budenz, 2008; Dubis et al., 2009; Huynh et al., 2007) although in these studies considerable individual variation was noted. In this study of optic disc structure inter-ocular symmetry has been shown to be present in all recruited cohorts; adults, children, amblyopes, non-amblyopic individuals (S/A) and visually normal controls, this has been a consistent finding in all retinal areas that have been investigated in this study.

359

10.6.4 Optic Disc Characteristics – Axial Length and Refractive Error

In this study a significant and positive effect of axial length on disc area was shown with increased disc area being associated with an increased axial length with disc area increasing by 0.14 for every 1mm increase in axial length (p<0.001). This is consistent with the findings of Oliveira et al, 2007. Refractive error (MSE) did not however demonstrate an effect on the optic disc characteristics other than the DM:DD Ratio (p=0.04). This lack of effect of refractive error (MSE) needs to be considered in the light of the fact that axial length has shown a significant effect on all of the measured characteristics. A study investigating optic disc parameters in visually normal eyes (Jonas et al., 1988) also found no correlation between refraction and optic disc size. The latter study limited the inclusion criteria to individuals with a refractive error below 8.0DS (mean -0.13±2.35DS range -7.50 to +7.50DS). The exclusion of individuals with high refractive errors may have influenced the findings; however, in this study where high refractive error was not excluded (mean -1.85DS range -13.5 to +4.00DS) no significant effect was demonstrated.

The DF:DD ratio was shown to be weakly affected by both axial length (coefficient: -0.06; p=0.05) and refractive error (coefficient: -0.03; p=0.04). This is difficult to explain as neither of the individual components of the ratio (Disc-fovea or disc diameter measurements are influenced by refractive error, but are influenced by axial length. The DF:DD ratio reported by Barr et al, 1999 (2.82±0.39) is slightly higher than this study but still falls well within the normative criteria set by Barr,

who suggests that a ratio of 4.20 or above is indicative of optic nerve hypoplasia (Barr et al., 1999). Comparisons of normative adult data are set out in Table 10.16.

10.6.5 Optic Disc Characteristics - Age

Optic disc dimensions have been shown to be variably affected by age. A number of studies of optic disc in children (De Silva et al., 2006; Hellstrom et al., 1997) and adults (Dacosta et al., 2008; Jonas et al., 1988) have found no significant correlation between optic disc dimensions and age. In this study the majority of measured disc parameters showed no significant association with age; the vertical diameter showed a weak negative effect (coefficient: -0.002; p=0.001), disc to fovea distance (DF:DD) showed a slight decrease with every 1 year increase in age (coefficient : -0.006; p<0.001). A very weak effect of age on disc area was also found with disc area reducing slightly with age (coefficient: -0.004; p=0.05). The effect of age on the DF:DD ratio has also been reported in studies investigating optic disc hypoplasia (Alvarez et al., 1988; Barr et al., 1999). Alverez et al, 1988 reported a DF:DD ratio of 2.62±0.21 in a paediatric population which was lower in comparison to Barrs findings for normal adults (2.82±0.39) (Barr et al., 1999), leading Barr to conclude that there was a significant difference between the ratio in adults and children. A difference between the disc to fovea measurement was also noted in a study of infant eyes where the disc to fovea (ODF) measurement was found to be 4.4±0.4mm (De Silva et al., 2006) this was smaller in comparison to the optic disc to fovea (ODF) measurement in an adult population (4.9±0.3mm) (Williams and Wilkinson, 1992). The conclusion derived by the authors from comparing the results between the different studies must however be considered

361

carefully, as although the mean measurements are smaller in the paediatric goups the means are still within 2 SD's of each other which would indicate that there is no significant difference, but only variation. This current study of optic disc parameters includes both adults and children, incorporating a wide range of age groups (4 - 66 years), most other studies reporting the effect of age have reported on either a purely paediatric (Alvarez et al., 1988; De Silva et al., 2006; Hellstrom et al., 1997; Huynh et al., 2006a) or a purely adult population (Barr et al., 1999; Jonas et al., 1992; Williams and Wilkinson, 1992). This may explain the insignificance found in terms of the relationship of age to disc parameters. That said the majority of disc parameters in this study have not shown any significant effect from age and those that have done so (vertical diameter, disc area and DF:DD) have demonstrated only a weak association (Tables 10.9 – 10.15).

10.6.6 Optic Disc Characteristics – Amblyopia

The research investigating optic disc characteristics (Lempert 1998, 2000, 2003, 2008) has presented evidence of smaller optic discs in amblyopic eyes, in comparison to their fellow eye and also in comparison to visually normal eyes. Optic disc area in amblyopic eyes has been reported as $1.72\pm0.73mm^2$ in comparison to their fellow eyes, with disc area of $1.95\pm0.69mm^2$ (Lempert, 2000). Although the disc area found in amblyopic eyes ($1.72\pm0.73mm^2$) by Lempert (2000) was comparable to that found with this study ($1.73\pm0.38mm^2$), the asymmetry between amblyopic eyes and their fellow eyes reported by Lempert was not demonstrated. In this present study a high degree of inter-ocular symmetry

was found between the optic disc area measurements of amblyopic eyes (1.73±0.38mm^2) and their fellow eyes (1.72±0.32mm^2) in adults and children, (amblyopic eye = 1.72±0.4mm^2 and fellow eye = 1.78±0.45mm^2) (Tables 10.4 and 10.6). Inter-ocular symmetry has been demonstrated in a study using magnetic resonance imaging (MRI) to investigate optic nerve and globe size and shape (Pineles and Demer, 2009). Pineles and Demer (2009) reported a symmetrical bilateral reduction in optic nerve size in amblyopes, this reduction in optic nerve size was however, subclinical, not appearing to be linked to the level of visual acuity. The report suggesting that optic disc area is reduced in amblyopic eyes (Lempert, 2000) has been criticised for not taking into account refractive error (Archer, 2000) and/or axial length (Lempert ,2003). In order to take account of any disproportionate reduction in optic disc area that may have been affected by the presence of hypermetropia and/or a shorter axial length, optic disc dimensions were reported in terms of the axial length to disc area ratio (Axl:DA) in follow-up retrospective studies (Lempert, 2003, 2004). In amblyopic esotropes Lempert (2003) found the Axl:DA to be 15.24±4.61mm^{-1} in the amblyopic eyes and 13.61±3.67mm^{-1} in the fellow eyes, this was found to be a significant difference (p=0.02) . No confidence interval is quoted for the difference between the group means; this would have been helpful in assessing the significance of the difference between the amblyopic and the fellow eyes which both have large standard deviations, making it possible that the difference is due to normal variation. In this study the Axl:DA in the amblyopic eyes of adults was found to be 13.56±2.89mm^{-1} and 13.62±2.44mm^{-1} in the fellow eyes (Table 10.4) and in children the Axl:DA in the amblyopic eyes was 12.95±2.45mm^{-1} and 12.81±2.48mm^{-1} in the fellow eyes,

respectively (Table 10.6). There has been a consistent picture of inter-ocular symmetry across the retina in this study (Chapter 7 to 9), where differences have been present it has been between the amblyopic and visually normal eyes (Chapter 7). The Axl:DA in the adult visually normal eyes was 12.71±2.27mm^{-1}, a direct comparison of the two groups did not show a significance between the two groups (2 sided t-test, p= 0.30; CI: -1.9 to 0.6).

The presence of amblyopia was shown to only just have a significant effect on one of the measured optic disc parameters, disc to fovea: disc diameter ratio (DF:DD) and this was only a weak effect (coefficient: 0.14; p=0.054) with the presence of amblyopia having a positive effect on the DF:DD ratio. The DF: DD ratio in amblyopic adult eyes was found to be 2.41±0.40 (Table 10.4) and 2.29±0.27 in visually normal eyes (Table 10.2) a direct comparison of the two groups did not show any significant difference (2 sided t-test, p=0.32; CI: -0.24 to 0.08). In a study of optic disc size using the DF:DD ratio (Barr et al., 1999), a DF:DD of 2.82±0.39 was found in the control group of visually normal adults, a small group of amblyopes was also recruited, the mean ratio was not reported, however, no significant difference was found between the amblyopic and fellow eyes and there was no significant difference between the groups (p=0.98).

10.7 Conclusion

Investigation of the optic disc characteristics has found no significant difference in structure in the presence of amblyopia, with only a weak effect evident on one parameter, DF:DD ratio (p=0.054). Where differences have been found between amblyopic and normal or fellow eyes in other studies (Bozkurt et al., 2008; Repka et al., 2009b; Yen et al., 2004) the amblyopic eye has been found to have a reduced optic disc area. Although optic disc dimensions in this study were similar that of the amblyopic eyes reported by Lempert (2000), unlike Lempert (2000, 2003, 2004) a significant degree of inter-ocular asymmetry was not found. Optic disc parameters, however have demonstrated a significant effect from axial length, particularly in the vertical diameter (p<0.001), horizontal diameter (p<0.001), disc area (p<0.001) and disc to fovea distance (p=0.01). As with the peripapillary retinal nerve fibre layer around the optic disc (Chapter 9), the optic disc itself was found to be similar in normals and amblyopes. The evidence from this study therefore suggests that amblyopia, or the conditions thought to cause amblyopia, are not associated with a change in optic disc structure.

Chapter 11. Retinal Structure in Amblyopes undergoing Occlusion Therapy: A Longitudinal Study

11.1 Introduction

The aim of the longitudinal phase of this study is to investigate the relationship between quantitative measures of retinal structure in children prior to amblyopia therapy, and to try to relate them to the post-therapy visual outcome.

Although the association of amblyopic deficits with differences in foveal structure (Chapter 7) provides retrospective evidence for the influence of retinal structural anomalies on therapy (since almost all the amblyopes (95%) in phase 1 had undergone therapy), the data cannot provide a critical test of the hypothesis that such anomalies limit the success of therapy. This can only be asserted conclusively with a prospective study. In the final phase of the project, the success or failure of occlusion therapy in children who are about to undergo amblyopia therapy for the first time will be examined. By relating the pre-therapy, quantitative measures obtained using the OCT imaging to the visual outcome achieved following standardised treatment protocols, the project will examine whether OCT measurements can identify children in whom a poor final visual result can be expected. In addition to being able to avoid unnecessary amblyopia treatment in these children, the opportunity to develop alternative treatment strategies is presented.

This longitudinal phase of the study will examine retinal structure both prior to and post occlusion therapy. Detailed measurements will be taken of the fovea, retinal nerve fibre layer (RNFL) in the peripapillary area and of the papillamacular bundle.

11.2 Foveal Topography in Amblyopia

11.2.1 Methods

A total of thirty-four children were recruited to the longitudinal arm of the study; nine with strabismus only (26.5%), 14 with anisometropia only (41.2%) 10 with both strabismus and anisometropia (29.4%) and one (2.9%) with a reduction in visual acuity but no detectable manifest deviation or refractive error (Table 11.1). The participants were recruited via the Ophthalmology and Orthoptic clinics at local hospitals. The majority of children (85%) recruited to the study were initially referred into the Ophthalmolgy service via the local school screening programme of reception age (4-5 years) school children having been identified as having reduced visual acuity and/ or a strabismus. This group of amblyopic children are from the same birth cohort of local school children who formed the group of visually normal children in phase 1 of this study (Chapter 7) and therefore are a representative sample of children that would be treated for amblyopia in the Hospital Eye Service (HES). The age range of this amblyopic cohort of children was from 4 to 7 years (mean = 5.1years). The mean spherical equivalent refractive error in the amblyopic eye ranged from -3.00DS to +6.50DS (mean = +2.5DS) and visual acuity ranged from +0.2 (6/9) to +1.0 logMAR (6/60) (mean = +0.46 logMAR (6/18 Snellen

equivalent)) . The mean spherical equivalent refractive error in the fellow eye ranged from -1.3DS to +5.50DS (mean = +1.5DS) and visual acuity in the fellow eyes ranged from 0.0 (6/5) to +0.275 (6/12[+1]) log units (mean = +0.085 (6/7.5[+1]). One participant with +0.275 logMAR visual acuity in the fellow eye had two lines difference between the amblyopic eye and the fellow eye and on this basis was therefore classified as a bilateral amblyope. Participants received a full eye examination that included recording ocular history, subjective refraction, visual acuity measurement (logMAR) with best correction, cover test (at distance and near, both with and without full refractive correction). Binocular function was assessed using measurement of prism fusion and stereoacuity using the Frisby stereotest measured to a best stereoacuity measurement of 55 sec of arc where appropriate. For the purposes of this study, amblyopia was defined as a reduction in the best corrected visual acuity in the amblyopic eye of $\geq$ 0.2 logMAR with at least 2 lines difference between the amblyopic eye and the fellow eye (Awan et al., 2005; Holmes and Clarke, 2006; Stewart et al., 2003) and anisometropia was defined as $\geq$ 1 dioptre difference in spherical equivalent (Donahue, 2005). It is important to stress that the treatment prescribed to the children was not altered in any way by participation in the study. Ethical approval was obtained from the local Ethics Committee (Bradford) prior to commencement of the study. Parents/careers of the participants gave informed, written consent and the study was conducted according to the tenets of the Declaration of Helsinki.

11.2.2 Treatment Prescribed

In order to insure that the visual outcome of the amblyopia treatment was related to the occlusion therapy and not solely from the wearing of glasses, occlusion was only instigated after a period of refractive adaptation, consistent with standard treatment protocols. This consisted of a period of glasses wear only for 4 months or 2 consecutive visits, with no visual improvement having been measured by logMAR visual acuity (Chapter 6). Occlusion using a conventional eye patch was prescribed for 4 hours daily to the fellow eye and the parents/carers issued with a diary in order to record the amount of daily occlusion (Chapter 2). The children were given follow-up appointments every 4 -6 weeks after commencing the occlusion therapy. Initially it was planned to perform the OCT scans once before the commencement of treatment and repeat after treatment. The capability of all the children to initially perform the scans was however reduced, this improved with familiarity with the imaging procedure. For this reason the scans were performed at each visit (including during the period of refractive adaptation) to ensure the greatest possible chance of obtaining good quality scans to be included in the data set. All of the clinical tests and the OCT imaging were conducted by the same researcher. The scans were not recorded or analysed until after all the children had completed their course of treatment, thus details about retinal structure were not known during the treatment period. The best pre-treatment and post treatment scans were chosen for analysis and the process of the foveal metric analysis using Data Thief was carried out blind to the result of the treatment. The processing via Matlab was carried out by a second researcher unaware of the treatment outcome.

Ten children did not complete all procedures . One child was withdrawn from the study, but not from treatment. One child moved from the area, five children failed to attend follow-up appointments and three were unable to be scanned, one due to lack of co-operation, one due to unsteady fixation and one due to photophobia. Of the twenty-four children receiving treatment, 9 (37.5%) had eccentric fixation assessed using an oculo-visuscope. Participants with no manifest deviation on cover test with eccentric fixation were classified as having micro-strabismus. None of the children had previously had treatment for their amblyopia, confirmed by ocular history from the parent/carer, except for one child who although had had treatment prescribed previously had not complied. Tables presenting the clinical details of the participants in each category are included in Chapter 6.

11.2.3 Treatment Outcomes

In Chapter 3 it was stated that the final visual outcome in the longitudinal phase of this study would be reported in 3 ways:

- Final level of the logMAR visual acuity in the amblyopic eye.
- Difference in the logMAR visual acuity between starting occlusion treatment and final recorded visual acuity when occlusion ceased.
- Proportional improvement as designed by the Monitored Occlusion Treatment Amblyopia Study (MOTAS) group (Stewart et al., 2003) (Chapter 3).

These outcomes for the longitudinal cohort of amblyopic children are presented in Table 11.1.

Table 11.1: The outcomes of the longitudinal phase of the study are presented in 5 ways; **1.** Final VA of amblyopic eye, **2.** Difference between VA at start of treatment and end of treatment, **3.** Improvement (%) in VA obtained, **4.** Final VA ≤ 0.2 LogMAR combined with % improvement of ≥ 50%, **5.** Improvement (%) in log units per hour of occlusion. S=strabismus only A=anisometropia only and S/A=combined strabismus and anisometropia.

ID	Diagn	Classific^n	Start VA Amblyopic eye (logMAR)	Final VA fellow eye (logMAR)	Final VA Amblyopic eye (logMAR) 1.	VA diffn 2.	% Improvement 3.	Combined Final VA & % imp 4.	Log unit Improvement per occln hour (10^{-3}) 5.	Hours Occln	Start Foveal Thk amblyopic eye (µm)
AB0074	S	MICRO	0.575	0.00	0.30	0.275	48	F	0.76	360	219.48
AB0123	A	ANI	0.80	0.00	0.00	0.80	100	S	3.35	239	179.22
AB0184	S/A	MICRO	0.675	0.20	0.20	0.475	100	S	1.05	452	206.80
AB0185	A	ANI	0.35	0.00	0.125	0.225	64	S	0.63	355	185.20
AB0186	S	ESO	1.00	0.00	1.00	0.0	0	F	0.00	480	191.64
AB0197	S/A	MICRO	0.250	0.00	0.125	0.125	50	S	0.55	228	180.22
AB0199	S	ESO	0.85	0.05	0.35	0.50	62	F	2.38	210	170.50
AB0200	S/A	MICRO	0.85	0.00	0.85	0.0	0	F	0.00	360	219.66
AB0204	S/A	ESO	0.40	0.10	0.20	0.20	66	S	0.48	421	147.81
AB0207	S	ESO	0.550	0.30	0.450	0.10	33	F	0.24	410	167.87
AB0208	A	ANI	0.25	0.025	0.025	0.225	90	S	3.38	66.5	157.09
AB0212	A	ANI	0.425	0.00	0.25	0.175	41	F	0.35	497	189.71
AB0214	A	ANI	0.275	0.05	0.05	0.225	90	S	0.92	244	151.27
AB0215	S	ESO	0.20	0.05	0.10	0.10	66.7	S	1.15	87	160.29
AB0217	A	ANI	0.325	0.075	0.075	0.25	77	S	0.75	335	154.07
AB0218	A	MICRO	0.325	0.05	0.2	0.125	45	F	0.79	158	180.52
AB0219	A	AM	0.275	0.05	0.075	0.20	72.7	S	0.85	234	162.39
AB0225	A	ANI	0.40	0.10	0.150	0.25	83	S	2.05	122	162.58
AB0241	A	ANI	0.40	0.10	0.20	0.20	66.7	S	0.69	289	157.85
AB0244	S/A	MICRO	0.20	0.05	0.075	0.125	83	S	0.44	282	166.72
AB0252	S/A	ANI	0.475	0.175	0.3	0.175	46.7	F	4.38	40	150.83
AB0255	A	ANI	0.40	0.00	0.075	0.325	81.25	S	2.64	123	166.22
AB0262	S/A	MICRO X	0.30	0.05	0.075	0.225	90	S	1.20	188	162.70
AB028	A	ANI	0.50	0.175	0.20	0.30	85	S	1.10	273	164.05

11.2.3.1 Foveal Topography in Amblyopic Children: Definition of Outcome

The definition of a successful outcome, final visual acuity of ≤ +0.2 logMAR combined with a % improvement score of ≥ 50% was based on previous peer reviewed research (Cleary, 2000, 2007; Stewart et al., 2003; Woodruff et al., 1994). This definition may however, influence the interpretation of the results found in the study. In Table 11.1 a number of defined outcome categories are therefore presented, the results of those children that would be classed as "Fail" are highlighted, thus indicating how the results would be modified with the change of outcome definition. Categories 1, 3, and 4 produce similar results with 1 and 3 producing 7 "failed" and 17 "successful" amblyopes and category 4 producing 8 "failed" and 16 "successful" amblyopes. Analysis using final outcomes 1, 3 or 4 does not produce any significant difference to the presented results. One participant (AB0199) (Table 11.1) would have changed from being defined as "failed" to that of "success" if the final outcome was changed from 4 to 3. This individual had a pre-treatment visual acuity of +0.85 logMAR and wore the occlusion for 210 hours, post-treatment the visual acuity was +0.35 logMAR with an improvement of 62%. Only one participant (AB0218) (Table 11.1) would have changed from being defined as "failed" to that of "success" if the final outcome was changed from 4 to 1. This individual had a pre-treatment visual acuity of +0.325 logMAR and wore the occlusion for 158 hours, post-treatment the visual acuity was +0.2 logMAR with an improvement of 45%. The refinement of the categorisation of final outcome from % improvement to final visual acuity did not significantly change the statistical significance found.

Category 2 indicates the difference between the amblyopic VA at the start and end of treatment, **any** difference is classed as a successful outcome, a category used in previous studies of amblyopia treatment (Bowman et al., 1998; Lithander and Sjostrand, 1991). Using this category only 2 amblyopes were deemed to fail, the results from category 2 will obviously vary depending on the chosen improvement deemed to produce "success", it is therefore variable and open to interpretation. It was for these reasons not chosen as the final outcome for analysis in this study. Category 5 is an improvement score in log units per hours of occlusion; the classification of "success" is set at ≥ 0.001 log unit per hour (4 letters per hour of occlusion). This category has not been reported previously and it is therefore difficult to use as a comparator. It is also more of an indication as to the speed of the improvement rather than the depth of the improvement indicated by the other four outcomes, making it difficult to make direct comparison with the other categories. It is however, important to know if the speed of the improvement is linked to the final outcome of treatment, i.e. do those children making the fastest improvement have the better visual outcomes? This does not appear to be the case and is illustrated by the results of 2 individual cases, AB0252 and AB0197. AB0197 would be classed as having a successful outcome under categories 1-4, with a VA improving from +0.25 logMAR to +0.125 logMAR with a % improvement of 50%. However, having had 228 hours of occlusion the log unit improvement per hour is only 0.05% which is slow, therefore despite having a good final VA they would be classified as a "Fail".

AB0252 if categorised using 1, 3 or 4 would "fail", this individual is the child who had poor compliance for treatment wearing the occlusion for 40 hours. The improvement in the VA during this time in the amblyopic eye was from +0.475 to +0.175 log units with a 46.7% improvement. However, when the log unit improvement is calculated the improvement per hour is 0.44 %, this is the fastest improvement change in the longitudinal cohort. Category 5 although providing information on the rate of change, does not accurately reflect the final visual outcome. It is therefore valid to analyse the data with the chosen category 4.

11.3 Statistical Analysis

Statistical analysis of the longitudinal phase of this study was carried out using commercially available Stata SE version 10.0. Paired t-tests were used to directly compare the inter-ocular symmetry between the eyes for the pre-treatment group for all measured foveal parameters (Figure 7.7 and Table 7.1). Paired t-tests were also used to explore the difference between pre-treatment and post-treatment measurements. Two sided t-tests were used to further explore differences between those amblyopes with a successful outcome and those amblyopes whose treatment outcome was deemed unsuccessful, as indicated in Table 11.1.

11.4 Results

11.4.1 Foveal Topography in Amblyopic Children: Pre-treatment

The methodology of the scan technique was the same as that used in Chapter 7. Foveal parameters (Figures 7.7, 7.8 and Table 7.1) were measured in both the horizontal and vertical meridians from scans that bisected the centre of the fovea (Figure 7.3). A summary of the results of all the foveal parameters in the pre-treatment amblyopes for both the horizontal (nasal – temporal meridian) and the vertical (superior – inferior meridian) scans is provided in Table 11.2. Pre-treatment the mean foveal thickness of the amblyopic eyes in the longitudinal cohort was found to be 173.11 ± 20.35µm measured in the horizontal meridian and 178.30 ± 23.44µm in the vertical meridian. The retinal thickness (highest point from the top of the pit (max) to the retinal pigment epithelium) (Figure 7.7 and Table 7.1) was 200.53 ± 20.64µm in the nasal meridian, 315.18 ± 23.31µm in the superior meridian and 310.84 ± 25.36µm in the inferior meridian. The temporal meridian was thinnest measuring 279.93 ± 18.70µm. (Table 11.2). The pit depth (max) (Chapter 7, Figure 7.7 and Table 7.1) for pre-treatment amblyopic eyes was 116.25µm (SD 25.53µm) in the horizontal meridian. The nasal pit slope was 12.40º (SD 3.2°) and the temporal slope was 11.19º (SD 3.25°). The slope of the foveal pit in the vertical meridian was steeper, with the superior slope measuring 14.37º (SD 3.62°) and the inferior slope measuring 14.43° (SD 3.63°). A summary of the results of parameters in pre-treatment amblyopes is provided in Table 11.2.

11.4.2 Inter-ocular Symmetry (IOS)

The pre-treatment amblyopic and fellow eyes were first examined in order to establish the degree of inter-ocular symmetry. As with the main amblyopic cohort investigated (see Chapter 7), a high degree of inter-ocular symmetry was found between the amblyopic eye and the fellow eye in all measured parameters (Table 11.2). For this reason only the results from the amblyopic eyes were therefore used in the analysis of pre versus post-treatment comparison of retinal structure and in the analysis of how retinal structure may be linked to treatment success.

Table 11.2 : Pre-treatment foveal topography measurements ± SD of both eyes in amblyopic children in the longitudinal phase. The results of paired t-tests between the amblyopic eye and fellow eye for each foveal parameter are shown. The foveal parameters are defined previously in Chapter 7 (Figure 7.7 and Table 7.1).

Foveal Parameter	Child (Pre-Treat) Amblyopic Eye (mean ± SD)	Child (Pre-Treat) Fellow Eye (mean ± SD)	Amblyopic v Fellow Treatment Eyes Paired t-test
Foveal Thickness *Horizontal*	173.11 μm (20.35)	173.45 μm (23.31)	p=0.88 CI: -4.08 to 4.75
Foveal Thickness *Vertical*	178.30 μm (23.44)	173.17 μm (33.96)	p=0.464 CI: -19.71 to 9.43
Nasal Thickness *(max)*	300.53 μm (20.64)	304.34 μm (19.68)	p=0.18 CI: -1.83 to 9.45
Superior Thickness *(max)*	315.53 μm (19.39)	305.99 μm (15.08)	p=0.27 CI: -8.19 to 27.28
Temporal Thickness *(max)*	280.07 μm (20.06)	281.72 μm (17.08)	p=0.81 CI: -6.8 to 8.67
Inferior Thickness *(max)*	310.84 μm (25.36)	303.86 μm (18.86)	p=0.189 CI: -17.80 to 3.84
Retinal Base Area *Nasal*	212367 μm^2 (38203)	204804 μm^2 (36291)	p=0.20 CI: -19478 to 4353
Retinal Triangle Area *Nasal*	77952 μm^2 (17993)	76879 μm^2 (17126)	p=0.59 CI:-5170 to 3022
Pit Depth *(max)* *Horizontal*	116.25 μm (25.53)	118.56 μm (29.45)	p=0.28 CI: -1.96 to 6.56
Pit Depth *(max)* *Vertical*	134.70 μm (33.87)	131.55 μm (39.20)	p=0.698 CI: -20.16 to 13.85
Horizontal Pit Diam.	2274 μm (345.13)	2198 μm (295.63)	p=0.14 CI: -180.77 to 27.99
Vertical Pit Diam.	2163 μm (867)	1961 μm (428)	p=0.889 CI: -196 to 170
Nasal Width *(max)*	1229 μm (176.75)	1183 μm (149.04)	p=0.145 CI:-109.96 to 17.15
Superior Width *(max)*	1049 μm (358.35)	1060 μm (201.01)	p=0.898 CI: -170.60 to 192.82
Foveal Slope *Nasal*	12.40° (3.20)	12.31° (3.37)	p=0.758 CI: -0.73 to 0.54
Foveal Slope *Superior*	14.37° (3.62)	13.62° (2.96)	p=0.284 CI: -1 to 3.36
Foveal Slope *Temporal*	11.19° (3.25)	11.05° (3.43)	p=0.646 CI: -0.71 to 0.45
Foveal Slope *Inferior*	14.43° (3.64)	13.22° (4.67)	p=0.60 CI: -1.63 to 2.76

11.4.3 Foveal Topography in Amblyopic Children: Pre v Post-treatment

The pre-treatment and post-treatment foveal parameters of children undergoing occlusion therapy were compared. No significant differences were found between the pre-treatment and post-treatment measurements across any of the measured foveal parameters. A summary of the results of the parameters in the amblyopic eyes both pre-treatment and post-treatment is provided in Table 11.3.The vertical scans of pre and post-treatment were not obtained for 9 of the 24 amblyopic eyes, mainly due to fixation difficulties such as movement and blink preventing the collection of pre-treatment scans. For this reason only the horizontal results are presented in Table 11.3.

Table 11.3: Foveal topography measurements ± SD pre and post treatment of the amblyopic eyes of children in the longitudinal phase. The results of paired t-tests between the amblyopic eye pre and post-treatment for each foveal parameter are shown. The foveal parameters are defined previously in Chapter 7 (Figure 7.7 and Table 7.1).

Foveal Parameter	Child (Pre-Treat) Measurements (mean μm ± SD)	Child (Post-Treat) Measurements (mean μm ± SD)	Post v Pre Amblyopic Eyes Paired t-test
Foveal Thickness *Horizontal*	173.11μm (20.35)	175.62μm (23.78)	p=0.69 CI: -10.47 to 15.49
Nasal Thickness *(max)*	300.53μm (20.64)	302.01μm (25.62)	p=0.83 CI: -12.16 to 15.12
Nasal Thickness *(mid)*	228.26μm (14.70)	228.51μm (17.85)	p=0.96 CI: -9.34 to 9.84
Temporal Thickness *(max)*	280.07μm (20.05)	279.01μm (21.31)	p=0.86 CI: -13.21 to 11.10
Retinal Base Area *Nasal*	212367μm^2 (38203)	209008μm^2 (35789)	p=0.760 CI: -25128 to 18412
Retinal Triangle Area *Nasal*	77953μm^2 (17993)	75447μm^2 (20733)	p=0.66 CI: -13896 to 8884
Pit Depth (max) *Horizontal*	117.19μm (25.44)	114.89μm (28.66)	p=0.77 CI: -18.20 to 13.61
Pit Depth (mid) *Horizontal*	50.99μm (10.82)	48.67μm (11.19)	p=0.47 CI: -8.71 to 4.07
Horizontal Pit Diam.	22743μm (345.13)	2215μm (304.23)	p=0.54 CI: -250.51 to 132.41
Top Width *Nasal*	1229.27μm (176.75)	1194.97μm (164.74)	p=0.495 CI: -134.79 to 66.19
Foveal Slope *Nasal*	12.40° (3.20)	11.75° (3.28)	p=0.49 CI: -2.56 to 1.25
Foveal Slope *Temporal*	11.19° (3.25)	10.54° (3.28)	p=0.50 CI: -2.57 to 1.27

378
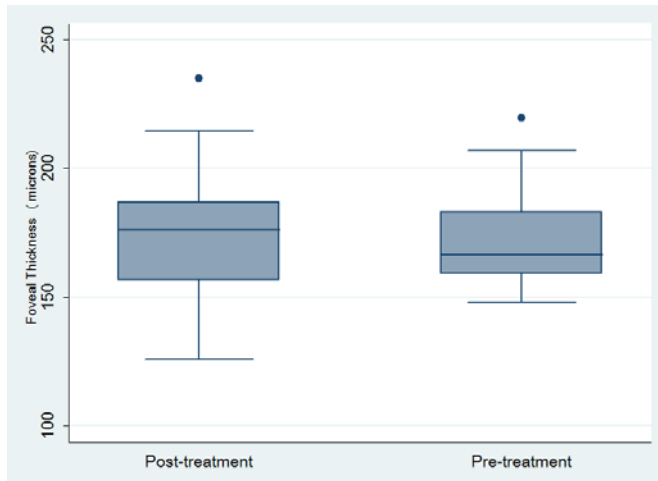
Figure 11.1: Box plots depicting the foveal thickness (µm) measurements pre and post-treatment (paired t-test diff: 2.5, p=0.69, CI: -10.47 to 15.49). The outliers are present both pre and post treatment and are data from AB0074).
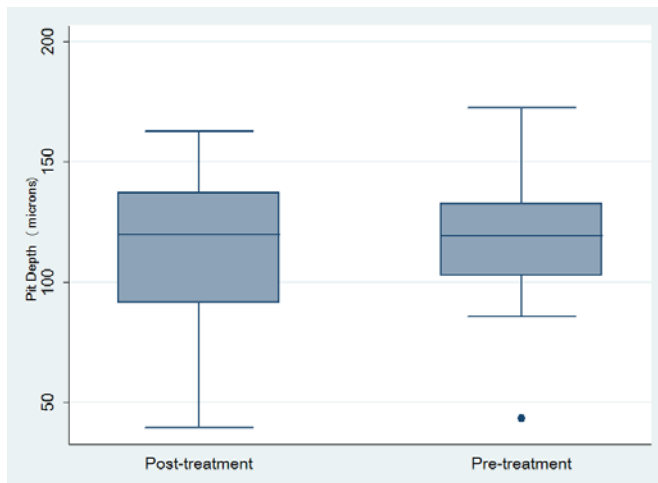
Figure 11.2: Box plots depicting the pit depth (µm), pre and post-treatment (paired t-test diff: -2.29, p=0.77, CI: -18.20 to 13.61). The outlier present pre-treatment is from AB0074, post-treatment this case also has the shallowest pit (39.69µm) but it is not shown as an outlier).
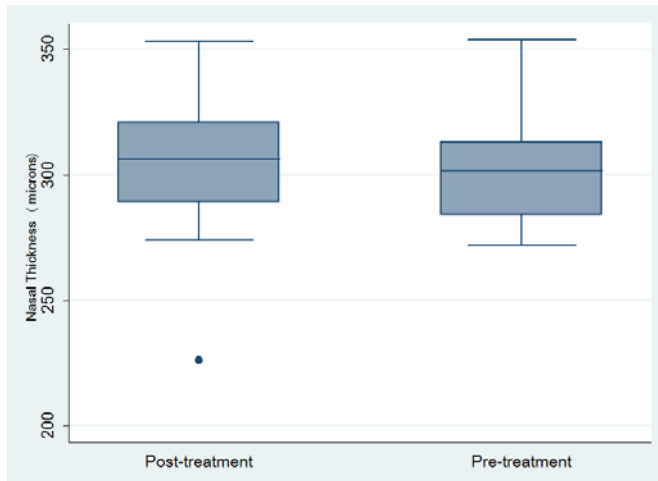
Figure 11.3: Box plots depicting the Nasal Thickness (µm) pre and post-treatment (paired t-test diff: 1.47, p=0.83, CI:-12.16 to 15.12). The outlier present post- treatment is from AB0208.
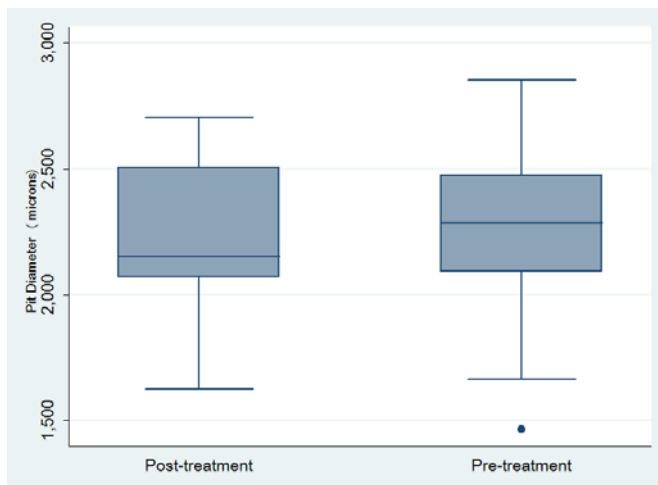
Figure 11.4: Box plots depicting the horizontal Pit Diameter (µm) pre and post-treatment (paired t-test, diff: -59.05, p=0.54, CI: -250.51 to 132.41). The outlier present pre-treatment is from AB0212; post- treatment although demonstrating the smallest measurement (1624µm) this case is not an outlier.

11.4.4 Foveal Topography in Amblyopic Children: Strabismus v Anisometropia

Twenty-four participants completed the longitudinal phase of the study. Of these, 5 had strabismus only, 12 had anisometropia only and 7 had combined strabismus and anisometropia (S/A). All the measured parameters were analysed using ANOVA to assess any differences that may be present due to the cause of the amblyopia i.e. strabismus and or anisometropia. The ANOVA of foveal topography by strabismus, anisometropia and S/A demonstrated no significant difference between the groups (Table 11.4). The closest parameters to producing a significant difference were temporal thickness, foveal thickness and the temporal foveal slope.

Table 11.4: Results of One-way ANOVA for the comparison of the pre-treatment measurements between the strabismic only, the anisometropic only and the combined strabismus and anisometropic amblyopic children (3 groups).

Foveal Parameters	Source of variation	Degrees of freedom	Sum of squares	Variance Ratio (F)	Probability
Foveal Thickness *Horizontal*	Between groups Within groups	2 21	2099.77 7428.88	2.97	**0.073**
Nasal Thickness *(max)*	Between groups Within groups	2 21	1748.05 8047.97	2.28	0.127
Temporal Thickness *(max)*	Between groups Within groups	2 21	2232.13 7022.25	3.34	**0.055**
Pit Depth *(max)*	Between groups Within groups	2 21	1447.52 13443.16	1.13	0.342
Nasal Base Area	Between groups Within groups	2 21	3794×10^{09} 2188×10^{10}	0.45	0.644
Nasal Triangle	Between groups Within groups	2 21	480185955 6.9657×10^{09}	0.72	0.497
Horizontal Pit Diam.	Between groups Within groups	2 21	350270 2389313	1.54	0.238
Top Width *Nasal*	Between groups Within groups	2 21	92925.68 625645.90	1.56	0.234
Foveal Slope *Nasal*	Between groups Within groups	2 21	46.57 189.33	2.58	0.099
Foveal Slope *Temporal*	Between groups Within groups	2 21	56.11 187.87	3.14	**0.064**

11.4.5 Foveal Topography in Amblyopic Children: Success v Failure

Twenty-four children completed the prescribed treatment regime. The occlusion diaries were collected and the total occlusion hours undertaken by each child summated. The amount of occlusion time varied from 40 to 497 hours (Table 11.1). Prior to analysis of the results, a successful outcome from the occlusion treatment was defined as ≥ 50% improvement and a final residual visual acuity in the amblyopic eye of ≤ 0.2 logMAR. This combination allows the improvement gained during treatment to be taken into account in the final outcome rather than solely the level of visual acuity achieved, which may not reflect the difference the treatment has made (see Chapter 3). Analysis of the pre-treatment parameters in children in the longitudinal phase of the study was examined in the light of treatment outcome of "success or "fail". Of the 24 children completing the treatment, 16 demonstrated a successful outcome from their treatment and were categorised as a "success", whereas 8 demonstrated a poor outcome and were categorised as a "fail". One child (AB0252) had poor compliance, regularly attending but only wearing the occlusion for a total of only 40 hours. His visual acuity improved during the period of occlusion but the final visual acuity obtained was only +0.3 LogMAR (6/12), and his treatment was therefore classed as a "fail".

On analysis of the data a number of differences between the amblyopic eyes with a successful outcome compared to the amblyopic eyes with a "failed" outcome were found to be significant. The foveal thickness parameter in the horizontal meridian was greater in the "failed" amblyopic eyes (188.11 ± 23.48 μm) compared to the

"success" amblyopic eyes (165.61 ± 14.07 µm), (two-tailed t-test of foveal thickness (fail v success): diff = 22.5µm, p = 0.007; CI: 6.68 to 38.32) (Figure 8.1). The foveal pit depth (max), was found to be shallower in the "failed" amblyopic eyes (97.17 ± 27.13 µm) compared to the "success" amblyopic eyes (127.20 ±18.13 µm); this was also found to be statistically significant (two-tail t-test of pit depth (fail v success): diff = -30.03µm, p = 0.004; CI: -49.25 to -10.80) (Figure 11.2). A summary of the results of the foveal parameters in the "success" or "failed" amblyopic eyes is provided in Table 11.5.

Table 11.5: Foveal topography measurements ± SD of the amblyopic and fellow eyes of children in the longitudinal phase deemed to have either had a "success" or a "fail" outcome. The results of paired t-tests between amblyopic and fellow eyes and 2 sided t-tests between the amblyopic "fail" and "success" eyes for each foveal parameter are shown.

Foveal Parameter	Child (fail) Amblyopic eye (mean ± SD) n=8	Child (fail) Fellow eye (mean ± SD) n=8	Amblyopic v Fellow Fail eyes Paired t-test	Child (success) Amblyopic eye (mean ± SD) n=16	Child (success) Fellow eye (mean ± SD) n=16	Amblyopic v Fellow Success eyes Paired t-test	Fail v Success Amblyopic eyes 2 sample t-test
Foveal Thickness *Horizontal*	188.11µm (23.48)	189.36µm (30.69)	p=0.82 CI: -32.78 to 26.59	165.61µm (14.07)	165.49µm (13.81)	p=0.84 CI: -9.32 to 11.40	**p= 0.007** CI: 6.68 to 38.32
Nasal Thickness *(max)*	294.38µm (23.36)	299.88µm (21.00)	p=0.90 CI: -24.23 to 21.50	303.61µm (19.19)	306.57µm (19.29)	p=0.48 CI: -19.50 to 9.44	p= 0.31 CI: -27.73 to 9.28
Temporal Thickness *(max)*	276.19µm (24.29)	279.84µm (16.22)	p=0.87 CI: -23.83 to 20.55	282.01µm (18.16)	282.66µm (17.93)	p=0.80 CI: -14.76 to 11.44	p= 0.52 CI: -24.05 to 12.42
Nasal Retinal Base Area	227991µm^2 (52309)	228580µm^2 (50830)	p=0.82 CI: -59332 to 48078	204554µm^2 (27669)	192916µm^2 (19012)	p=0.14 CI: -4772 to 33086	p=0.161 CI:-10075 to 56948
Nasal Retinal Triangle Area	63005µm^2 (13651)	66327µm^2 (18627)	p=0.99 CI: -18943 to 19232	85427µm^2 (15188)	82155µm^2 (14097)	p=0.78 CI: -9364 to 12440	**p= 0.002** CI: -35637 to -9206
Pit Depth (max) *Horizontal*	97.17µm (27.13)	100.49µm (31.09)	p=0.92 CI: -30.28 to 33.46	127.20µm (18.13)	129.13µm (23.26)	p=0.58 CI: -20.35 to 11.59	**p= 0.004** CI: -49.25 to -10.80
Pit Depth (mid) *Horizontal*	42.92µm (11.39)	44.89µm (14.83)	p=0.99 CI: -14.67 to 14.75	55.03µm (7.63)	54.93µm (9.08)	p=0.77 CI: -7.18 to 5.37	**p= 0.005** CI: -20.19 to -4.03
Pit Diameter (max) *Horizontal*	2246µm (447)	2228µm (437)	p=0.99 CI: -461 to 458	2287µm (298)	2182µm (209)	p=0.23 CI: -77.34 to 308.32	p= 0.79 CI:-357.82 to 274.9
Nasal Width *(max)*	1211µm (223.39)	1213µm (229.27)	p=0.89 CI: -250.6 to 219.04	1238µm (156)	1167µm (93.80)	p=0.11 CI: -18.9 to 173.91	p=0.728 CI:-189.25 to 134.4
Foveal Slope *Nasal*	11.07° (4.32)	10.56° (3.89)	p=0.73 CI: -3.6 to 5.04	13.07° (2.37)	13.18° (2.81)	p=0.82 CI: -2.16 to 1.73	p= 0.155 CI: -4.79 to 0.81
Foveal Slope *Temporal*	9.81° (4.40)	9.32° (4.39)	p=0.80 CI: -4.13 to 5.25	11.88° (2.39)	11.93°(2.58)	p=0.93 CI: -1.9 to 1.73	p= 0.145 CI: -4.92 to 0.77
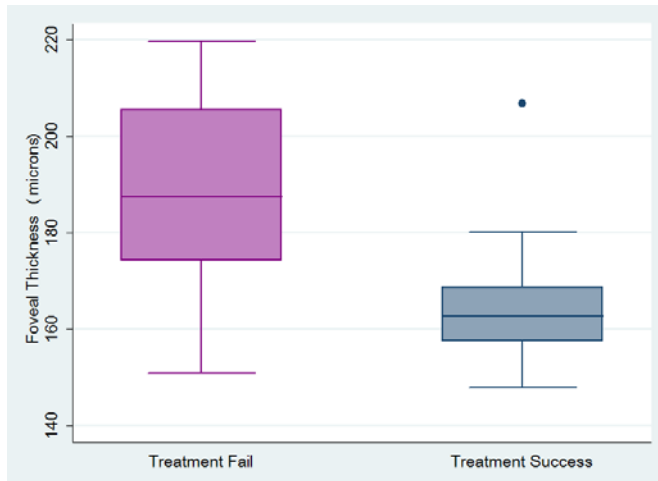
Figure 11.5: Box plots depicting the foveal thickness (horizontal)
measurements in microns (μm) of (2 sided t-test of "failed" v "success"
amblyopic eyes, diff: +22.50, p=0.007, CI: 6.68 to 38.32). One outlier is
present in the success eye data; the difference remains significant if
removed.
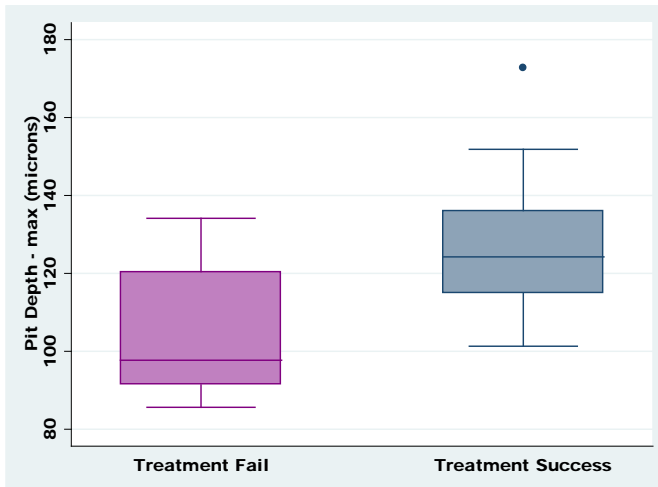
Figure 11.6: Box plots depicting the pit depth (horizontal) measurements in
microns (μm) of (2 sided t-test of "failed" v "success" amblyopic eyes, diff:
+30.03 p=0.004, CI: -49.25 to -10.80). One outlier is present in the success
eye data; the difference remains significant if removed.

11.4.6 Amblyopic Children: Comparison with Visual Normals

The amblyopic children in this cohort (success and fail categories both included) demonstrate increased foveal thickness and shallower pit depths; however, to establish the degree of difference it is necessary to compare this group with visually normal children. In order to evaluate the findings it was thought reasonable to compare the results directly to those of the visually normal children recruited to phase 1 of the study (Chapter7). The cohort of visually normal children recruited to phase 1 of the study were from the local schools visual screening programme of 4-5 year old children. The majority (85%) of children recruited into phase 2 of the study were also from the local school's vision screening programme conducted in the same year as recruitment and it is therefore valid to compare the two groups.

The data from each foveal parameter (horizontal meridian only) of the visually normal children was first compared directly to that of the phase 2 amblyopic children, 2 tail t-tests were carried out. Significant differences were found between the visually normal eyes and the amblyopic eyes in a number of parameters (Table 11.6). The foveal thickness parameter was greater in the amblyopic eyes (173.11± 20.35µm) compared to the visually normal eyes (165.09±14.78µm) (p = 0.044; CI: -15.82 to -0.21). The pit depth also demonstrated a significant difference being shallower in the amblyopic eyes (117.19±25.44µm) in comparison to the visually normal eyes (130.56±20.82µm) (p = 0.01; CI: 2.87 to 23.89). A summary of the results of the foveal parameters for the visually normal and amblyopic eyes is provided in Table 11.6.

Table 11.6: Foveal topography measurements ± SD of the visually normal eyes from phase1 (chapter 7) and the amblyopic eyes of children in the longitudinal phase. The results of t-tests for each foveal parameter are shown.

Foveal Parameter	Visually Normal Measurements (mean ± SD) (n=65)	Amblyopic (Pre-treat) Measurements (mean ± SD) (n=24)	Normal v Pre-treat Amblyopic Eyes Unpaired t-test
Foveal Thickness *Horizontal*	165.09µm (14.78)	173.11µm (20.35)	**p=0.044** CI: -15.82 to -0.21
Nasal Thickness *(max)*	307.38µm (16.36)	300.53µm (20.64)	p=0.11 CI: 1.50 to 15.20
Temporal Thickness *(max)*	283.93µm (16.68)	280.07µm (20.05)	p=0.36 CI: -4.510145 12.23
Nasal Retinal Base Area	179897µm^2 (24720)	212367µm^2 (38203)	**p<0.001** CI: -46191 to -18748
Nasal Retinal Triangle Area	77900µm^2 (16261)	77953µm^2 (17993)	p=0.99 CI: -7998 to 7893
Pit Depth (max) *Horizontal*	130.56µm (20.82)	117.19µm (25.44)	**p=0.01** CI: 2.87 to 23.88
Pit Diameter *Horizontal*	2068.46µm (269.12)	22743µm (345.13)	**p=0.004** CI: -343.73 to -67.29
Top Width *Nasal*	1092.87µm (140.56)	1229.27µm (176.75)	**P<0.001** CI: -208.07 to -64.72
Foveal Slope *Nasal*	13.76° (2.56)	12.40° (3.20)	**p=0.04** CI: 0.05 to 2.66
Foveal Slope *Temporal*	12.42° (2.51)	11.19° (3.25)	p=0.06 CI: -0.07 to 2.52

The data from the visually normal eyes were compared with the amblyopic eyes in relation to the classification of "success" or "fail". The results of the ANOVA with post-hoc analysis are presented in Table 11.7. Significant differences were found between the visually normal eyes and the amblyopic eyes in a number of parameters (Table 11.7). The foveal thickness parameter was greater in the "failed" amblyopic eyes (186.28±24.30µm) compared to both the "successful" amblyopic eyes (166.53± 4.86µm) and the visually normal eyes (165.09± 4.78µm).This difference was found to be significant (Table 11.7) (Figure 11.7).The pit depth also demonstrated a significant difference being shallower in the failed amblyopic eyes

(102.08± 8.27µm) in comparison to both the successful amblyopic eyes

(124.74±20.90µm) and the visually normal eyes (130.56±0.82µm) (Table 11.7)

(Figure 11.8).

Table 11.7: The results of a one-way ANOVA for the comparison of the pre-treatment measurements of the "fail"and "success" amblyopic eyes and the visually normal eyes (3 groups).

Foveal Parameters	Source of variation	Degrees of freedom	Sum of squares	Variance Ratio (F)	Probability	Post-hoc Significance	Post-hoc Non-Significance
Foveal Thickness *Horizontal*	Between groups Within groups	2 86	3206.37 21438.19	6.43	**0.003**	**Norm v Fail p=0.002** **Succ v Fail p=0.015**	Succ v Norm p=1.00
Nasal Thickness *(max)*	Between groups Within groups	2 86	871.21 26886	1.39	0.25		Succ v Norm p=0.72 Norm v Fail p=0.55 Succ v Fail p=1.00
Temporal Thickness *(max)*	Between groups Within groups	2 86	303.58 27028.5	0.48	0.62		Succ v Norm p=1.00 Norm v Fail p=1.00 Succ v Fail p=1.00
Pit Depth *(max)*	Between groups Within groups	2 86	5874.91 39895.15	6.33	**0.003**	**Norm v Fail p=0.002** **Succ v Fail p=0.05**	Succ v Norm p=1.00
Nasal Base Area	Between groups Within groups	2 86	1.9825e+10 7.1331e+10	11.95	**<0.001**	**Succ v Norm p=0.003** **Norm v Fail p<0.001**	Succ v Fail p=0.62
Nasal Triangle	Between groups Within groups	2 86	1.5817e+09 2.2787e+10	2.98	**0.05**	**Succ v Fail p=0.05**	Succ v Norm p=0.617 Norm v Fail p=0.193
Pit Diameter *Horizontal*	Between groups Within groups	2 86	767152 7348024	4.49	**0.014**	**Succ v Norm p=0.018**	Norm v Fail p=0.46 Succ v Fail p=1.00
Top Width *Nasal*	Between groups Within groups	2 86	338355 1970690	7.38	**0.001**	**Succ v Norm p=0.002**	Norm v Fail p=0.21 Succ v Fail p=1.00
Foveal Slope *Nasal*	Between groups Within groups	2 86	47.50 642.56	3.18	**0.05**	**Norm v Fail p=0.05**	Succ v Norm p=0.91 Succ v Fail p=0.47
Foveal Slope *Temporal*	Between groups Within groups	2 86	46.96 628.85	3.21	**0.05**	**Norm v Fail p=0.043**	Succ v Norm p=1.00 Succ v Fail p=0.30
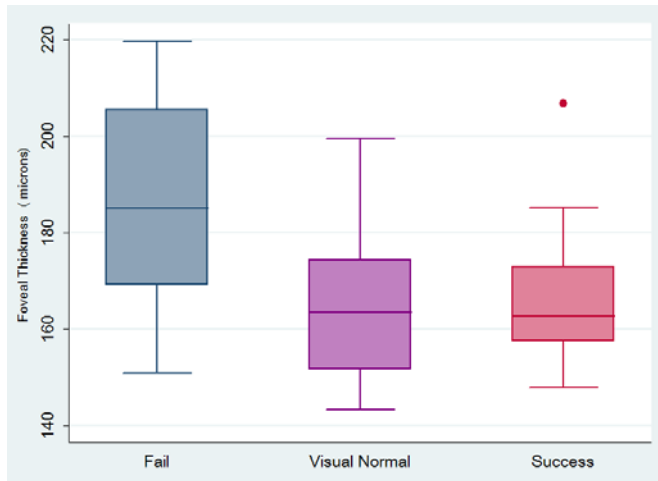
Figure 11.7: Box plots depicting the Foveal Thickness (µm) of "failed", "success" and visually normal eyes. Norm v Fail p=0.002, Succ v Fail p=0.015, Succ v Vis Norm p=1.00. One outlier (AB0184) is present in the success eye data.
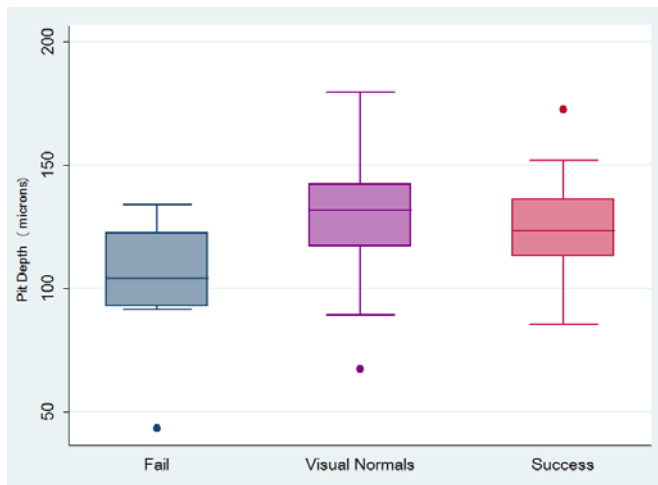
Figure 11.8: Box plots of Pit Depth (µm) in "failed", "success" and visually normal eyes Norm v Fail p=0.002, Succ v Fail p=0.05. One outlier is present in each data set (fail – AB0074, success – AB0225, normal – AB0165).

In order to assess if the biggest differences in foveal thickness and pit depth were related to either the final level of visual acuity achieved (logMAR) or the degree of improvement achieved (% improvement) the variables were compared. The foveal thickness was compared to the final level of visual acuity achieved and the individual measurements are identified as "success" or "fail" in terms of visual outcome (Figure 11.8). The visually normal eyes and the "success" eyes with the lowest logMAR scores are generally those with the lower foveal thickness measurements. A notable exception to this is AB0252 who demonstrates the lowest foveal thickness (150.83µm) but is in the "fail" group. However, this individual had poor compliance only completing 40 hours of occlusion, showing improvement during this time, but was classed as "fail" as the final visual acuity was only +0.3 logMAR. Also the individual AB0184 in the "success" group with the greatest foveal thickness (206.8µm) had complied with occlusion treatment for 452 hours with an improvement in the visual acuity from +0.675 to +0.2 logMAR. Pit depth was also compared to final level of visual acuity achieved, identifying individual measurements (Figure 11.9). The pit depth is generally shown to be shallower in those individuals who have "failed" the occlusion treatment, again there are some exceptions. The shallowest pit depth in the success group belongs to AB0185 (82.22µm) this individual has a strabismus and had 355 hours of occlusion achieving a final visual acuity of 0.125 logMAR. The shallowest pit depth (43.39µm) in the "failed" group belongs to AB0074; this individual also has the greatest foveal thickness (219.5µm). The individual with the deepest pit (134.13µm)

in the "failed" group is AB0212 who received the greatest number of occlusion

hours (497 hours) and improved from +0.425 to +0.25 logMAR.
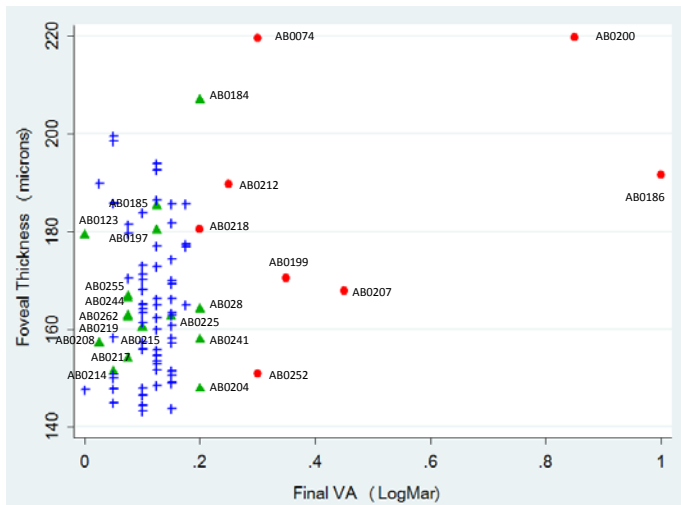
Figure 11.9: Scatter plot of Foveal Thickness (μm) v Final level of visual acuity (LogMar). + = visual normals △ = "successful" amblyopic eyes and ●= "failed" amblyopic eyes.
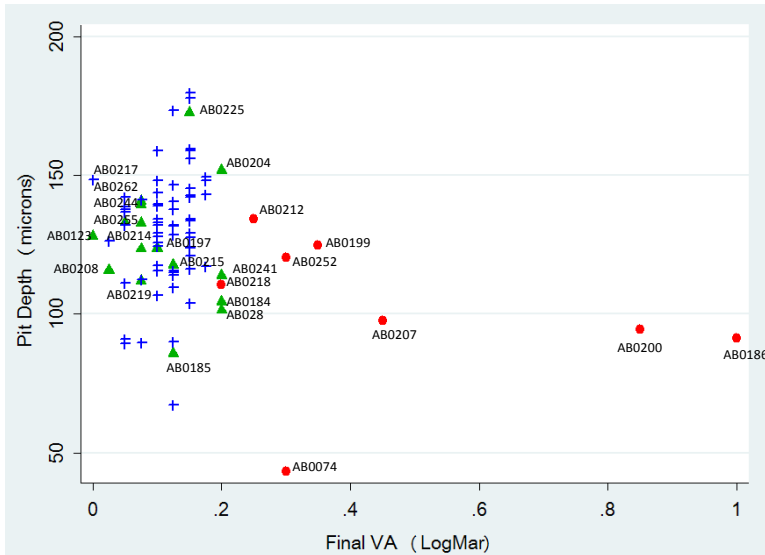
Figure 11.10: Scatter plot of Pit Depth (µm) v Final level of visual acuity(LogMar).
+ = visual normals, ▲ = "successful" amblyopic eyes and ● = "failed" amblyopic
eyes.

In order to assess the effect of treatment success on foveal thickness and pit depth

a linear regression analysis was carried out. The foveal thickness is shown to

decrease with increased improvement; the equation for the regression line is

(Figure 11.10):

$$y = -0.355x + 196.04. \quad R^{2=}0.23.$$

Conversely Pit depth increases with improvement; the equation for the regression

line is (Figure 11.11):

$y = 0.417x + 90.26.\ R^{2} = 0.20.$
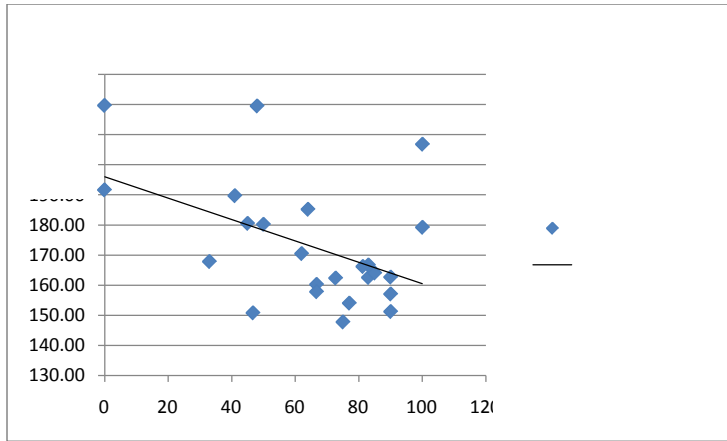
Figure 11.11: Linear regression of mean Foveal Thickness (µm) v % Improvement in amblyopic eyes. Equation for the regression line is $y = -0.355x + 196.04$. $R^{2}=0.23$
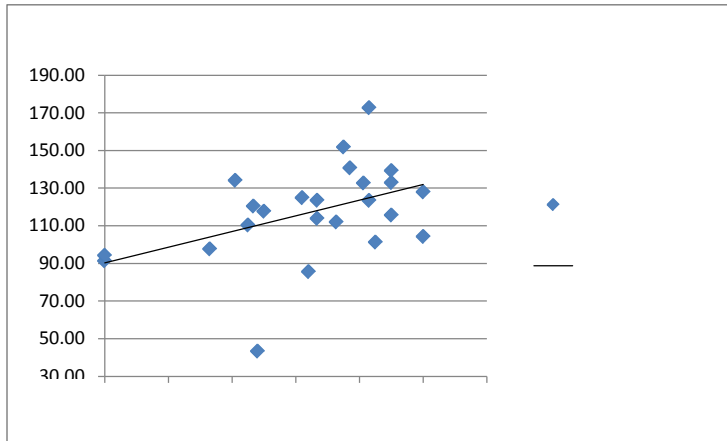
Figure 11.12: Linear regression of mean Pit Depth (µm) v % Improvement in amblyopic eyes. Equation for the regression line is $y =0.417x + 90.26$. $R^{2}=0.20$

11.5 Sensitivity and Specificity

The foveal thickness measurement appears to provide an indication of the likelihood of achieving a successful outcome from the occlusion treatment. This was chosen over pit depth as although they appear to be inversely related, the foveal thickness measurement is slightly more significant p= 0.15 R^2=0.022 as opposed to p=0.05 R^2=0.20. Also in practical terms the foveal thickness can be easily measured clinically using most time-domain and fourier domain OCT's, whereas pit depth is not routinely measured with either types of OCT. The data was examined in order to provide information on the efficacy of the procedure. The measures tested were, sensitivity, specificity, positive predictive value (PPV) and negative predictive value (NPV) (Table 11.8 and Table 11.9). Initially on visual inspection of the data the cut-off point between sensitivity and specificity appears to be approximately 180μm. The four measures were therefore initially calculated at a foveal thickness of 180μm.

Table 11.8: Determination of True Positive (TP), False Positive (FP), False Negative (FN) and True Negative status using the **180μm** cut-off point.

Criteria 180μm	+ve Failed Amblyope	-ve Failed Amblyope	Total
Test +ve	5 True +ve	3 False +ve	8
Test -ve	3 False -ve	13 True -ve	16
Total	8	16	24

Table 11.9: Diagnostic test efficacy estimates using foveal thickness **180μm** cut-off point

Criteria 180μm	Probability	Formula	%
Sensitivity	$P(T+|D+)$	$\dfrac{^nTP}{^nTP+^nFN}$	62.5
Specificity	$P(T-|D-)$	$\dfrac{^nTN}{^nFP+^nTN}$	81.25
PPV	$P(D+|T+)$	$\dfrac{nTP}{^nTP+^nFP}$	62.5
NPV	$P(D-|T-)$	$\dfrac{nTN}{^nTN+^nFN}$	81.25

Using the 180μm cut-off point produces a high level of specificity (81.25%) but the sensitivity is low (62.5%). In order to find the optimum point a receiver operator curve (ROC) was produced, analysing the cut-off points of sensitivity, the true positive rate, on the *y* axis, against the false positive rate (1- specificity), on the *x* axis. The optimal cut-off point is the point on the curve closest to the top left corner; this is the point which maximises the area under the curve (AUC) (Figure 11.13).
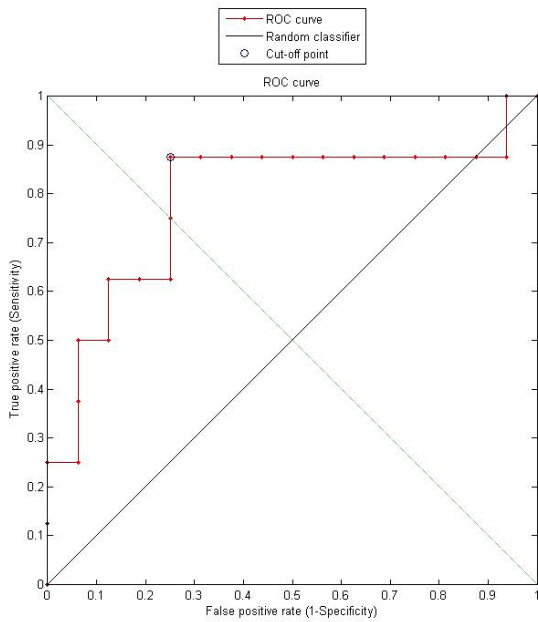
Figure 11.13: The Receiver operating characteristic **(**ROC) curve for the foveal thickness measurement where the cut-off point will be used to determine a "success" or "fail" criterion. Cut-off point for best Sensitivity and Specificity (circle in plot) = 166.22μm. The solid black diagonal line represents a diagnostic test that does not discriminate between those with and those without the condition.

Table 11.10: Results from the receiver operating characteristic (ROC) analysis with the cut-off point for best Sensitivity and Specificity identified as 166.22μm.

Area under curve (SE)	p- value	95% CI
0.789 (0.107)	0.0035	0.58 to 0.99

Table 11.11: Determination of True Positive (TP), False Positive (FP), False Negative (FN) and True Negative status using the **166.22μm** cut-off point

Criteria 166.22μm	+ve Failed Amblyope	-ve Failed Amblyope	Total
Test +ve	7 True +ve	5 False +ve	12
Test -ve	1 False -ve	11 True -ve	12
Total	8	16	24

Table 11.12: Diagnostic test efficacy estimates using foveal thickness **166.22μm** cut-off point.

Criteria 166.22μm	Probability	Formula	%
Sensitivity	$P(T+|D+)$	$\dfrac{^{n}TP}{^{n}TP + ^{n}FN}$	87.5
Specificity	$P(T-|D-)$	$\dfrac{^{n}TN}{^{n}FP + ^{n}TN}$	68.75
PPV	$P(D+|T+)$	$\dfrac{nTP}{^{n}TP + ^{n}FP}$	58.33
NPV	$P(D-|T-)$	$\dfrac{nTN}{^{n}TN + ^{n}FN}$	91.66

When the cut-off point is changed from 180μm to 166.22μm the area under the

operator characteristic (ROC) is 0.789 (Table 11.10) suggesting that this cut-off

point would produce a reasonable prediction of individuals who would fail

398

amblyopia treatment. The number classified as being a true positive, false positive, false negative and true negative changes in line with the cut-off point (Table 11.11) and the balance between sensitivity and specificity also changes (Table 11.12); with an increase in sensitivity from 62.5% to 87.5% and a decrease in specificity from 81.25% to 68.75%. The PPV also decreases slightly from 62.5% to 58.33%, whilst the NPV increases from 81.25% to 91.66%. This trade-off between sensitivity and specificity in identifying those amblyopes who are likely to fail treatment is not crucial to the treatment of amblyopia. The treatment is likely to be instigated whether "fail" or "success" is indicated by the foveal thickness measurement, therefore currently, although adding useful information to the treatment regime of amblyopia, providing an indication as to whether to continue treatment despite limited improvement, the use of OCT foveal thickness measurement as a routine test would not alter the treatment instigated.

11.6 Foveal Architecture in Amblyopic Eyes:Identification of Retinal layers

In this study using foveal metrics it is not possible to define and identify the exact retinal layers contributing towards the detected differences. However, with rapidly advancing imaging technology it is possible using commercially available high–resolution Fourier-domain OCT to produce images which delineate a greater number of retinal layers than was possible even with previous OCT devices (Marmor et al., 2008).The detailed identification of the retinal layers would help strengthen the findings of foveal structural change in some eyes that were diagnosed as amblyopic. In order to address this issue, further analysis of the

horizontal B-scans of the children forming the longitudinal phase of the study was

undertaken and the participants had their horizontal B-scans measured using the

inbuilt 3D-1000 Topcon measurement callipers. The technology used for this study,

3D-1000 Topcon OCT delineates 4 layers on each B-scan (Figure 11.3); layer 1 –

inner limiting membrane (ILM),

layer 2 – inner segment and outer segment of the photoreceptors (IS/OS),

layer 3 – retinal pigment epithelium (RPE) and layer 4 – border between RPE and

choroid. In order to further identify the retinal layers that influence the foveal

measurements, the internal calliper from the 3D-1000 Topcon was used to

manually measure the distance between layers 1 and 2 (ILM to IS/OS) and

between layers 2 and 3 (IS/OS to RPE) (Figure 11.14).
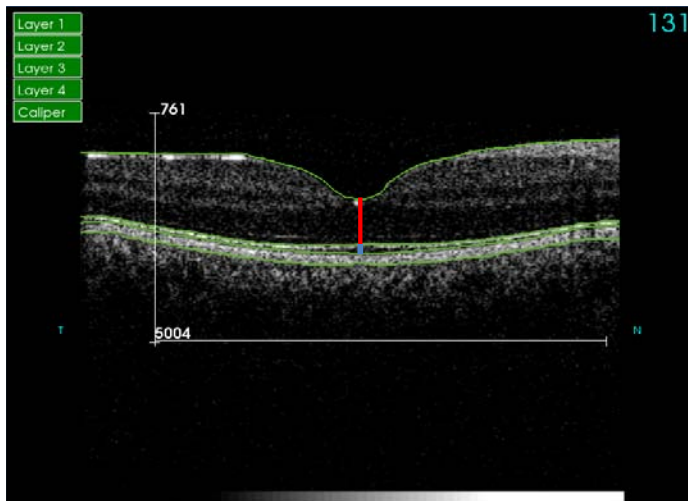
Figure 11.14: Foveal B-scan (horizontal) from 3D-1000 Topcon. The green lines delineate the layers identified by the OCT's software. Callipers are used (not depicted) to measure layers 1-2 (ILM to IS/OS) = red line and layers 2-3 (IS/OS to RPE) = blue line.

Table 11.13: Foveal calliper measurements ± SD of the amblyopic eyes of children in the longitudinal phase deemed to have either had "success" or "fail" treatment outcome. The results of 2 sided t-tests between the amblyopic eyes for each layer are shown. ILM=inner limiting membrane, IS/OS = junction between inner and outer segment of the photoreceptors, RPE= retinal pigment epithelium.

Foveal Parameter *calliper measurement*	All Children (mean ± SD) n=24	Fail (mean ± SD) n=8	Success (mean ± SD) n=16	2 sample t-test
Combined Thickness *(layer 1-3)*	183.63 µm (20.58)	196.63 µm (23.26)	177.13 µm (16.19)	**p= 0.025** CI: 2.68 to 36.32
ILM to IS/OS *(layer 1-2)*	144.83 µm (19.12)	156.88 µm (22.36)	138.81 µm (14.53)	**p= 0.025** CI: 2.43 to 33.69
IS/OS to RPE *(layer 2-3)*	38.79 µm (6.88)	39.75 µm (10.94)	38.31 µm (3.99)	p= 0.64 CI: -4.85 to 7.72

The foveal B scans for this longitudinal cohort were all well delineated and non of the boundaries were displaced, allowing accurate manual measurement of the thickness between layers with the internal callipers. The foveal structure when measured with the callipers (Table 11.13) shows a similar picture to that measured using the foveal metrics (Table 11.5). The total foveal thickness (layers 1-3) for all amblyopic children in the longitudinal phase ("success" and "fail") was found to be 183.63 ± 20.58 µm, the thickness of layer 1-2 was 144.83±19.2µm and layer 2 - 3 was found to be 38.79±6.88µm (Table 11.13). In "failed" amblyopic eyes the total foveal thickness (layers 1-3) is increased (196.63±23.26µm) in comparison to "successful" amblyopic eyes (177.13±16.19µm). On more detailed examination of the foveal structure a significant difference is shown in the thickness between the ILM and the IS/OS layer (layers 1 – 2) with the "failed group" demonstrating significantly thicker measurements (two-tailed t-test of layers 1-2 (fail v success): diff = 18.07µm, p = 0.025; CI: 2.43 to 33.69). Analysis of the thickness between the

IS/OS to RPE (layers 2-3) showed no significant difference in the thickness measurement between the "failed" amblyopic eyes (39.75±10.94µm) in comparison to "success" amblyopic eyes (38.31±3.99µm) (p= 0.64) (Table 11.13). Thus, where differences exist in foveal structure between amblyopic eyes these results suggest that they reflect differences in ILM to IS/OS change rather than IS/OS to RPE thickness differences.

The "failed" group of amblyopes consisted of 4 participants with strabismus only, 2 participants with anisometropia only and 2 participants with combined strabismus and anisometropia. However, the previously reported ANOVA (Table 11.4) showed that aetiology did not appear to influence foveal structure.

11.7 Discussion

11.7.1 Foveal Topography in Amblyopic Children: Pre-treatment

The foveal topography found in this group of amblyopes is similar in comparison to the group of amblyopic children described in phase 1 (Chapter 7, Table 13). In this longitudinal phase of the study the mean foveal thickness measurement was found to be 173.11±20.35µm compared to 176.63±23.29µm of the child amblyopes in phase 1. The pit depth in this group was however shallower 117.19±25.44µm compared to 130.04±22.87µm in the phase 1 group. This may be due to the presence of large amounts of individual variation due to sample size (phase 1 child amblyopes = 34 and phase 2 child amblyopes= 24). It may be an effect of the

occlusion treatment that phase 1 children had undergone prior to scanning or it may be an effect of development of the fovea with the children in phase 1 being older (mean age= 7.5 years) compared to those in phase 2 (mean age = 5.1years). The results in this longitudinal, second phase of the study have not demonstrated a significant difference between the retinal structure pre- and post-treatment (Table 11.3). It is, therefore, unlikely that the treatment itself is the cause of the difference. The mean age of the phase 1 child amblyopes is slightly older than the mean age of the children taking part in the longitudinal phase; it is therefore possible that the phase 2 children have not completed their physiological foveal development. However, in other studies changes to the foveal structure have been identified in amblyopes of differing ages (Huynh et al., 2009). The age of onset of the visual assault is unknown for either group of amblyopes. This is an important factor in assessing the degree of structural change, as the fovea will be at differing degrees of maturity prior to the onset of visual assault. The only method by which this information can be obtained is to carry out a longitudinal cohort study following children from birth to visual maturity to assess their visual development in comparison to structural development. There have been very few longitudinal studies assessing the development of visual function (Williams et al., 2008) and currently no longitudinal study exists of retinal structure.

11.7.1.2 Foveal Topography in Amblyopic Children: Inter-ocular symmetry

A high degree of inter-ocular symmetry was found in all the measured foveal parameters in the children participating in the longitudinal study. This has been a

consistent finding within all groups and in all phases of this research. Inter-ocular symmetry has previously been noted in studies of both the adult and child macula using OCT (Dubis et al., 2009; Huynh et al., 2007). Both studies however comment on large amounts of individual variation.

11.7.1.3 Foveal Topography in Amblyopic Children: Pre v Post-treatment

No significant differences were found between the pre-treatment and post-treatment measurements across any of the measured foveal parameters (Table 11.3). This is perhaps not surprising; firstly the high degree of intra-ocular symmetry has demonstrated that the change in foveal structure alone cannot be responsible for differences in the level of visual acuity between the eyes of amblyopes being affected. Secondly the anatomical development of the fovea is a slow protracted process taking place from birth to around 7 years (Provis et al., 1998; Provis and Hendrickson, 2008). It is therefore unlikely that any significant change would be evident in the relatively short period of time (maximum occlusion time= 497 hours taking approximately 6 months) during which the occlusion therapy was undertaken.

11.7.1.4 Foveal Topography in Amblyopic Children: Success v Failure

Factors contributing to the success of occlusion therapy are important to establish as it provides a benchmark for comparison between those children for whom treatment is likely to succeed and those in whom there is unlikely to be a positive

404

treatment response. The ability to identify these factors in advance of treatment would allow an informed decision to be made regarding the instigation of treatment and the length of time for which it should be continued. The analysis of the foveal parameters compared to the outcome of occlusion therapy, "success" or "fail", suggests that the contributing factors to a successful outcome are the foveal thickness and the pit depth. The foveal thickness, demonstrates increased thickness in those that have "failed" treatment (188.11±23.48µm as opposed to those with a "successful" outcome 165.61± 4.07µm, (p=0.007) (Table 11.5). The pit depth demonstrates a shallower measurement in those that have "failed" treatment (97.17±27.13µm) compared to those that have had a "successful" outcome (127.20±18.13µm), (p=0.004) (Table 11.5). On exploring the combined foveal thickness and pit depth, the overall combined measurement (293µm) of the foveal thickness (165µm) and pit depth (127µm) in "successful" amblyopes is close to the combined measurement (285µm) of foveal thickness (188µm) and pit depth (97µm) of the "failed" amblyopes (Figure 11.15). This finding is similar to that found previously in phase 1 (Figure 7.26) and is an indication that the reduction in pit depth is most likely related to the increased thickening of the fovea.
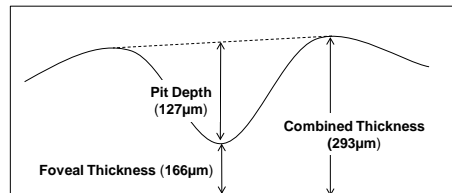
Foveal thickness to pit depth ratio in "successful" amblyopes
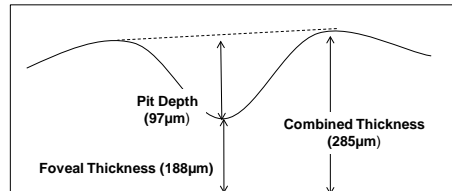
Foveal thickness to pit depth ratio in "failed" amblyopes

Figure 11.15: Schematic of combined foveal thickness and pit depth for amblyopic eyes in children in relation to the treatment outcome.

The foveal thickness measurement (188.11µm), although significantly increased in the "failed" amblyopes, is subject to a large amount of individual variation with wide confidence intervals (two-tail t-test of foveal thickness (fail v success): diff = 22.5µm, p = 0.007; CI: 6.68 to 38.32). This variation makes it difficult to suggest a definitive thickness measurement which would identify those children unlikely to achieve a successful result from their treatment. The information provided by the ROC curve indicates a foveal thickness measurement of 166.22µm would provide a good level of sensitivity (87.5%) and specificity (68.75%) (Table 11.12). Clinically it is unlikely that amblyopia treatment would be withheld on the basis of the foveal

406

thickness measurement, however, the measurement could provide information on which to base a clinical decision regarding the continuation of long term occlusion, preventing prolonged and unnecessary treatment. It could also influence the clinical decision to continue treatment in eyes where the foveal thickness is not increased and where improvement is limited by other factors such as compliance.

11.7.1.5 Foveal Architecture in Amblyopic Eyes:
 Identification of Retinal layers

The rapid development of imaging technology has produced commercially available OCT units that produce detailed measurements of multiple retinal layers (Charbel Issa et al., 2008; Marmor et al., 2008). The technology used for this study, 3D-1000 Topcon OCT delineates 4 layers (Figure 7.3). The internal calliper measurements used to manually measure the layers are not directly comparable with the foveal metric measurements which have been processed via Matlab, which were derived from curve fitting and which took magnification into account. However, the calliper measurements do provide an alternative method by which the foveal thickness can be examined. The results of the calliper measurements indicate that the increased foveal thickening in "failed" treatment is mainly contributed to by layers 1-2 and not by layer 2-3 thickening. This is the area between the inner limiting membrane (ILM) and the layer between the inner and outer segments of the photoreceptors (IS/OS). In this area between layers 1-2 lies the outer plexiform layer, the Henlé nerve fibre layer, the outer nuclear layer, the outer limiting membrane and the inner segments of the photoreceptors. In an

imaging study of foveal hypoplasia, widening in the central area of the outer nuclear layer and lengthening of the cone outer segments was noted (Marmor et al., 2008). This would equate to an increase of thickness in layers 1-2 and layers 2-3. In an imaging study of retinopathy of prematurity (ROP) using foveal metrics (Hammer et al., 2008), an increase in the overall foveal thickness was found. This was measured from the ILM to the RPE and the scan processed in a similar fashion to this study. In Hammer et al.'s study, a change in the photoreceptor thickness between the control group and the ROP group was not detected. The findings from this study indicate that the foveal thickness increase, particularly noted in "failed" amblyopes (Table 11.6) is located between the ILM and the IS/OS border in amblyopic eyes. In the few animal studies investigating monocular deprivation that have been carried out the increased thickness has been shown to be produced by lengthening of the outer segments of the photoreceptors (Liang et al., 1995). Further more detailed imaging is however, required to identify exactly which elements contribute to the increased foveal thickness in human amblyopia.

11.7.3 Results from Studies of Human Ocular Disease

Increased foveal thickness has been noted in other ocular conditions such as foveal hypoplasia, retinopathy of prematurity and oculocutaneous albinism (Charbel Issa et al., 2008; Hammer et al., 2008; Marmor et al., 2008). In a study of foveal architecture in a small number of subjects (n=4) with foveal hypoplasia, Marmor et al. described widening of the outer nuclear layer and lengthening of the cone outer segments in foveal hypoplasia using high-resolution Fourier-domain

OCT. The study provides evidence that the anatomical structure of the foveal pit is not directly related to the level of visual acuity with good levels of visual acuity being present despite the absence of the foveal pit.

In a study of a small number of adults (n=5) with resolved retinopathy of prematurity (ROP), (Hammer et al., 2008) found the foveal pit to be shallower in the ROP subjects and that the foveal thickness measurement in the subjects with ROP was increased in comparison to a control group (270μm v 190μm). The study also found the pit depth and volume measurements to be similar between the eyes except in one participant with ROP who had a dragged macula. No difference was found in the photoreceptor layer thickness between the ROP subjects and the control group. A study investigating foveal thickness and macular volume in oculocutaneous albinism (OCA) (Izquierdo et al., 2007) found subjects with OCA had thicker foveas (p=0.0009) and less macular volume (p=0.0022) than the general population, no indication of the inter-ocular asymmetry was given in this study.

These research findings demonstrate that some structural change appears to occur in different pathological and developmental disorders of vision. They present the structural characteristics of increased foveal thickness and elongation of the photoreceptors associated with lower levels of visual acuity. Taking these facts into account there is a strong suggestion that the structural changes are secondarily associated with the condition.

11.8 Conclusion

As suggested previously (Chapter 7), there are 3 ways in which these structural defects in amblyopia could be interpreted. The first is that the structural defects reflect the primary cause of the visual deficit, with strabismus and anisometropia occurring secondary to this, although possibly contributing to the visual deficit. This has now been discounted from the results of the study presented in Chapter 7 and is supported by the findings from this second phase of the study confirming the inter-ocular symmetry found previously. This leaves two options to consider:

1. The structural defects are caused by the visual insult, primarily produced by the presence of strabismus and/ or anisometropia.

2. The structural defects could be caused by some as yet unknown defect, other than strabismus and/ or anisometropia, perhaps at the level of the visual cortex, which leads to the secondary occurrence of strabismus, anisometropia and retinal structural defects.

The structural changes could be secondary changes produced by a developmental response to the visual insult produced by the presence of amblyogenic factors such as strabismus and/ or anisometropia (option 1above) leading to visual loss. This in turn could produce structural change. This option is supported by the results from this study, from the evidence of structural change found in other ocular

conditions and from animal studies in which deprivation generating amblyopia of one eye caused anatomical changes in both eyes (Chapter 7 Discussion).

It is also possible that the structural differences, along with strabismus and anisometropia are caused by some, as yet undiscovered defect, perhaps at the level of the visual cortex, however, further studies are required to either rule out or substantiate this second option. Thus the results of this study currently cannot distinguish between option 1 and option 2 but the evidence available to date currently favours option 1.

11.9 Papillomacular Bundle Structure in Amblyopic Children: Pre-treatment

11.9.1 Introduction

The methodology of the scan technique was the same as that described in Chapter 10. The paillomacular bundle parameters, P1, P2, S1, S2, I1 and I2 (Chapter 9 Figure 9.3 and Table 9.1) were measured. Of the twenty-four children who completed the occlusion treatment, scans were obtained from 22 children. Of these children, only 9 had pre-treatment scans for both the amblyopic and the fellow eye, and 13 had post-treatment scans for both the amblyopic and the fellow eye. Thus either pre- or post-treatment scans of the amblyopic and fellow eyes were obtained from all 22 children. The retinal nerve fibre layer (RNFL) thickness extending between the macula and the optic disc was imaged and measurements produced for the six sectors (Chapter 9 Table 9.1).

As with the papillomacular bundle in phase 1, this longitudinal cohort of amblyopic children was found to have a pattern of thicker RNFL in the superior and inferior sectors in comparison to the central sectors and the sectors closest to the optic disc (P1, S1 and I1) were thicker than the sectors closest to the macula (P2, S2, I2). A summary of the results of all the papillomacular RNFL measurements is provided in Table 11.14.

11.9.2 Inter-ocular Symmetry (IOS)

The pre-treatment amblyopic and fellow eyes were first examined in order to establish the degree of inter-ocular symmetry. As with the main amblyopic cohort investigated, a high degree of inter-ocular symmetry was found between the amblyopic eye and the fellow eye in all measured pre-treatment parameters (Table 11.14). A high degree of inter-ocular symmetry was also shown in the post-treatment scans (Table 11.15). Due to the small number of pre-treatment pairs of scans the symmetry between the amblyopic and the fellow post-treatment pairs were also combined and analysed (Table 11.16) to ensure that the small number of scans was not unduly influencing the results. As with the separate categories the combined data set also demonstrated a high degree of inter-ocular symmetry across all the RNFL sectors (Table 11.16).

> **Table 11.14 : Pre-treatment** Papillomacular RNFL measurements (µm) ± SD of the 6 sectors in amblyopic and fellow eyes of amblyopic children. Paired t-tests for each sector are shown. The parameters are defined previously in Chapter 9 (Figures 9.3 and Table 9.1).

Papillomacular Sector	Amblyopic Eye (mean ± SD) (n=9)	Fellow Eye (mean ± SD) (n=9)	Fellow v Amblyopic Eye Paired t-test
P1	63.89 µm (10.19)	55.56 µm (10.46)	p=0.06 CI: -16.99 to 0.33
P2	40.56 µm (19.62)	34.11 µm (8.19)	p=0.35 CI:-21.52 to 8.64
S1	73.11 µm (8.71)	71.11 µm (15.75)	p=0.54 CI:-9.15 to 5.15
S2	45.09 µm (7.36)	44.78 µm (9.99)	p=0.94 CI:-7.55 to 7.11
I1	85.89 µm (31.47)	62.89 µm (29.12)	p=0.20 CI:-60.61 to 14.61
I2	44.89 µm (13.04)	32.89 µm (16.65)	p=0.18 CI:-30.89 to 6.89

Table 11.15 : **Post-treatment** Papillomacular RNFL measurements (µm) ± SD of the 6 sectors in amblyopic and fellow eyes of amblyopic children. Paired t-tests for each sector are shown. The parameters are defined previously in Chapter 9 (Figures 9.3 and Table 9.1).

Papillomacular Sector	Amblyopic Eye (mean ± SD) (n=13)	Fellow Eye (mean ± SD) (n=13)	Fellow v Amblyopic Eye Paired t-test
P1	53.46 µm (15.53)	57.54 µm (10.46)	p=0.16 CI: -1.87 to 10.02
P2	35.62 µm (19.87)	41.46 µm (24.82)	p=0.44 CI:-10.07 to 21.76
S1	63.08 µm (8.19)	62.23 µm (10.26)	p=0.72 CI:-5.79 to 4.11
S2	40.54 µm (11.55)	39.69 µm (5.23)	p=0.77 CI:-6.87 to 5.19
I1	75.23 µm (31.47)	77.31 µm (17.83)	p=0.80 CI:-15.40 to 19.56
I2	37.31 µm (16.11)	45.54 µm (10.67)	p=0.13 CI:-2.66 to 19.12

Table 11.16: **Combined Pre & Post-treatment** papillomacular RNFL measurements (µm) ± SD of the 6 sectors in amblyopic and fellow eyes of amblyopic children. Paired t-tests for each sector are shown. The parameters are defined previously in Chapter 9 (Figures 9.3 and Table 9.1).

Papillomacular Sector	Amblyopic Eye (mean ± SD) (n=22)	Fellow Eye (mean ± SD) (n=22)	Fellow v Amblyopic Eye Paired t-test
P1	57.73 µm (14.31)	56.73 µm (11.01)	p=0.70 CI: -6.30 to 4.30
P2	37.64 µm (19.05)	38.45 µm (19.78)	p=0.88 CI:-9.87 to 11.51
S1	67.18 µm (12.60)	65.86 µm (13.21)	p=0.47 CI:-5.07 to 2.43
S2	42.36 µm (10.09)	41.77 µm (7.76)	p=0.78 CI:-4.84 to 3.65
I1	79.59 µm (32.71)	71.41 µm (23.61)	p=0.34 CI:-25.63 to 9.27
I2	40.41 µm (15.09)	40.36 µm (14.53)	p=0.99 CI:-10.15 to 10.06

Tables 11.14, 11.15 and 11.16 present the mean measurements of the two eyes in the longitudinal cohort of children. On analysis of the individual variation a wide range of differences was found with the inter-ocular difference in sector P1 ranging from -30µm to +18µm, with a mean individual difference of -1.0µm; in sector P2, the difference ranged from -19µm to +82µm, with a mean individual difference of 4.11µm. The 82µm difference in sector P2 was from subject AB0218 (Chapter 7, Table 7.1) a failed amblyope with combined strabismus and anisometropia, his difference appears to be an outlier. Sector I1 also demonstrated a wide range of inter-individual differences with a range of -94µm to 38µm with a mean individual difference of   -4.11µm. The outlier is from subject AB0186 another failed amblyope with combined strabismus and anisometropia. The individual inter-ocular differences for sectors P2 and I1 indicating these outliers are shown in Figure 11.16.
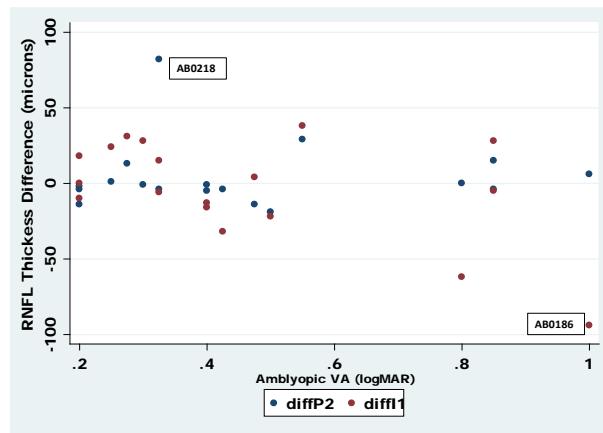
Figure 11.16: Scatter plot of individual difference measurements (μm) between the amblyopic eye and the fellow eye in sectors P2 ● and I1 ● in comparison to level of visual acuity in the amblyopic eye (logMAR).The outliers belong to AB0218 (82μm difference) a "failed" amblyope with combined strabismus and anisometropia (S/A) and 0.325 logMAR VA and AB0186 (94μm difference) a "failed" amblyope with also with S/A and 1.0 logMAR VA. A positive difference indicates that the fellow eye had a thicker (μm) measurement in comparison to the fellow eye, a negative difference indicates that the amblyopic eye has the thicker measurement.

11.9.3 Papillomacular Bundle in Amblyopic Children: Pre v Post-treatment

The pre-treatment and post-treatment measurements of all the papillomacular bundle sectors of children undergoing occlusion therapy were compared. 22 scans from the amblyopic eyes (9 pre-treatment and 13 post-treatment) were obtained. No significant differences were found between the pre-treatment and post-treatment measurements across any of the measured sectors. A summary of the results of the parameters in the amblyopic eyes both pre-treatment and post-treatment is provided in Table 11.17.

Table 11.17: Papillomacular bundle RNFL measurements ± SD **pre v post treatment** of the amblyopic eyes of children in the longitudinal phase. The results of paired t-tests between the amblyopic eye pre and post-treatment for each sector are shown. The parameters are defined previously in Chapter 10 (Figures 9.3 and Table 9.1).

Papillomacular Sector	Pre-Treatment Measurements (mean ± SD) (n=9)	Post-Treatment Measurements (mean ± SD) (n=13)	Fellow v Amblyopic Eye Paired t-test
P1	63.89 μm (10.19)	53.46 μm (15.53)	p=0.09 CI: -22.77 to 1.92
P2	40.56 μm (19.62)	35.62 μm (19.87)	p=0.56 CI:-22.45 to 12.56
S1	73.11 μm (8.71)	63.08 μm (8.19)	p=0.06 CI:-20.74 to 0.67
S2	45.00 μm (7.36)	40.54 μm (11.55)	p=0.32 CI:-13.59 to 4.66
I1	85.89 μm (31.47)	75.23 μm (31.47)	p=0.47 CI:-40.57 to 19.25
I2	44.89 μm (13.04)	37.31 μm (16.11)	p=0.26 CI:-21.12 to 5.95

11.9.4 Papillomacular Bundle in Amblyopic Children: Success v Failure

Twenty-four children completed the prescribed treatment regime. The occlusion diaries were collected and the total occlusion hours undertaken by each child summated. The amount of occlusion time varied from 40 to 497 hours (Table 11.1). Prior to analysis of the results, a successful outcome from the occlusion treatment was defined as ≥ 50% improvement and a final residual visual acuity in the amblyopic eye of ≤ 0.2 logMAR (see Chapter 2 and Chapter 8). Analysis of the pre-treatment parameters in children in the longitudinal phase of the study was examined in the light of treatment outcome of "success or "fail" (Chapter 11). In the

analysis of the papillomacular bundle, 9 children completed the treatment and had a scan which was obtained pre-treatment; 6 demonstrated a successful outcome from their treatment and were categorised as a "success", whereas 3 demonstrated a poor outcome and were categorised as a "fail". As there was only a small number of scans, the pre-treatment and post-treatment scans were combined to analyse "success" v "fail". On analysis of the combined data, no significant differences between the amblyopic eyes with a successful outcome compared to the amblyopic eyes with a "failed" outcome were found (Table 11.18).

Table 11.18 : Papillomacular bundle RNFL (µm) measurements ± SD of the amblyopic eyes of children in the longitudinal phase deemed to have either had a "success" or a "fail" treatment outcome. The results of 2 sample t-tests between the amblyopic eyes are shown.

Papillomacular Sector	Child (fail) Amblyopic eye (mean ± SD) n=9	Child (success) Amblyopic eye (mean ± SD) n=13	Fail v Success Amblyopic eyes 2 sample t-test
P1	56.78µm (12.47)	58.38µm (15.93)	p=0.80 CI: -14.86 to 11.64
P2	36.67µm (21.90)	38.30µm (17.72)	p=0.85 CI: -19.28 to 15.99
S1	66.22µm (11.95)	67.85µm (13.48)	p=0.77 CI: -13.28 to 10.03
S2	41.33µm (11.68)	43.08µm (11.68)	p=0.70 CI: -11.07 to 7.58
I1	73.11µm (34.75)	84.08µm (31.85)	p=0.45 CI: -40.85 to 18.92
I2	39.78µm (18.37)	40.85µm (13.16)	p=0.87 CI: -15.05 to 12.91

11.9.5 Papillomacular Bundle in Amblyopic Children:

Strabismus v Anisometropia

Of the 22 participants with scans of their amblyopic eye (12 pre-treatment and 18 post-treatment), pre-treatment scans included 1 individual with strabismus only, 7 with anisometropia only and 4 with combined strabismus and anisometropia (S/A). The post-treatment scans included 6 with strabismus only, 7 with anisometropia and 5 with S/A. All the measured sectors were analysed using ANOVA to assess any differences that may be present due to the presumed cause of the amblyopia i.e. strabismus and/ or anisometropia. As there was a greater number of post-treatment scans encompassing all diagnosis categories and no significant difference had been found between the pre- and post-treatment scans the post-treatment scans (n=18) were used in the ANOVA of papillomacular sectors analysed by diagnosis, (strabismus, anisometropia and S/A). The analysis demonstrated no significant difference between the groups (Table 11.19).

Table 11.19 : Results of One-way ANOVA for the comparison of the post-treatment papillomacular bundle RNFL (μm) measurements between the strabismic only, the anisometropic only and the combined strabismus and anisometropic amblyopic children (3 groups). 18 scans were included in this analysis.

Papillomacular Sector	Source of variation	Degrees of freedom	Sum of squares	Variance Ratio (F)	Probability
P1	Between groups Within groups	2 15	76.78 181.53	0.42	0.66
P2	Between groups Within groups	2 15	119.82 246.05	0.49	0.62
S1	Between groups Within groups	2 15	279.05 197.99	1.41	0.27
S2	Between groups Within groups	2 15	28.85 129.89	0.22	0.80
I1	Between groups Within groups	2 15	42.25 842.27	0.05	0.95
I2	Between groups Within groups	2 15	46.4 155.95	0.30	0.75

11.9.6 Amblyopic Children: Comparison with Visual Normals

The amblyopic children in this cohort (success and fail categories both included) have not demonstrated statistically significant differences in the papillomacular bundle thickness. However, in order to further evaluate the findings it was thought reasonable to compare the results directly to those of the visually normal children recruited to phase 1 of the study (Chapter 7). The cohort of visually normal children recruited to phase 1 of the study were from the local schools visual screening programme of 4-5 year old children. The majority (85%) of children recruited into

phase 2 of the study were also from the local school's vision screening programme conducted in the same year as recruitment and it is therefore valid to compare the two groups. The data from the visually normal children was compared directly to that of the phase 2 amblyopic children, 2 tailed t-tests were carried out. Significant differences were found between the visually normal eyes and the amblyopic eyes in two of the measured papillomacular bundle sectors, P2 and I1 (Table 11.20). The papillomacular bundle sectors were further explored to investigate sectors P2 and I1 (Figure 11.17 and Figure 11.18).

Table 11.20: Papillomacular bundle RNFL (μm) measurements ± SD of the visually normal eyes from phase1 (Chapter 7) and the amblyopic eyes (post-treatment) of children in the longitudinal phase. The results of t-tests for each sector are shown. The results in red are the statistical analysis with the outliers removed.

Papillomacular Sector	Child (phase 1) Visually normal eye (mean ± SD) n=50	Child (phase 2) Amblyopic eye (mean ± SD) n=18	Amblyopic (phase 2) v Visually normal eyes (phase 1) 2 sample t-test
P1	50.56μm (10.73)	54.44μm (13.00)	p=0.22 CI: -2.35 to 10.12
P2	27.72μm (8.69)	36.44μm (15.21) 32.33μm (10.20)	**p=0.004** CI: 2.82 to 14.62 p=0.07 CI:-0.38 to 9.60
S1	65.67μm (14.40)	63.26μm (9.84)	p=0.44 CI: -3.74 to 8.55
S2	38.00μm (8.79)	42.33μm (10.86)	p=0.10 CI: -0.81 to 9.48
I1	62.14μm (19.44)	75.17μm (27.35) 68.13μm (18.16)	**p=0.03** CI: 1.10 to 24.96 p=0.29 CI:-5.28 to 17.27
I2	33.84μm (12.55)	38.33μm (11.96)	p=0.19 CI: -2.31 to 11.30
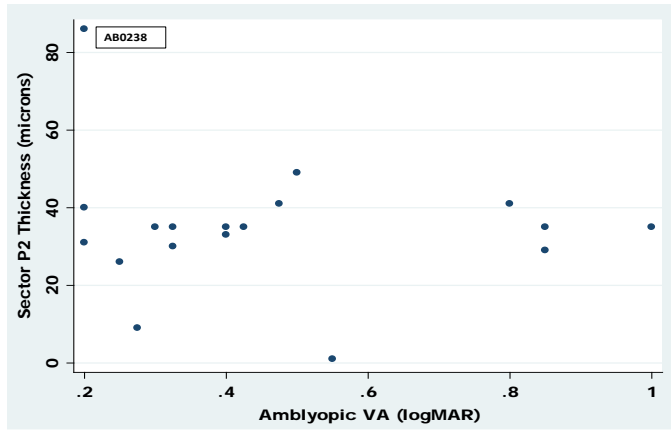
Figure 11.17: Scatter plot of individual P2 sector measurements in comparison to level of visual acuity (logMAR) of the amblyopic eyes of children pre-treatment. The one outlier belongs to AB0238 a "failed" amblyope with anisometropia and 0.2 logMAR VA.
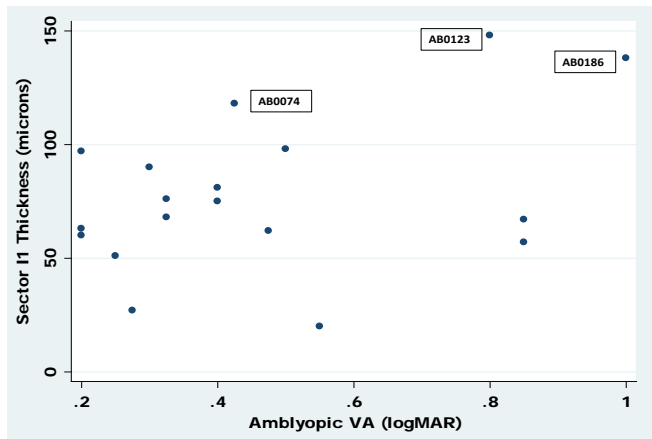
Figure 11.18: Scatter plot of individual I1 sector measurements in comparison to level of visual acuity (logMAR) of the amblyopic eyes of children pre-treatment. The outlier s belong to AB0074, AB0186 "failed" amblyopes with strabismus and 0.575 and 1.00 logMAR VA, respectively, and AB0123 a "successful" amblyope with 0.8 logMAR VA.

11.10 Discussion

11.10.1 Papillomacular bundle structure in Amblyopic Children:
Pre-treatment

In this longitudinal phase of the study the papillomacular RNFL thickness measurements (Chapter 9, Figure 9.3 and Table 9.1) produced a similar pattern to that found in phase 1 of the study, with thicker superior and inferior sectors in comparison to the central sectors, and the sectors closest to the optic disc (P1, S1 and I1) being thicker than the sectors closest to the macula (P2, S2, I2).

11.10.2 Papillomacular bundle in Amblyopic Children:
Inter-ocular symmetry

A high degree of inter-ocular symmetry was found in all measured papillomacular sectors (both pre-treatment and post-treatment), in the children participating in the longitudinal study. This has been a consistent finding within all cohorts and in all phases of this research. However, when examining the inter-ocular differences in detail (Figure 11.16) it can be seen that there are outliers within this cohort, which will affect the findings. The outliers demonstrating the greatest differences are both "failed" amblyopes one with +0.325 logMAR (AB0218) visual acuity in the amblyopic eye and one with +1.0 logMAR (AB0186) visual acuity. This variation is likely to have occurred due to poor fixation in the amblyopic eye rather than caused by the amblyopia itself as the direction of the difference varies vastly and is positive in the case of AB0218 and negative for AB0186.

424

In comparison to the visually normal children from phase 1, statistically significant differences were found, with the amblyopic eyes demonstrating increased thickness in sectors P2 and I1 (Table 11.20). However, on further detailed examination of the data it is clear that one outlier in sector P2 , AB0238; a "failed" amblyope with anisometropic amblyopia and +0.2 logMAR visual acuity, and 3 outliers in sector I1, 2 failed amblyopes (AB0186 and AB0074) and one successfully treated anisometropic amblyope (AB0123) with +0.8 logMAR visual acuity, are responsible for the increase in the mean measurement for the amblyopic group. On running the 2 sample t-tests again without the outliers no significant difference is found (sector P2, $p=0.07$; sector I1, $p=0.29$) (Table 11. 20). This further statistical analysis is an indication that the measurements are subject to significant individual variation.

11.10.3 Papillomacular bundle structure in Amblyopic Children: Pre v Post-treatment

No difference between the retinal structure pre- and post-treatment was found in this longitudinal phase of the study (Table 11.17); there were no significant differences between the eyes or indeed between pre-treatment and post-treatment visits in children who underwent occlusion therapy. The results indicate that there is no significant change in papillomacular bundle structure at any sector during treatment for amblyopia. As well as suggesting that the two eyes of amblyopes are not structurally different, these results suggest however occlusion therapy works it is not significantly altering the papillomacular thickness.

11.10.4 Papillomacular bundle structure in Amblyopic Children: Success v Failure

In the analysis of the measured papillomacular bundle sectors no contributing factors were identified that could be linked to the success or fail status achieved after completion of occlusion therapy.

11.11 Conclusion

Structural measurements of the papillomacular bundle have not been published previously, either for children or adults, however a pattern of thicker superior and inferior sectors in comparison to the central sectors and the sectors closest to the optic disc (P1, S1 and I1) being thicker than the sectors closest to the macula (P2, S2, I2) has been constant in both phase 1 and the longitudinal phase 2 of this study (Chapter 9, Figure 9.7).

Investigation of the papillomacular bundle in this longitudinal phase of the study has found no significant difference in structure in the presence of amblyopia. A high degree of inter-ocular symmetry in the children participating in the longitudinal study was found, this is consistent with all the retinal areas measured (Chapters 7 to 11). The degree of symmetry does, however, vary considerably between individuals producing outliers in measures which must be taken into account when analysing data. This variability may have been exacerbated in this phase of the study due to the ability of these young children (age 4-5 years) to maintain an off-

426

centre fixation position during the scan, compounded by the lower level of visual acuity in the amblyopic eye.

11.12 Peripapillary RNFL Structure in Amblyopic Children: Pre-treatment

11.12.1 Introduction

The methodology of the scan technique was the same as that described in Chapter 8. Optic disc parameters (Figures 8.1, 8.2, 8.3, 8.4) were measured in six sectors; nasal, upper nasal, upper temporal, temporal, lower temporal and lower nasal (Figure 8.3). Of the twenty-four children who completed the occlusion treatment optic disc scans were obtained from 20 children, of these children 8 had pre-treatment scans for both the amblyopic and the fellow eye, and 9 had post-treatment scans for both the amblyopic and the fellow eye. Pre- and post-treatment scans of the amblyopic eyes were obtained from 14 children; the low number of complete sets of scans was mainly due to fixation difficulties. In order to scan the disc the observer has to maintain an eccentric viewing position, obtained by fixing a small target positioned off centre. The children in this cohort, aged between 4-5 years found this eye position very difficult to maintain, leading to eye movement and blink. In this longitudinal phase of the study the commonly described pattern of thicker superior and inferior sectors compared to the nasal and temporal sectors

427

was demonstrated. A summary of the results of the RNFL parameters in pre-treatment amblyopes is provided in Table 11.21.

11.12.2 Inter-ocular Symmetry (IOS)

The pre-treatment amblyopic and fellow eyes were first examined in order to establish the degree of inter-ocular symmetry. As with the main amblyopic cohort investigated, a high degree of inter-ocular symmetry was found between the amblyopic eye and the fellow eye in all measured parameters (Table 11.21). Due to the small number of pre-treatment pairs of scans the symmetry between the amblyopic and the fellow post-treatment pairs were also analysed (Table 11.22). A high degree of inter-ocular symmetry was also shown in the post-treatment scans. For this reason both groups were combined to ensure that the small number of scans was not unduly influencing the results (Table 11.23). As with the separate categories the combined data set also demonstrated a high degree of inter-ocular symmetry across all the RNFL sectors (Table 11.23).

Disc Sector (n=8)	Child Amblyopic Eye (mean ± SD)	Child Fellow Eye (mean ± SD)	Fellow v Amblyopic Eye Paired t-test
Nasal	75.13µm (12.44)	77.86µm (4.64)	p=0.44 CI:-5.14 to 10.64
Upper Nasal	108.25µm (20.74)	109.25µm (19.33)	p=0.87 CI:-12.9 to 14.90
Upper Temporal	108.25µm (15.53)	112.13µm (19.66)	p=0.62 CI:-13.88 to 21.63
Temporal	63.38µm (12.67)	63.81µm (6.0)	p=0.93 CI:-10.6 to 9.85
Lower Temporal	112.75µm (24.09)	128.5µm (17.15)	p=0.13 CI:-6.17 to 37.67
Lower Nasal	119µm (16.56)	120.5µm (22.20)	p=0.89 CI:-24.28 to 27.28

Table 11.21 : Pre-treatment RNFL measurements ± SD of both eyes in amblyopic children in the longitudinal phase. The results of paired t-tests between the amblyopic eye and fellow eye for each peripapillary sector are shown. The RNFL sectors are defined previously in Chapter 8 (Figures 8.1, 8.2, 8.3, 8.4).

Disc Sector (n=9)	Child Amblyopic Eye (mean ± SD)	Child Fellow Eye (mean ± SD)	Fellow v Amblyopic Eye Paired t-test
Nasal	80µm (12.18)	73.56µm (12.33)	p=0.14 CI:-15.73 to 2.84
Upper Nasal	115.67µm (26.38)	115.78µm (20.70)	p=0.98 CI:-13.17 to 13.39
Upper Temporal	105.78µm (20.39)	113.67µm (16.05)	p=0.25 CI:-6.71 to 22.49
Temporal	60.11µm (15.38)	65µm (10.54)	p=0.06 CI:-0.17 to 9.6
Lower Temporal	115.56µm (44.47)	116.11µm (16.10)	p=0.97 CI:-29.94 to 31.05
Lower Nasal	112.22µm (35.56)	106.89µm (19.94)	p=0.56 CI:-25.52 to 14.86

Table 11.22 : Post-treatment RNFL measurements ± SD of both eyes in amblyopic children in the longitudinal phase. The results of paired t-tests between the amblyopic eye and fellow eye for each peripapillary sector are shown. The RNFL sectors are defined previously in Chapter 8 (Figures 8.1, 8.2, 8.3, 8.4).

Disc Sector (n=17)	Child Amblyopic Eye (mean ± SD)	Child Fellow Eye (mean ± SD)	Fellow v Amblyopic Eye Paired t-test
Nasal	77.70µm (12.17)	75.59µm (9.51)	p=0.46 CI:-8.07 to 3.84
Upper Nasal	112.18µm (23.47)	112.70µm (19.72)	p=0.89 CI:-7.93 to 8.99
Upper Temporal	106.94µm (17.75)	112.94µm (17.28)	p=0.22 CI:-4.05 to 16.05
Temporal	61.65µm (13.83)	64.06µm (8.5)	p=0.31 CI:-2.51 to 7.33
Lower Temporal	114.23µm (35.28)	121.94µm (17.29)	p=0.36 CI:-9.72 to 25.13
Lower Nasal	115µm (27.65)	113.29µm (21.53)	p=0.76 CI:-16.41 to 12.18

Table 11.23 : RNFL measurements ± SD of amblyopic and their fellow eyes in children in the longitudinal phase, pre- and post-treatment scans are included in the analysis. The results of paired t-tests between the amblyopic eye and fellow eye for each peripapillary sector are shown. The RNFL sectors are defined previously in Chapter 8 (Figures 8.1, 8.2, 8.3, 8.4).

11.12.3 Peripapillary RNFL in Amblyopic Children: Pre v Post-treatment

The pre-treatment and post-treatment measurements of all the RNFL sectors of children undergoing occlusion therapy were compared. Only 28 scans (14 pre-treatment and 14 post-treatment) were obtained from the 24 child amblyopes in the longitudinal cohort. No significant differences were found between the pre-treatment and post-treatment measurements across any of the measured RNFL sectors. A summary of the results of the parameters in the amblyopic eyes both pre-treatment and post-treatment is provided in Table 11.24.

Table 11.24: RNFL measurements ± SD pre and post treatment of the amblyopic eyes of children in the longitudinal phase. The results of paired t-tests between the amblyopic eye pre and post-treatment for each sector are shown. The RNFL parameters are defined previously in Chapter 8 (Figures 8.1, 8.2, 8.3, 8.4).

Disc Sector (n=14)	Child (Pre-Treat) Measurements (mean ± SD)	Child (Post-Treat) Measurements (mean ± SD)	Post v Pre Amblyopic Eyes Paired t-test
Nasal	78µm (16.62)	81.85µm (19.78)	p=0.51 CI:-16.13 to 8.42
Upper Nasal	94.29µm (28.14)	103.64µm (25.85)	p=0.44 CI:-34.54 to 15.83
Upper Temporal	100.86µm (23.81)	114.43µm (16.91)	p=0.06 CI:-27.93 to 0.79
Temporal	61.86µm (17.96)	65.36µm (16.22)	p=0.46 CI:-13.41 to 6.41
Lower Temporal	99.5µm (28.04)	108.71µm (23.70)	p=0.37 CI:-30.83 to 12.40
Lower Nasal	118.14µm (36.23)	123 µm (33.21)	p=0.75 CI:-37.45 to 27.74

11.12.4 RNFL in Amblyopic Children: Success v Failure

As previously described 24 children completed the prescribed treatment regime.
Analysis of the pre-treatment parameters in children in the longitudinal phase of the
study was examined in the light of treatment outcome of "success or "fail". In the
analysis of the RNFL thickness of the peripapillary area around the optic disc 13
children completed the treatment and had an optic disc scan which was obtained
pre-treatment, 9 demonstrated a successful outcome from their treatment and were
categorised as a "success", whereas 4 demonstrated a poor outcome and were
categorised as a "fail". On analysis of the data no significant differences between
the amblyopic eyes with a successful outcome compared to the amblyopic eyes
with a "failed" outcome were found (Table 11.25).

> **Table 11.25:** RNFL (µm) measurements ± SD pre-treatment of the amblyopic
> eyes of children in the longitudinal phase deemed to have either had a "success" or
> a "fail" outcome. The results of 2 sample t-tests between the amblyopic eyes are shown.

Disc Sector (n=13)	Child (fail) Amblyopic eye (mean ± SD) n=4	Child (success) Amblyopic eye (mean ± SD) n=9	Fail v Success Amblyopic eyes 2 sample t-test
Nasal	69µm (12.96)	82.22µm (15.53)	p=0.17 CI: -32.89 to 6.45
Upper Nasal	113.75µm (22.19)	96.11µm (29.88)	p=0.32 CI: -19 to 54.67

Upper Temporal	101.5µm (21.02)	99.56µm (33.94)	p=0.92 CI: -39 to 42.89	
Temporal	66.25µm (8.73)	69.33µm (10.98)	p=0.47 CI: -24.12 to 11.96	
Lower Temporal	116.75µm (39.39)	119.56µm (19.99)	p=0.86 CI: -38.14 to 32.53	
Lower Nasal	116.25µm (18.48)	123.33µm (33.36)	p=0.70 CI: -46.82 to 32.65	

11.12.5 RNFL in Amblyopic Children: Strabismus v Anisometropia

Of the 20 participants with scans of their amblyopic eye (13 pre-treatment and 7 post-treatment), 5 had strabismus only, 9 had anisometropia only and 6 had combined strabismus and anisometropia (S/A). All the measured RNFL sectors were analysed using ANOVA to assess any differences that may be due to the present cause of the amblyopia i.e. strabismus and/ or anisometropia. The ANOVA of RNFL thickness analysed by diagnosis, (strabismus, anisometropia and S/A) demonstrated no significant difference between the groups (Table 11.26).

Table 11.26: Results of One-way ANOVA for the comparison of the pre-treatment RNFL (µm) measurements between the strabismic only, the anisometropic only and the combined strabismus and anisometropic amblyopic children (3 groups) 20 scans are included for analysis 13 pre-treatment and 7 post-treatment.

Disc Sector (n=20)	Source of variation	Degrees of freedom	Sum of squares	Variance Ratio (F)	Probability

Nasal	Between groups Within groups	2 17	470.76 3344.03	1.20	0.33
Upper Nasal	Between groups Within groups	2 17	30.64 16463.56	0.02	0.98
Upper Temporal	Between groups Within groups	2 17	524.28 11696.52	0.38	0.69
Temporal	Between groups Within groups	2 17	49.94 3367.86	0.13	0.88
Lower Temporal	Between groups Within groups	2 17	430.64 22242.36	0.16	0.85
Lower Nasal	Between groups Within groups	2 17	560.69 15602.26	0.31	0.74

11.12.6 Amblyopic Children: Comparison with Visual Normals

The amblyopic children in this cohort (success and fail categories both included) have not demonstrated any significant differences in RNFL thickness between those who achieve a successful outcome, relative to those who don't. Again, in order to further evaluate the findings it was thought reasonable to compare the results directly to those of the visually normal children recruited to phase 1 of the study (Chapter 7). The data from the visually normal children was compared directly to those of the phase 2 amblyopic children, 2 tail t-tests were carried out. No significant differences were found between the visually normal eyes and the amblyopic eyes in any of the RNFL sectors (Table 11.27). A summary of the results of the RNFL thickness measurements for the visually normal and amblyopic eyes is provided in Table 11.27.

Table 11.27: RNFL (µm) measurements ± SD of the visually normal eyes from phase1 (chapter 7) and the amblyopic eyes of children in the longitudinal phase. The results of t-tests for each RNFL sector are shown.

Disc Sector	Child (phase 1) Visually normal eye (mean ± SD) n=39	Child (phase 2) Amblyopic eye (mean ± SD) n=20	2 sample t-test
Nasal	74.31µm (11.01)	77.6µm (14.17)	p=0.33 CI: -3.4 to 9.98
Upper Nasal	109.67µm (25.30)	107.3µm (29.46)	p=0.75 CI: -17.1 to 12.37
Upper Temporal	106.67µm (24.44)	103.6µm (25.36)	p=0.65 CI: -16.69 to 10.56
Temporal	61.10µm (8.92)	64.1µm (13.41)	p=0.31 CI: -2.86 to 8.85
Lower Temporal	108.33µm (27.37)	115.5µm (34.54)	p=0.39 CI: -9.33 to 23.66
Lower Nasal	116.25µm (18.48)	123.33µm (33.36)	p=0.70 CI: -46.82 to 32.65

RNFL rhickness (microns)

0   50   100   150   200

Figure 11.19: Box plots of RNFL (µm) thickness measurements for all 6 sectors around the optic disc in Phase 2 amblyopic children and Phase 1 visually normal children. Dots indicate outliers.

11.13 Discussion

11.13.1 RNFL thickness in Amblyopic Children: Pre-treatment

In this longitudinal phase of the study the RNFL thickness measurements (Table 11.21) produced the commonly described thickness pattern of thicker superior and inferior quadrants in comparison to the nasal and temporal quadrants. The RNFL thickness found in this cohort of amblyopic children is similar in comparison to the group of amblyopic children described in phase 1 (Chapter 8, Table 8.13) except for the nasal sector. The nasal sector in this cohort (77.6µm) was closer to the nasal sector found in the visually normal group of children (74.31µm) in the phase 1 group. This finding is likely to be due to the presence of large amounts of individual variation in RNFL thickness. In other studies measuring RNFL thickness where differences have been found, these have not always been significant (Repka et al., 2009b; Yen et al., 2004). The two studies that have found significant differences (Yen et al., 2004; Yoon et al., 2005), reported differences between

retinal nerve fibre layer (RNFL) thickness in the amblyopic eye in comparison to the fellow eye in anisometropic amblyopes with the amblyopic eyes demonstrating increased RNFL thickness. This was not a finding in this study, with considerable inter-ocular symmetry demonstrated with all cohorts, visual normals, amblyopes, adults or children.

11.13.2 RNFL thickness in Amblyopic Children: Inter-ocular symmetry

A high degree of inter-ocular symmetry was found in all measured RNFL sectors in the peripapillary disc area in the children participating in the longitudinal study. This has been a consistent finding within all cohorts and in all phases of this research.

11.13.3 RNFL thickness in Amblyopic Children: Pre v Post-treatment

The results from this longitudinal, second phase of the study have not demonstrated a significant difference between the retinal structure pre- and post-treatment (Table 11.24). The investigation of the peripapillary RNFL thickness in this longitudinal study has not found any significant differences either between the eyes or indeed between pre-treatment and post-treatment visits in children having occlusion therapy. Although other studies have been carried out on children(Huynh et al., 2009), the age of this cohort undergoing treatment (4-5years) is significantly younger than previous studies; this has reduced the number and quality of scans

collected for analysis. That said, this study is the only prospective study of retinal structure carried out during treatment for amblyopia. The results indicate that there is no significant change in RNFL thickness in any sector during treatment for amblyopia.

11.13.4 RNFL thickness in Amblyopic Children: Success v Failure

In the analysis of the RNFL sectors in the peripapillary disc area around the disc no contributing factors were found to be linked to the success or fail status achieved after completion of occlusion therapy.

11.14 Conclusion

A high degree of inter-ocular symmetry in the children participating in the longitudinal study was found, consistent with all the retinal areas measured (Chapters 7 to 11). The investigation of the peripapillary RNFL thickness has found no significant difference in thickness in the presence of amblyopia either in phase 1 or in the longitudinal phase 2. The evidence from this study therefore suggests amblyopia, or the conditions thought to cause amblyopia, are not associated with a change in peripapillary RNFL thickness.

11.15 Optic Disc Parameters in Amblyopic Children: Pre-treatment

11.16 Introduction

The methodology of image measurement was the same as that described in Chapter 10. Optic disc parameters (Figure 10.2, 10.3 and Table 10.1) were measured. Of the twenty-four children who completed the occlusion treatment optic disc images were obtained from 22 children, of these children 15 had pre-treatment scans for both the amblyopic and the fellow eye, and 7 had post-treatment scans for both the amblyopic and the fellow eye. Two images one pre and one post treatment did not have a visible fovea preventing the disc to fovea distance and the disc-fovea to disc diameter ratio (DF:DD) to be measured. A summary of the results of all the disc parameters in the pre-treatment amblyopes is provided in

Table 11.28. Pre-treatment the typical oval pattern of an increased vertical

diameter compared to the horizontal diameter was demonstrated in both eyes. The

vertical diameter in the amblyopic eye was found to be 1.62±0.23mm and

1.44±0.24mm in the horizontal diameter.

11.17 Inter-ocular Symmetry (IOS)

The pre-treatment amblyopic and fellow eyes were first examined in order to

establish the degree of inter-ocular symmetry. As with the main amblyopic cohort

investigated, a high degree of inter-ocular symmetry was found in the pre-

Optic Disc parameter	Child Amblyopic Eye (mean ± SD) (n=15)	Child Fellow Eye (mean ± SD) (n=15)	Fellow v Amblyopic Eye Paired t-test
Vertical diameter	1.62mm (0.23)	1.67mm (0.17)	p=0.28 CI:-0.05 to 0.15
Horizontal diameter	1.44mm (0.24)	1.49mm (0.19)	p=0.12 CI:-0.16 to 0.12
Disc to Fovea diameter	4.40mm (0.33)	4.37mm (0.39)	p=0.66 CI:-0.23 to 0.15
Disc Area	1.86mm^2 (0.53)	1.97mm^2 (0.42)	p=0.18 CI:-0.06 to 0.28
Vetical:Horizontal Ratio	1.13 (0.12)	1.13 (0.11)	p=0.93 CI:-0.07 to 0.06
Axial length :Disc Area Ratio	12.61mm^{-1} (3.96)	11.75mm^{-1} (2.84)	p=0.15 CI:-2.07 to 0.35
Disc-Fovea:Disc Diameter Ratio	2.47 (0.48)	2.30 (0.33)	**p=0.04** CI:-0.32 to -0.01

439

Table 11.28 : Pre-treatment optic disc parameters ± SD of both eyes in amblyopic children in the longitudinal phase. The results of paired t-tests between the amblyopic eye and fellow eye for each parameter are shown. The optic disc parameters are defined previously in Chapter 10 (Figures 10.3, 10.4 and Table 10.1).

treatment images between the amblyopic eye and the fellow eye in all measured

parameters (Table 11.28) with the exception of the disc-fovea:disc diameter ratio

(DF:DD). The DF:DD demonstrated a significant difference between the amblyopic

Optic Disc parameter	Child Amblyopic Eye (mean ± SD) (n=7)	Child Fellow Eye (mean ± SD) (n=7)	Fellow v Amblyopic Eye Paired t-test
Vertical diameter	1.64mm (0.24)	1.66mm (0.16)	p=0.71 CI:-0.11 to 0.15
Horizontal diameter	1.52mm (0.22)	1.52mm (0.16)	p=0.97 CI:-0.09 to 0.09
Disc to Fovea diameter	4.25mm (0.29)	4.21mm (0.26)	p=0.34 CI:-0.13 to 0.05

Table 11.29 : Post-treatment optic disc parameters ± SD of both eyes in amblyopic children in the longitudinal phase. The results of paired t-tests between the amblyopic eye and fellow eye for each parameter are shown. The optic disc parameters are defined previously in Chapter 10 (Figures 10.3, 10.4 and Table 10.1).

eye and the fellow eye (paired t-test, diff=0.17 p=0.04 CI: -0.32 to -0.01) with the

amblyopic eye demonstrating an increased ratio mean (2.47) in comparison to the

fellow eye mean (2.30). As with the RNFL (Chapter 11) the symmetry between the

amblyopic and the fellow post-treatment pairs was also analysed (Table 11.29). A

high degree of inter-ocular symmetry was shown in the post-treatment images for

all parameters (Table 11.29).

Disc Area	1.99mm^2 (0.57)	2.00mm^2 (0.39)	p=0.92 CI:-0.26 to 0.28
Vetical:Horizontal Ratio	1.08 (0.09)	1.09 (0.09)	p=0.34 CI:-0.02 to 0.04
Axial length :Disc Area Ratio	11.71mm^{-1} (3.20)	11.27mm^{-1} (1.99)	p=0.56 CI:-2.19 to 1.31
Disc-Fovea:Disc Diameter Ratio	2.22 (0.36)	2.15 (0.29)	p=0.44 CI:-0.27 to 0.13

Tables 11.28 and 11.29 present the differences between the mean measurements in the longitudinal cohort of children; individually pre-treatment no subject had an inter-ocular difference in the vertical diameter greater than 0.36mm (mean individual difference of 0.02mm). In the horizontal diameter no individual had a difference greater than 0.24mm (mean individual difference of 0.05mm). The greatest inter-ocular difference of the disc to fovea distance was 0.66mm with a mean individual difference of 0.13mm and the greatest inter-ocular difference of the disc area was 0.53mm^2 with a mean individual difference of 0.06mm^2. The greatest difference in the axial length to disc area ratio (Axl:DA) was 5.36mm^{-1}. The Axl:DA ratio did not always show the amblyopic eye as the eye with the larger ratio and in 4 cases (AB0207 diff = -1.33mm^{-1}, AB0215 diff = -0.36mm^{-1}, AB0218 diff = -0.49mm^{-1}, and AB0244 diff = -3.88mm^{-1}) the amblyopic eye demonstrated the smaller ratio. The greatest difference in the DF: DD ratio was 0.6. Two individuals demonstrated a lower ratio in their amblyopic eyes (AB0200 diff = -0.03 and AB0207 diff = -0.37).

11.18 Optic Disc Parameters in Amblyopic Children: Pre v Post-treatment

The pre-treatment and post-treatment measurements of the amblyopic eyes, of the children undergoing occlusion therapy were compared. Thirty-two optic disc images of amblyopic eyes, (16 pre-treatment pairs and 16 post-treatment pairs) were obtained from the 24 child amblyopes completing the longitudinal phase of the study. No significant differences were found between the pre-treatment and post-treatment measurements across any of the measured optic disc parameters. A summary of the results of the parameters in the amblyopic eyes compared pre-treatment and post-treatment is provided in Table 11.30.

Table 11.30: Pre-treatment v Post-treatment optic disc parameters ± SD of the amblyopic eyes in the longitudinal phase. The results of paired t-tests between the amblyopic eye pre and post-treatment for each sector are shown. The optic disc parameters are defined previously in Chapter 10 (Figures 10.3, 10.4 and Table 10.1).

No significant difference was found between the pre and post treatment images in

Optic Disc parameter	Child (Pre-Treat) Measurements (mean ± SD) (n=16)	Child (Post-Treat) Measurements (mean ± SD) (n=16)	Pre v Post Amblyopic Eyes Paired t-test
Vertical diameter	1.63mm (0.23)	1.63mm (0.21)	p=0.78 CI:-0.05 to 0.06
Horizontal diameter	1.48mm (0.26)	1.49mm (0.23)	p=0.75 CI:-0.04 to 0.03
Disc to Fovea diameter	4.40mm (0.31)	4.36mm (0.33)	p=0.48 CI:-0.08 to 0.17
Disc Area	1.94mm^2 (0.56)	1.92mm^2 (0.49)	p=0.78 CI:-0.09 to 0.12
Vetical:Horizontal Ratio	1.11 (0.10)	1.10 (0.11)	p=0.29 CI:-0.01 to 0.03
Axial length :Disc Area Ratio	12.27mm^{-1} (4.01)	12.21mm^{-1} (3.34)	p=0.86 CI:-0.65 to 0.78
Disc-Fovea:Disc Diameter Ratio	2.39 (0.49)	2.35 (0.42)	p=0.40 CI:-0.07 to 0.16

any of the parameters (Table 11.30). For this reason both groups were combined

(Table 11.31) to ensure that the low number of images in the post treatment group

was not unduly influencing the results. As with the separate categories the

combined data set also demonstrated a high degree of inter-ocular symmetry

across the optic disc parameters, with the exception of the DF:DD ratio (Table

11.31 and Figure 11.20).

443

Table 11.31 : Combined Pre-treatment and post-treatment optic disc parameter measurements ± SD of both eyes in amblyopic children in the longitudinal phase. The results of paired t-tests between the amblyopic eye and fellow eye for each optic disc parameter are shown. The optic disc parameters are defined previously in Chapter 10 (Figures10.3, 10.4 and Table 10.1).

Optic Disc parameter	Child Amblyopic Eye (mean ± SD) (n=22)	Child Fellow Eye (mean ± SD) (n=22)	Fellow v Amblyopic Eye Paired t-test
Vertical diameter	1.63mm (0.23)	1.67mm (0.16)	p=0.25 CI:-0.03 to 0.11
Horizontal diameter	1.47mm (0.23)	1.50mm (0.18)	p=0.16 CI:-0.16 to 0.09
Disc to Fovea diameter	4.35mm (0.32)	4.31mm (0.36)	p=0.51 CI:-0.16 to 0.08
Disc Area	1.91mm^2 (0.53)	1.98mm^2 (0.40)	p=0.23 CI:-0.05 to 0.21
Vetical:Horizontal Ratio	1.12 (0.10)	1.12 (0.10)	p=0.92 CI:-0.04 to 0.05
Axial length :Disc Area Ratio	12.33mm^{-1} (3.68)	11.60mm^{-1} (2.56)	p=0.11 CI:-1.64 to 0.19
Disc-Fovea:Disc Diameter Ratio	2.39 (0.45)	2.25 (0.32)	**p=0.02** CI:-0.25 to -0.02
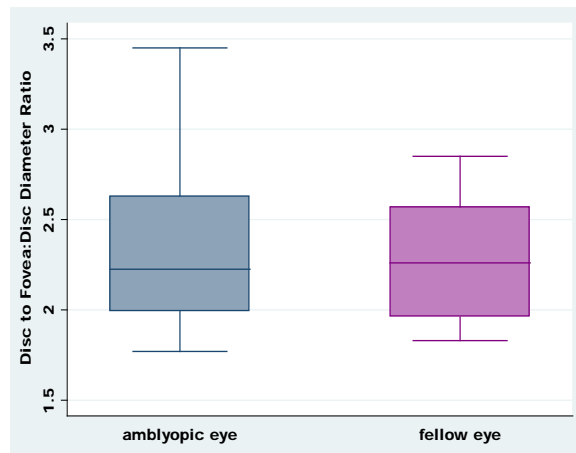
Figure 11.20: Box plots depicting the DF:DD ratio for the amblyopic and fellow eyes (including pre and post-treatment images) paired t-test diff: 0.14, p=0.02, CI: -0.25 to -0.02.

11.19 Optic Disc Parameters in Amblyopic Children: Strabismus v Anisometropia

Twenty-two participants completing the longitudinal phase of the study had pre-treatment optic disc images of the amblyopic eye. Of these, 5 had strabismus only, 12 had anisometropia only and 5 had combined strabismus and anisometropia (S/A). All the measured parameters were analysed using ANOVA to assess any differences that may be present due to the presumed cause of the amblyopia i.e. strabismus and or anisometropia. The ANOVA of the optic disc parameters by strabismus, anisometropia and S/A demonstrated no significant difference between the groups (Table 11.32).

Table 11.32: Results of One-way ANOVA for the comparison of the pre-treatment measurements between the strabismic only, the anisometropic only and the combined strabismus and anisometropic (S/A) amblyopic children (3 groups).						
Optic Disc parameter						
Vertical diameter	Between groups Within groups	2 19	0.10 1.05	0.91	0.42	
Horizontal diameter	Between groups Within groups	2 19	0.23 0.96	2.27	0.13	
Disc to Fovea diameter	Between groups Within groups	2 19	0.54 1.61	3.22	0.06	
Disc Area	Betw	2	1.07	1.95	0.17	

445

	een groups Within groups	19	5.22		
Vetical:Horizontal Ratio	Between groups Within groups	2 19	0.02 0.19	0.87	0.43
Axial length :Disc Area Ratio	Between groups Within groups	2 19	21.13 267	0.75	0.49
Disc-Fovea:Disc Diameter Ratio	Between groups Within groups	2 19	0.05 4.48	0.10	0.90

11.20 Optic Disc Parameters in Amblyopic Children: Success v Failure

Twenty-two children completed the prescribed treatment regime and had pre-treatment optic disc images of the amblyopic eye. Analysis of the pre-treatment parameters in children in the longitudinal phase of the study was examined in the light of treatment outcome of "success or "fail". In the analysis of the optic disc parameters 22 children completed the treatment and had optic disc images of the amblyopic eye obtained pre-treatment, 13 demonstrated a successful outcome from their treatment and were categorised as a "success", whereas 9

demonstrated a poor outcome and were categorised as a "fail". On analysis of the

data no significant differences between the amblyopic eyes with a successful

outcome compared to the amblyopic eyes with a "failed" outcome were found. A

summary of the results of the optic disc parameters in the "success" or "failed"

amblyopic eyes is provided in Table 11.33.

Table 11.33: Optic Disc parameter measurements ± SD of the amblyopic and fellow eyes of children in the longitudinal phase deemed to have either had a "success" or a "fail" outcome. The results of paired t-tests between amblyopic and fellow eyes and 2 sided t-tests between the amblyopic "fail" and "success" eyes for each parameter are shown.

Optic Disc parameter	Child (fail) Amblyopic eye (mean ± SD) n=9	Child (fail) Fellow eye (mean ± SD) n=9	Amblyopic v Fellow Fail eyes Paired t-test	Child (success) Amblyopic eye (mean ± SD) n=13	Child (success) Fellow eye (mean ± SD) n=13	Amblyopic v Fellow Success eyes Paired t-test	Fail v Success Amblyopic eyes 2 sample t-test
Vertical diameter	1.65 (0.28)mm	1.68 (0.19)	p=0.77 CI:-0.27 to 0.20	1.62 (0.21)mm	1.66 (0.15)mm	p=0.56 CI:-0.19 to 0.11	p=0.79 CI:-0.19 to 0.24
Horizontal diameter	1.47 (0.28)mm	1.52 (0.18)	p=0.68 CI:-0.28 to 0.19	1.47 (0.21)mm	1.49 (0.19)mm	p=0.77 CI:-0.19 to 0.14	p=0.98 CI:-0.22 to 0.22
Disc to Fovea diameter	4.40 (0.31)mm	4.53 (0.24)mm	p=0.35 CI:-0.42 to 0.16	4.29 (0.33)mm	4.18 (0.36)mm	p=0.44 CI:-0.17 to 0.39	p=0.42 CI:-0.18 to 0.41
Disc Area	1.95 (0.66)mm	2.02 (0.43)	p=0.80 CI:-0.62 to 0.49	1.89 (0.49)mm	1.96 (0.39)mm	p=0.70 CI:-0.42 to 0.29	p=0.82 CI:-0.45 to 0.56
Vetical:Horizontal Ratio	1.13 (0.11)	1.11 (0.09)	p=0.74 CI:-0.08 to 0.11	1.10 (0.10)	1.12 (0.12)	p=0.71 CI:-0.10 to 0.07	p=0.59 CI:-0.07 to 0.12
Axial length :Disc Area Ratio	12.51 (4.39)	11.57 (2.89)	p=0.60 CI:-2.77 to 4.66	12.14 (3.33)	11.62 (2.43)	p=0.66 CI:-1.84 to 2.88	p=0.82 CI:-3.06 to 3.8
Disc-Fovea:Disc Diameter Ratio	2.38 (0.41)	2.39 (0.41)	p=0.98 CI:-0.36 to 0.35	2.33 (0.52)	2.17 (0.34)	p=0.36 CI:-0.19 to 0.51	p=0.81 CI:-0.38 to 0.48

11.21 Amblyopic Children: Comparison with Visual Normals

The amblyopic children in this longitudinal cohort (success and fail categories both included) demonstrated a difference between the DM:DD ratio between the amblyopic eye and the fellow eye with the amblyopic eyes demonstrating an increase in the DM:DD ratio. However, as with the investigation of foveal topography, in order to establish the degree of difference it is necessary to compare this group with visually normal children. To assess the findings it was thought reasonable to compare the results directly to those of the visually normal children recruited to phase 1 of the study (Chapter 7). The data from each optic disc parameter of the visually normal children was directly compared to that of the phase 2 amblyopic children, 2 tail t-tests were carried out. No significant differences were found between the visually normal eyes and the amblyopic eyes in any of the optic disc parameters. A summary of the results of the optic disc parameters for the visually normal and amblyopic eyes is provided in Table 11.34.

Table 11.34: Optic disc parameter measurements ± SD of the visually normal eyes from phase1 (Chapter 7) and the amblyopic eyes of children in the longitudinal phase. The results of 2 sided t-tests for each parameter are shown.

Optic Disc parameter	Visually Normal Measurements (mean ± SD) (n=55)	Amblyopic (Pre-treat) Measurements (mean ± SD) (n=22)	Amblyopic (Pre-treat) v Normal Eyes 2 sample t-test
Vertical diameter	1.65 (0.17)mm	1.63 (0.23)mm	p=0.64 CI: -0.12 to 0.07
Horizontal diameter	1.44 (0.16)mm	1.47 (0.24)mm	p=0.56 CI: -0.07 to 0.12
Disc to Fovea diameter	4.40 (0.27)mm	4.34 (0.32)mm	p=0.37 CI: -0.21 to 0.08
Disc Area	1.89 (0.37)mm	1.92 (0.55)mm	p=0.79 CI: -0.19 to 0.24
Vetical:Horizontal Ratio	1.15 (0.10)	1.11 (0.10)	p=0.16 CI: -0.09 to 0.14
Axial length :Disc Area Ratio	12.13 (2.48)mm^{-1}	12.29 (3.70)mm^{-1}	p=0.82 CI: -1.28 to 1.6
Disc-Fovea:Disc Diameter Ratio	2.37 (0.30)	2.35 (0.46)	p=0.85 CI: -0.20 to 0.17

In order to further investigate the DF:DD ratio which has shown a difference between the amblyopic eyes and the fellow eyes in the longitudinal cohort but no significant difference relative to the eyes of the visually normal children from phase 1, analysis of the DF:DD was undertaken in relation to the level of pre-treatment visual acuity in the amblyopic eye. The DF:DD is shown to be higher in 2 individual amblyopes in the longitudinal cohort and it is these results that appear to be influencing the overall increase in the mean value of the DF:DD (Figure 11.21). Individuals AB0225 (DF:DD=3.45) a "successful" amblyope with anisometropia and +0.4 logMAR visual acuity and AB0185 (DF:DD=3.13) a "successful" amblyope with anisometropia and +0.35 logMAR visual acuity.
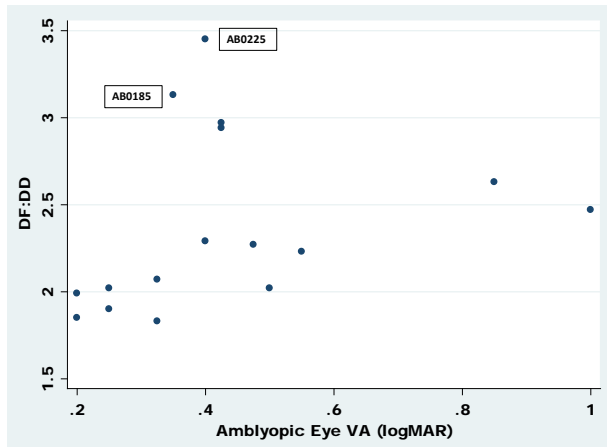
Figure 11.21: Scatter plot of DF:DD v visual acuity (logMAR) of amblyopic eyes. Individual outliers AB0225 and AB0185 are indicated.

11.22 Discussion

11.22.1 Optic Disc Parameters in Amblyopic Children: Pre-treatment

In this longitudinal phase of the study the optic disc measurements (Table 11.28) produced the commonly described pattern of increased vertical diameter (1.62±0.23mm) in comparison to the horizontal diameter (1.44±0.24mm). The optic disc parameters in this cohort of amblyopic children are similar in comparison to the group of amblyopic children described in phase 1 (Chapter 10, Table 10.6). The vertical to horizontal diameter ratio is similar to the findings of Jonas (Jonas et al., 1988), (Jonas et al., 1999), who reported the variation between the horizontal to vertical disc diameter to vary between 0.70 and 1.37, the vertical to horizontal ratio in this study was found to be 1.13. The optic disc to fovea distance in this phase of the study (4.4±0.33mm) is similar to that found in the amblyopic children in phase 1 of this study (4.31±0.33mm) (Table 10.6) and the same as that reported in a study of pre-term and full term infants (4.4±0.4mm) (De Silva et al., 2006). The optic disc area in the longitudinal cohort of children was found to be 1.86±0.53mm^2. This is slightly greater than the amblyopic cohort of children (1.72±0.40mm^2) in phase 1 and similar to the visually normal children in phase 1 (1.87±0.37mm^2). Optic disc area has been shown to vary significantly (Hellstrom et al., 1997; Huynh et al., 2006a). In a study of visually normal children using OCT (Huynh et al., 2006a) the disc area was found to be 2.20±0.39mm^2 with a range of 1.09 to 4.27mm^2. In this present study (phase1, Chapter 10) the disc area was found to be 1.87±0.37mm^2 with a range of 0.92mm^2 to 2.81mm^2, this variability within a normal

population makes it difficult to detect any significant difference that could be caused by factors such as amblyopia.

11.22.2 Optic Disc Parameters in Amblyopic Children: Inter-ocular symmetry

A high degree of inter-ocular symmetry was found in the majority of measured optic disc parameters in the children participating in the longitudinal study with the exception of the disc-fovea: disc diameter ratio (DF:DD). The DF:DD is commonly used to assess the degree of optic nerve hypoplasia (Barr et al., 1999; Wakakura and Alvarez, 1987; Zeki et al., 1991). The accurate measurement of intraocular structures is difficult to achieve due to the variation of the size and shape of the ocular structures (globe, cornea and intra-ocular lens). Therefore as photographic images are equally affected by optical variation, the use of a ratio as a comparator provides a more accurate assessment of the optic disc images. The ratio assumes that the parameters will bear a constant relationship to each other reducing the likelihood of optical variation. The DF:DD ratio in this study demonstrated a significant difference between the amblyopic eye and the fellow eye (p=0.04), with the amblyopic eye showing a higher ratio (2.47±0.48) compared to the fellow eye (2.30±0.33). This finding was consistent both in the pre treatment (Table 11.28) and in the combined group of pre and post treatment measurements (p=0.02) (Table 11.31). This increase in the DF:DD was also detected in the regression analysis of the optic disc parameters in Chapter 10, where the presence of amblyopia had a borderline significant effect on the DF:DD ratio (p=0.054).

The axial length to disc area ratio (Axl:DA) was not found to differ significantly (p=0.15) between the amblopic eye ($12.61\pm3.96mm^{-1}$) and the fellow eye ($11.75\pm2.84mm^{-1}$). These findings are not consistent with those of (Lempert, 2003, 2004), who found a higher ratio in the amblyopic eye compared to the fellow eye. Although the Axl:DA of the amblyopic eyes was shown to be higher in this study it did not reach significance and was not consistently higher with the ratio ranging from - $3.88mm^{-1}$ to $0.53mm^{-1}$. Lempert's original paper (Lempert, 2000) reported a significant difference between the disc area of the amblyopic and fellow eyes. These claims are not supported by the results of this study which, although finds the amblyopic eyes to have smaller disc area ($1.86\pm0.53mm^2$) compared to the fellow eyes ($1.97\pm0.42mm^2$) does not show a significant difference between the amblyopic and fellow eyes (p= 0.18). The findings in this study are similar to that reported by the imaging study using MRI (Pineles and Demer, 2009), with amblyopes showing subtle optic disc differences to visually normal eyes, the optic disc area being smaller and DF:DD ratio increased. The optic disc area has been shown to be subject to a high degree of variation (Jonas et al., 1999) with inter-individual variation of between $0.8mm^2$ to $6.00mm^2$ in visual normals. This degree of normal variation may mask the full effect of any structural differences in amblyopic eyes (Chapter 10 and Chapter 11).

11.22.3 Optic Disc Parameters in Amblyopic Children:

Pre v Post-treatment

No significant differences were found between the majority of pre-treatment and post-treatment measurements across any of the measured optic disc parameters (Table 11.30). This is perhaps not surprising as the anatomical development of the optic disc has been shown to develop in three phases (Hellstrom et al., 1997) with 75% 0f the development occurring by birth. Therefore it would be unlikely that any significant change would be evident in the relatively short period of time (approximately 6 months) during which the occlusion therapy was undertaken. The lack of significant change between the pre and post-treatment groups could also be due to the fact that the number of paired scans in the post-treatment group is smaller (7 pairs) in comparison with the pre-treatment group (15 pairs). The limited sample size may have contributed to the results found in the post-treatment group. Where the data sets for pre and post treatment are combined and the amblyopic eye compared to the fellow eye, the DF:DD continues to maintain a significant difference between the amblyopic and fellow eyes (p=0.02) (Table 11.31).

11.22.4 Optic Disc parameters in Amblyopic Children: Success v Failure

In the analysis of the optic disc parameters no contributing factors were found to predict the "success" or "fail" status achieved after completion of occlusion therapy.

11.23 Conclusion

The optic disc dimensions in this study were similar to the amblyopic eyes reported by Lempert (2000), smaller optic disc area and greater axial length to disc area ratio (Axl:DA) in comparison to the fellow eyes (Table 11.28). However, unlike Lempert (2000, 2003, 2004) a significant degree of inter-ocular asymmetry was not found in the majority of parameters, including those reported by Lempert as having significant asymmetry.

Investigation of the optic disc in this longitudinal study has found no significant difference in structure in the presence of amblyopia for the majority of parameters with the exception of one parameter, the disc-fovea to disc diameter ratio (DF:DD) (p=0.04). This ratio which is used to estimate the degree of optic disc hypoplasia (Barr et al., 1999; Wakakura and Alvarez, 1987; Zeki et al., 1991) was found to be greater in the amblyopic eyes, compared to the fellow eyes, the degree of hypoplasia present is however still far from the level that would be classified as pathological (>3.70) (Barr et al., 1999; Zeki et al., 1991). On detailed examination of the individual DF:DD measurements in relation to the level of visual acuity in the amblyopic eyes (Figure 11.21) it can be seen that 4 of the 16 measurements have a higher than average DF:DD which is causing the mean measurement to increase. The degree of hypoplasia as measured by the DF:DD is not linearly associated with reduced visual acuity (Brodsky, 1994; Frisen and Holmegaard, 1978) and it is likely that the higher DF:DD found in this longitudinal phase of the study is not produced by a subtle degree of hypoplasia, but is produced by a small number of amblyopes (Figure 11.21) having a higher DF:DD, bordering on what would be

regarded as clinically significant. Optic nerve hypoplasia is not generally reported with amblyopia and is not generally a clinical finding, however, hypoplasia has been shown to vary widely (Brodsky, 1994; Frisen and Holmegaard, 1978) the few amblyopes with a higher DF:DD measurement have influenced the findings in this phase.

A consistent increase in the DF:DD in the presence of amblyopia can be seen in both phase1 (Chapter10) and the longitudinal phase 2 (Chapter 11) (each investigating separate cohorts of amblyopes), indicating a subtle effect on retinal structure from the presence of amblyopia. However, there is considerable variation in normals. Thus, while the ratio is significantly different in amblyopic eyes relative to the fellow eyes, it is difficult to attribute clinical significance to this finding.

Chapter 12. Discussion

12.1 Overall Summary of Findings

The research described in this thesis investigates in detail the anatomical integrity of the retinal and optic disc structure in eyes diagnosed with amblyopia, in order to establish if some of those diagnosed have an underlying, subtle, ocular defect. The aim was to either confirm or reject the hypothesis that visual loss in some patients presumed to be functionally amblyopic is due wholly or in part to a co-existing organic cause. The presence of a subtle structural difference in a presumed amblyopic eye could be the primary cause of the visual loss or it could be caused by secondary changes developing from adaptation to a visual assault, caused by, for example, anisometropia or strabismus. It is also possible that structural change could be caused by an as yet unknown cause perhaps at the level of the visual cortex. This research has investigated the amblyopic eyes of children and adults, following the visual pathway across the retina from the fovea, via the paramacular bundle to the optic disc, where peripapillary retinal nerve fibre thickness has been imaged and optic disc size and shape and subjected to detailed measures.

12.2 Foveal Structure in Amblyopia

The results have shown a clear picture of inter-ocular symmetry structure in all individuals, visually normal, amblyopic and non-amblyopic with the presence of strabismus and/ or anisometropia (S/A). This was the case for both adult and child eyes. Where differences were shown to occur such as thickening of the fovea and reduction of the foveal pit depth (Chapter 7 and Chapter 11), they were found to be both bilateral and symmetrical. This structural change cannot therefore be the primary cause of the visual loss as the fellow eye is also affected structurally, despite having a good level of visual acuity.

The longitudinal follow up of amblyopes undergoing occlusion therapy has demonstrated that structural differences exist to a greater extent in both eyes of amblyopes who have failed to show a successful outcome to their treatment. The amblyopes taking part in this study were carefully assessed and their treatment monitored and recorded. However, the one unknown factor in the study, is the timing of the onset of the amblyopia or the factor associated with the amblyopia and it is not known at what point in time the strabismus and/ or anisometropia presented. The timing of the onset may be key to the amount of structural change demonstrated at the fovea and could be a proxy for the "success" or "fail" status achieved after occlusion therapy. Amblyopes with the greatest structural change are those shown to fail to demonstrate improvement in their visual acuity level from occlusion therapy. These amblyopes are likely to be those with the earliest onset of strabismus and /or anisometropia and subsequently do not respond well. This bilateral, symmetrical structural change found at the fovea, which has not been

previously reported is therefore most likely to be a secondary developmental response to visual deprivation and is not the primary cause of the visual loss which has been diagnosed as amblyopia. Even though it is not the cause of the visual loss, the presence of structural differences in amblyopic individuals is very significant, for the reason that amblyopia is defined as a condition in which the eye is healthy and structurally normal.

Two published studies examining macular thickness have also found an increase in the thickness at the macula of the amblyopic eye (Huynh et al., 2006b; Kee et al., 2006). Kee (2006) investigated both the thickness of the fovea and the retinal nerve fibre layer in children with strabismic and anisometropic amblyopia; no difference was found between amblyopic eyes and the visually normal control eyes. However, a significant difference was found between the amblyopic eye and the fellow eye. Huynh (2009) also found a significant difference in foveal and macular thickness in amblyopic eyes in comparison to his control group. The latter study also investigated the macular thickness difference between treated and untreated amblyopes. There was however a degree of variation and the results did not achieve statistical significance. Huynh hypothesises that the increase in foveal thickness may be associated with reduction in the level of visual acuity, although from his large population study, it is not possible to support this association, as the untreated group of amblyopes is small (n=12) in comparison to the recruited total (n=4118). In the longitudinal phase of the present study, although foveal thickness was found to be increased in amblyopes with a poor visual outcome, it cannot be directly linked to the level of visual acuity as the fellow eyes are also affected

structurally but maintain a good level of visual acuity. There is therefore no evidence to link the level of visual acuity with increased foveal thickness.

It must therefore be considered why both eyes demonstrate structural change. From the published literature it has been shown that the visual pathway has its own internal feedback system (Kind et al., 2002; Zhang et al., 2005). It is possible that when a visual insult occurs either from optical blur or a confused and diplopic image affecting one eye to a greater extent than the other, the visual cortex receives incongruous information and via the feedback system attempts to maintain the binocular status.

Bilateral structural change at the level of the photoreceptors has been shown to occur in animals studies following monocular deprivation from birth (Liang et al 1995, Rucker and Wallman 2008) and has also been reported in ophthalmic conditions such as retinopathy of prematurity and ocular albinism (Hammer,2008, Marmor 2008, Charbel Issa 2008). It is therefore, possible that the visual system utilises the internal feedback system to produce a bilateral adaptation to the visual assault by accelerating the development of the fovea in an attempt to compensate. In the longitudinal phase of this study no significant change in foveal structure was found to occur in response to treatment, although this may be due to the fact that the treatment phase was short. The structural differences found were present prior to treatment and were not changed by the treatment. In order to prove beyond doubt that the presence of foveal thickening is a developmental response to the presence of amblyopia or indeed if it precedes the development of amblyopia, a

longitudinal study investigating the development of retinal structure from birth would be required.

12.3 Papillomacular Bundle Structure in Amblyopia

The papillomacular bundle is formed from the retinal ganglion axons as they pass from the fovea to the optic disc. The dimensions of this structure in amblyopia have not been reported previously and considering it is the major pathway of the retinal nerve fibre layer (RNFL) it was thought logical to image the papillomacular bundle in detail. The results, like those from all retinal areas have shown a clear picture of structural inter-ocular symmetry in all eye categories. In this study no structural differences in the papillomacular bundle were found to be associated with the presence of amblyopia, nor was there any association between the level of visual acuity and the measured structure.

12.4 Peripapillary Retinal Nerve Fibre Layer (RNFL) Thickness in Amblyopia

No significant difference was found in the RNFL thickness in any of the sectors of the peripapillary region of the optic disc in the presence of amblyopia.

Two previously published studies have found a significant difference in RNFL thickness in the presence of amblyopia (Yen et al., 2004; Yoon et al., 2005) demonstrating an increase in RNFL thickness, but only in anisometropic amblyopes. The majority of studies have failed to find differences in amblyopic eyes (Reche-Sainz et al., 2006; Repka et al., 2006; Repka et al., 2009b) relative to fellow eyes or eyes in visually normal controls. The majority of the studies

462

investigating retinal structure have used the fellow eye as the control with which to compare measurements from the amblyopic eye (Altintas et al., 2005; Dickmann et al., 2009; Repka et al., 2006; Yoon et al., 2005) and this may result in any bilateral change being masked. In the studies where the fellow eye was used as the control and there is no specific control group, the results showed no significant differences between the amblyopic eye and the fellow eye (Altintas et al., 2005; Repka et al., 2006; Yoon et al., 2005). In this study no structural differences in the peripapillary RNFL were found to be associated with the presence or depth of amblyopia.

12.5 Optic Disc Dimensions in Amblyopia

The current investigation of optic disc characteristics revealed no structural abnormalities in amblyopes. Although optic disc dimensions in this study were similar to that of the amblyopic eyes reported by Lempert (2000), unlike Lempert (2000, 2003, 2004) no difference was found between the amblyopic eye and the fellow eye. Lempert (2000) claims that 48% of the amblyopes in his study exhibited a structural hyoplasia of the amblyopic disc. In phase 1 of this study no significant difference was found between the amblyopic and the fellow eyes and indeed no difference in optic disc structure was found between the eyes of amblyopes and visual normals for any of the measured disc parameters. In the longitudinal phase 2 when a significant difference in the DF:DD ratio between the amblyopic eye and the fellow eye was demonstrated, indicating a subclinical hypoplasia, further analysis showed a small number of outliers influencing the mean measurement .These outliers were children who had failed to improve despite

occlusion therapy; this may be an indicator of subtle subclinical hypoplasia preventing improvement or it may be due to variability caused by poor vision and leading to difficulty maintaining the steady fixation required to produce accurate images. The amblyopic eyes have demonstrated a wide range of structural measures, however, this diversity is also found in visually normal eyes. The wide ranging inter –individual variation, present in optic disc structure (Jonas, 1988) indicates that the change in the DF:DD is due to normally occurring variation that exists in optic disc structure. This would not be surprising as clinically amblyopia is not associated with an obvious hypoplasia, and it would be unexpected to find significant hypoplasia which is not generally found clinically.

Lempert (2003) suggests that the axial-length to disc area ratio (Axl:DA) amongst the general population is between 8.66 - 9.5 mm^{-1}. This normative range of data is however, derived from a number of differing studies, measuring subjects of different ages and including ophthalmic conditions such as glaucoma and cataract. In the present study the normative Axl:DA was higher than that suggested by Lempert, both for visually normal adults (12.71±2.27mm^{-1}) and children (12.18±2.25mm^{-1}). A recent study measuring the optic disc area in a group of adolescents has demonstrated very substantial variability in the size of the optic disc area in the normal population, with the disc area varying by over 100% (Chapter 4,Figure 4.13) (Huynh et al., 2008). Huynh (2008) reports a mean disc area in a visually normal group of children to be 2.57mm^2. Although the mean disc area measurements from this study are lower (visually normal adults =

1.95±0.39mm^{-1} and visually normal children = 1.87±0.37mm^{-1}) than those reported by Huynh (2008) they are well within the reported normative range. The measurements taken from Lempert's study of esotropic children (Lempert, 2003) both normals and amblyopes, would also fit into this normative distribution, with the amblyopic measurements being on the edge of the normative curve (1.55 mm^2). The amblyopic disc area measurements from the present study (amblyopic adults = 1.73±0.39mm^2 and amblyopic children = 1.72±0.40mm^2) would also be situated on the edge of the normative curve (Chapter 4, Figure 4.13).The suggestion by Lempert (Lempert, 2003) that a smaller disc area in amblyopic eyes leads to a reduction of the retinal nerve fibre layer thickness and thus a reduction in visual acuity, has not been supported by the results of this study, nor is it reflected in the findings reported by any of the published imaging studies investigating amblyopia. The optic disc area of amblyopic eyes has not been found to be significantly reduced, nor has the level of visual acuity been linked to any change in retinal structure.

12.6 Conclusion

Structural changes at retinal level are not the primary cause of amblyopia and therefore the current consensus theory of the amblyopic defect being at the level of the visual cortex must still hold true. The pioneering work of Hubel and Weisel (1963, 1965,1968) demonstrating the adaptive changes at the level of the visual cortex with a decline in the binocularly driven neurones remains unchallenged by the findings from this present research. Current definitions for amblyopia therefore appear intact.

From a clinical stand point, subtle structural abnormalities should not be routinely examined for using the techniques used in the study. However, in cases where there is little benefit from occlusion therapy despite presumed compliance, subtle structural anomalies should be searched for.

BIBLIOGRAPHY

Abrahamsson, M., Fabian, G., Andersson, A. K. & Sjostrand, J. (1990) A longitudinal study of a population based sample of astigmatic children. I. Refraction and amblyopia. *Acta Ophthalmol (Copenh),* 68**,** 428-34.

Adams, D. (2005) Normal and Abnormal Visual Development. IN Taylor, D. & Hoyt, G. (Eds.) *Pediatric Ophthalmology and Strabismus* 3rd ed. Edinburgh Elsevier Saunders

Adams, D. L. & Horton, J. C. (2009) Ocular Dominance Columns: Enigmas and Challenges. *Neuroscientist,* 15**,** 62-77.

Adler, D. C., Ko, T. H. & Fujimoto, J. G. (2004) Speckle reduction in optical coherence tomography images by use of a spatially adaptive wavelet filter. *Opt Lett,* 29**,** 2878-80.

Alamouti, B. & Funk, J. (2003) Retinal thickness decreases with age: an OCT study. *Br J Ophthalmol,* 87**,** 899-901.

Almeder, L. M., Peck, L. B. & Howland, H. C. (1990) Prevalence of anisometropia in volunteer laboratory and school screening populations. *Invest Ophth Vis Sci,* 31**,** 2448-2455.

Altintas, O., Yuksel, N., Ozkan, B. & Caglar, Y. (2005) Thickness of the retinal nerve fiber layer, macular thickness, and macular volume in patients with strabismic amblyopia. *J Pediat Ophth Strab,* 42**,** 216-21.

Alvarez, E., Wakakura, M., Khan, Z. & Dutton, G. N. (1988) The disc-macula distance to disc diameter ratio: a new test for confirming optic nerve hypoplasia in young children. *J Pediat Ophth Strab,* 25**,** 151-4.

Anderson, S. J. & Swettenham, J. B. (2006) Neuroimaging in human amblyopia. *Strabismus,* 14**,** 21-35.

Ansari-Shahrezaei, S., Maar, N., Biowski, R. & Stur, M. (2001) Biomicroscopic measurement of the optic disc with a high-power positive lens. *Invest Ophth Vis Sci,* 42**,** 153-157.

Archer, S. M. (2000) Amblyopia? *J AAPOS,* 4**,** 257-257.

Arden, G. B., Vaegan, Hogg, C. R., Powell, D. J. & Carter, R. M. (1980) Pattern ERG's are Abnormal in many Amblyopes. *T Ophth Soc U K,* 100**,** 453-460.

Arden, G. B. & Wooding, S. L. (1985) Pattern ERG in amblyopia. *Invest Ophth Vis Sci,* 26**,** 88-96.

Arnold, J. V., Gates, J. W. C. & Taylor, K. M. (1993) Possible Errors in the Measurement of Retinal Lesions. *Invest Ophth Vis Sci,* 34**,** 2576-2580.

Ashburner, J. & Friston, K. J. (2000) Voxel-based morphometry--the methods. *Neuroimage,* 11**,** 805-21.

Attebo, K., Mitchell, P., Cumming, R., Smith, W., Jolly, N. & Sparkes, R. (1998) Prevalence and causes of amblyopia in an adult population. *Ophthalmology,* 105**,** 154-159.

Awan, M., Proudlock, F. A. & Gottlob, I. (2005) A randomized controlled trial of unilateral strabismic and mixed amblyopia using occlusion dose monitors to record compliance. *Invest Ophth Vis Sci,* 46**,** 1435-1439.

Baddini-Caramelli, C., Hatanaka, M., Polati, M., Umino, A. T. & Susanna, R., Jr. (2001) Thickness of the retinal nerve fiber layer in amblyopic and normal eyes: a scanning laser polarimetry study. *J AAPOS,* 5**,** 82-4.

Bal, T., Debay, D. & Destexhe, A. (2000) Cortical feedback controls the frequency and synchrony of oscillations in the visual thalamus. *J Neurosci,* 20**,** 7478-88.

Barishak, Y. R. (1992) Embryology of the eye and its adnexae. *Dev Ophthalmol,* 24**,** 1-142.

Barnard, A. R., Hattar, S., Hankins, M. W. & Lucas, R. J. (2006) Melanopsin regulates visual processing in the mouse retina. *Curr Biol,* 16**,** 389-95.

Barnes, G. R., Hess, R. F., Dumoulin, S. O., Achtman, R. L. & Pike, G. B. (2001) The cortical deficit in humans with strabismic amblyopia. *J Physiol,* 533**,** 281-97.

Barnes, G. R., Li, X., Thompson, B., Singh, K. D., Dumoulin, S. O. & Hess, R. F. (2010) Decreased gray matter concentration in the lateral geniculate nuclei in human amblyopes. *Invest Ophth Vis Sci,* 51**,** 1432-8.

Barr, D. B., Weir, C. R. & Purdie, A. T. (1999) An appraisal of the disc-macula distance to disc diameter ratio in the assessment of optic disc size. *Ophthal Physl Opt,* 19**,** 365-375.

Barrett, B. T., Bradley, A. & Mcgraw, P. V. (2004) Understanding the neural basis of amblyopia. *Neuroscientist,* 10**,** 106-117.

Barrett, B. T., Candy, T. R., Mcgraw, P. V. & Bradley, A. (2005) Probing the causes of visual acuity loss in patients diagnosed with functional amblyopia. *Ophthal Physl Opt,* 25**,** 175-178.

Barrett, B. T., Pacey, I. E., Bradley, A., Thibos, L. N. & Morrill, P. (2003) Nonveridical visual perception in human amblyopia. *Invest Ophth Vis Sci,* 44**,** 1555-67.

Beck, R. W. & Grp, P. E. D. I. (2003) A randomized trial of prescribed patching regimens for treatment of severe amblyopia in children. *Ophthalmology,* 110**,** 2075-2087.

Bedell, H. D. & Flom, M. C. (1981) Monocular spatial distortion in strabismic amblyopia. *Invest Ophth Vis Sci,* 20**,** 263-8.

Bedell, H. E. & Flom, M. C. (1985) Bilateral oculomotor abnormalities in strabismic amblyopes: evidence for a common central mechanism. *Doc Ophthalmol,* 59**,** 309-21.

Bedell, H. E., Flom, M. C. & Barbeito, R. (1985) Spatial aberrations and acuity in strabismus and amblyopia. *Invest Ophth Vis Sci,* 26**,** 909-16.

Bedell, H. E., Yap, Y. L. & Flom, M. C. (1990) Fixational drift and nasal-temporal pursuit asymmetries in strabismic amblyopes. *Invest Ophth Vis Sci,* 31**,** 968-76.

Bengtsson, B. & Krakau, C. E. T. (1992) Correction of Optic Disk Measurements on Fundus Photographs. *Graefes Arch Clin Exp Ophthalmol,* 230**,** 24-28.

Bennett, A. G., Rudnicka, A. R. & Edgar, D. F. (1994) Improvements on Littmann Method of Determining the Size of Retinal Features by Fundus Photography. *Graefes Arch Clin Exp Ophthalmol,* 232**,** 361-367.

Berson, D. M., Dunn, F. A. & Takao, M. (2002) Phototransduction by retinal ganglion cells that set the circadian clock. *Science,* 295**,** 1070-3.

Bienenstock, E. L., Cooper, L. N. & Munro, P. W. (1982) Theory for the development of neuron selectivity: orientation specificity and binocular interaction in visual cortex. *J Neurosci,* 2**,** 32-48.

Birch, E. E. & Stager, D. R. (1985) Monocular acuity and stereopsis in infantile esotropia. *Invest Ophth Vis Sci,* 26**,** 1624-30.

Birch, E. E. & Swanson, W. H. (2000) Hyperacuity deficits in anisometropic and strabismic amblyopes with known ages of onset. *Vision Res,* 40**,** 1035-40.

Birt, C. M., Shin, D. H., Samudrala, V., Hughes, B. A., Kim, C. & Lee, D. (1997) Analysis of reliability indices from Humphrey visual field tests in an urban glaucoma population. *Ophthalmology,* 104**,** 1126-1130.

Blakemore, C. & Eggers, H. M. (1978) Effects of artificial anisometropia and strabismus on the kitten's visual cortex. *Arch Ital Biol,* 116**,** 385-9.

472

Blakemore, C. & Price, D. J. (1987) The organization and postnatal development of area 18 of the cats visual cortex. . *J. Physiol.-London,* 384**,** 263-292.

Blakemore, C. & Vital-Durand, F. (1979) Development of the neural basis of visual acuity in monkeys: speculation on the origin of deprivation amblyopia. *T Ophthal Soc UK,* 99**,** 363-8.

Blakemore, C. & Vitaldurand, F. (1986) Effects of visual deprivation on the development of the monkeys lateral geniculate nucleus. *J. Physiol.-London,* 380**,** 493-511.

Bland, M. (1995) *An introduction to medical statistics,* Oxford, Oxford University Press.

Blumenthal, E. Z., Parikh, R. S., Pe'er, J., Naik, M., Kaliner, E., Cohen, M. J., Prabakaran, S., Kogan, M. & Thomas, R. (2009) Retinal nerve fibre layer imaging compared with histological measurements in a human eye. *Eye,* 23**,** 171-5.

Blumenthal, E. Z., Williams, J. M., Weinreb, R. N., Girkin, C. A., Berry, C. C. & Zangwill, L. M. (2000) Reproducibility of nerve fiber layer thickness measurements by use of optical coherence tomography. *Ophthalmology,* 107**,** 2278-2282.

Bone, R. A. & Landrum, J. T. (1992) Distribution of macular pigment components, zeaxanthin and lutein, in human retina. *Methods Enzymol,* 213**,** 360-6.

Bonhoeffer, T. (1996) Neurotrophins and activity-dependent development of the neocortex. *Curr Opin Neurobiol,* 6**,** 119-26.

Bouvier, S. E., Cardinal, K. S. & Engel, S. A. (2008) Activity in visual area V4 correlates with surface perception. *J Vis,* 8**,** 28 1-9.

Bowman, R. J., Williamson, T. H., Andrews, R. G., Aitchison, T. C. & Dutton, G. N. (1998) An inner city preschool visual screening programme: long-term visual results. *Br J Ophthalmol,* 82**,** 543-8.

Boyd, J. D., Mavity-Hudson, J. A. & Casagrande, V. A. (2000) The Connections of Layer 4 Subdivisions in the Primary Visual Cortex (V1) of the Owl Monkey. *Cereb. Cortex,* 10**,** 644-662.

Bozkurt, B., Irkec, M. & Arslan, U. (2008) Asymmetry in optic disc morphometry as measured by confocal scanning laser ophthalmoscopy in subjects with hyperopic anisometropia. *J Pediat Ophth Strab,* 45**,** 156-160.

Bozkurt, B., Irkec, M., Orhan, M. & Karaagaoglu, E. (2003) Thickness of the retinal nerve fiber layer in patients with anisometropic and strabismic amblyopia. *Strabismus,* 11**,** 1-7.

Bradley, A. & Freeman, R. D. (1981) Contrast sensitivity in anisometropic amblyopia. *Invest Ophth Vis Sci,* 21**,** 467-76.

Bradley, A. & Freeman, R. D. (1985) Is reduced vernier acuity in amblyopia due to position, contrast or fixation deficits? *Vision Res,* 25**,** 55-66.

Bradley, A., Freeman, R. D. & Applegate, R. (1985) Is amblyopia spatial frequency or retinal locus specific? *Vision Res,* 25**,** 47-54.

Bradley, A., Rabin, J. & Freeman, R. D. (1983) Nonoptical determinants of aniseikonia. *Invest Ophth Vis Sci,* 24**,** 507-512.

Briggs, F. & Usrey, W. M. (2005) Temporal properties of feedforward and feedback pathways between the thalamus and visual cortex in the ferret. *Thalamus Relat Syst,* 3**,** 133-139.

Briggs, F. & Usrey, W. M. (2007) Cortical activity influences geniculocortical spike efficacy in the macaque monkey. *Front Integr Neurosci,* 1**,** 3.

Briggs, F. & Usrey, W. M. (2008) Emerging views of corticothalamic function. *Curr Opin Neurobiol,* 18**,** 403-407.

Brock, F. W. & Givner, I. (1952) Fixation anomalies in amblyopia. *Arch Ophthalmol,* 47**,** 775-86.

Brodsky, M. C. (1994) Congenital optic disk anomalies. *Surv Ophthalmol,* 39**,** 89-112.

Brose, K., Bland, K. S., Wang, K. H., Arnott, D., Henzel, W., Goodman, C. S., Tessier-Lavigne, M. & Kidd, T. (1999) Slit proteins bind Robo receptors and have an evolutionarily conserved role in repulsive axon guidance. *Cell,* 96**,** 795-806.

Brown, S. M., Archer, S. & Del Monte, M. A. (1999) Stereopsis and binocular vision after surgery for unilateral infantile cataract. *J AAPOS,* 3**,** 109-13.

Bruce, A., Pacey, I. E., Dharni, P., Scally, A. J. & Barrett, B. T. (2009) Repeatability and reproducibility of macular thickness measurements using fourier domain optical coherence tomography. *Open Ophth J,* 3**,** 10-4.

Bruce V, Green P R & Georgeson M A (2004) *Visual Perception : physiology, psychology and ecology,* New York, Psychology Press.

Budenz, D. L. (2008) Symmetry between the right and left eyes of the normal retinal nerve fiber layer measured with optical coherence tomography (an AOS thesis). *T Am Ophth Soc,* 106**,** 252-75.

Budenz, D. L., Anderson, D. R., Varma, R., Schuman, J., Cantor, L., Savell, J., Greenfield, D. S., Patella, V. M., Quigley, H. A. & Tielsch, J. (2007) Determinants of normal retinal nerve fiber layer thickness measured by Stratus OCT. *Ophthalmology,* 114**,** 1046-52.

Budenz, D. L., Chang, R. T., Huang, X. R., Knighton, R. W. & Tielsch, J. M. (2005) Reproducibility of retinal nerve fiber thickness measurements using the stratus OCT in normal and glaucomatous eyes. *Invest Ophth Vis Sci,* 46**,** 2440-2443.

Burian, H. M. (1967) The behavior of the amblyopic eye under reduced illumination and the theory of functional amblyopia. *Doc Ophthalmol,* 23**,** 189-202.

Burian, H. M. & Cortimiglia, R. M. (1962) Visual acuity and fixation pattern in patients with strabismic amblyopia. *Am Orthopt J,* 12**,** 169-74.

Burian, H. M. & Von Noorden, G. K. (1980) *Burian-von Noorden's Binocular vision and ocular motility,* St Louis, The C. V. Mosby Company.

Callaway, E. M. (1998) Local circuits in primary visual cortex of the macaque monkey. *Annu Rev Neurosci,* 21**,** 47-74.

Callaway, E. M. (2005) Structure and function of parallel pathways in the primate early visual system. *J. Physiol.-London,* 566**,** 13-19.

Campos, E. (1995) AMBLYOPIA. *Surv Ophthalmol,* 40**,** 23-39.

Campos, E. C. (1989) Amblyopia revisited: evidence for the heterogeneity of the syndrome. *Int Ophthalmol,* 13**,** 327-30.

Chan, A., Duker, J. S., Ko, T. H., Fujimoto, J. G. & Schuman, J. S. (2006) Normal macular thickness measurements in healthy eyes using stratus optical coherence tomography. *Arch Ophthalmol,* 124**,** 193-198.

Chan, S. T., Tang, K. W., Lam, K. C., Chan, L. K., Mendola, J. D. & Kwong, K. K. (2004) Neuroanatomy of adult strabismus: a voxel-based morphometric analysis of magnetic resonance structural scans. *Neuroimage,* 22**,** 986-994.

Charbel Issa, P., Foerl, M., Helb, H. M., Scholl, H. P. & Holz, F. G. (2008) Multimodal fundus imaging in foveal hypoplasia: combined scanning laser ophthalmoscope imaging and spectral-domain optical coherence tomography. *Arch Ophthalmol,* 126**,** 1463-5.

Chatterjee, S. & Callaway, E. M. (2003) Parallel colour-opponent pathways to primary visual cortex. *Nature,* 426**,** 668-71.

Chen, J. & Lee, L. (2007) Clinical applications and new developments of optical coherence tomography: an evidence-based review. *Clin Exp Optom,* 90**,** 317-335.

Chen, P.-L., Chen, J.-T., Tai, M.-C., Fu, J.-J., Chang, C.-C. & Lu, D.-W. (2007) Anisometropic Amblyopia Treated with Spectacle Correction Alone: Possible Factors Predicting Success and Time to Start Patching. *Am J Ophthalmol,* 143**,** 54-60.

Choi, R. Y. & Kushner, B. J. (1998) The accuracy of experienced strabismologists using the Hirschberg and Krimsky tests. *Ophthalmology,* 105**,** 1301-6.

Ciuffreda, K. J., Levi, D. M. & Selenow, A. (1991) *Amblyopia: basic and clinical aspects.,* Stoneham, MA, Butterworth-Heinemann.

Clarke, M. P. (2010) Review of amblyopia treatment: are we overtreating children with amblyopia? *Br Ir Orthop J,* 7**,** 3-7.

Clarke, M. P., Wright, C. M., Hrisos, S., Anderson, J. D., Henderson, J. & Richardson, S. R. (2003) Randomised controlled trial of treatment of unilateral visual impairment detected at preschool vision screening. *BMJ,* 327**,** 1251-1254.

Cleary, M. (2000) Efficacy of occlusion for strabismic amblyopia: can an optimal duration be identified? *Br J Ophthalmol,* 84**,** 572-578.

Cleary, M. (2007) Amblyopia treatment: from research to practice. *Br Ir Orthop J,* 4**,** 9-14.

Cleland, B. G., Crewther, D. P., Crewther, S. G. & Mitchell, D. E. (1982) Normality of spatial-resolution of retinal ganglion-cells in cats with strabismic amblyopia. *J. Physiol.-London,* 326**,** 235-249.

Clothiaux, E. E., Bear, M. F. & Cooper, L. N. (1991) Synaptic plasticity in visual cortex: comparison of theory with experiment. *J Neurophysiol,* 66**,** 1785-804.

Colen, T. P., De Faber, J. T. & Lemij, H. G. (2000) Retinal nerve fiber layer thickness in human strabismic amblyopia. *Binocul Vis Strabismus Q,* 15**,** 141-6.

Coletta, N. J. & Williams, D. R. (1987) Psychophysical estimate of extrafoveal cone spacing. *J Opt Soc Am A,* 4**,** 1503-13.

Conradi, N. & Sjostrand, J. (1993) A morphometric and stereologic analysis of ganglion cells of the central human retina. *Graefes Arch Clin Exp Ophthalmol,* 231**,** 169-74.

Cornish, E. E., Xiao, M., Yang, Z. T., Provis, J. M. & Hendrickson, A. E. (2004) The role of opsin expression and apoptosis in determination of cone types in human retina. *Exp Eye Res,* 78**,** 1143-1154.

Costa, R. A., Calucci, D., Skaf, M., Cardillo, J. A., Castro, J. C., Melo, L. A., Jr., Martins, M. C. & Kaiser, P. K. (2004) Optical Coherence Tomography 3: Automatic

Delineation of the Outer Neural Retinal Boundary and Its Influence on Retinal Thickness Measurements. *Invest Ophth Vis Sci,* 45**,** 2399-2406.

Costa, R. A., Skaf, M., Melo, L. A. S., Calucci, D., Cardillo, J. A., Castro, J. C., Huang, D. & Wojtkowski, M. (2006) Retinal assessment using optical coherence tomography. *Prog Retin Eye Res,* 25**,** 325-353.

Cotter, S., Astle, W. F., Beck, R. W., Birch, E. E., Chandler, D. L., Davitt, B. V., Holmes, J. M., Kraker, R. T., Miller, M. M., Repka, M. X., Saunders, R. A., Wallace, D. K. & Grp, P. E. D. I. (2003) The course of moderate amblyopia treated with atropine in children: Experience of the amblyopia treatment study. *Am J Ophthalmol,* 136**,** 630-639.

Cotter, S. A., Pediatric Eye Disease Investigator, G., Edwards, A. R., Wallace, D. K., Beck, R. W., Arnold, R. W., Astle, W. F., Barnhardt, C. N., Birch, E. E., Donahue, S. P., Everett, D. F., Felius, J., Holmes, J. M., Kraker, R. T., Melia, M., Repka, M. X., Sala, N. A., Silbert, D. I. & Weise, K. K. (2006) Treatment of anisometropic amblyopia in children with refractive correction. *Ophthalmology,* 113**,** 895-903.

Cowey, A., Stoerig, P. & Perry, V. H. (1989) Trans-Neuronal Retrograde Degeneration of Retinal Ganglion-Cells after Damage to Striate Cortex in Macaque Monkeys - Selective Loss of P-Beta Cells. *Neuroscience,* 29**,** 65-80.

Coxson, H. O., Quiney, B., Sin, D. D., Xing, L., Mcwilliams, A. M., Mayo, J. R. & Lam, S. (2008) Airway wall thickness assessed using computed tomography and optical coherence tomography. *Am J Resp Crit Care,* 177**,** 1201-6.

Crawford, M. L. & Harwerth, R. S. (2004) Ocular dominance column width and contrast sensitivity in monkeys reared with strabismus or anisometropia. *Invest Ophth Vis Sci,* 45**,** 3036-42.

Crowley, J. C. & Katz, L. C. (2002) Ocular dominance development revisited. *Curr Opin Neurobiol,* 12**,** 104-9.

Curcio, C. A. & Allen, K. A. (1990) Topography of ganglion cells in human retina. *J Comp Neurol,* 300**,** 5-25.

Dacey, D. M., Peterson, B. B., Robinson, F. R. & Gamlin, P. D. (2003) Fireworks in the primate retina: In vitro photodynamics reveals diverse LGN-projecting ganglion cell types. *Neuron,* 37**,** 15-27.

Dacosta, S., Bilal, S., Rajendran, B. & Janakiraman, P. (2008) Optic disc topography of normal Indian eyes: An assessment using optical coherence tomography. *Indian J Ophthalmol,* 56**,** 99-102.

Daw, N. W. (1998) Critical periods and amblyopia. *Arch Ophthalmol,* 116**,** 502-5.

De Buffon, M. (1743) Dissertation sur la cause de strabisme on des yeux louches. *Hist Acad R Sci***,** 231.

481

De Silva, D. J., Cocker, K. D., Lau, G., Clay, S. T., Fielder, A. R. & Moseley, M. J. (2006) Optic Disk Size and Optic Disk-to-Fovea Distance in Preterm and Full-Term Infants. *Invest Ophth Vis Sci,* 47**,** 4683-4686.

Deiner, M. S., Kennedy, T. E., Fazeli, A., Serafini, T., Tessierlavigne, M. & Sretavan, D. W. (1997) Netrin-1 and DCC mediate axon guidance locally at the optic disc: Loss of function leads to optic nerve hypoplasia. *Neuron,* 19**,** 575-589.

Del Rio, T. & Feller, M. B. (2006) Early retinal activity and visual circuit development. *Neuron,* 52**,** 221-222.

Dickmann, A., Petroni, S., Salerni, A., Dell'omo, R. & Balestrazzi, E. (2009) Unilateral amblyopia: An optical coherence tomography study. *J AAPOS,* 13**,** 148-50.

Donahue, S. P. (2005) The relationship between anisometropia, patient age, and the development of amblyopia. *T Am Ophth Soc,* 103**,** 313-36.

Donnelly, U. M., Stewart, N. M. & Hollinger, M. (2005) Prevalence and outcomes of childhood visual disorders. *Ophthal Epidemiol,* 12**,** 243-50.

Drexler, W. (2007) Cellular and Functional Optical Coherence Tomography of the Human Retina The Cogan Lecture. *Invest Ophth Vis Sci,* 48**,** 5340-5351.

Drexler, W., Findl, O., Menapace, R., Rainer, G., Vass, C., Hitzenberger, C. K. & Fercher, A. F. (1998) Partial coherence interferometry: a novel approach to biometry in cataract surgery. *Am J Ophthalmol,* 126**,** 524-34.

Drexler, W. & Fujimoto, J. G. (2008) State-of-the-art retinal optical coherence tomography. *Prog Retin Eye Res,* 27**,** 45-88.

Drexler, W., Sattmann, H., Hermann, B., Ko, T. H., Stur, M., Unterhuber, A., Scholda, C., Findl, O., Wirtitsch, M., Fujimoto, J. G. & Fercher, A. F. (2003) Enhanced Visualization of Macular Pathology With the Use of Ultrahigh-Resolution Optical Coherence Tomography. *Arch Ophthalmol,* 121**,** 695-706.

Dubis, A., Mcallister, J. T. & Carroll, J. (2009) Reconstructing foveal pit morphology from optical coherence tomography imaging. *Br J Ophthalmol.*

Duong, T. Q., Pardue, M. T., Thule, P. M., Olson, D. E., Cheng, H. Y., Nair, G., Li, Y. X., Kim, M., Zhang, X. D. & Shen, Q. (2008) Layer-specific anatomical, physiological and functional MRI of the retina. *NMR Biomed,* 21**,** 978-996.

Durand, J. B., Zhu, S. P., Celebrini, S. & Trotter, Y. (2002) Neurons in parafoveal areas V1 and V2 encode vertical and horizontal disparities. *J. Neurophysiol.,* 88**,** 2874-2879.

Earl.Treatment.Diabetic.Retinopathy.Study. (1985) Photocoagulation for diabetic macular edema. Early Treatment Diabetic Retinopathy Study report number 1. . *Arch Ophthalmol,* 103**,** 1796-1806.

El-Dairi, M. A., Asrani, S. G., Enyedi, L. B. & Freedman, S. F. (2009) Optical Coherence Tomography in the Eyes of Normal Children. *Arch Ophthalmol,* 127**,** 50-58.

Elkington, A. R., Frank, H. J. & Greaney, M. J. (1999) *Clinical Optics*, Blackwell.

Elsner, A. E., Burns, S. A., Beausencourt, E. & Weiter, J. J. (1998) Foveal cone photopigment distribution: small alterations associated with macular pigment distribution. *Invest Ophth Vis Sci,* 39**,** 2394-404.

Ergun, E., Hermann, B., Wirtitsch, M., Unterhuber, A., Ko, T. H., Sattmann, H., Scholda, C., Fujimoto, J. G., Stur, M. & Drexler, W. (2005) Assessment of Central Visual Function in Stargardt's Disease/Fundus Flavimaculatus with Ultrahigh-Resolution Optical Coherence Tomography. *Invest Ophth Vis Sci,* 46**,** 310-316.

Erskine, L. & Herrera, E. (2007) The retinal ganglion cell axon's journey: Insights into molecular mechanisms of axon guidance. *Dev Biol,* 308**,** 1-14.

Feldheim, D. A., Vanderhaeghen, P., Hansen, M. J., Frisen, J., Lu, Q., Barbacid, M. & Flanagan, J. G. (1998) Topographic guidance labels in a sensory projection to the forebrain. *Neuron,* 21**,** 1303-1313.

Fercher, A. F., Hitzenberger, C. K., Kamp, G. & Elzaiat, S. Y. (1995) Measurement of Intraocular Distances by Backscattering Spectral Interferometry. *Opt Commun,* 117**,** 43-48.

Ferguson, R. D., Hammer, D. X., Paunescu, L. A., Beaton, S. & Schuman, J. S. (2004) Tracking optical coherence tomography. *Opt Lett,* 29**,** 2139-41.

Fernandez, D. C., Salinas, H. M. & Puliafito, C. A. (2005) Automated detection of retinal layer structures on optical coherence tomography images. *Opt Express,* 13**,** 10200-10216.

Fielder, A. R., Irwin, M., Auld, R., Cocker, K. D., Jones, H. S. & Moseley, M. J. (1995) Compliance in amblyopia therapy: objective monitoring of occlusion. *Br J Ophthalmol,* 79**,** 585-589.

Filous, A., Hlozánek, M., Osmera, J. & Hladíková, M. (2008) Retinal nerve fiber layer assessment in healthy children using scanning laser polarimetry with variable corneal compensation. *J AAPOS,* 12**,** 466-470.

Flom, M. C. & Bedell, H. E. (1985) Identifying amblyopia using associated conditions, acuity, and nonacuity features. *Am J Optom Physiol Opt,* 62**,** 153-60.

Foley-Nolan, A., Mccann, A. & O'keefe, M. (1997) Atropine penalisation versus occlusion as the primary treatment for amblyopia. *Br J Ophthalmol,* 81**,** 54-7.

Fox, P. T., Miezin, F. M., Allman, J. M., Van Essen, D. C. & Raichle, M. E. (1987) Retinotopic organization of human visual cortex mapped with positron-emission tomography. *J Neurosci,* 7**,** 913-22.

Frenkel, S., Morgan, J. E. & Blumenthal, E. Z. (2005) Histological measurement of retinal nerve fibre layer thickness. *Eye,* 19**,** 491-498.

Frisen, L. (1980) The neurology of visual acuity. *Brain,* 103**,** 639-70.

Frisen, L. & Holmegaard, L. (1978) Spectrum of optic nerve hypoplasia. *Br J Ophthalmol,* 62**,** 7-15.

Frohns, F., Mager, M. & Layer, P. G. (2009) Basic fibroblast growth factor increases the precursor pool of photoreceptors, but inhibits their differentiation and apoptosis in chicken retinal reaggregates. *Eur J Neurosci,* 29**,** 1931-42.

Fujita, N., Tanaka, H., Takanashi, M., Hirabuki, N., Abe, K., Yoshimura, H. & Nakamura, H. (2001) Lateral geniculate nucleus: anatomic and functional identification by use of MR imaging. *Am J Neuroradiol,* 22**,** 1719-26.

Garway-Heath, D. F., Rudnicka, A. R., Lowe, T., Foster, P. J., Fitzke, F. W. & Hitchings, R. A. (1998) Measurement of optic disc size: equivalence of methods to correct for ocular magnification. *Br J Ophthalmol,* 82**,** 643-649.

Georges, P., Madigan, M. & Provis, J. (1999) Apoptosis during development of the human retina: Relationship to foveal development and retinal synaptogenesis. *J. Comp. Neurol.,* 413**,** 198-208.

Gerckens, U., Buellesfeld, L., Mcnamara, E. & Grube, E. (2003) Optical Coherence Tomography (OCT). Potential of a new high-resolution intracoronary imaging technique. *Herz,* 28**,** 496-500.

Gold, V. & International Union of Pure and Applied Chemistry. (1987) *Compendium of chemical terminology : IUPAC recommendations,* Oxford, Blackwell Scientific.

Goldberg, J. L., Vargas, M. E., Wang, J. T., Mandemakers, W., Oster, S. F., Sretavan, D. W. & Barres, B. A. (2004) An oligodendrocyte lineage-specific semaphorin, sema5A, inhibits axon growth by retinal ganglion cells. *J. Neurosci,* 24**,** 4989-4999.

Gonzalo, N., Serruys, P. W., Okamura, T., Shen, Z. J., Onuma, Y., Garcia-Garcia, H. M., Sarno, G., Schultz, C., Van Geuns, R. J., Ligthart, J. & Regar, E. (2009) Optical Coherence Tomography Assessment Of The Acute Effects Of Stent Implantation On The Vessel Wall. A Systematic Quantitative Approach. *Heart*.

Goodale, M. A., Meenan, J. P., Bulthoff, H. H., Nicolle, D. A., Murphy, K. J. & Racicot, C. I. (1994) Separate neural pathways for the visual analysis of object shape in perception and prehension. *Curr Biol,* 4**,** 604-10.

Gottlob, I. & Welge-Lussen, L. (1987) Normal pattern electroretinograms in amblyopia. *Invest Ophth Vis Sci,* 28**,** 187-91.

Greenfield, D. S., Knighton, R. W., Feuer, W. J., Schiffman, J. C., Zangwill, L. & Weinreb, R. N. (2002) Correction for corneal polarization axis improves the discriminating power of scanning laser polarimetry. *Am J Ophthalmol,* 134**,** 27-33.

Group, P. E. I. (2003) The course of moderate amblyopia treated with patching in children: Experience of the amblyopia treatment study. *Am J Ophthalmol,* 136**,** 620-629.

Guler, A. D., Ecker, J. L., Lall, G. S., Haq, S., Altimus, C. M., Liao, H. W., Barnard, A. R., Cahill, H., Badea, T. C., Zhao, H., Hankins, M. W., Berson, D. M., Lucas, R. J., Yau, K. W. & Hattar, S. (2008) Melanopsin cells are the principal conduits for rod-cone input to non-image-forming vision. *Nature,* 453**,** 102-5.

Hainline, B. C., Sprunger, D. C., Plager, D. A., Neely, D. E. & Guess, M. G. (2009) Reverse amblyopia with atropine treatment. *Binocul Vis Strabismus Q,* 24**,** 25-31.

Hammer, D. X., Ferguson, R. D., Iftimia, N. V., Ustun, T., Wollstein, G., Ishikawa, H., Gabriele, M. L., Dilworth, W. D., Kagemann, L. & Schuman, J. S. (2005a) Advanced scanning methods with tracking optical coherence tomography. *Opt Express,* 13**,** 7937-7947.

Hammer, D. X., Ferguson, R. D., Magill, J. C., Paunescu, L. A., Beaton, S., Ishikawa, H., Wollstein, G. & Schuman, J. S. (2005b) Active retinal tracker for clinical optical coherence tomography systems. *J Biomed Opt,* 10**,** 024038.

Hammer, D. X., Iftimia, N. V., Ferguson, R. D., Bigelow, C. E., Ustun, T. E., Barnaby, A. M. & Fulton, A. B. (2008) Foveal Fine Structure in Retinopathy of Prematurity: An Adaptive Optics Fourier Domain Optical Coherence Tomography Study. *Invest Ophth Vis Sci,* 49**,** 2061-2070.

Hammond, B. R., Jr. & Fuld, K. (1992) Interocular differences in macular pigment density. *Invest Ophth Vis Sci,* 33**,** 350-5.

Harwerth, R. S. & Levi, D. M. (1983) Psychophysical studies on the binocular processes of amblyopes. *Am J Optom Physiol Opt,* 60**,** 454-63.

Harwerth, R. S., Smith, E. L., 3rd, Duncan, G. C., Crawford, M. L. & Von Noorden, G. K. (1986) Multiple sensitive periods in the development of the primate visual system. *Science,* 232**,** 235-8.

Hattar, S., Liao, H. W., Takao, M., Berson, D. M. & Yau, K. W. (2002) Melanopsin-containing retinal ganglion cells: architecture, projections, and intrinsic photosensitivity. *Science,* 295**,** 1065-70.

Haynes, J. D., Deichmann, R. & Rees, G. (2005) Eye-specific effects of binocular rivalry in the human lateral geniculate nucleus. *Nature,* 438**,** 496-499.

Headon, M. P., Sloper, J. J., Hiorns, R. W. & Powell, T. P. (1985) Effects of monocular closure at different ages on deprived and undeprived cells in the primate lateral geniculate nucleus. *Brain Res,* 350**,** 57-78.

Hee, M. R., Fujimoto, J. & Ko, T. (2004) Interpretation of the optical coherence tomography image. IN Schuman, J., Puliafito, C. A. & Fujimoto, J. (Eds.) *Optical Coherence Tomography of Ocular Diseases.* 2nd ed. Thorofare, NJ.

Hee, M. R., Izatt, J. A., Swanson, E. A., Huang, D., Schuman, J. S., Lin, C. P., Puliafito, C. A. & Fujimoto, J. G. (1995) Optical coherence tomography of the human retina. *Arch Ophthalmol,* 113**,** 325-332.

Hee, M. R., Puliafito, C. A., Duker, J. S., Reichel, E., Coker, J. G., Wilkins, J. R., Schuman, J. S., Swanson, E. A. & Fujimoto, J. G. (1998) Topography of diabetic macular edema with optical coherence tomography. *Ophthalmology,* 105**,** 360-370.

Hellstrom, A., Hard, A. L., Chen, Y., Niklasson, A. & Albertsson-Wikland, K. (1997) Ocular fundus morphology in preterm children. Influence of gestational age, birth size, perinatal morbidity, and postnatal growth. *Invest Ophth Vis Sci,* 38**,** 1184-1192.

Helveston, E. M., Saunders, R. A. & Ellis, F. D. (1980) Unilateral cataracts in children. *Ophthalmic Surg,* 11**,** 102-8.

Helveston, E. M. & Von Noorden, G. K. (1967) Microtropia. A newly defined entity. *Arch Ophthalmol,* 78**,** 272-81.

Hendry, S. H. C. & Reid, R. C. (2000) The Koniocellular Pathway in Primate Vision. *Annu Rev Neurosci,* 23**,** 127-153.

Hess, R. F. (1982) Developmental sensory impairment: amblyopia or tarachopia? *Hum Neurobiol,* 1**,** 17-29.

Hess, R. F. (2001) Amblyopia: site unseen. *Clin Exp Optom,* 84**,** 321-336.

Hess, R. F., Baker, C. L., Jr., Verhoeve, J. N., Keesey, U. T. & France, T. D. (1985) The pattern evoked electroretinogram: its variability in normals and its relationship to amblyopia. *Invest Ophth Vis Sci,* 26**,** 1610-1623.

490

Hess, R. F., Campbell, F. W. & Zimmern, R. (1980) Differences in the neural basis of human amblyopias: the effect of mean luminance. *Vision Res,* 20**,** 295-305.

Hess, R. F. & Pointer, J. S. (1985) Differences in the neural basis of human amblyopia: the distribution of the anomaly across the visual field. *Vision Res,* 25**,** 1577-94.

Hess, R. F., Thompson, B., Gole, G. & Mullen, K. T. (2009) Deficient responses from the lateral geniculate nucleus in humans with amblyopia. *Eur. J. Neurosci.,* 29**,** 1064-1070.

Hilz, R., Rentschler, I. & Brettel, H. (1977) Myopic and strabismic amblyopia: substantial differences in human visual development. *Exp Brain Res,* 30**,** 445-6.

Hitzenberger, C. K. (1991) Optical measurement of the axial eye length by laser Doppler interferometry. *Invest Ophth Vis Sci,* 32**,** 616-24.

Holmes, G. (1945) The organisation of the visual cortex in man. *Proc R Soc Lond Series B (Biol),* 132**,** 348-361.

Holmes, J. M., Beck, R. W., Repka, M. X., Leske, D. A., Kraker, R. T., Blair, R. C., Moke, P. S., Birch, E. E., Saunders, R. A., Hertle, R. W., Quinn, G. E., Simons, K. A. & Miller, J. M. (2001) The amblyopia treatment study visual acuity testing protocol. *Arch. Ophthalmol.,* 119**,** 1345-1353.

Holmes, J. M. & Clarke, M. P. (2006) Amblyopia. *The Lancet,* 367**,** 1343-1351.

Holmes, J. M., Kraker, R. T., Beck, R. W., Birch, E. E., Cotter, S. A., Everett, D. F., Hertle, R. W., Quinn, G. E., Repka, M. X., Scheiman, M. M., Wallace, D. K. & Pediatric Eye Disease Investigator, G. (2003) A randomized trial of prescribed patching regimens for treatment of severe amblyopia in children. *Ophthalmology,* 110**,** 2075-87.

Hood, D. C., Fortune, B., Arthur, S. N., Xing, D., Salant, J. A., Ritch, R. & Liebmann, J. M. (2008) Blood vessel contributions to retinal nerve fiber layer thickness profiles measured with optical coherence tomography. *J Glaucoma,* 17**,** 519-28.

Hood, D. C., Salant, J. A., Arthur, S. N., Ritch, R. & Liebmann, J. M. (2009) The Location of the Inferior and Superior Temporal Blood Vessels and Interindividual Variability of the Retinal Nerve Fiber Layer Thickness. *J Glaucoma.*

Horton, J. C. & Hocking, D. R. (1996a) An adult-like pattern of ocular dominance columns in striate cortex of newborn monkeys prior to visual experience. *J Neurosci,* 16**,** 1791-807.

Horton, J. C. & Hocking, D. R. (1996b) Intrinsic variability of ocular dominance column periodicity in normal macaque monkeys. *J Neurosci,* 16**,** 7228-39.

Horton, J. C. & Hocking, D. R. (1996c) Pattern of ocular dominance columns in human striate cortex in strabismic amblyopia. *Vis Neurosci,* 13**,** 787-795.

Horton, J. C. & Hocking, D. R. (1998) Effect of early monocular enucleation upon ocular dominance columns and cytochrome oxidase activity in monkey and human visual cortex. *Vis Neurosci,* 15**,** 289-303.

Horton, J. C. & Hoyt, W. F. (1991a) Quadrantic visual field defects. A hallmark of lesions in extrastriate (V2/V3) cortex. *Brain,* 114 (Pt 4)**,** 1703-18.

Horton, J. C. & Hoyt, W. F. (1991b) The representation of the visual field in human striate cortex. A revision of the classic Holmes map. *Arch Ophthalmol,* 109**,** 816-24.

Huang, D. (2006) *Retinal imaging,* Philadelphia, PA, Mosby Elsevier.

Huang, D., Swanson, E. A., Lin, C. P., Schuman, J. S., Stinson, W. G., Chang, W., Hee, M. R., Flotte, T., Gregory, K., Puliafito, C. A. & Fujimoto, J. G. (1991) Optical Coherence Tomography. *Science,* 254**,** 1178-1181.

Huang, J., Liu, X., Wu, Z., Guo, X., Xu, H., Dustin, L. & Sadda, S. (2010) Macular and Retinal Nerve Fiber Layer Thickness Measurements in Normal Eyes With the Stratus OCT, the Cirrus HD-OCT, and the Topcon 3D OCT-1000. *J Glaucoma.*

Hubel, D. H. (1963) The Visual Cortex of the Brain. *Sci Am,* 209**,** 54-62.

Hubel, D. H. & Wiesel, T. N. (1965) Binocular interaction in striate cortex of kittens reared with artificial squint. *J Neurophysiol,* 28**,** 1041-59.

Hubel, D. H. & Wiesel, T. N. (1968) Receptive fields and functional architecture of monkey striate cortex. *J Physiol,* 195**,** 215-43.

493

Hubel, D. H. & Wiesel, T. N. (1998) Early exploration of the visual cortex. *Neuron, 20*, 401-412.

Hubel, D. H., Wiesel, T. N. & Levay, S. (1977) Plasticity of Ocular Dominance Columns in Monkey Striate Cortex. *Philos T Roy Soc B, 278*, 377-&.

Hubel, D. H., Wiesel, T. N. & Stryker, M. P. (1978) Anatomical demonstration of orientation columns in macaque monkey. *J. Comp. Neurol., 177*, 361-379.

Huberman, A. D. (2007) Mechanisms of eye-specific visual circuit development. *Curr Opin Neurobiol, 17*, 73-80.

Huberman, A. D., Murray, K. D., Warland, D. K., Feldheim, D. A. & Chapman, B. (2005) Ephrin-As mediate targeting of eye-specific projections to the lateral geniculate nucleus. *Nat Neurosci, 8*, 1013-21.

Huberman, A. D., Speer, C. M. & Chapman, B. (2006) Spontaneous retinal activity mediates development of ocular dominance columns and binocular receptive fields in V1. *Neuron, 52*, 247-254.

Hug, T. (2004) Full-time occlusion compared to part-time occlusion for the treatment of amblyopia. *Optometry, 75*, 241-4.

Huynh, S. C., Samarawickrama, C., Wang, X. Y., Rochtchina, E., Wong, T. Y., Gole, G. A., Rose, K. A. & Mitchell, P. (2009) Macular and nerve fiber layer thickness in amblyopia: the Sydney Childhood Eye Study. *Ophthalmology, 116*, 1604-9.

Huynh, S. C., Wang, X. Y., Burlutsky, G. & Mitchell, P. (2007) Symmetry of optical coherence tomography retinal measurements in young children. *Am J Ophthalmol,* 143**,** 518-520.

Huynh, S. C., Wang, X. Y., Burlutsky, G., Rochtchina, E., Stapleton, F. & Mitchell, P. (2008) Retinal and Optic Disc Findings in Adolescence: A Population-Based OCT Study. *Invest Ophth Vis Sci,* 49**,** 4328-4335.

Huynh, S. C., Wang, X. Y., Rochtchina, E., Crowston, J. G. & Mitchell, P. (2006a) Distribution of optic disc parameters measured by OCT: findings from a population-based study of 6-year-old Australian children. *Invest Ophth Vis Sci,* 47**,** 3276-85.

Huynh, S. C., Wang, X. Y., Rochtchina, E. & Mitchell, P. (2006b) Distribution of macular thickness by optical coherence tomography: findings from a population-based study of 6-year-old children. *Invest Ophth Vis Sci,* 47**,** 2351-7.

Huynh, S. C., Wang, X. Y., Rochtchina, E. & Mitchell, P. (2006c) Peripapillary retinal nerve fiber layer thickness in a population of 6-year old children - Findings by optical coherence tomography. *Ophthalmology,* 113**,** 1583-1592.

Ikeda, H. (1980) Visual acuity, its development and amblyopia. *J R Soc Med,* 73**,** 546-55.

Ikeda, H. & Tremain, K. E. (1979) Amblyopia occurs in retinal ganglion cells in cats reared with convergent squint without alternating fixation. *Exp Brain Res,* 35**,** 559-82.

495

Ikeda, H. & Wright, M. J. (1972a) Differential effects of refractive errors and receptive field organization of central and peripheral ganglion cells. *Vision Res,* 12**,** 1465-76.

Ikeda, H. & Wright, M. J. (1972b) Receptive field organization of 'sustained' and 'transient' retinal ganglion cells which subserve different function roles. *J Physiol,* 227**,** 769-800.

Ikeda, H. & Wright, M. J. (1974) Is amblyopia due to inappropriate stimulation of the "sustained" pathway during development? *Br J Ophthalmol,* 58**,** 165-75.

Ingram, R. M., Gill, L. E. & Lambert, T. W. (2003) Emmetropisation in normal and strabismic children and the associated changes of anisometropia. *Strabismus,* 11**,** 71-84.

Izquierdo, N. J., Emanuelli, A., Izquierdo, J. C., Garcia, M., Cadilla, C. & Berrocal, M. H. (2007) Foveal thickness and macular volume in patients with oculocutaneous albinism. *Retina,* 27**,** 1227-30.

Jaffe, G. J. & Caprioli, J. (2004) Optical coherence tomography to detect and manage retinal disease and glaucoma. *Am J Ophthalmol,* 137**,** 156-169.

Jakobsson, P., Kvarnstrom, G., Abrahamsson, M., Bjernbrink-Hornblad, E. & Sunnqvist, B. (2002) The frequency of amblyopia among visually impaired persons. *Acta Ophthalmol Scand,* 80**,** 44-46.

496

Jensen, H. & Goldschmidt, E. (1986) Visual acuity in Danish school children. *Acta Ophthalmol (Copenh),* 64**,** 187-91.

Johnson, C. A., Sample, P. A., Zangwill, L. M., Vasile, C. G., Cioffi, G. A., Liebmann, J. R. & Weinreb, R. N. (2003) Structure and function evaluation (SAFE): II. Comparison of optic disk and visual field characteristics. *Am J Ophthalmol,* 135**,** 148-54.

Johnson, E. C., Guo, Y., Cepurna, W. O. & Morrison, J. C. (2009) Neurotrophin roles in retinal ganglion cell survival: lessons from rat glaucoma models. *Exp Eye Res,* 88**,** 808-15.

Jonas, J. B., Budde, W. M. & Panda-Jonas, S. (1999) Ophthalmoscopic evaluation of the optic nerve head. *Surv Ophthalmol,* 43**,** 293-320.

Jonas, J. B. & Dichtl, A. (1996) Evaluation of the retinal nerve fiber layer. *Surv Ophthalmol,* 40**,** 369-378.

Jonas, J. B., Gusek, G. C. & Naumann, G. O. (1988) Optic disc, cup and neuroretinal rim size, configuration and correlations in normal eyes. *Invest Ophth Vis Sci,* 29**,** 1151-8.

Jonas, J. B., Schmidt, A. M., Muller-Bergh, J. A., Schlotzer-Schrehardt, U. M. & Naumann, G. O. (1992) Human optic nerve fiber count and optic disc size. *Invest Ophth Vis Sci,* 33**,** 2012-2018.

Kandel, G. L., Grattan, P. E. & Bedell, H. E. (1980) Are the dominant eyes of amblyopes normal? *Am J Optom Physiol Opt,* 57**,** 1-6.

Katsanos, A., Kothy, P., Papp, A. & Hollo, G. (2004) Influence of subfoveal choroidal neovascularisation on macular imaging with scanning laser polarimetry of the retinal nerve fibre layer. *Eye,* 19**,** 117-122.

Katz, L. C. & Crowley, J. C. (2002) Development of cortical circuits: lessons from ocular dominance columns. *Nat Rev Neurosci,* 3**,** 34-42.

Katz, L. M., Levi, D. M. & Bedell, H. E. (1984) Central and peripheral contrast sensitivity in amblyopia with varying field size. *Doc Ophthalmol,* 58**,** 351-73.

Kee, S., Lee, S. & Lee, Y. (2006) Thickness of the fovea and retinal nerve fiber layer in amblyopic and normal eyes in children. *Korean J Ophthalmol,* 20**,** 177-181.

Kee, S. P. M., Levi, D. M. & Movshon, J. A. (2003) The pattern of visual deficits in amblyopia. *J Vision,* 3**,** 380-405.

Kelly, J. P., Weiss, A. H., Zhou, Q., Schmode, S. & Dreher, A. W. (2003) Imaging a Child's Fundus Without Dilation Using a Handheld Confocal Scanning Laser Ophthalmoscope. *Arch Ophthalmol,* 121**,** 391-396.

Khan, A. A., Wadhwa, S. & Bijlani, V. (1994) Development of human lateral geniculate nucleus: an electron microscopic study. *Int J Dev Neurosci,* 12**,** 661-72.

Kheterpal, S., Jones, H. S., Auld, R. & Moseley, M. J. (1996) Reliability of visual acuity in children with reduced vision. *Ophthalmic Physiol Opt,* 16**,** 447-9.

Kidd, T., Bland, K. S. & Goodman, C. S. (1999) Slit is the midline repellent for the robo receptor in Drosophila. *Cell,* 96**,** 785-94.

Kind, P. C., Mitchell, D. E., Ahmed, B., Blakemore, C., Bonhoeffer, T. & Sengpiel, F. (2002) Correlated binocular activity guides recovery from monocular deprivation. *Nature,* 416**,** 430-433.

Kiorpes, L. (2006) Visual processing in amblyopia: animal studies. *Strabismus,* 14**,** 3-10.

Kiorpes, L. & Kiper, D. C. (1996) Development of contrast sensitivity across the visual field in macaque monkeys (Macaca nemestrina). *Vision Res,* 36**,** 239-47.

Kiorpes, L. & Wallman, J. (1995) Does experimentally-induced amblyopia cause hyperopia in monkeys? *Vision Res,* 35**,** 1289-97.

Kiss, B., Findl, O., Menapace, R., Wirtitsch, M., Drexler, W., Hitzenberger, C. K. & Fercher, A. F. (2002) Biometry of cataractous eyes using partial coherence interferometry: clinical feasibility study of a commercial prototype I. *J Cataract Refr Surg,* 28**,** 224-9.

Klein, B. E., Klein, R. & Lee, K. E. (2004) Heritability of risk factors for primary open-angle glaucoma: the Beaver Dam Eye Study. *Invest Ophth Vis Sci,* 45**,** 59-62.

Knight, O. R. J., Chang, R. T., Feuer, W. J. & Budenz, D. L. (2009) Comparison of Retinal Nerve Fiber Layer Measurements Using Time Domain and Spectral Domain Optical Coherent Tomography. *Ophthalmology,* 116**,** 1271-1277.

Ko, T. H., Fujimoto, J. G., Duker, J. S., Paunescu, L. A., Drexler, W., Baumal, C. R., Puliafito, C. A., Reichel, E., Rogers, A. H. & Schuman, J. S. (2004) Comparison of ultrahigh- and standard-resolution optical coherence tomography for imaging macular hole pathology and repair. *Ophthalmology,* 111**,** 2033-2043.

Landisman, C. E. & Ts'o, D. Y. (2002) Color processing in macaque striate cortex: relationships to ocular dominance, cytochrome oxidase, and orientation. *J Neurophysiol,* 87**,** 3126-37.

Langenbucher, A., Seitz, B. & Viestenz, A. (2003) Computerised calculation scheme for ocular magnification with the Zeiss telecentric fundus camera. *Ophthalmic Physiol Opt,* 23**,** 449-455.

Lawwill, T. (1978) Electrophysiologic aspects of amblyopia. *Ophthalmology,* 85**,** 451-64.

Leguire, L. E., Rogers, G. L. & Bremer, D. L. (1990) Amblyopia: the normal eye is not normal. *J Pediat Ophth Strab,* 27**,** 32-8; discussion 39.

Lempert, P. (2000) Optic nerve hypoplasia and small eyes in presumed amblyopia. *J AAPOS,* 4**,** 258-266.

Lempert, P. (2003) Axial Length-Disc Area Ratio in Esotropic Amblyopia. *Arch Ophthalmol,* 121**,** 821-824.

500

Lempert, P. (2004) The axial length/disc area ratio in anisometropic hyperopic amblyopia: A hypothesis for decreased unilateral vision associated with hyperopic anisometropia. *Ophthalmology,* 111**,** 304-308.

Lempert, P. (2008) Retinal Area and Optic Disc Rim Area in Amblyopic, Fellow, and Normal Hyperopic Eyes: A Hypothesis for Decreased Acuity in Amblyopia. *Ophthalmology,* 115**,** 2259-2261.

Lepard, C. W. (1975) Comparative changes in the error of refraction between fixing and amblyopic eyes during growth and development. *Am J Ophthalmol,* 80**,** 485-90.

Leung, C. K.-S., Cheung, C. Y. L., Weinreb, R. N., Lee, G., Lin, D. S., Pang, C.-P. & Lam, D. S. C. (2008) Comparison of Macular Thickness Measurements between Time Domain and Spectral Domain Optical Coherence Tomography. *Invest. Ophthalmol. Vis. Sci.***,** iovs.07-1326.

Leung, C. K., Cheng, A. C., Chong, K. K., Leung, K. S., Mohamed, S., Lau, C. S., Cheung, C. Y., Chu, G. C., Lai, R. Y., Pang, C. C. & Lam, D. S. (2007) Optic disc measurements in myopia with optical coherence tomography and confocal scanning laser ophthalmoscopy. *Invest Ophth Vis Sci,* 48**,** 3178-83.

Leung, C. K., Cheung, C. Y., Weinreb, R. N., Qiu, Q., Liu, S., Li, H., Xu, G., Fan, N., Huang, L., Pang, C. P. & Lam, D. S. (2009) Retinal nerve fiber layer imaging with spectral-domain optical coherence tomography: a variability and diagnostic performance study. *Ophthalmology,* 116**,** 1257-63, 1263 e1-2.

Leung, C. K. S., Chan, W. M., Yung, W. H., Ng, A. C. K., Woo, J., Tsang, M. K. & Tse, R. K. K. (2005) Comparison of macular and peripapillary measurements for the detection of glaucoma - An optical coherence tomography study. *Ophthalmology,* 112**,** 391-400.

Leung, C. K. S., Mohamed, S., Leung, K. S., Cheung, C. Y. L., Chan, S. L. W., Cheng, D. K. Y., Lee, A. K. C., Leung, G. Y. O., Rao, S. K. & Lam, D. S. C. (2006) Retinal nerve fiber layer measurements in myopia: An optical coherence tomography study. *Invest Ophth Vis Sci,* 47**,** 5171-5176.

Leung, M. M., Huang, R. Y. & Lam, A. K. (2010) Retinal nerve fiber layer thickness in normal Hong Kong chinese children measured with optical coherence tomography. *J Glaucoma,* 19**,** 95-9.

Levay, S., Wiesel, T. N. & Hubel, D. H. (1980) The Development of Ocular Dominance Columns in Normal and Visually Deprived Monkeys. *J Comp Neurol,* 191**,** 1-51.

Levi-Montalcini, R. (1975) Nerve Growth Factor. *Science,* 187**,** 113.

Levi, D. M. (2006) Visual processing in amblyopia: human studies. *Strabismus,* 14**,** 11-9.

Levi, D. M., Klein, S. A. & Chen, I. (2008) What limits performance in the amblyopic visual system: seeing signals in noise with an amblyopic brain. *J Vis,* 8**,** 1 1-23.

Levi, D. M., Klein, S. A. & Yap, Y. L. (1987) Positional uncertainty in peripheral and amblyopic vision. *Vision Res,* 27**,** 581-97.

Levi, D. M. & Manny, R. E. (1982) The pathophysiology of amblyopia: electrophysiological studies. *Ann N Y Acad Sci,* 388**,** 243-63.

Levitt, J. B., Schumer, R. A., Sherman, S. M., Spear, P. D. & Movshon, J. A. (2001) Visual response properties of neurons in the LGN of normally reared and visually deprived macaque monkeys. *J Neurophysiol,* 85**,** 2111-29.

Li, T. & Shotton, K. (2009) Conventional occlusion versus pharmacologic penalization for amblyopia. *Cochrane Database Syst Rev***,** CD006460.

Liang, H., Crewther, D. P., Crewther, S. G. & Barila, A. M. (1995) A Role for Photoreceptor Outer Segments in the Induction of Deprivation Myopia. *Vision Res,* 35**,** 1217-1225.

Lim, C. S., O'brien, C. & Bolton, N. M. (1996) A simple clinical method to measure the optic disc size in glaucoma. *J Glaucoma,* 5**,** 241-5.

Lithander, J. & Sjostrand, J. (1991) Anisometropic and strabismic amblyopia in the age group 2 years and above: a prospective study of the results of treatment. *Br J Ophthalmol,* 75**,** 111-6.

Littmann, H. (1977) [A schematic fundus completing Gullstrand's schematic eye (author's transl)]. *Klin Monatsbl Augenheilkd,* 170**,** 59-63.

Littmann, H. (1979) [On the peripheral refraction of the human eye (author's transl)]. *Klin Monatsbl Augenheilkd,* 174**,** 139-46.

Littmann, H. (1982) [Determination of the real size of an object on the fundus of the living eye]. *Klin Monatsbl Augenheilkd,* 180**,** 286-9.

Littmann, H. (1988) [Determining the true size of an object on the fundus of the living eye]. *Klin Monatsbl Augenheilkd,* 192**,** 66-7.

Littmann, H. (1992) Determination of the true size of an object on the fundus of the living eye. By H. Littmann from the original article, "Zur Bestimmung der wahren Grosse eines Objektes auf dem Hintergrund des lebenden Auges," which originally appeared in Klinisches Monatsblatter fur Augenheilkunde 1982; 180:286-9. Translated by TD Williams. *Optom Vis Sci,* 69**,** 717-20.

Livingstone, M. S. & Hubel, D. H. (1984) Anatomy and Physiology of a Color System in the Primate Visual-Cortex. *J. Neurosci,* 4**,** 309-356.

Loudon, S. E., Fronius, M., Looman, C. W. N., Awan, M., Simonsz, B., Van Der Maas, P. J. & Simonsz, H. J. (2006) Predictors and a remedy for noncompliance with amblyopia therapy in children measured with the occlusion dose monitor. *Invest Ophth Vis Sci,* 47**,** 4393-4400.

Loudon, S. E., Polling, J. R., Simonsz, B. & Simonsz, H. J. (2004) Objective survey of the prescription of occlusion therapy for amblyopia. *Graefes Arch Clin Exp Ophthalmol,* 242**,** 736-40.

504

Lyon, D. C. & Kaas, J. H. (2002) Evidence for a modified V3 with dorsal and ventral halves in macaque monkeys. *Neuron,* 33**,** 453-61.

Lyon, D. C., Xu, X., Casagrande, V. A., Stefansic, J. D., Shima, D. & Kaas, J. H. (2002) Optical imaging reveals retinotopic organization of dorsal V3 in New World owl monkeys. *Proc Natl Acad Sci U S A,* 99**,** 15735-42.

Maguire, G. W., Smith, E. L., 3rd, Harwerth, R. S. & Crawford, M. L. (1982) Optically induced anisometropia in kittens. *Invest Ophth Vis Sci,* 23**,** 253-64.

Mann, F., Harris, W. A. & Holt, C. E. (2004) New views on retinal axon development: a navigation guide. *Int J Dev Biol,* 48**,** 957-64.

Mansour, A. M. (1992) Racial variation of optic disc parameters in children. *Ophthalmic Surg,* 23**,** 469-71.

Markwell, E. L., Feigl, B. & Zele, A. J. (2010) Intrinsically photosensitive melanopsin retinal ganglion cell contributions to the pupillary light reflex and circadian rhythm. *Clin Exp Optom,* 93**,** 137-49.

Marmor, M. F., Choi, S. S., Zawadzki, R. J. & Werner, J. S. (2008) Visual insignificance of the foveal pit: reassessment of foveal hypoplasia as fovea plana. *Arch Ophthalmol,* 126**,** 907-13.

Martinez, L. M. & Alonso, J. M. (2001) Construction of complex receptive fields in cat primary visual cortex. *Neuron,* 32**,** 515-25.

Massin, P., Vicaut, E., Haouchine, B., Erginay, A., Paques, M. & Gaudric, A. (2001) Reproducibility of retinal mapping using optical coherence tomography. *Arch. Ophthalmol.,* 119**,** 1135-1142.

Mc Allister, A. K., Katz, L. C. & Lo, D. C. (1999) Neurotrophins and synaptic plasticity. *Annu Rev Neurosci,* 22**,** 295-318.

Mc Fadzean, R., Brosnahan, D., Hadley, D. & Mutlukan, E. (1994) Representation of the visual field in the occipital striate cortex. *Br J Ophthalmol,* 78**,** 185-90.

Mc Graw, P., Winn, B. & Whitaker, D. (1995) Reliability of the Snellen chart. *BMJ,* 310**,** 1481-2.

Mc Graw, P. V., Winn, B., Gray, L. S. & Elliott, D. B. (2000) Improving the reliability of visual acuity measures in young children. *Ophthalmic Physiol Opt,* 20**,** 173-84.

Mc Guire, D. E., Weinreb, R. N. & Goldbaum, M. H. (2003) Foveal hypoplasia demonstrated in vivo with optical coherence tomography. *Am J Ophthalmol,* 135**,** 112-114.

Medeiros, F. A., Zangwill, L. M., Bowd, C., Sample, P. A. & Weinreb, R. N. (2006) Influence of disease severity and optic disc size on the diagnostic performance of imaging instruments in glaucoma. *Invest Ophth Vis Sci,* 47**,** 1008-15.

Medeiros, F. A., Zangwill, L. M., Bowd, C. & Weinreb, R. N. (2004) Comparison of the GDx VCC scanning laser polarimeter, HRT II confocal scanning laser

ophthalmoscope, and stratus OCT optical coherence tomograph for the detection of glaucoma. *Arch. Ophthalmol.,* 122**,** 827-837.

Mendola, J. D., Conner, I. P., Roy, A., Chan, S. T., Schwartz, T. L., Odom, J. V. & Kwong, K. K. (2005) Voxel-based analysis of MRI detects abnormal visual cortex in children and adults with amblyopia. *Hum Brain Mapp,* 25**,** 222-236.

Menke, M. N., Knecht, P., Sturm, V., Dabov, S. & Funk, J. (2008) Reproducibility of nerve fiber layer thickness measurements using 3D fourier-domain OCT. *Invest Ophth Vis Sci,* 49**,** 5386-91.

Meyer, C. H., Lapolice, D. J. & Freedman, S. F. (2002) Foveal hypoplasia in oculocutaneous albinism demonstrated by optical coherence tomography. *Am J Ophthalmol,* 133**,** 409-410.

Miller, N. R. (2005) *Walsh & Hoyt's Clinical Neuro-Ophthalmology,* Philadelphia, London.

Minckler, D. S. (1980) The organization of nerve fiber bundles in the primate optic nerve head. *Arch Ophthalmol,* 98**,** 1630-6.

Missotten, L. (1974) Estimation of the ratio of cones to neurons in the fovea of the human retina. *Invest Ophth Vis Sci,* 13**,** 1045-9.

Mitchell, D. E., Kind, P. C., Sengpiel, F. & Murphy, K. (2003) Brief daily periods of binocular vision prevent deprivation-induced acuity loss. *Curr Biol,* 13**,** 1704-1708.

Mok, K. H., Lee, V. W. H. & So, K. F. (2004) Increasing scans per examination improves the reproducibility on retinal nerve fiber layer measurements by optical coherence tomography. *Optom Vis Sci,* 81**,** 268-271.

Moller, H. U. (2005) Milestones and Normative Data. *Pediatric Ophthalmology and Strabismus 3rd ed.Edinburgh Elseveir Saunders*
3rd ed.

Morita, T., Kochiyama, T., Yamada, H., Konishi, Y., Yonekura, Y., Matsumura, M. & Sadato, N. (2000) Difference in the metabolic response to photic stimulation of the lateral geniculate nucleus and the primary visual cortex of infants: a fMRI study. *Neurosci Res,* 38**,** 63-70.

Moseley, M. & Fielder, A. R. (2001) *Amblyopia : a multidisciplinary approach,* Oxford, Butterworth-Heinemann.

Moseley, M. J., Fielder, A. R., Irwin, M., Jones, H. S. & Auld, R. J. (1997) Effectiveness of occlusion therapy in ametropic amblyopia: a pilot study. *Br J Ophthalmol,* 81**,** 956-961.

Moseley, M. J., Neufeld, M., Mccarry, B., Charnock, A., Mcnamara, R., Rice, T. & Fielder, A. (2002) Remediation of refractive amblyopia by optical correction alone. *Ophthal. Physiol. Opt.,* 22**,** 296-299.

Moses, R. A. (Ed.) (1981) *Adler's Physiology of the eye,* St. louis, Toronto, London, The C.V. Mosby Company.

Nassi, J. J. & Callaway, E. M. (2009) Parallel processing strategies of the primate visual system. *Nat Neurosci,* 10**,** 360-372.

Nassif, N., Cense, B., Park, B. H., Yun, S. H., Chen, T. C., Bouma, B. E., Tearney, G. J. & De Boer, J. F. (2004) In vivo human retinal imaging by ultrahigh-speed spectral domain optical coherence tomography. *Opt Lett,* 29**,** 480-482.

Neuringer, M., Sandstrom, M. M., Johnson, E. J. & Snodderly, D. M. (2004) Nutritional manipulation of primate retinas, I: effects of lutein or zeaxanthin supplements on serum and macular pigment in xanthophyll-free rhesus monkeys. *Invest Ophth Vis Sci,* 45**,** 3234-43.

Nolan, J. M., Stringham, J. M., Beatty, S. & Snodderly, D. M. (2008) Spatial Profile of Macular Pigment and Its Relationship to Foveal Architecture. *Invest Ophth Vis Sci,* 49**,** 2134-2142.

Nucci, C., Piccirilli, S., Nistico, R., Morrone, L. A., Cerulli, L. & Bagetta, G. (2003) Apoptosis in the mechanisms of neuronal plasticity in the developing visual system. *Eur J Ophthalmol,* 13 Suppl 3**,** S36-43.

Nucci, C., Piccirilli, S., Rodino, P., Nistico, R., Grandinetti, M., Cerulli, L., Leist, M., Nicotera, P. & Bagetta, G. (2000) Apoptosis in the dorsal lateral geniculate nucleus

after monocular deprivation involves glutamate signaling, NO production, and PARP activation. *Biochem Biophys Res Commun,* 278**,** 360-7.

Ogden, T. E. (1983) Nerve-Fiber Layer of the Primate Retina - Thickness and Glial Content. *Vision Res,* 23**,** 581-587.

Ogden, T. E. (1984) Nerve-Fiber Layer of the Primate Retina - Morphometric Analysis. *Invest Ophth Vis Sci,* 25**,** 19-29.

Ohlsson, J., Baumann, M., Sjostrand, J. & Abrahamsson, M. (2002) Long term visual outcome in amblyopia treatment. *Br J Ophthalmol,* 86**,** 1148-1151.

Oliveira, C., Harizman, N., Girkin, C. A., Xie, A., Tello, C., Liebmann, J. M. & Ritch, R. (2007) Axial length and optic disc size in normal eyes. *Br J Ophthalmol,* 91**,** 37-9.

Olson, R. J. & Scott, W. E. (1997) A practical approach to occlusion therapy for amblyopia. *Semin Ophthalmol,* 12**,** 161-165.

Oster, S. F., Bodeker, M. O., He, F. L. & Sretavan, D. W. (2003) Invariant Sema5A inhibition serves an ensheathing function during optic nerve development. *Development,* 130**,** 775-784.

Oster, S. F., Deiner, A., Birgbauer, E. & Sretavan, D. W. (2004) Ganglion cell axon pathfinding in the retina and optic nerve. *Semin Cell Dev Biol,* 15**,** 125-136.

Oster, S. F. & Sretavan, D. W. (2003) Connecting the eye to the brain: the molecular basis of ganglion cell axon guidance. *Br J Ophthalmol,* 87**,** 639-645.

Osterberg, G. (1935) Topography of the layer of rods and cones in the human retina. *Acta Ophthalmologica* Suppl. 13:6**,** 1-102.

Pakravan, M., Aramesh, S., Yazdani, S., Yaseri, M. & Sedigh-Rahimabadi, M. (2009) Peripapillary Retinal Nerve Fiber Layer Thickness Measurement by Three-Dimensional Optical Coherence Tomography in a Normal Population. *J Ophthalmic Vis Res,* 4**,** 220 -227.

Parikh, R. S., Parikh, S. R., Sekhar, G. C., Prabakaran, S., Babu, J. G. & Thomas, R. (2007) Normal Age-Related Decay of Retinal Nerve Fiber Layer Thickness. *Ophthalmology,* 114**,** 921-926.

Parker, A. J. (2007) Binocular depth perception and the cerebral cortex. *Nat Neurosci,* 8**,** 379-391.

Parravano, M., Oddone, F., Sampalmieri, M. & Gazzaniga, D. (2007) Reliability of the IOLMaster in axial length evaluation in silicone oil-filled eyes. *Eye,* 21**,** 909-11.

Paunescu, L. A., Schuman, J. S., Price, L. L., Stark, P. C., Beaton, S., Ishikawa, H., Wollstein, G. & Fujimoto, J. G. (2004) Reproducibility of Nerve Fiber Thickness, Macular Thickness, and Optic Nerve Head Measurements Using StratusOCT. *Invest Ophth Vis Sci,* 45**,** 1716-1724.

Pediatric Eye Disease Investigator, G. (2008) A Randomized Trial of Atropine vs Patching for Treatment of Moderate Amblyopia: Follow-up at Age 10 Years. *Arch Ophthalmol,* 126**,** 1039-1044.

Persson, H. E. & Wanger, P. (1982) Pattern-reversal electroretinograms in squint amblyopia, artificial anisometropia and simulated eccentric fixation. *Acta Ophthalmol (Copenh),* 60**,** 123-32.

Pfeiffenberger, C., Cutforth, T., Woods, G., Yamada, J., Renteria, R. C., Copenhagen, D. R., Flanagan, J. G. & Feldheim, D. A. (2005) Ephrin-As and neural activity are required for eye-specific patterning during retinogeniculate mapping. *Nat Neurosci,* 8**,** 1022-7.

Pineles, S. L. & Demer, J. L. (2009) Bilateral Abnormalities of Optic Nerve Size and Eye Shape in Unilateral Amblyopia. *Am J Ophthalmol,* 148**,** 551-557.e2.

Plump, A. S., Erskine, L., Sabatier, C., Brose, K., Epstein, C. J., Goodman, C. S., Mason, C. A. & Tessier-Lavigne, M. (2002) Slit1 and Slit2 cooperate to prevent premature midline crossing of retinal axons in the mouse visual system. *Neuron,* 33**,** 219-232.

Poinoosawmy, D., Fontana, L., Wu, J. X., Fitzke, F. W. & Hitchings, R. A. (1997) Variation of nerve fibre layer thickness measurements with age and ethnicity by scanning laser polarimetry. *Br J Ophthalmol,* 81**,** 350-354.

Polito, A., Del Borrello, M., Isola, M., Zemella, N. & Bandello, F. (2005) Repeatability and reproducibility of fast macular thickness mapping with stratus optical coherence tomography. *Arch Ophthalmol,* 123**,** 1330-1337.

Pollock, S. C. & Miller, N. R. (1986) The retinal nerve fiber layer. *Int Ophthalmol Clin,* 26**,** 201-21.

Polyak, S. L. (1941) *The Retina*, University of Chicago Press.

Pons, M. E. & Garcia-Valenzuela, E. (2005) Redefining the Limit of the Outer Retina in Optical Coherence Tomography Scans. *Ophthalmology,* 112**,** 1079-1085.

Povazay, B., Hermann, B., Unterhuber, A., Hofer, B., Sattmann, H., Zeiler, F., Morgan, J. E., Falkner-Radler, C., Glittenberg, C., Blinder, S. & Drexler, W. (2007) Three-dimensional optical coherence tomography at 1050 nm versus 800 nm in retinal pathologies: enhanced performance and choroidal penetration in cataract patients. *J Biomed Opt,* 12**,** 041211.

Powell, C., Porooshani, H., Bohorquez, M. C. & Richardson, S. (2005a) Screening for amblyopia in childhood. *Cochrane Database of Systematic Reviews***,** -.

Powell, C., Wedner, S. & Richardson, S. (2005b) Screening for correctable visual acuity deficits in school-age children and adolescents. *Cochrane Database of Systematic Reviews***,** -.

Provis, J. M. (1987) Patterns of Cell-Death in the Ganglion-Cell Layer of the Human-Fetal Retina. *J. Comp. Neurol.,* 259**,** 237-246.

Provis, J. M., Diaz, C. M. & Dreher, B. (1998) Ontogeny of the primate fovea:a central issue in retinal development. *Prog Neurobiol,* 54**,** 549-581.

Provis, J. M. & Hendrickson, A. E. (2008) The foveal avascular region of developing human retina. *Arch. Ophthalmol.,* 126**,** 507-511.

Provis, J. M., Vandriel, D., Billson, F. A. & Russell, P. (1985) Development of the Human Retina - Patterns of Cell Distribution and Redistribution in the Ganglion-Cell Layer. *Journal of Comparative Neurology,* 233**,** 429-451.

Purves, D., Fitzpartick, D., S.M, W., Mcnamara, J., Augustine, G. J., Katz, L. C. & Lamantia, A. (Eds.) (2001) *Neuroscience,* Sunderland (MA), Sinauer Associates.

Quigley, H. A. & Addicks, E. M. (1982) Quantitative studies of retinal nerve fiber layer defects. *Arch Ophthalmol,* 100**,** 807-14.

Quigley, H. A., Mckinnon, S. J., Zack, D. J., Pease, M. E., Kerrigan-Baumrind, L. A., Kerrigan, D. F. & Mitchell, R. S. (2000) Retrograde axonal transport of BDNF in retinal ganglion cells is blocked by acute IOP elevation in rats. *Invest Ophth Vis Sci,* 41**,** 3460-6.

Quigley, M. G. & Dube, P. (2003) A New Fundus Camera Technique to Help Calculate Eye-Camera Magnification: A Rapid Means to Measure Disc Size. *Arch Ophthalmol,* 121**,** 707-709.

Rabbione, M. M., Roagna, B., Tonetti, S., Morgese, A., Rolle, T., Musso, M. & Grignolo, F. M. (2004) Optical coherence tomography measurements of retinal nerve fiber layer thickness in amblyopic and non-amblyopic eyes. *Invest Ophth Vis Sci,* 45**,** 2574-.

Rahi, J. S., Cumberland, P. M. & Peckham, C. S. (2006) Does amblyopia affect educational, health, and social outcomes? Findings from 1958 British birth cohort. *BMJ,* 332**,** 820-824.

Rajan, M. S., Keilhorn, I. & Bell, J. A. (2002) Partial coherence laser interferometry vs conventional ultrasound biometry in intraocular lens power calculations. *Eye,* 16**,** 552-6.

Rapaport, D. H. & Stone, J. (1982) The site of commencement of maturation in mammalian retina: observations in the cat. *Brain Res,* 281**,** 273-9.

Reche-Sainz, J. A., Domingo-Gordo, B. & Toledano-Fernandez, N. (2006) [Study of the retinal nerve fiber layer in childhood strabismus]. *Arch Soc Esp Oftalmol,* 81**,** 21-5.

Repka, M. X., Goldenberg-Cohen, N. & Edwards, A. R. (2006) Retinal nerve fiber layer thickness in amblyopic eyes. *Am J Ophthalmol,* 142**,** 247-51.

Repka, M. X., Kraker, R. T., Beck, R. W., Birch, E., Cotter, S. A., Holmes, J. M., Hertle, R. W., Hoover, D. L., Klimek, D. L., Marsh-Tootle, W., Scheiman, M. M., Suh, D. W., Weakley, D. R. & Pediatric Eye Disease Investigator, G. (2009a) Treatment of severe amblyopia with weekend atropine: results from 2 randomized clinical trials. *J AAPOS,* 13**,** 258-63.

515

Repka, M. X., Kraker, R. T., Tamkins, S. M., Suh, D. W., Sala, N. A. & Beck, R. W. (2009b) Retinal Nerve Fiber Layer Thickness in Amblyopic Eyes. *Am J Ophthalmol,* 148**,** 143-147.

Repka, M. X. & Quigley, H. A. (1989) The effect of age on normal human optic nerve fiber number and diameter. *Ophthalmology,* 96**,** 26-32.

Repka, M. X., Wallace, D. K., Beck, R. W., Kraker, R. T., Birch, E. E., Cotter, S. A., Donahue, S., Everett, D. F., Hertle, R. W., Holmes, J. M., Quinn, G. E., Scheiman, M. M., Weakley, D. R. & Pediatric Eye Disease Investigator, G. (2005) Two-year follow-up of a 6-month randomized trial of atropine vs patching for treatment of moderate amblyopia in children. *Arch Ophthalmol,* 123**,** 149-57.

Richer, S., Stiles, W., Statkute, L., Pulido, J., Frankowski, J., Rudy, D., Pei, K., Tsipursky, M. & Nyland, J. (2004) Double-masked, placebo-controlled, randomized trial of lutein and antioxidant supplementation in the intervention of atrophic age-related macular degeneration: the Veterans LAST study (Lutein Antioxidant Supplementation Trial). *Optometry,* 75**,** 216-30.

Rockhill, R. L., Daly, F. J., Macneil, M. A., Brown, S. P. & Masland, R. H. (2002) The diversity of ganglion cells in a mammalian retina. *J Neurosci,* 22**,** 3831-43.

Rosa, M. G., Palmer, S. M., Gamberini, M., Tweedale, R., Pinon, M. C. & Bourne, J. A. (2005) Resolving the organization of the New World monkey third visual complex: the dorsal extrastriate cortex of the marmoset (Callithrix jacchus). *J Comp Neurol,* 483**,** 164-91.

516

Rowe, M. H. & Dreher, B. (1982) Functional morphology of beta cells in the area centralis of the cat's retina: a model for the evolution of central retinal specializations. *Brain Behav Evol,* 21**,** 1-23.

Rucker, F. J. & Wallman, J. (2008) Cone signals for spectacle-lens compensation: Differential responses to short and long wavelengths. *Vision Res,* 48**,** 1980-1991.

Rudnicka, A. R., Burk, R. O. W., Edgar, D. F. & Fitzke, F. W. (1998) Magnification characteristics of fundus imaging systems. *Ophthalmology,* 105**,** 2186-2192.

Sadda, S. R., Wu, Z., Walsh, A. C., Richine, L., Dougall, J., Cortez, R. & Labree, L. D. (2006) Errors in Retinal Thickness Measurements Obtained by Optical Coherence Tomography. *Ophthalmology,* 113**,** 285-293.

Sakata, L. M., Deleon-Ortega, J., Sakata, V. & Girkin, C. A. (2009) Optical coherence tomography of the retina and optic nerve - a review. *Clin Exp Ophthalmol,* 37**,** 90-9.

Salchow, D. J., Oleynikov, Y. S., Chiang, M. F., Kennedy-Salchow, S. E., Langton, K., Tsai, J. C. & Al-Aswad, L. A. (2006) Retinal nerve fiber layer thickness in normal children measured with optical coherence tomography. *Ophthalmology,* 113**,** 786-791.

Samarawickrama, C., Wang, X. Y., Huynh, S. C., Burlutsky, G., Stapleton, F. & Mitchell, P. (2007) Effects of Refraction and Axial Length on Childhood Optic Disk

517

Parameters Measured by Optical Coherence Tomography. *Am J Ophthalmol,* 144**,** 459-461.

Sanchez-Cano, A., Baraibar, B., Pablo, L. E. & Honrubia, F. M. (2008) Magnification characteristics of the Optical Coherence Tomograph STRATUS OCT 3000. *Ophthalmic Physiol Opt,* 28**,** 21-28.

Sasaki, Y., Cheng, H., Smith, E. L., 3rd & Chino, Y. (1998) Effects of early discordant binocular vision on the postnatal development of parvocellular neurons in the monkey lateral geniculate nucleus. *Exp Brain Res,* 118**,** 341-51.

Savini, G., Zanini, M., Carelli, V., Sadun, A. A., Ross-Cisneros, F. N. & Barboni, P. (2005) Correlation between retinal nerve fibre layer thickness and optic nerve head size: an optical coherence tomography study. *Br J Ophthalmol,* 89**,** 489-492.

Schmitt, J. M., Xiang, S. H. & Yung, K. M. (1999) Speckle in optical coherence tomography. *J. Biomed. Opt.,* 4**,** 95-105.

Schuman, J. S., Pedutkloizman, T., Hertzmark, E., Hee, M. R., Wilkins, J. R., Coker, J. G., Puliafito, C. A., Fujimoto, J. G. & Swanson, E. A. (1996) Reproducibility of nerve fiber layer thickness measurements using optical coherence tomography. *Ophthalmology,* 103**,** 1889-1898.

Schuman, J. S., Wollstein, G., Farra, T., Hertzmark, E., Aydin, A., Fujimoto, J. G. & Paunescu, L. A. (2003) Comparison of optic nerve head measurements obtained

by optical coherence tomography and confocal scanning laser ophthalmoscopy. *Am J Ophthalmol,* 135**,** 504-512.

Searle, A., Norman, P., Harrad, R. & Vedhara, K. (2002) Psychosocial and clinical determinants of compliance with occlusion therapy for amblyopic children. *Eye (Lond),* 16**,** 150-5.

Selenow, A. & Ciuffreda, K. J. (1986) Vision function recovery during orthoptic therapy in an adult esotropic amblyope. *J Am Optom Assoc,* 57**,** 132-40.

Sherbondy, A. J., Dougherty, R. F., Napel, S. & Wandell, B. A. (2008) Identifying the human optic radiation using diffusion imaging and fiber tractography. *J Vis,* 8**,** 12 1-11.

Shotton, K., Powell, C., Voros, G. & Hatt, S. R. (2008) Interventions for unilateral refractive amblyopia. *Cochrane Database Syst Rev***,** CD005137.

Simons, K., Gotzler, K. C. & Vitale, S. (1997) Penalization versus part-time occlusion and binocular outcome in treatment of strabismic amblyopia. *Ophthalmology,* 104**,** 2156-60.

Sincich, L. C. & Horton, J. C. (2002) Divided by cytochrome oxidase: a map of the projections from V1 to V2 in macaques. *Science,* 295**,** 1734-7.

Sireteanu, R. & Fronius, M. (1981) Naso-temporal asymmetries in human amblyopia consequence of long-term interocular suppression. *Vision Res,* 21**,** 1055-63.

Slyshalova, N. N. & Shamshinova, A. M. (2008) [Retinal bioelectrical activity in amblyopia]. *Vestn Oftalmol,* 124**,** 32-6.

Smith, A. T., Greenlee, M. W., Singh, K. D., Kraemer, F. M. & Hennig, J. (1998) The processing of first- and second-order motion in human visual cortex assessed by functional magnetic resonance imaging (fMRI). *J Neurosci,* 18**,** 3816-30.

Smith, E. L., 3rd, Harwerth, R. S. & Crawford, M. L. (1985) Spatial contrast sensitivity deficits in monkeys produced by optically induced anisometropia. *Invest Ophth Vis Sci,* 26**,** 330-42.

Smith, M., Frost, A., Graham, C. M. & Shaw, S. (2007) Effect of pupillary dilatation on glaucoma assessments using optical coherence tomography. *Br J Ophthalmol,* 91**,** 1686-1690.

Snodderly, D. M., Brown, P. K., Delori, F. C. & Auran, J. D. (1984) The macular pigment. I. Absorbance spectra, localization, and discrimination from other yellow pigments in primate retinas. *Invest Ophth Vis Sci,* 25**,** 660-73.

Solomon, S. G. & Lennie, P. (2007) The machinery of colour vision. *Nat Rev Neurosci,* 8**,** 276-86.

Springer, A. D. & Hendrickson, A. E. (2005) Development of the primate area of high acuity, 3: Temporal relationships between pit formation, retinal elongation and cone packing. *Visual Neurosci,* 22**,** 171-185.

Sretavan, D. W. (1990) Specific Routing of Retinal Ganglion-Cell Axons at the Mammalian Optic Chiasm during Embryonic-Development. *J Neurosci,* 10**,** 1995-2007.

Steele, A. L., Bradfield, Y. S., Kushner, B. J., France, T. D., Struck, M. C. & Gangnon, R. E. (2006) Successful treatment of anisometropic amblyopia with spectacles alone. *J AAPOS,* 10**,** 37-43.

Stein, D. M., Ishikawa, H., Hariprasad, R., Wollstein, G., Noecker, R. J., Fujimoto, J. G. & Schuman, J. S. (2006a) A new quality assessment parameter for optical coherence tomography. *Br J Ophthalmol,* 90**,** 186-190.

Stein, D. M., Wollstein, G., Ishikawa, H., Hertzmark, E., Noecker, R. J. & Schuman, J. S. (2006b) Effect of Corneal Drying on Optical Coherence Tomography. *Ophthalmology,* 113**,** 985-991.

Stellwagen, D. & Shatz, C. J. (2002) An Instructive Role for Retinal Waves in the Development of Retinogeniculate Connectivity. *Neuron,* 33**,** 357-367.

Stewart-Brown, S. L. & Snowdon, S. K. (1998) Evidence-based dilemmas in pre-school vision screening. *Arch Dis Child,* 78**,** 406-407.

Stewart, C. E. (2000) Comparison of Snellen and log-based acuity scores for school-aged children. *Br Orthop J,* 57**,** 32-38.

Stewart, C. E., Fielder, A. R., Stephens, D. A. & Moseley, M. J. (2002) Design of the Monitored Occlusion Treatment of Amblyopia Study (MOTAS). *Br J Ophthalmol,* 86**,** 915-919.

Stewart, C. E., Fielder, A. R., Stephens, D. A. & Moseley, M. J. (2005) Treatment of unilateral amblyopia: Factors influencing visual outcome. *Invest Ophth Vis Sci,* 46**,** 3152-3160.

Stewart, C. E., Moseley, M. J. & Fielder, A. R. (2003) Defining and measuring treatment outcome in unilateral amblyopia. *Br J Ophthalmol,* 87**,** 1229-1231.

Stewart, C. E., Moseley, M. J., Fielder, A. R., Stephens, D. A. & Cooperative, M. (2004a) Refractive adaptation in amblyopia: quantification of effect and implications for practice. *Br J Ophthalmol,* 88**,** 1552-6.

Stewart, C. E., Moseley, M. J., Stephens, D. A. & Fielder, A. R. (2004b) Treatment dose-response in amblyopia therapy: The Monitored Occlusion Treatment of Amblyopia Study (MOTAS). *Invest Ophth Vis Sci,* 45**,** 3048-3054.

Stewart, C. E., Stephens, D. A., Fielder, A. R. & Moseley, M. J. (2007) Objectively monitored patching regimens for treatment of amblyopia: randomised trial. *BMJ,* 335**,** 707-711.

Symonds, L. L. & Rosenquist, A. C. (1984) Corticocortical connections among visual areas in the cat. *J Comp Neurol,* 229**,** 1-38.

Tan, J. H. Y., Thompson, J. R. & Gottlob, I. (2003) Differences in the management of amblyopia between European countries. *Br J Ophthalmol,* 87**,** 291-296.

Taylor, D. (2005) Optic nerve axons: life and death before birth. *Eye,* 19**,** 499-527.

Tejedor, J. & Ogallar, C. (2008) Comparative efficacy of penalization methods in moderate to mild amblyopia. *Am J Ophthalmol,* 145**,** 562-9.

Testoni, P. A. (2007) Optical coherence tomography. *ScientificWorldJournal,* 7**,** 87-108.

The Pediatric Eye Disease Investigator, G. (2002a) The Clinical Profile of Moderate Amblyopia in Children Younger Than 7 Years. *Arch Ophthalmol,* 120**,** 281-287.

The Pediatric Eye Disease Investigator, G. (2002b) A Randomized Trial of Atropine vs Patching for Treatment of Moderate Amblyopia in Children. *Arch Ophthalmol,* 120**,** 268-278.

The Pediatric Eye Disease Investigator, G. (2003) A Randomized Trial of Patching Regimens for Treatment of Moderate Amblyopia in Children. *Arch Ophthalmol,* 121**,** 603-611.

The Pediatric Eye Disease Investigator, G. (2005) Two-Year Follow-up of a 6-Month Randomized Trial of Atropine vs Patching for Treatment of Moderate Amblyopia in Children. *Arch Ophthalmol,* 123**,** 149-157.

Thomas, O. M., Cumming, B. G. & Parker, A. J. (2002) A specialization for relative disparity in V2. *Nat Neurosci,* 5**,** 472-8.

Troilo, D., Xiong, M. J., Crowley, J. C. & Finlay, B. L. (1996) Factors controlling the dendritic arborization of retinal ganglion cells. *Visual Neurosci,* 13**,** 721-733.

Trotter, Y., Celebrini, S. & Durand, J. B. (2004) Evidence for implication of primate area V1 in neural 3-D spatial localization processing. *J Physiol,* 98**,** 125-134.

Ts'o, D. Y., Roe, A. W. & Gilbert, C. D. (2001) A hierarchy of the functional organization for color, form and disparity in primate visual area V2. *Vision Res,* 41**,** 1333-49.

Van Horck, F. P. G., Weinl, C. & Holt, C. E. (2004) Retinal axon guidance: novel mechanisms for steering. *Curr Opin Neurobiol,* 14**,** 61-66.

Van Velthoven, M. E. J., Faber, D. J., Verbraak, F. D., Van Leeuwen, T. G. & De Smet, M. D. (2007) Recent developments in optical coherence tomography for imaging the retina. *Prog Retin Eye Res,* 26**,** 57-77.

Van Velthoven, M. E. J., Van Der Linden, M. H., De Smet, M. D., Faber, D. J. & Verbraak, F. D. (2006) Influence of cataract on optical coherence tomography image quality and retinal thickness. *Br J Ophthalmol,* 90**,** 1259-1262.

Vandriel, D., Provis, J. M. & Billson, F. A. (1990) Early differentiation of ganglion, amacrine, bipolar, and muller cells in the developing fovea of human retina. *J. Comp. Neurol.,* 291**,** 203-219.

Varma, R., Skaf, M. & Barron, E. (1996) Retinal nerve fiber layer thickness in normal human eyes. *Ophthalmology,* 103**,** 2114-2119.

Vizzeri, G., Bowd, C., Medeiros, F. A., Weinreb, R. N. & Zangwill, L. M. (2008) Effect of improper scan alignment on retinal nerve fiber layer thickness measurements using Stratus optical coherence tomograph. *J Glaucoma,* 17**,** 341-9.

Von Noorden, G. K. (1985) Idiopathic amblyopia. *Am J Ophthalmol,* 100**,** 214-7.

Von Noorden, G. K., Crawford, M. L. & Levacy, R. A. (1983) The lateral geniculate nucleus in human anisometropic amblyopia. *Invest Ophth Vis Sci,* 24**,** 788-790.

Wakakura, M. & Alvarez, E. (1987) A simple clinical method of assessing patients with optic nerve hypoplasia. The disc-macula distance to disc diameter ratio (DM/DD). *Acta Ophthalmol (Copenh),* 65**,** 612-7.

Wallace, D. K., Pediatric Eye Disease Investigator, G., Edwards, A. R., Cotter, S. A., Beck, R. W., Arnold, R. W., Astle, W. F., Barnhardt, C. N., Birch, E. E., Donahue, S. P., Everett, D. F., Felius, J., Holmes, J. M., Kraker, R. T., Melia, M., Repka, M. X., Sala, N. A., Silbert, D. I. & Weise, K. K. (2006) A randomized trial to evaluate 2 hours of daily patching for strabismic and anisometropic amblyopia in children. *Ophthalmology,* 113**,** 904-12.

Wang, K., Yuan, M. K., Jiang, Y. R., Bao, Y. Z. & Li, X. X. (2009) Axial length measurements before and after removal of silicone oil: a new method to correct the axial length of silicone-filled eyes for optical biometry. *Ophthal Physl Opt,* 29**,** 449-57.

Wang, X. Y., Huynh, S. C., Burlutsky, G., Ip, J., Stapleton, F. & Mitchell, P. (2007) Reproducibility of and effect of magnification on optical coherence tomography measurements in children. *Am J Ophthalmol,* 143**,** 484-488.

Wang, Y., Xu, L., Zhang, L., Yang, H., Ma, Y. & Jonas, J. B. (2006) Optic disc size in a population based study in northern China: the Beijing Eye Study. *Br J Ophthalmol,* 90**,** 353-6.

Watts, P. O., Neveu, M. M., Holder, G. E. & Sloper, J. J. (2002) Visual evoked potentials in successfully treated strabismic amblyopes and normal subjects. *J AAPOS,* 6**,** 389-392.

Weaver, M. & Hogan, B. (2001) Powerful ideas driven by simple tools: lessons from experimental embryology. *Nat Cell Biol,* 3**,** E165-7.

Weinreb, R. N., Bowd, C., Greenfield, D. S. & Zangwill, L. M. (2002) Measurement of the magnitude and axis of corneal polarization with scanning laser polarimetry. *Arch Ophthalmol,* 120**,** 901-6.

Weinreb, R. N., Bowd, C. & Zangwill, L. M. (2003) Glaucoma Detection Using Scanning Laser Polarimetry With Variable Corneal Polarization Compensation. *Arch Ophthalmol,* 121**,** 218-224.

Weinreb, R. N., Zangwill, L., Berry, C. C., Bathija, R. & Sample, P. A. (1998) Detection of Glaucoma With Scanning Laser Polarimetry. *Arch Ophthalmol,* 116**,** 1583-1589.

Weisberg, O. L., Sprunger, D. T., Plager, D. A., Neely, D. E. & Sondhi, N. (2005) Strabismus in pediatric pseudophakia. *Ophthalmology,* 112**,** 1625-8.

Wiesel, T. N. & Hubel, D. H. (1963) Single-Cell Responses in Striate Cortex of Kittens Deprived of Vision in One Eye. *J Neurophysiol,* 26**,** 1003-17.

Wiesel, T. N. & Hubel, D. H. (1965) Comparison of the effects of unilateral and bilateral eye closure on cortical unit responses in kittens. *J Neurophysiol,* 28**,** 1029-40.

Williams, C., Northstone, K., Harrad, R., Sparrow, J. M., Harvey, I. & Study, A. (2003a) Amblyopia treatment outcomes after preschool screening v school entry screening: observational data from a prospective cohort study. *Br J Ophthalmol,* 87**,** 988-993.

Williams, C., Northstone, K., Harrad, R. A., Sparrow, J. M. & Harvey, I. (2003b) Amblyopia treatment outcomes after preschool screening v school entry screening: observational data from a prospective cohort study. *Br J Ophthalmol,* 87**,** 988-993.

Williams, C., Northstone, K., Harrad, R. A., Sparrow, J. M., Harvey, I. & Team, A. S. (2002) Amblyopia treatment outcomes after screening before or at age 3 years: follow up from randomised trial. *BMJ,* 324**,** 1549-+.

Williams, C., Northstone, K., Howard, M., Harvey, I., Harrad, R. A. & Sparrow, J. M. (2008) Prevalence and risk factors for common vision problems in children: data from the ALSPAC study. *Br J Ophthalmol,* 92**,** 959-64.

Williams, D. R. (1980) Visual consequences of the foveal pit. *Invest Ophth Vis Sci,* 19**,** 653-67.

Williams, D. R. (1985) Aliasing in human foveal vision. *Vision Res,* 25**,** 195-205.

Williams, T. D. & Wilkinson, J. M. (1992) Position of the fovea centralis with respect to the optic nerve head. *Optom Vis Sci,* 69**,** 369-77.

Wojtkowski, M., Leitgeb, R., Kowalczyk, A., Bajraszewski, T. & Fercher, A. F. (2002) In vivo human retinal imaging by Fourier domain optical coherence tomography. *J Biomed Opt,* 7**,** 457-63.

Wojtkowski, M., Srinivasan, V., Fujimoto, J., Ko, T., Schuman, J., Kowalczyk, A. & Duker, J. (2005) Three-dimensional Retinal Imaging with High-Speed Ultrahigh-Resolution Optical Coherence Tomography. *Ophthalmology,* 112**,** 1734-1746.

Wojtkowski, M., Srinivasan, V. J., Ko, T. H., Fujimoto, J. G., Kowalczyk, A. & Duker, J. S. (2004) Ultrahigh-resolution, high-speed, Fourier domain optical coherence tomography and methods for dispersion compensation. *Opt Express,* 12**,** 2404-2422.

Woodruff, G., Hiscox, F., Thompson, J. R. & Smith, L. K. (1994) Factors affecting the outcome of children treated for amblyopia. *Eye,* 8 (Pt 6)**,** 627-31.

Worth, C. (1901) The orthoptic tretment of convergent squint in young children. *T Ophthal Soc UK,* 21**,** 245-258.

Wu, Z., Vazeen, M., Varma, R., Chopra, V., Walsh, A. C., Labree, L. D. & Sadda, S. R. (2007) Factors Associated with Variability in Retinal Nerve Fiber Layer Thickness Measurements Obtained by Optical Coherence Tomography. *Ophthalmology,* 114**,** 1505-1512.

Xiao, J. X., Xie, S., Ye, J. T., Liu, H. H., Gan, X. L., Gong, G. L. & Jiang, X. X. (2007) Detection of abnormal visual cortex in children with amblyopia by voxel-based morphometry. *Am J Ophthalmol,* 143**,** 489-93.

Yamada, E. (1969) Some structural features of the fovea centralis in the human retina. *Arch Ophthalmol,* 82**,** 151-9.

Yen, M. Y., Cheng, C. Y. & Wang, A. G. (2004) Retinal nerve fiber layer thickness in unilateral amblyopia. *Invest Ophth Vis Sci,* 45**,** 2224-2230.

Yoon, S. W., Park, W. H., Baek, S. H. & Kong, S. M. (2005) Thicknesses of macular retinal layer and peripapillary retinal nerve fiber layer in patients with hyperopic anisometropic amblyopia. *Korean J Ophthalmol,* 19**,** 62-7.

Yoshioka, T. & Hendry, S. H. C. (1995) Compartmental Organization of Layer Iva in Human Primary Visual-Cortex. *J. Comp. Neurol.,* 359**,** 213-220.

Yücel, Y. H., Zhang, Q., Weinreb, R. N., Kaufman, P. L. & Gupta, N. (2003) Effects of retinal ganglion cell loss on magno-, parvo-, koniocellular pathways in the lateral geniculate nucleus and visual cortex in glaucoma. *Prog Retin Eye Res,* 22**,** 465-481.

Yuodelis, C. & Hendrickson, A. (1986) A qualitative and quantitative analysis of the human fovea during development. *Vision Res,* 26**,** 847-55.

Zeki, S. M. (1969) Representation of central visual fields in prestriate cortex of monkey. *Brain Res,* 14**,** 271-91.

Zeki, S. M., Dudgeon, J. & Dutton, G. N. (1991) Reappraisal of the ratio of disc to macula/disc diameter in optic nerve hypoplasia. *Br J Ophthalmol,* 75**,** 538-41.

Zhang, B., Bi, H., Sakai, E., Maruko, I., Zheng, J. H., Smith, E. L. & Chino, Y. M. (2005) Rapid plasticity of binocular connections in developing monkey visual cortex (V1). *P Nat Acad Sci USA,* 102**,** 9026-9031.

Zhang, N., Zhu, X. H., Zhang, Y. & Chen, W. (2008) An fMRI study of neural interaction in large-scale cortico-thalamic visual network. *Neuroimage,* 42**,** 1110-7.